Aston University

Some parts of this thesis may have been removed for copyright restrictions.

If you have discovered material in AURA which is unlawful e.g. breaches copyright, (either yours or that of a third party) or any other law, including but not limited to those relating to patent, trademark, confidentiality, data protection, obscenity, defamation, libel, then please read our Takedown Policy and contact the service immediately

PRESTRESSED CONCRETE BEAMS

IN TORSION, BENDING AND SHEAR

- by -

MICHAEL JOHN COOPER, M.A., C.ENG., M.I.C.E.,

A THESIS SUBMITTED FOR THE DEGREE OF DOCTOR OF PHILOSOPHY

24 AUG 1976

DEPARTMENT OF CIVIL ENGINEERING

THE UNIVERSITY OF ASTON IN BIRMINGHAM

MARCH 1976

SYNOPSIS

This paper examines prestressed concrete rectangular beams subjected to torsion and a single point load. Forty beams of 100 x 174 mm cross section were tested with two shear spans and two types of post-tensioned, unbonded tendons. No stirrups or bonded longitudinal steel were incorporated in the test length.

Using the skewed bending approach, theoretical expressions are developed for the ultimate capacity of the beam under the combined loading condition, which agree well with the experimental values. The results of other research workers are compared with theoretical moment/torque interaction diagrams.

Complete moment/torque/shear interaction surfaces are presented for the author's beams; only part of this surface is, however, substantiated by the limited test results available.

ACKNOWLEDGMENTS

Thanks are due to Professor M. Holmes, B.Sc., Ph.D., C.Eng., F.I.C.E., F.I.Struct.E., F.I.Mun.E., Head of the Department of Civil Engineering, The University of Aston in Birmingham, for allowing this research to be undertaken part-time and to L.H. Martin, B.Sc., Ph.D., C.Eng., M.I.C.E., who supervised the project and gave every help and encouragement. The author is indebted to Dr P.J. Wainwright, for the design of the test rig; to Mr W. Parsons, Chief Technician and to the members of the staff of the Concrete and Structures Laboratories for their help during the casting and testing of the beams.

THE AUTHOR

After graduating in 1952 the author pursued his practical training in East Africa with the Public Works Department for three years. He then joined English Electric Atomic Power Division and from 1955 to 1966 was engaged on the design and development of atomic power stations, working in steel, reinforced and prestressed concrete.

Since 1966 the author has been Senior Lecturer in the Civil Engineering and Building Department, Faculty of Engineering, Lanchester Polytechnic, Coventry, teaching Structural Analysis and Design to Degree students.

No part of this work has been submitted in support of an application for another degree or qualification.

NOTATION

A_{s1} , A_{s2} , A_{s3}	cross sectional areas of lower, centre and upper layers of prestressing steel
a_v	distance of load from nearest support
B	bond slip factor
b	breadth of section
c_t	St. Venant constant
D_{s1} , D_{s2}	dowel forces due to torsion in lower and centre steel
d_1, d_2 , d_3	depths of centroids of lower, centre and upper layers of prestressing steel
E_c , E_s	Young's Modulus for concrete, steel
f'_c	uniaxial cylinder compressive strength of concrete.
f_{cm}	maximum direct stress in concrete due to bending normal to axis of beam
f_{cmi}	maximum direct stress in concrete due to bending normal to skew failure plane
f_{cu}	uniaxial cube crushing strength of concrete
f_r	modulus of rupture of concrete, 100 mm deep specimen
f'_r	modulus of rupture of concrete, 174 mm deep specimen
f_s	cylinder splitting strength of concrete
f_{s1} , f_{s2}	increase in stress in lower and centre prestressing steel
f_t	uniaxial tensile strength of concrete
G_s	modulus of rigidity of steel
h	overall depth of section
l_1 , l_2	lever arms for dowel force in lower and centre steel

NOTATION (continued)

M	bending moment applied to member
M_1 , M_2 , M_3	theoretical moments, Modes 1, 2, 3
M_{c1}	bending moment at first crack, Mode 1
M_u	ultimate moment of member, in pure bending
M_{u1} , M_{u2} , M_{u3}	theoretical ultimate moments, Modes 1, 2, 3
m	modular ratio steel/concrete
P_{s1} , P_{s2} , P_{s3}	initial prestressing forces in lower, centre and upper steel
p_{c1}	stress at bottom of beam due to prestress
p_{c2}	stress at centre of side of beam due to prestress
p_{c3}	stress at top of beam due to prestress
T	torsional moment applied to member
T_1 , T_2 , T_3	theoretical torsional moments, Modes 1, 2, 3
T_{c1}	torsional moment at first crack, Mode 1
T_u	ultimate torsional moment of member, in pure torsion
T_{u1} , T_{u2} , T_{u3}	theoretical ultimate torsional moments, Modes 1, 2, 3
V	shear force applied to member
V_1 , V_2	theoretical shear forces, Modes 1 and 2
V_u	ultimate shear force applied to member
V_{u1} , V_{u2}	theoretical ultimate shear forces, Modes 1 and 2
v_c	maximum shear stress in concrete on plane normal to axis of beam
v_{ct}	maximum shear stress in concrete on plane normal to axis of beam, due to torsional moment
v_{cv}	maximum shear stress in concrete on plane normal to axis of beam, due to shear force

NOTATION (continued)

x	depth to neutral axis
z	lever arm in bending
z_t	lever arm in torsion
β	angle of inclination of concrete failure envelope
ϵ_{c1}	direct strain in concrete adjacent to lower layer of steel due to applied moment, on plane normal to axis of beam
ϵ_{c1i}	Ditto, but normal to skew plane
ϵ_{cm}	maximum strain in concrete due to bending normal to axis of beam
ϵ_{cmi}	Ditto, but normal to skew plane
ϵ_{s1}	direct strain in lower layer of prestressing steel due to applied moment, normal to axis of beam
θ	angle of failure plane in compressive zone of concrete
θ'	modified angle of failure plane in compressive zone of concrete

TABLE OF CONTENTS

TABLE OF CONTENTS (continued)

TABLE OF CONTENTS (continued)

LIST OF FIGURES

LIST OF FIGURES (continued)

LIST OF FIGURES (continued)

LIST OF TABLES

1. INTRODUCTION

Torsion has, in the past, generally been ignored in the design of concrete structures. Of course, where structural forms such as spiral staircases and curved elevated roads occurred, torsion was a primary consideration, and ways had to be found for dealing with it. But for the vast majority of structures it was considered a secondary effect which was covered by the safety factor employed.

With the advent of ultimate strength design and the use of realistic load factors it becomes more important to understand the way in which the loads are distributed around the structure. To-day's plane frame analysis will become to-morrow's space frame, in which torsional moment will play an important part in resisting the loads.

1.1 Design for Torsion

When the various code requirements for torsion design were reviewed by Fisher and Zia (1)* in 1964, neither the American nor the British codes gave a design method for torsion. Reinforced concrete Designers in this country generally used the Australian code until the publication of the British Standard CP 110 (2) in 1972.

However, CP 110 gives little guidance for the design of pre-stressed concrete in torsion, stating in clause 4.3.6 'the method adopted for reinforced concrete beams .... may generally be used'. The Australian code (3) does give a complete design procedure for prestressed concrete beams subjected to combined torsion, bending and shear. This is based on equations developed by Rangan and Hall (4, 5) which they expanded into a design method (6) and is only applicable to under-reinforced beams with both longitudinal and

* Number in brackets refers to list of references.

transverse bonded steel. The theory is based on yielding of the steel, an empirical expression being used to ensure that the concrete does not fail in the 'shear compression' mode.

1.2 Previous Research

Many reviews of previous research are available (7, 8, 9, 10, 11) and only a few authors will be mentioned here.

1.2.1 Plain Concrete

The analysis of homogeneous and elastic sections was carried out by St. Venant in 1853, whilst Nadai produced his plastic theory in 1931. The failure of a plain concrete section could then be predicted by equating either the elastic or the plastic principal tensile stresses to the ultimate tensile strength of the concrete. Neither method gave very good results.

In 1959 Lessig considered the failure of reinforced concrete sections to be on a skewed plane, and in 1968 Hsu (12, 13) showed that this type of failure actually occurred in plain concrete. From his tests, Hsu determined an empirical constant in the relationship between torque and the tensile strength of the concrete. He also found expressions relating the tensile strength of the concrete, f_t to the compressive cylinder strength f'_c , which are useful where no tensile strength has been measured.

In 1971, Martin (14) used a trapezoidal approximation to the distorted skew failure plane and found a theoretical basis for the empirical constant used by Hsu. This approach gave good agreement with experimental results, especially where the tensile strength of the concrete had been measured.

1.2.2 Reinforced Concrete

Following Lessig, many researchers have used the skewed plane approach in reinforced concrete. Normally both links and longitudinal steel are used, part or all of which yield at failure. To ensure that this is so, the section is always under-reinforced and the properties of the concrete have a negligible effect on the loads at failure. This case is, therefore, so different to that covered by the author that reinforced concrete results will not be considered further.

1.2.3 Prestressed Concrete

The detailed review of rectangular section prestressed concrete beams is left to Section 2.

Some research has been carried out on I - section (15, 16, 17, 18), on T - section (19) and on box section beams (20). These sections are, of course, commonly used in practice, and much more research remains to be carried out. However, the author feels that the simpler, rectangular section should be examined in detail first, before proceeding to the more complicated sections. Following the same line of argument, no bonded steel has been incorporated in the test zone of the author's beams, with the express intention of solving the simplest cases first.

1.3 Object and Scope of Study

The object of this research was to investigate the behaviour of rectangular post-tensioned prestressed concrete beams loaded in combined torsion, bending and shear. It was designed to complement the work of Wainwright (7) and of Evans and Khalil (21) who

tested similar beams, but without shear action.

The main attention was on the prediction of the ultimate conditions for the beams, but strains, deflections and rotations of the beams were measured for each load increment.

The scope of the study involved testing forty beams in two series with different types of post-tensioned steel, one with a large diameter alloy bar, the other with four high tensile steel wires. In both cases the prestress at the top of the beam was approximately zero.

Two values of shear span were used, and the only other variable was the ratio of applied moment to torque, which varied from zero to infinity.

2. PREVIOUS STUDIES OF TORSION ON PRESTRESSED CONCRETE - RECTANGULAR BEAMS

It was soon realised that by prestressing a concrete member the strength under torsional loads could be greatly improved, because the compressive prestress must first be overcome before the tensile torsional stresses become effective.

For pure torsional loads the most effective distribution of prestress will be uniform over the section, and many investigators have used this distribution; others have used eccentric prestress, the eccentricity varying up to the maximum value of h/6 for a rectangular beam. This latter, 'triangular' distribution of prestress will be the most appropriate for beams resisting high bending moments, and has been used by the author for all his tests.

The prestress may be applied by means of pre- or post-tensioned tendons. The latter have the advantage,to the research worker,that the force may be measured directly. By using post-tensioning the author was able to compare his results with Wainwright (7) and Evans (21).

In post-tensioned beams, the type of duct and the degree of bond, if any, may also be varied. It is important to know the duct size to determine whether dowel action is likely to take place. Not all research workers give sufficient information in their reports.

The size and type of tendon are also important variables, as is its position in the section when ultimate loads are considered.

Many previous tests have been on beams with bonded steel in the test zone, either longitudinal or web, or both. The beams tested by the author, however, did not incorporate such steel.

2.1 Pure Torsion

Extensive tests have been carried out by Zia (16) and Humphreys (22), whilst many other investigators have tested a few beams as part of a series under combined loads.

In all cases, where no bonded reinforcement has been included, failure has been sudden and has taken place at the cracking load.

As Hsu (12) has pointed out for uniformly prestressed beams, or for slender beams with triangular prestress, the first crack forms at the centre of the long side (Mode 2); for beams of nearly square cross section with little prestress on the upper face, the critical crack may form at the centre of this face (Mode 3).

Hsu also observes that neither the elastic nor the plastic stress criterion agree with the experimental results and proposes a formula based on skew bending theory and empirical constants. Martin and Wainwright (23) have derived a similar formula from first principles using skew bending on a spiral failure plane, with derived constants. This gives good agreement with the available results.

2.2 Torsion and bending

Many investigators have worked on this combined loading case, using rectangular or triangular prestress distributions.

Cowan and Armstrong (24) tested five 152 x 203 mm beams, one concentrically and four eccentrically prestressed, with 16 mm diameter unbonded McAlloy bars, and web steel. The $^{M}/_{T}$ ratios varied between 2 and 8. The tests were, however, carried out over rather a short length which may have forced failure to occur at a rather steeper angle than normal and led to erroneous results.

Reynolds (25) tested a total of twelve beams with $^{M}/_{T}$ ratios varying between 1.2 and 6.7. All beams were of 64 x 91 mm cross section, with post-tensioned grouted cables giving a triangular distribution of prestress. With his loading arrangement, however, he was not able to apply pure torsion.

Okada (26) carried out twelve tests on post-tensioned uniformly prestressed beams of 100 x 200 mm cross section, half of the beams being reinforced with both web and longitudinal bonded steel. The $^{M}/_{T}$ ratios varied between 0.4 and 2.4.

Murashkin (27) tested ten beams of 170 x 210 mm cross section, with a constant $^{M}/_{T}$ ratio of 2.5. The four prestressing tendons gave concentric or eccentric loading. Half the beams had web steel.

Warwaruk and Mukherjee (28, 29) tested twenty beams of 152 x 305 mm cross section pretensioned with either 8 or 12 mm diameter strands giving a uniform or a triangular distribution of prestress. The $^{M}/_{T}$ ratios varied between 0.3 and 3.0. All beams had longitudinal and web bonded steel.

Ganga Rao (30, 31) tested thirty three beams of 152 x 305 mm cross section, pretensioned with four or five 9.5 mm diameter strands giving a uniform or slightly eccentric prestress. The $^{M}/_{T}$ ratios varied between 0.6 and 8.4. All beams had web steel, some had longitudinal bonded steel also.

Wainwright (7) tested seventeen beams of 100 x 174 mm cross section, post-tensioned with one unbonded McAlloy bar of 22 mm diameter giving a triangular distribution of prestress. The $^{M}/_{T}$ ratios varied between 0.3 and 17.8. These beams were thus the same as the Author's 'Series One' beams.

Evans (21) tested thirty one beams of 127 x 203 mm cross section, post-tensioned with four 7 mm diameter unbonded wires. The $^{M}/_{T}$ ratios varied between 0.8 and 12.7. Of the specimens with no bonded reinforcement, twelve had triangular and seven had uniform prestress.

The former were thus very similar to the Author's 'Series Two' beams.

Farley (32) tested ten beams of 30 x 80 mm cross section, with M/T ratios varying between .13 and 3.0. These specimens were of micro-concrete, with an external system of prestressing applying a triangular stress distribution.

For beams with no mild steel reinforcement, Martin and Wainwright (23) have derived formulae for the three observed modes of failure.

Mode 1 occurs when the M/T ratio is high and cracking occurs before failure. The compressive face is at the top of the beam, but the failure plane is inclined. A dowel force is usually present between the concrete and the prestressing steel.

In Mode 2 the bending moment does not appear in the equation, which is the same as that for pure torsion.

In Mode 3 the pure torsion equation is modified due to the presence of the bending moment.

In their paper, the theory is compared with one hundred and twenty five test results, but over half of these are for pure torsion. The correlation is, however, good.

2.3 Torsion, Bending and Shear

Of the four investigators who have previously examined this problem, three have included both web and longitudinal bonded steel in all their beams.

Bishara (33) tested eight beams of 102 x 305 mm cross section, pretensioned with three strands of 11 mm diameter giving a uniform or eccentric prestress. The M/T ratios varied between 0.7 and 2.8 and V/V_{u2} ratios between .03 and .17. All beams had both longitudinal and web bonded steel. The test length was extremely short which may have induced failures at higher values than expected.

Henry (8, 34) tested a total of thirty two beams of 152 x 305 mm cross section, pretensioned with four or five strands of 9.5 mm diameter, giving a uniform or eccentric prestress. The $^{M}/_{T}$ ratios varied between .4 and 13.4 and $^{V}/_{V_{u2}}$ ratios between .08 and .56. All beams had both longitudinal and web bonded steel.

Warwaruk and Mukherjee (28, 29) tested twenty beams of 152 x 305 mm cross section, pretensioned with either 8 or 12 mm diameter strands giving a uniform or a triangular distribution of prestress. The $^{M}/_{T}$ ratios varied between 0.2 and 11.5 and $^{V}/_{V_{u2}}$ ratios between .03 and .26. All beams had longitudinal and web bonded steel.

McMullen (35) tested a total of twenty one beams of 152 x 305 mm cross section, pretensioned with six 13 mm diameter strands giving an eccentric prestress. The $^{M}/_{T}$ ratios varied between 1.7 and 84 and $^{V}/_{V_{u2}}$ ratios between 0 and .26. Fifteen beams had stirrups; the remaining six beams had no bonded steel.

These last beams tested by McMullen are the only directly comparable tests to those undertaken by the Author.

Bishara (33), McMullen (35), Warwaruk and Mukherjee (28, 29) have each produced empirical formulae for moment/torque and torque/shear interaction diagrams, based on their own test results.

Using the skew bending method, Henry and Zia (8, 34) have derived theoretical formulae for both bending and torsional mode failures, where beams incorporate both longitudinal and transverse bonded steel.

In a similar manner, Rangan and Hall (4, 5) have analysed three modes of failure theoretically, but have used an empirical expression for their 'shear compression' mode.

Lampert (36) has modified the space truss theory to suit pre-stressed concrete, with an additional check for crushing of the concrete.

The three theories above are only applicable to beams having both longitudinal and transverse bonded steel, being based on yielding of all or part of that steel.

Woodhead and McMullen (37) have used the skew bending method for bending and torsional modes of failure, utilising both the steel and concrete properties. The concrete strain at failure is, however, assumed to follow an empirical relationship. Their method is claimed to be suitable for under - and over-reinforced sections, with or without longitudinal and transverse bonded steel.

A synopsis of the test results available for torsion and bending is given in table 2.1, and for torsion, bending and shear in table 2.2.

The paucity of results indicated by this latter table led the author to undertake this study.

TABLE 2.1 PREVIOUS TESTS ON PRESTRESSED CONCRETE RECTANGULAR BEAMS UNDER TORSION AND BENDING

Author	Ref.	Width mm	Depth mm	Type of pre-stress	Bonded ?	Number of beam tests					
						Bonded Steel		Torque only	Moment only	Torque & moment	Total
						web	longi-tudinal				
Cowan	24	152	203	Post	No	9	0	2	2	5	9
Evans	21	127	203	Post	No	12	0	2	2	31	35
Farley	32	30	80	External	No	0	0	2	1	10	13
Ganga Rao	31	152	305	Pre	Yes	40	14	7	0	33	40
~~Henry~~	~~8~~	~~152~~	~~305~~	~~Pre~~	~~Yes~~	~~32~~	~~32~~	~~0~~	~~0~~	~~32~~	~~32~~
Kurashkin	27	170	210	?	?	5	0	0	0	10	10
Okada	26	100	200	?	?	0	10	4	4	12	20
Reynolds	25	64	91	Post	Yes	0	0	0	0	12	12
Wainwright	7	100	174	Post	No	0	0	2	3	17	22
Warwaruk	28	152	305	Pre	Yes	28	28	4	4	20	28
						TOTAL		23	16	~~182~~ 150	~~221~~ 189

Author	Ref.	Width mm.	Depth mm.	Type of pre-stress	Bonded ?	Number of beam tests					
						Bonded Steel		Torque only	Moment & shear	Moment, torque & shear	Total
						web	longi-tudinal				
Bishara	33	102	305	Pre	Yes	8	8	0	0	8	8
Henry	8	152	305	Pre	Yes	32	32	0	0	32	32
McMullen	35.	152	305	Pre	Yes	18	0	3	2	21	26
Warwaruk	28	152	305	Pre	Yes	26	26	2	4	20	26
						TOTAL		5	6	81	92

TABLE 2.2 PREVIOUS TESTS ON PRESTRESSED CONCRETE RECTANGULAR BEAMS UNDER TORSION, BENDING AND SHEAR

3. EXPERIMENTAL INVESTIGATION

3.1. Numbering System

The beams were numbered in the order of testing from 0 - 41. However, beams 8 and 24 were incorrectly tested and only the concrete control tests for these beams have been used.

The number appears on both sides of the beam and identifies the photographs, the letters F F and B F being added to refer to the front and back faces respectively. In the front face the torsional and flexural shearing stresses are additive.

3.2. Materials

3.2.1 Concrete

The fine and coarse aggregates were obtained from Packington and Perry Barr respectively and had the sieve analyses shown in table 3.1. The coarse aggregate came in several batches, one of which was such that the mix design had to be modified. Ordinary Portland Cement was used, the nominal mix being 1 : 1.5 : 3.0 by weight with a water/cement ratio of 0.5. The nominal cube strength of the mix of 42 N/mm^2 at 28 days was normally well exceeded - see table 3.2.

The concrete was made in a Liner 'Cumflow' No. 1 A mixer, sufficient to cast one beam and its associated control specimens. Two batches were required for Series 1 beams; one sufficed for Series 2 as the number of control tests were reduced in this case. All concrete was placed with the help of a poker vibrator.

The control tests were :-

(a) Three 150 mm cubes for compression test - f_{cu}

(b) Three 150 x 300 mm cylinders for compression test - f'_c

(c) Three 150 x 300 mm cylinders for the indirect tensile (or 'split cylinder') test - f_s

(d) Two 150 x 300 mm cylinders for Young's Modulus determination - E_c

(e) Three 100 x 174 x 1000 mm beams for a transverse bending test, giving a modulus of rupture - f_r' for Series 1 beams only.

(f) Two 100 x 100 x 600 mm beams for the standard modulus of rupture test - f_r (beams 9 to 41 only)

The tests were carried out in accordance with the British Standards except :-

(1) In test (d) the strains were measured with electrical resistance type strain gauges from the same batch as those used on the beam itself. Thus the gauge lengths used were only 50 mm, smaller than that specified in the British Standard.

(2) In test (e) no B.S. is available. The loading system was similar to the B.S. being at the third points on a span of 800 mm., the rate of loading giving an increase in stress at the extreme fibres of 1.6 N/mm^2/ min.

The results of the tests are given in table 3.2. All tests were conducted on the same day as the main beam was loaded to failure, i.e., 28 days after casting.

Beam and control specimens were cured in a thermostatically controlled enclosure and automatically sprayed with water once a day. They were removed on the 27th day and left in the laboratory for the surface to dry sufficiently for the attachment of the strain gauges.

The relationships between the various concrete properties have been examined, see figures 3.8 to 3.13 and the following points are noted.

(a) Modulus of Rupture

Two types of specimen were tested, one 100 mm and one 174 mm deep. Fig. 3.8 indicates that either may be used; analysis of the mean values and the coefficients of variation in each case (table 3.2) supports this. It appears to be perfectly satisfactory to use the British Standard Test for determining the modulus of rupture for beams of this size and this grade of concrete.

This finding does not agree with Hsu (13) who gives an empirical relationship between f_r, f'_c and depth of beam h.

Fig. 3.9 compares this relationship with f_r.

The variation of modulus of rupture agrees reasonably well with the small spread of cylinder strength, but no variation with size of specimen is apparent.

An equation agreeing more closely with the Author's results would be

$$f_r = 1.10 \sqrt[3]{f'_c}$$

(b) Split cylinder strength f_s.

As shown in table 3.2. the coefficient of variation of f_s was larger than that for f_r. Fig. 3.10 compares the two. For the type and strength of concrete used we may take

$$f_s = 0.83 \ f_r \qquad \ldots \ (3 - 1)$$

The variation of f_s with cylinder strength is shown in Fig. 3.11

The corresponding equation valid for the Author's results would be

$$f_s = 0.91 \sqrt[3]{f'_c}$$

(c) Cylinder strength

Agreement between the cylinder and the cube strengths (Fig. 3.12) was generally good, although the coefficient of variation for the cylinders was higher. For the type of concrete used we can write

$$f'_c = 0.80 \ f_{cu} \qquad \ldots \ (3 - 2)$$

which is the accepted value.

(d) Young's Modulus

A typical curve obtained for the determination of Young's Modulus E_c is shown in Fig. 3.5.

The variation of Young's Modulus with cylinder strength is shown in Fig. 3.13. The empirical relationship $E_c = 5000 \sqrt{f'_c}$ where the units are N/mm^2, is also plotted.

3.2.2 Steel

Series 1 :-

The tendon used was a 'McAlloy' high tensile alloy steel bar of 22 mm diameter with threaded ends. The ultimate load of the one bar tested was 400 kN. The actual loads used were not more than 167 kN.

Two specimens were tested to determine Young's Modulus; the results are shown in Fig. 3.6

Series 2 :-

The four tendons used were high tensile steel wire of 7 mm diameter with an ultimate load of 61 kN. The actual loads used were not more than 39 kN.

Two specimens were tested to determine Young's Modulus; the results are shown in Fig. 3.7

3.3 Details of Beams

General arrangements of the beams used are shown in Fig. 3.1 ; beams were cast in plastic faced wooden moulds, the overall dimensions being 100 x 174 x 3000 mm.

Series 1

Twenty seven days after casting the beams were post-tensioned using a standard 'McAlloy' jack to a force of about 140 kN sufficient to give an average of 2000 $\mu\epsilon$ in the four strain gauges.

On the twenty seventh day the concrete strain gauges were affixed. The number and position of these depended on the proposed loading and the expected mode of failure. The positions are shown in figures 8.1 to 8.22, together with the crack patterns after test. The strain gauges were either Tinsley type 7 A, of 50 mm gauge length, fixed with 'Tridox' F 88 adhesive or Tokyosokkikenkyujo type TML, of 60 mm gauge length, fixed with the maker's adhesive.

Series 2

Twenty seven days after casting the beams were gauged as shown in Fig. 8.23 to 8.40. The strain gauges were either Tinsley type 7 A,

50 mm gauge length, or Tokyosokkikenkyujo type TML, of 60 mm gauge length, both fixed with the same adhesives as in the Series One beams.

The beam was then post tensioned with the two central wires to a low value for handling purposes. After assembly in the test rig the final prestress was applied on the twenty eighth day immediately before the test, the values of load actually applied being measured by load cells placed under each wire.

Before being placed in the test rig all beams were given a thin coat of white emulsion paint so that the cracks could be distinguished clearly.

3.4. Testing of Beams

A general view of the test rig is shown in figure 3.3 . It has been described previously by Wainwright (7) in an arrangement for giving a constant bending moment along the central portion. Here a point load is applied so that the bending moment varies throughout the length and consequently shearing forces appear in the test length. This point load was applied either 600 or 800 mm from the left hand support of the 2.5 m simply supported span.

The first ten beams were tested by applying the full vertical load, and then increasing the torsional moment to failure. However, it was felt that an approximately constant $^{M}/_{T}$ ratio might lead to different crack patterns and hence, possibly, a different type of failure. Thus beams 10 to 41 were tested in the following manner :-

(a) Increase vertical load to 20 kN

(b) Decrease vertical load to zero

(c) Read strain gauges and deflections

(d) Increase vertical load by first increment

(e) Increase torsional load by first increment

(f) Read strains and deflection gauges

(g) Examine for cracks and mark extent of cracking with the load increment number

(h) Increase vertical load by second increment, etc.

At each stage of the loading care was taken to keep the beam horizontal under the vertical load by adjusting the restraining torsion arm.

In Series 1 beams the strain gauges were read using a Peekel indicator type B 105, the deflections using ordinary dial gauges reading in mm and each set of readings took approximately two minutes.

In Series 2 beams all readings were recorded by a Data Logger. A programme was already in existence for reading strain gauges and printing the results. This was modified to read in addition :-

(a) the voltage output of a Hayes Type 403 Load Cell, supplied with a constant voltage supply. This output was multiplied by a constant and printed out directly as a load in kN. The loads measured were (1) vertical load (2) torsion load (3) all four loads in the prestress wires.

(b) the voltage output of an Ether Type P D 20 linear transducer for measuring deflections and rotations. Again constants were written into the programme so that the printed output was the required deflection in mm.

With the use of the data logger each set of readings could be completed in about ten seconds.

The number of load increments varied, but averaged fifteen. When near failure some time, up to five minutes, might have to be allowed for the deflections and strains to settle down before the readings could be taken. Tests usually occupied about one and a half to two hours.

Due to the method of loading, at failure the vertical loading system attempted to keep a constant force on the beam; the torsional loading jack kept a constant rotation, the force, therefore, falling off with time. When the torsional moment fell off so quickly that the

hand pump could not keep the moment constant, the beam was assumed to have failed and both jacks were retracted simultaneously.

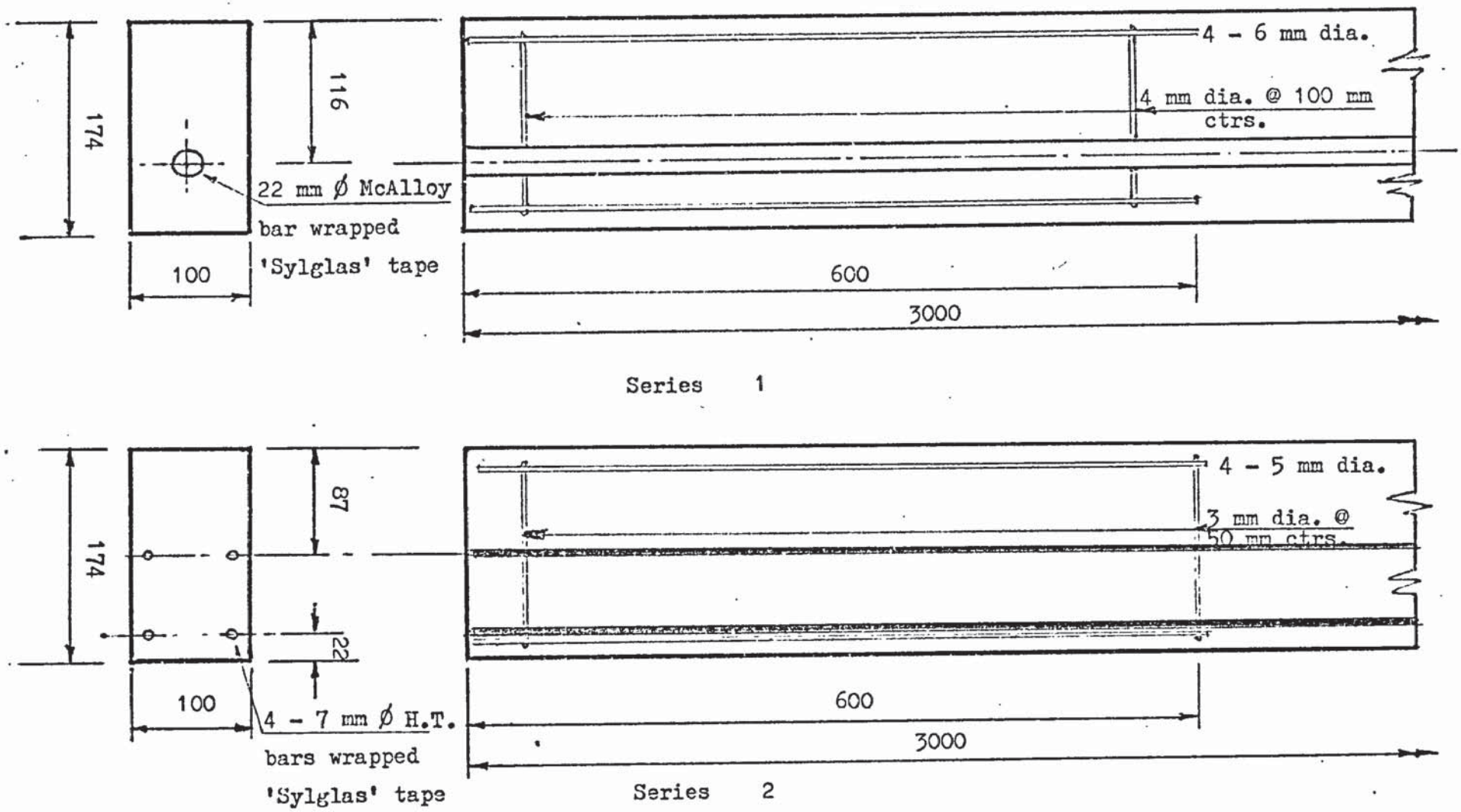

FIGURE 3.1 DETAILS OF TEST BEAMS

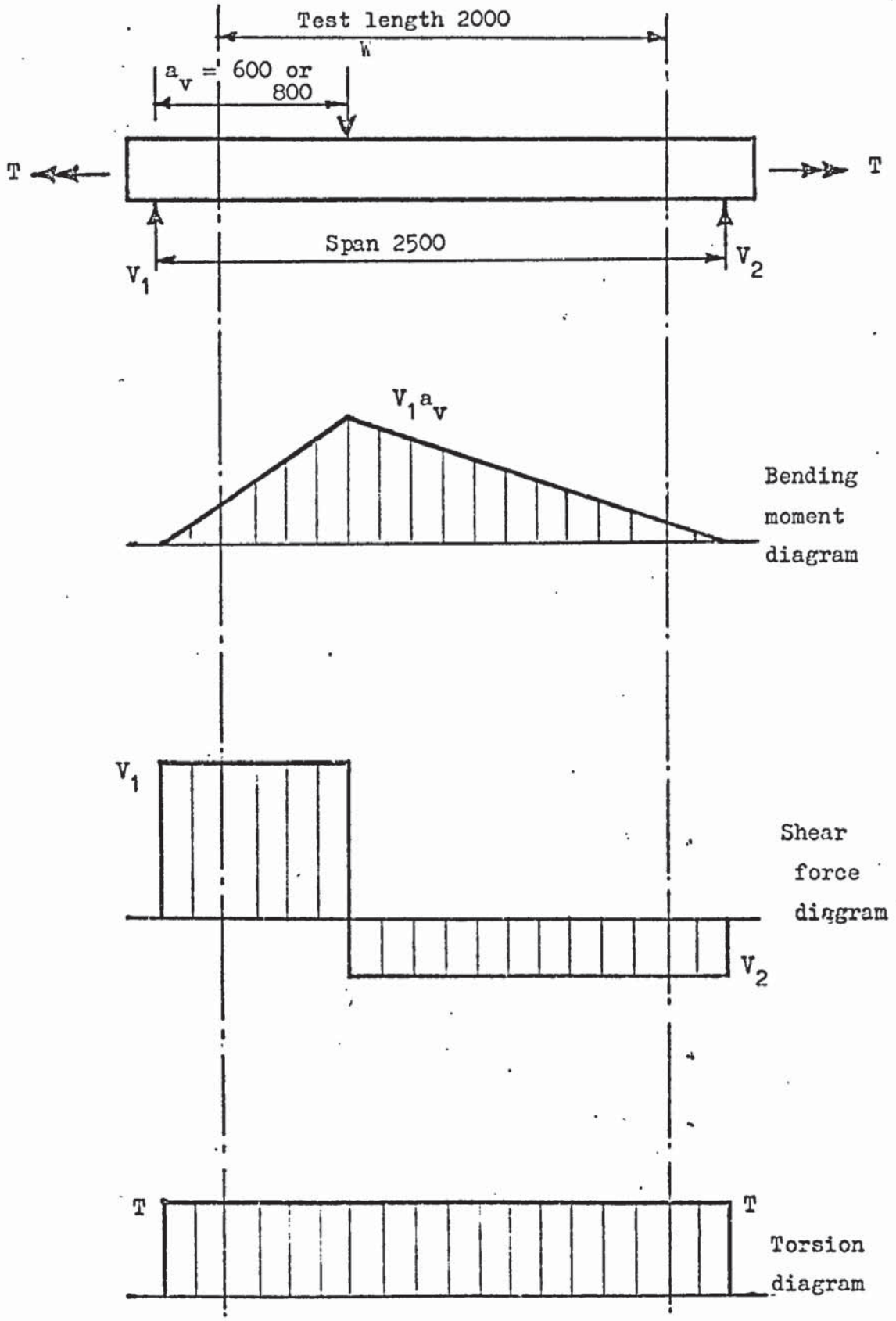

N.B. Self weight also taken into account

FIGURE 3.2 DIAGRAM OF TEST ARRANGEMENT

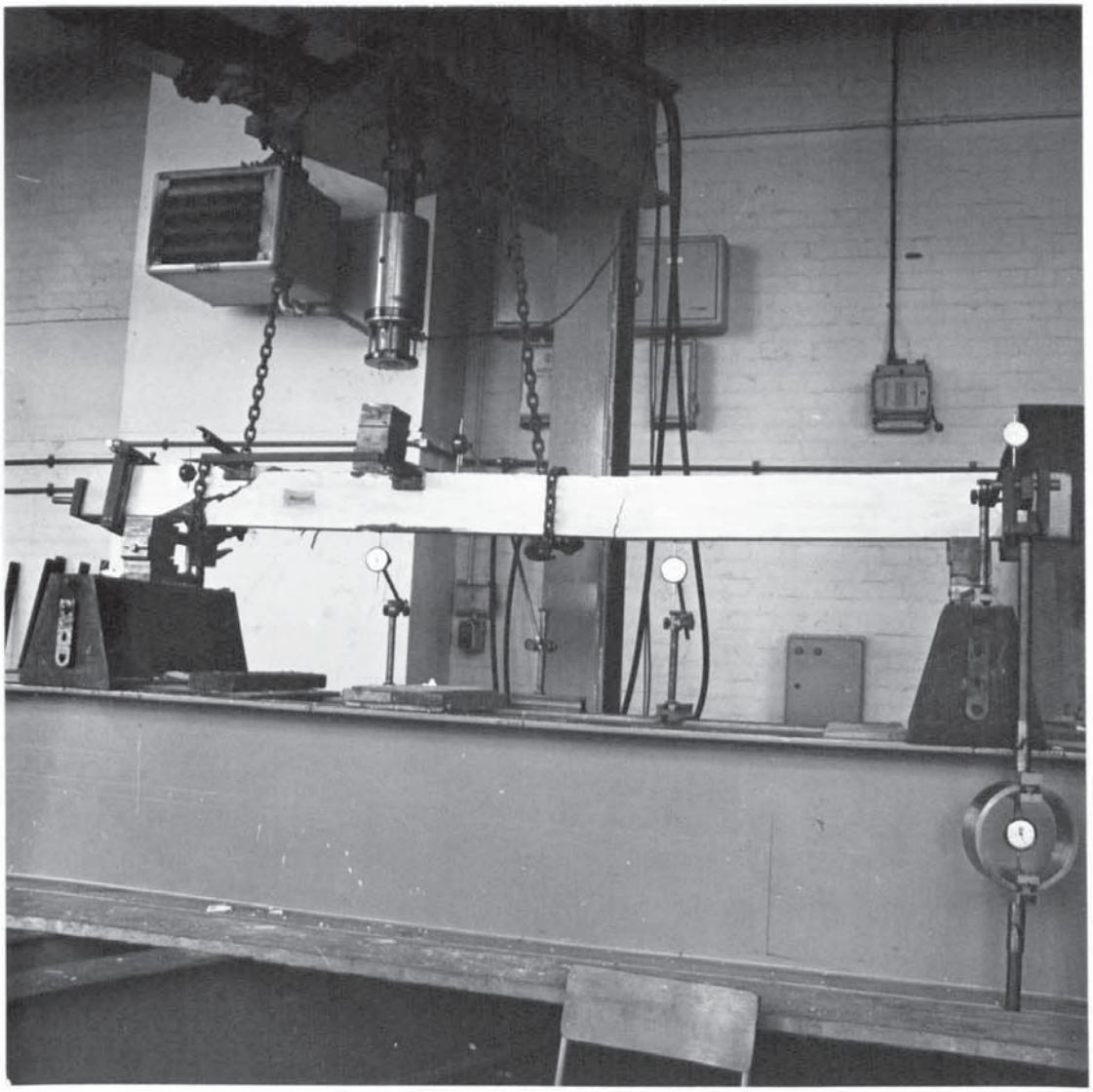

FIGURE 3.3 VIEW OF TEST RIG - SERIES 1
BEAM 7 AFTER FAILURE

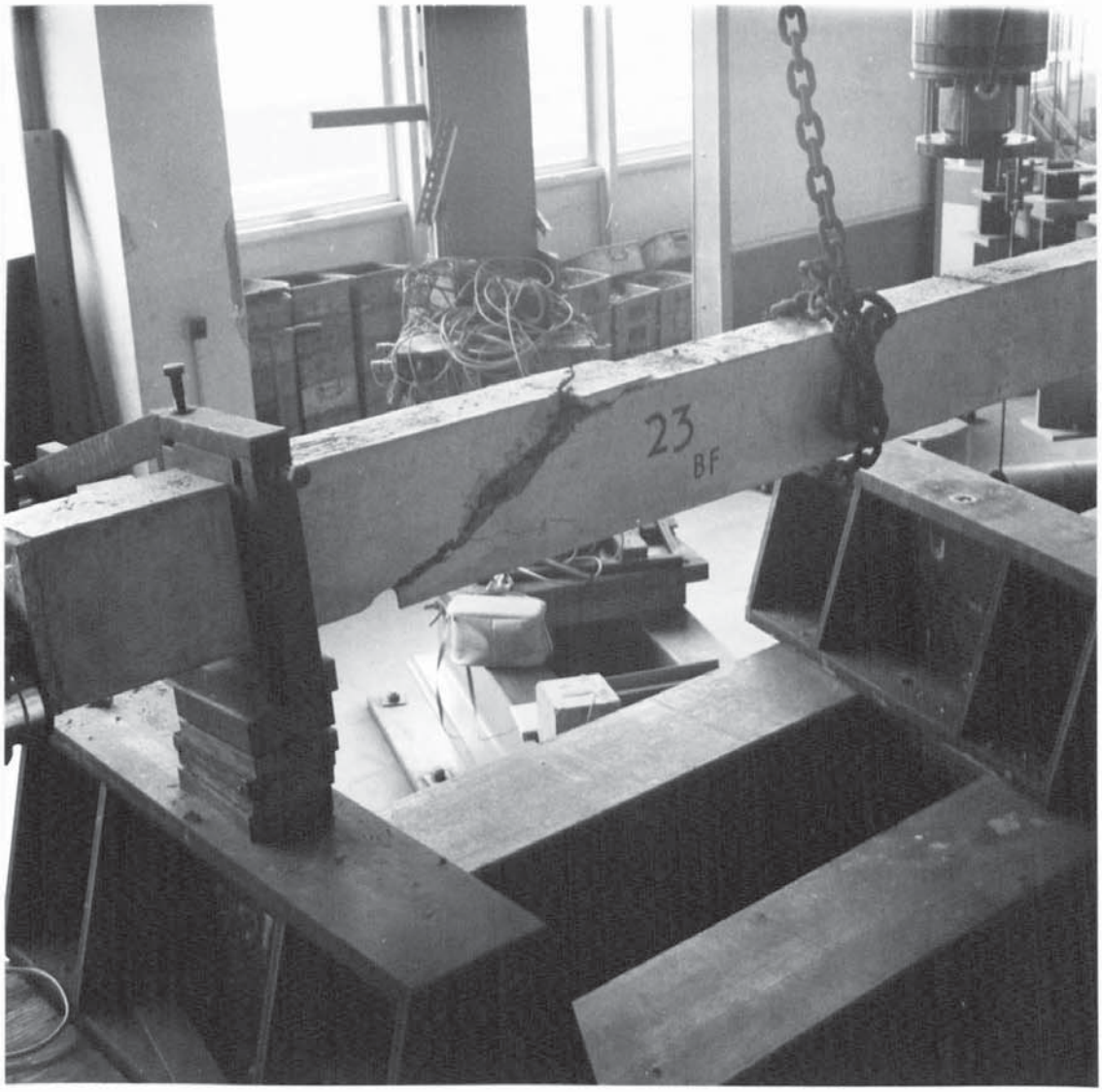

FIGURE 3.4 VIEW OF TEST RIG - SERIES 2
BEAM 23 AFTER FAILURE

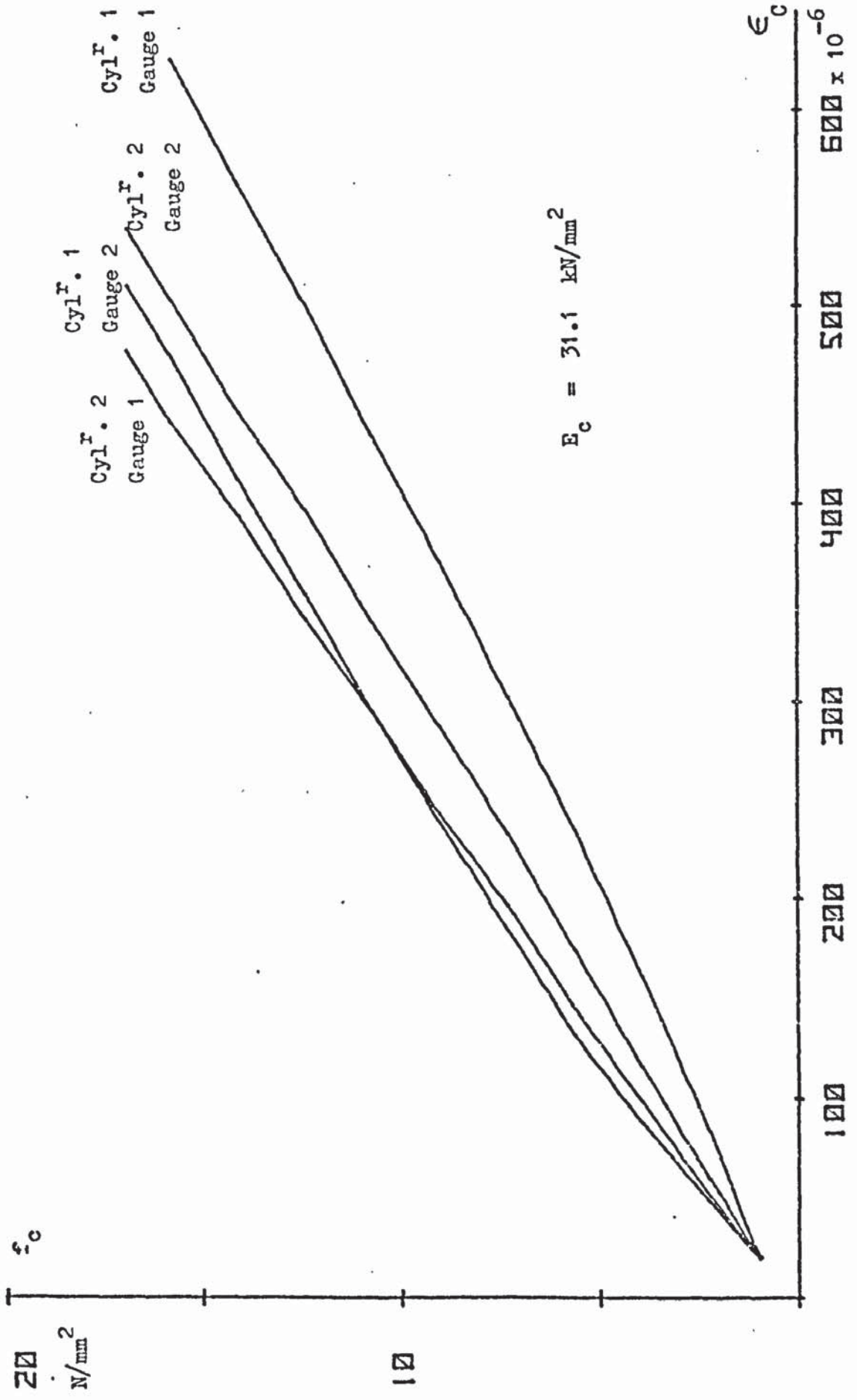

FIGURE 3.5 STRESS / STRAIN CURVE FOR CONCRETE - BEAM 14

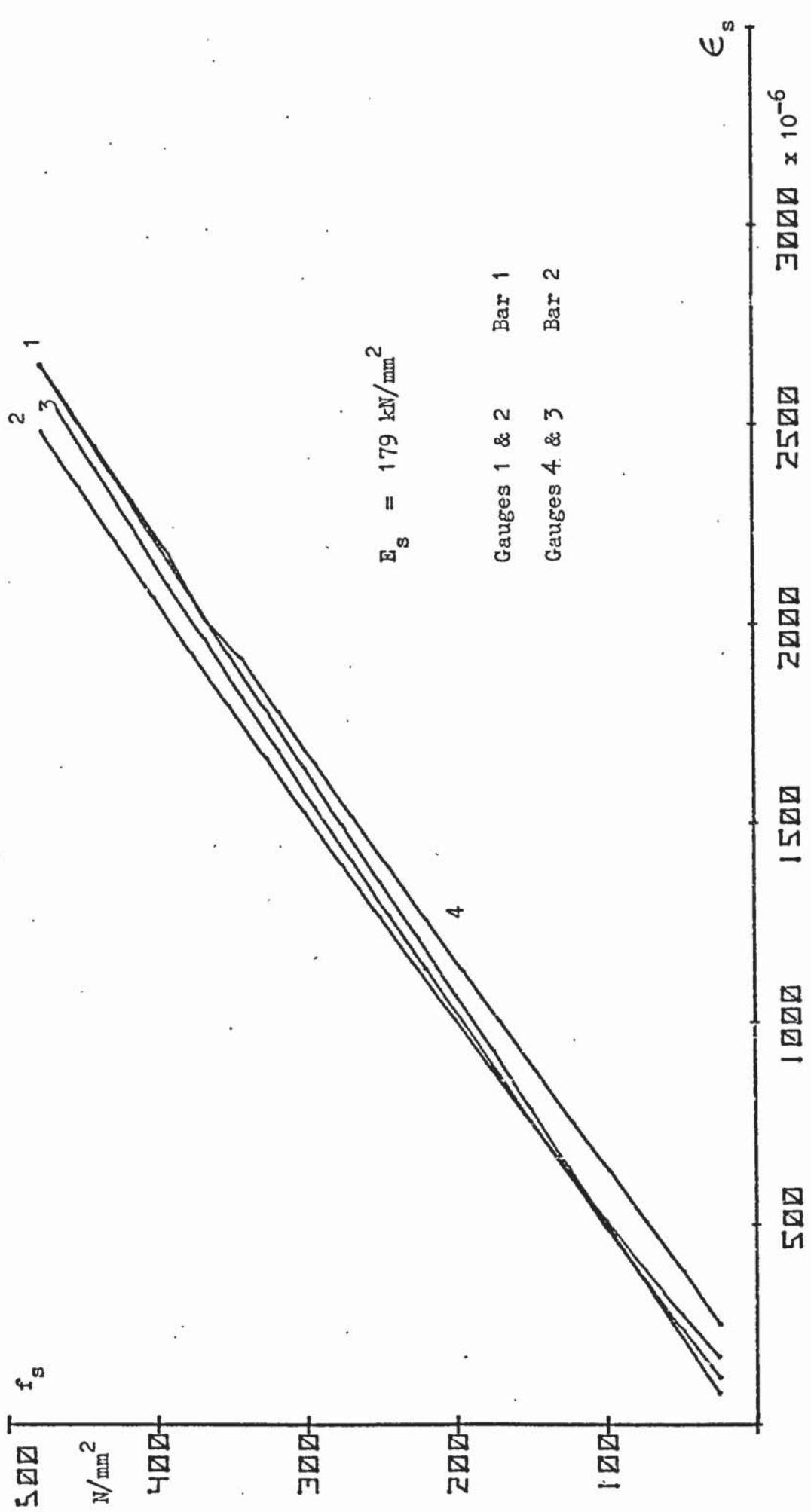

FIGURE 3.6 STRESS / STRAIN CURVE FOR PRESTRESSING STEEL - SERIES 1

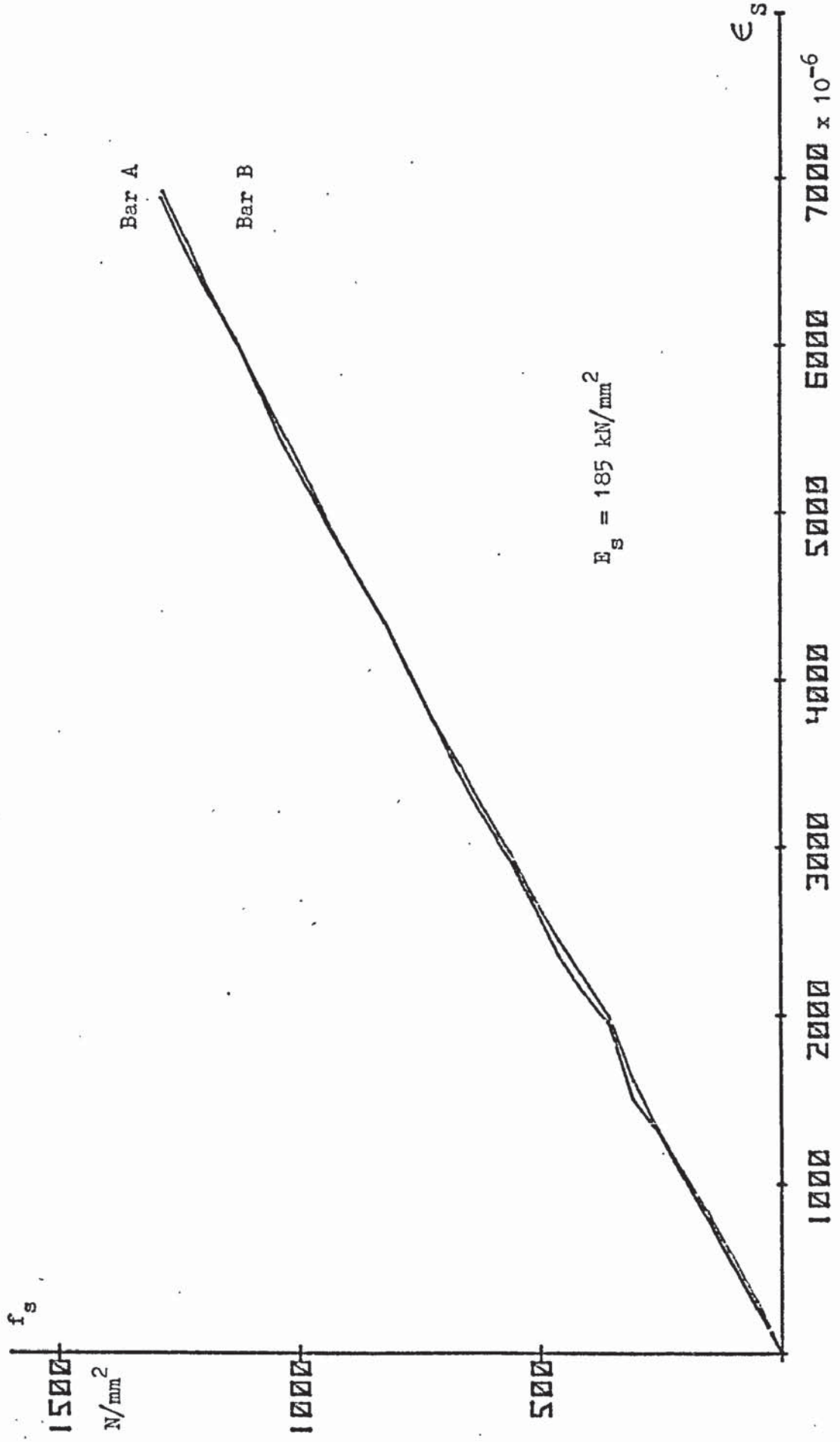

FIGURE 3.7 STRESS / STRAIN CURVE FOR PRESTRESSING STEEL - SERIES 2

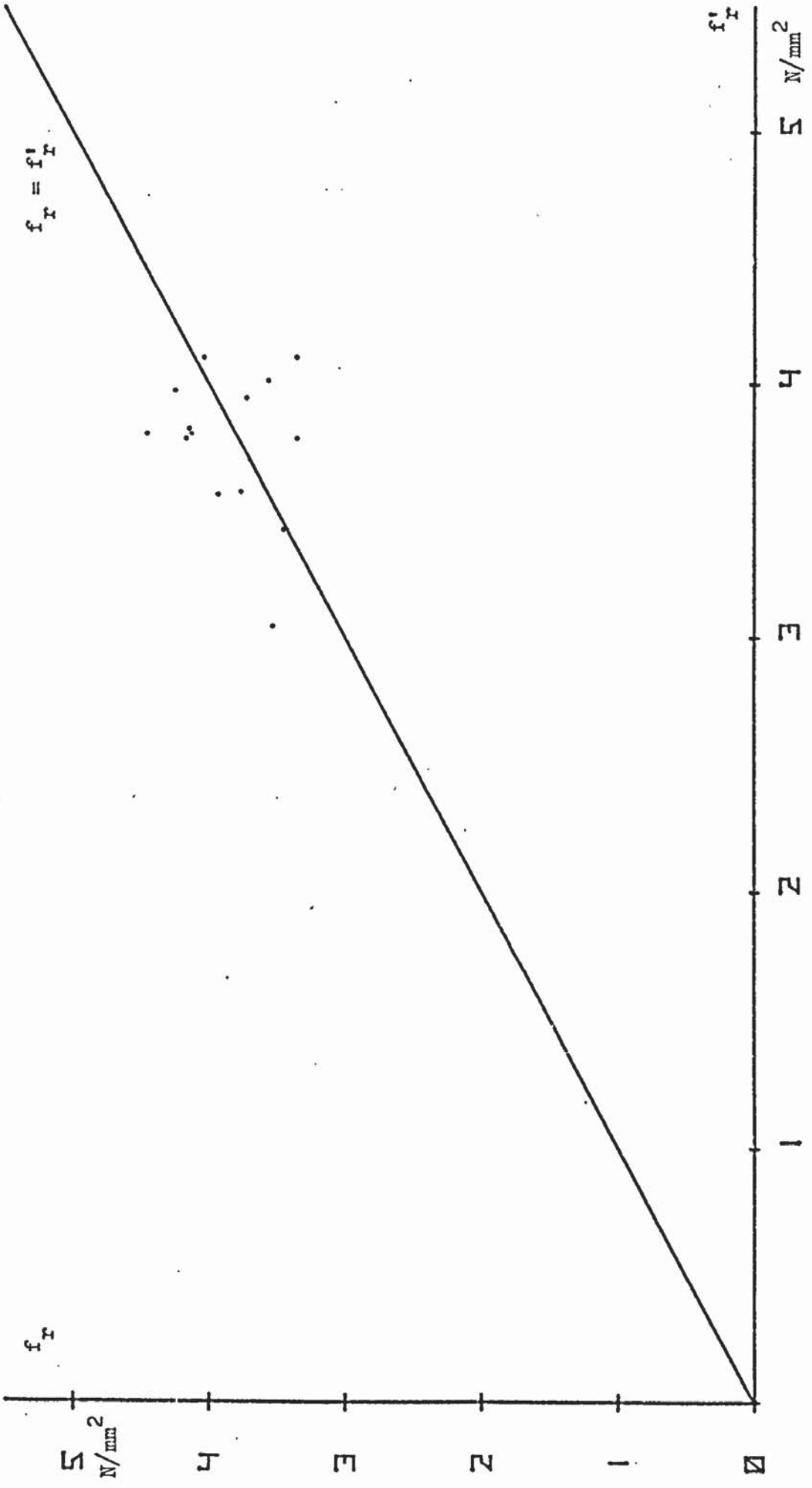

FIGURE 3.8 RELATIONSHIP BETWEEN MODULI OF RUPTURE FOR DIFFERENT SIZED TEST SPECIMENS

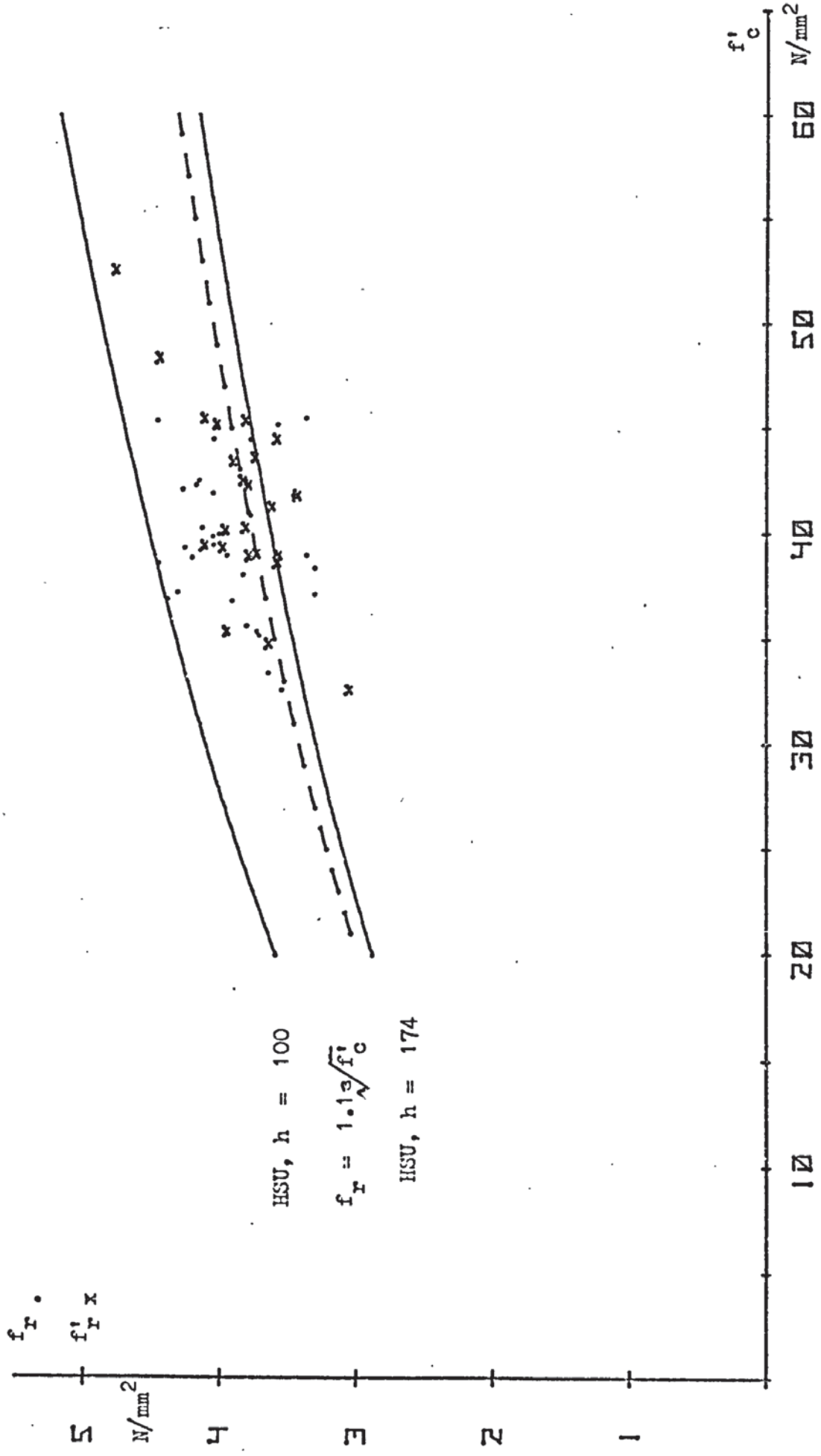

FIGURE 3.9 EMPIRICAL RELATIONSHIP BETWEEN MODULUS OF RUPTURE AND CYLINDER STRENGTH

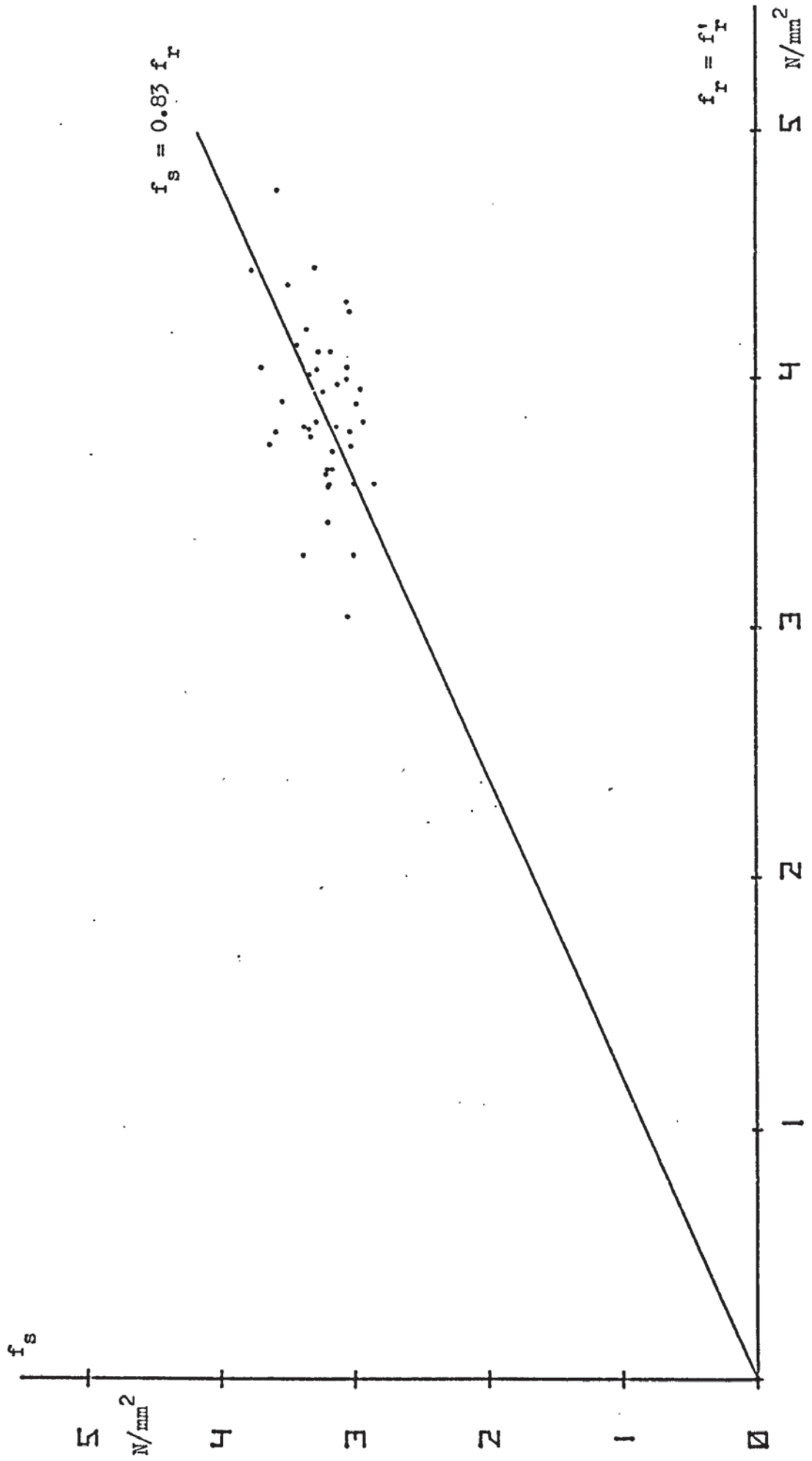

FIGURE 3.10 RELATIONSHIP BETWEEN MODULUS OF RUPTURE AND CYLINDER SPLITTING STRENGTH

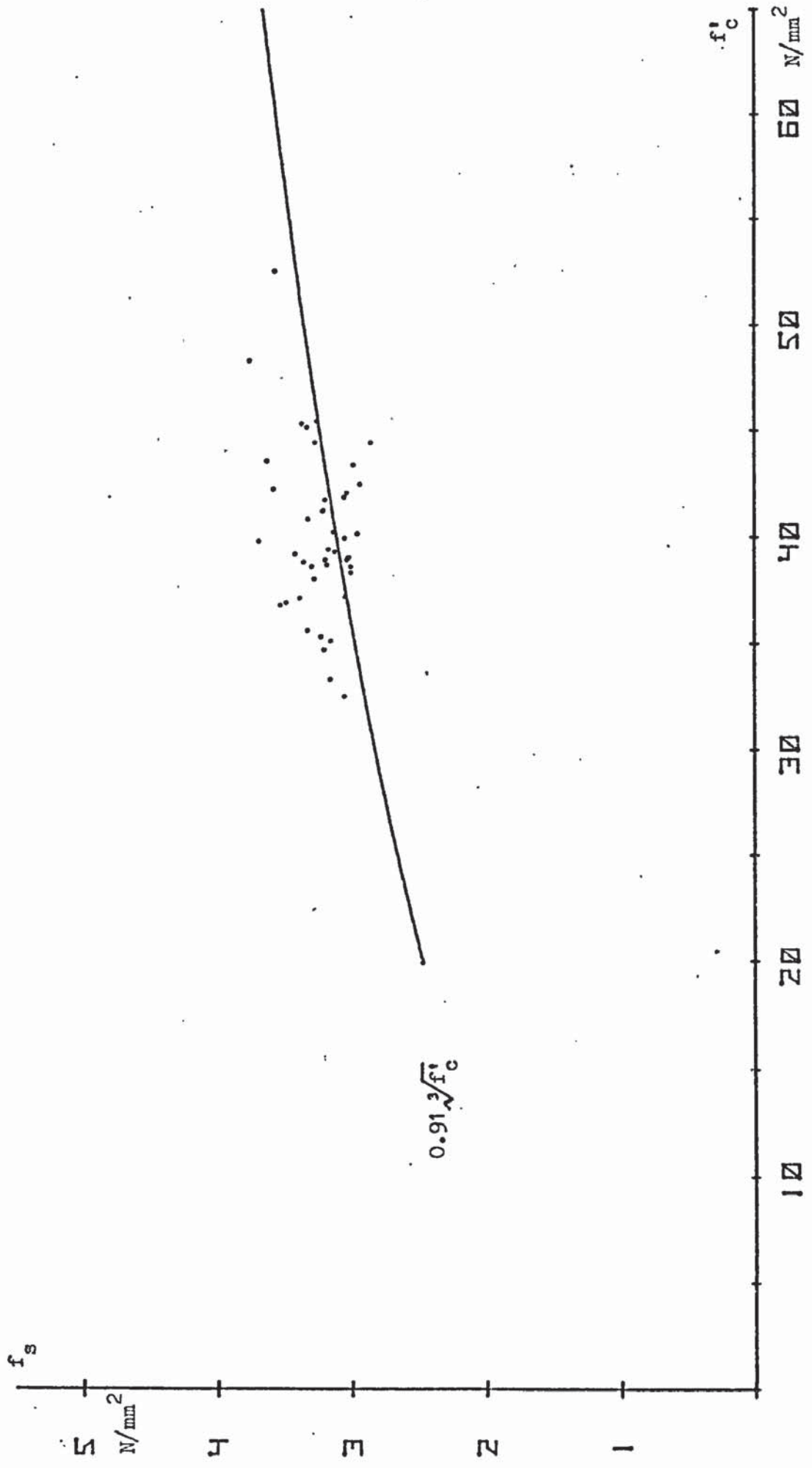

FIGURE 3.11 RELATIONSHIP BETWEEN CYLINDER SPLITTING STRENGTH AND CYLINDER STRENGTH

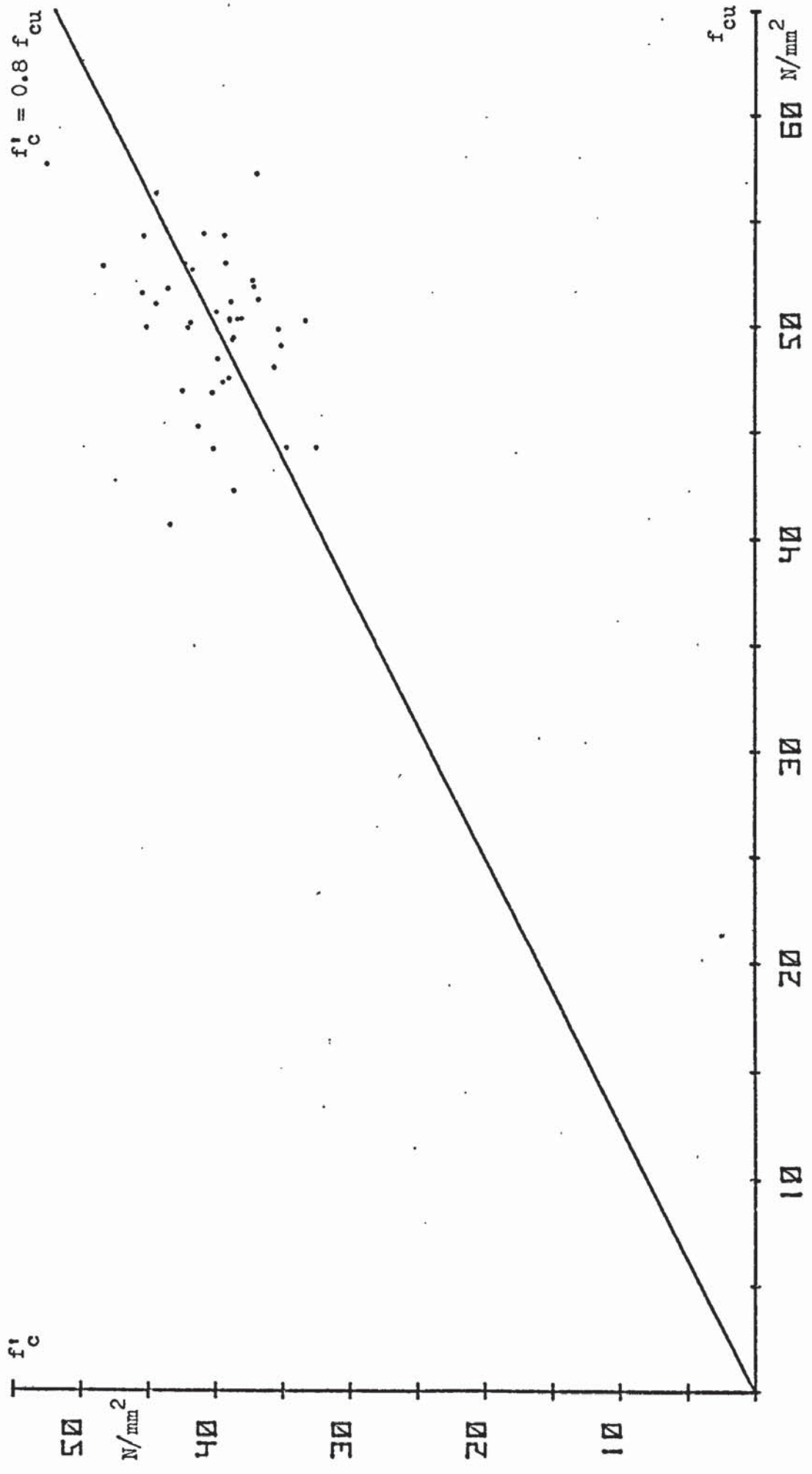

FIGURE 3.12 RELATIONSHIP BETWEEN CUBE STRENGTH AND CYLINDER STRENGTH.

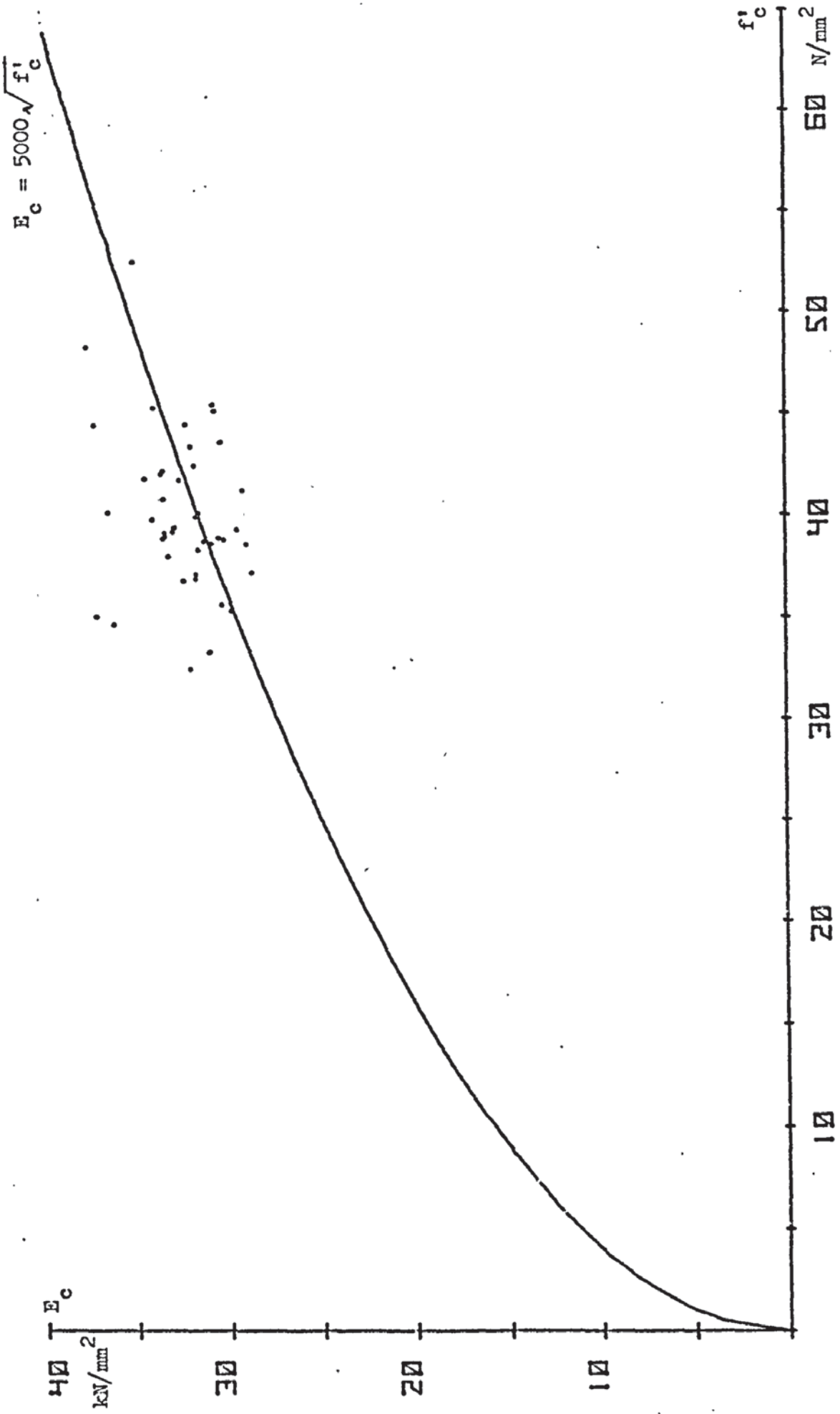

FIGURE 3.13 RELATIONSHIP BETWEEN YOUNG'S MODULUS AND CYLINDER STRENGTH

COARSE AGGREGATE	BATCH		
	1	2	3
% retained 9.5 mm	2.2	5.3	2.7
% retained 4.8 mm	81.9	92.2	82.3
% passed 4.8 mm	15.9	2.5	15.0

FINE AGGREGATE	BATCH	
	1	2
% retained 4.8 mm	7.4	6.9
% retained 2.4 mm	18.2	11.0
% retained 1.2 mm	11.2	5.1
% retained 0.60 mm	11.0	14.6
% retained 0.30 mm	33.7	40.0
% retained 0.15 mm	14.7	19.4
% passed 0.15 mm	3.9	2.8

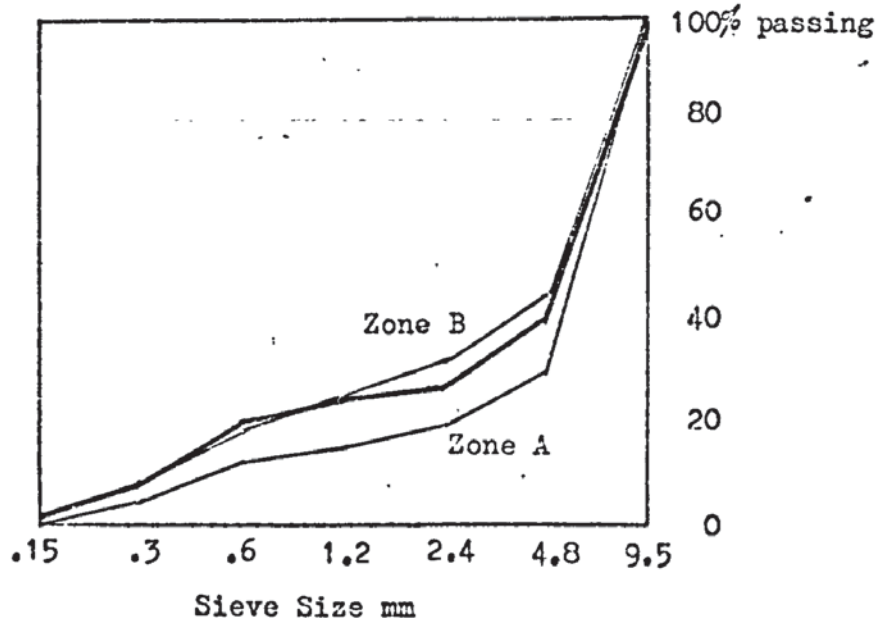

GRADING CURVE FOR MIXED AGGREGATE, COMPARED WITH TYPICAL ZONE A AND ZONE B AGGREGATES.

TABLE 3.1 ANALYSES OF AGGREGATES

BEAM NO.	f_{cu} N/mm^2	f'_c N/mm^2	f_s N/mm^2	f'_r N/mm^2	f_r N/mm^2	E_c kN/mm^2
0	47.6	39.1	3.02	3.73	-	33.5
1	51.8	43.6	3.63	3.74	-	30.5
2	42.3	38.7	3.00	3.58	-	29.1
3	40.7	43.4	2.96	3.90	-	32.1
4	57.7	52.6	3.57	4.76	-	35.2
5	52.9	48.4	3.76	4.44	-	37.7
6	44.3	34.8	3.20	3.64	-	36.3
7	44.2	40.2	2.95	3.96	-	31.7
8	45.3	41.3	3.21	3.62	-	29.3
9	50.3	39.0	3.19	3.57	3.94	33.6
10	52.7	41.8	3.19	3.43	3.46	32.7
11	50.4	39.0	3.03	3.79	3.36	30.6
12	49.9	35.4	3.23	3.95	3.73	29.9
13	44.3	32.6	3.05	3.05	3.54	31.3
14	47.6	42.5	2.93	3.83	4.15	31.1
15	50.0	45.2	3.33	4.02	3.57	30.8
16	46.9	40.3	3.13	3.81	4.13	36.6
17	47.4	39.5	3.17	4.11	4.04	33.0
18	51.6	45.5	3.26	4.11	3.36	30.9
19	53.0	42.3	3.58	3.79	4.17	33.6
20	51.1	44.5	2.85	3.58	3.77	32.4
21	54.3	45.4	3.37	3.81	4.46	34.1
22	54.3	39.4	3.12	3.98	4.25	29.6
23	56.3	44.5	3.27	-	4.04	37.3
24	48.1	35.7	3.33	-	3.80	30.4
25	50.0	42.1	3.03	-	4.27	33.7
26	49.1	35.2	3.16	-	3.71	37.2
27	50.3	33.4	3.16	-	3.64	31.1
28	50.4	38.4	3.00	-	3.30	31.7
29	50.4	38.1	3.28	-	3.83	33.3
30	48.5	39.9	3.69	-	4.05	34.2
31	51.9	37.2	3.38	-	3.30	31.8
32	49.5	38.7	3.29	-	4.45	31.9
33	57.2	37.0	3.49	-	4.38	31.8
34	49.4	38.8	3.18	-	3.58	31.4
35	53.9	39.3	3.42	-	4.14	33.1
36	51.2	38.9	3.35	-	4.29	30.3
37	54.4	40.9	3.32	-	3.77	33.6
38	51.3	36.9	3.53	-	3.91	32.5
39	50.2	41.9	3.05	-	4.05	34.6
40	52.8	37.3	3.05	-	4.31	28.8
41	50.7	40.0	3.05	-	4.00	31.3
MEAN	50.1	40.2	3.23	3.84	3.90	32.5
Coeff.^{t} of Var.^{n} %	7.4	9.8	6.8	8.9	8.8	7.0

TABLE 3.2 CONTROL TEST RESULTS

4. THEORETICAL ANALYSIS OF ULTIMATE STRENGTH

4.1 Introduction

In this section, theoretical expressions for the ultimate torsional strength of prestressed rectangular concrete beams subjected to combined torsion, bending and shear are developed.

Previous investigators into the effects of combined torsion and bending have observed three modes of failure. In the present tests, only two failure modes occurred (see Section 5), but for completeness all three modes have been analysed.

In mode 1, the strength is related to the cylinder strength, f'_c, using the Cowan failure criterion for the concrete in the compressive zone at the top of the beam.

In modes 2 and 3, the strength is dependent on the tensile strength or modulus of rupture of the concrete in the tensile zone at the side, or top of the beam, respectively.

The theory is developed for a rectangular beam with three layers of steel, one in the compressive and two in the tensile zone; all steel remains elastic to failure. The bond slip factor may be modified to cover pre and post-tensioned cases. No transverse steel is considered.

4.2 Mode 1

This mode is characterised by a failure surface of the type shown in fig. 4.1, and occurs when the M/T ratio is high. Extensive cracking occurs in the bottom of the beam, whilst crushing of the concrete at the top face may occur at failure.

The concrete in the compression zone is subjected to

(a) direct stress, due to prestressing force and bending moment

(b) shear stress, due to torsion and to shear. For these combined stresses, the Cowan (38) failure theory has been used previously by Martin and Wainwright (23). Here, the theory will be extended to include the effect of shear force on the beam.

The stress and strain distributions across a section at right angles to the axis of the beam are shown in fig. 4.2. Normally the prestressing steel cannot move laterally in the duct, and dowel forces will be set up, balanced by shear forces in the concrete as shown. Where the ducts are large, these dowel forces cannot arise and the equations must be modified.

Taking moments about an axis through the centroid of the lowest steel, and perpendicular to the axis of the beam

$$M_1 + (P_{s2} + A_{s2} f_{s2})(d_1 - d_2) + P_{s3}(d_1 - d_3) = \frac{2}{3} bxzf_{cm} \qquad \ldots (4.1)$$

Similarly, taking moments parallel to the axis of the beam

$$T_1 = \frac{2}{3} bxv_{ct} z_t \qquad \ldots (4.2)$$

or

$$T_1 = (D_{s1} + D_{s2}) z_t \qquad \ldots (4.3)$$

where z_t is the torsional moment lever arm.

Resolving vertically, and neglecting any dowel force due to vertical shear

$$V_1 = \frac{2}{3} bxv_{cv}$$

Taking $v_c = v_{cv} + v_{ct}$, and using the Cowan failure envelope, fig. 4.3, with $\sin\beta = 0.6$

$$25\left[\frac{v_c}{f'_c}\right]^2 + 4\left[\frac{f_{cm}}{f'_c}\right]^2 - 3\left[\frac{f_{cm}}{f'_c}\right] = 1 \qquad \ldots (4.4)$$

Substituting values for v_c and f_{cm} in 4.4

$$25\left[\frac{V_1 z_t + T_1}{\frac{2}{3}bxz_t f'_c}\right]^2 + 4\left[\frac{M_1 + (P_{s2} + A_{s2}f_{s2})(d_1 - d_2) + P_{s3}(d_1 - d_3)}{\frac{2}{3}bxzf'_c}\right]^2$$

$$- 3\left[\frac{M_1 + (P_{s2} + A_{s2}f_{s2})(d_1 - d_2) + P_{s3}(d_1 - d_3)}{\frac{2}{3}bxzf'_c}\right] = 1 \qquad \ldots (4.5)$$

This basic equation relating M_1, T_1, and V_1, cannot at the moment be solved as it contains the unknowns f_{s2}, x, z and z_t.

Resolving forces on the skew failure plane

$$\frac{2b}{3\cos\theta_1} xf_{cmi} = (A_{s1}f_{s1} + A_{s2}f_{s2} + P_{s1} + P_{s2} + P_{s3})\cos\theta_1 + (D_{s1} + D_{s2})\sin\theta_1 \qquad \ldots (4.6)$$

The strain distribution over the depth of the section is assumed to be linear across both the skew and square bending planes. The strain in the concrete normal to the skew plane is

$$\epsilon_{c1i} = \epsilon_{c1}\cos^2\theta_1 + \frac{D_{s1}}{A_{s1}G_s}\sin\theta_1\cos\theta_1 \qquad \ldots (4.7)$$

But $$\frac{\epsilon_{cmi}}{x} = \frac{\epsilon_{c1i}}{d_1 - x} = \frac{\epsilon_{c2i}}{d_2 - x} \qquad \ldots (4.8)$$

and $$\epsilon_{c1} = \frac{\epsilon_{s1}}{B} \qquad \ldots (4.9)$$

where a bond slip factor B is assumed.

Now $E_c \epsilon_{cmi} = f_{cmi}$ ... (4.10)

$E_s \epsilon_{s1} = f_{s1}$ and $E_s \epsilon_{s2} = f_{s2}$ ... (4.11)

Combining equations (4.7) to (4.11)

$$f_{s1} = B\left[\frac{f_{cmi} m(d_1 - x)}{x\cos^2\theta_1} - \frac{D_{s1}E_s\tan\theta_1}{A_{s1}G_s}\right] \quad \text{... (4.12)}$$

A similar equation may be written down for f_{s2} , but an approximate expression will be used here, assuming that the stress increases are proportional to the distance from the neutral axis, i.e. :-

$$f_{s2} = f_{s1}\frac{(d_2 - x)}{(d_1 - x)} \quad \text{... (4.13)}$$

In a similar manner, the dowel forces are assumed to be proportional to their distance from the upper arm of the couple :-

$$D_{s1} = \frac{T_1 l_1}{l_1^2 + l_2^2} \quad \text{and} \quad D_{s2} = \frac{T_1 l_2}{l_1^2 + l_2^2} \quad \text{... (4.14)}$$

where $l_1 = d_1 - 0.375x$ and $l_2 = d_2 - 0.375x$ ... (4.15)

Taking moments of forces about an axis normal to the skew plane and through the centroid of the lowest steel :-

$$M_1\cos\theta_1 + T_1\sin\theta_1 = \frac{2bxzf_{cmi}}{3\cos\theta_1} - (P_{s2} + A_{s2}f_{s2})(d_1 - d_2)\cos\theta_1$$

$$- D_{s2}(d_1 - d_2)\sin\theta_1 - P_3(d_1 - d_3)\cos\theta_1 \quad \text{... (4.16)}$$

Equations (4.6), (4.12) and (4.16) include θ_1 , the angle of inclination of the compression hinge. Following Wainwright (7), we assume that this angle is determined by the M/T ratio on loading.

Taking moments about the neutral axis on the skew failure plane at the first crack

$$M_{c1}\cos\theta_1 + T_{c1}\sin\theta_1 = \frac{bh^2(f_r + p_{c1}\cos\theta_1)}{6\cos\theta_1} \qquad \ldots (4.17)$$

$$\text{rearranging} \quad T_{c1} = \frac{bh^2}{6} f_r \left[\frac{1 + \tan^2\theta_1 + p_{c1}/f_r}{M_{c1}/T_{c1} + \tan\theta_1} \right] \qquad \ldots (4.18)$$

If the M/T ratio is constant during the test we can write $M_{c1}/T_{c1} = M_1/T_1$ and the minimum value of T_{c1} occurs when

$$\tan\theta_1 = \sqrt{(M_1/T_1)^2 + 1 + p_{c1}/f_r} - M_1/T_1 \qquad \ldots (4.19)$$

Equations (4.6), (4.12) to (4.16) and (4.19) may now be solved for x. Using this value, M_1 may be determined from (4.5), for given values of T_1 and V_1 .

4.3. Mode 2

This mode is characterised by a failure surface of the type shown in fig. 4.4 . Normally the initial cracking occurs on the front face where the shear stresses due to flexural shear and torsion are additive. With high flexural moments, however, the initial cracks may form at the bottom of the beam; the failure surface will not then incorporate these initial cracks.

4.3.1 Stress Method

With this method of analysis, failure is assumed to occur when the maximum principal tensile stress in the concrete reaches the uniaxial tensile stress f_t, determined experimentally.

At the centre of the front face :-

Shear stress due to flexural shear $= \dfrac{1.5\ V_2}{bh}$

Shear stress due to torsional moment $= \dfrac{T_2}{c_t\ hb^2}$

Direct stress due to prestress $= p_{c2}$

$$f_t = \sqrt{\left[\frac{1.5\ V_2}{bh} + \frac{T_2}{c_t hb^2}\right]^2 + \left[\frac{p_{c2}}{2}\right]^2} - \frac{p_{c2}}{2}$$

or $$\frac{1.5V_2}{bh} + \frac{T_2}{c_t hb^2} = \sqrt{f_t\ (\ p_{c2} + f_t\ )}$$

When $T_2 = 0$ $V_2 = V_{u2} = \dfrac{bh}{1.5}\sqrt{f_t\ (\ p_{c2} + f_t\ )}$

When $V_2 = 0$ $T_2 = T_{u2} = c_t hb^2\ \sqrt{f_t\ (\ p_{c2} + f_t\ )}$

$$\frac{V_2}{V_{u2}} + \frac{T_2}{T_{u2}} = 1. \qquad \ldots (\ 4.\ 20\ )$$

There is thus a linear relationship between V_2 and T_2. The flexural moment M does not appear in the equation.

4.3.2 Skew Bending Method

It is now assumed that the critical stress is the modulus of rupture, and it occurs at an angle θ_2 to the vertical on an inclined, rectangular plane, fig. 4.5.

Taking moments about the centroid of the full concrete section :-

$$T_2 \sin\theta_2 = \frac{hb^2}{6\cos\theta_2}\left[f_{r2} + p_{c2}\cos^2\theta_2 - \frac{V_2 \sin\theta_2\cos\theta_2}{bh}\right]$$

$$\text{or } T_2 + \frac{V_2 b}{6} = \frac{hb^2}{6}\left[\frac{f_{r2} + p_{c2}\cos^2\theta_2}{\sin\theta_2\cos\theta_2}\right]$$

For constant V, T is a minimum when $\tan\theta_2 = \sqrt{1 + p_{c2}/f_{r2}}$ ... (4.21)

$$\text{and then } T_2 + \frac{V_2 b}{6} = \frac{hb^2}{3}\sqrt{f_{r2}(p_{c2} + f_{r2})}$$

If a more realistic, trapezoidal failure plane is assumed, then following Martin (23) we may approximate this by modifying the constant 3 in the above equation, which becomes

$$T_2 + \frac{V_2 b}{6} = \frac{hb^2}{3 + \left[\frac{b}{h}\right]^{\frac{1}{2}} + 0.35\left[\frac{b}{h}\right]^{\frac{1}{2}}\left[\frac{p_{c2}}{f_{r2}}\right]^{\frac{1}{2}}}\sqrt{f_{r2}(p_{c2} + f_{r2})}$$

$$\text{When } T_2 = 0,\ V_2 = V'_{u2} = \frac{6bh}{3 + \left[\frac{b}{h}\right]^{\frac{1}{2}} + 0.35\left[\frac{b}{h}\right]^{\frac{1}{2}}\left[\frac{p_{c2}}{f_{r2}}\right]^{\frac{1}{2}}}\sqrt{f_{r2}(p_{c2} + f_{r2})}$$

$$\text{When } V_2 = 0,\ T_2 = T'_{u2} = \frac{hb^2}{3 + \left[\frac{b}{h}\right]^{\frac{1}{2}} + 0.35\left[\frac{b}{h}\right]^{\frac{1}{2}}\left[\frac{p_{c2}}{f_{r2}}\right]^{\frac{1}{2}}}\sqrt{f_{r2}(p_{c2} + f_{r2})}$$

$$\text{and } \frac{T_2}{T'_{u2}} + \frac{V_2}{V'_{u2}} = 1 \qquad \text{... (4. 22)}$$

is the general interaction form of the equation.

4.4 Mode 3

None of the beams tested were observed to fail with this Mode, but for completeness it will be included in the analysis.

The type of failure surface is shown in fig. 4. 6. Cracking occurs on the top and both sides, with rotation about a compressive zone at the bottom of the beam.

4.4.1 Stress Method

If failure follows formation of the first crack, a principal tensile stress criterion may be used.

The shear stress at the centre of the top face will only be dependent on the torsional moment and will equal $\frac{T_3}{c_t bh^2}$

The direct stress at the same point = $\frac{M_3}{bh^2/6} + p_{c3}$

Then $f_t = \sqrt{\left[\frac{T_3}{c_t bh^2}\right]^2 + \left[\frac{3M_3}{bh^2} + \frac{p_{c3}}{2}\right]^2} - \left[\frac{3M_3}{bh^2} + \frac{p_{c3}}{2}\right]$

which gives $\left[\frac{T_3}{c_t bh^2 f_t}\right]^2 - \frac{6M_3}{bh^2 f_t} = 1 + \frac{p_{c3}}{f_t}$

when $M_3 = 0$, $T_3 = T_{u3} = f_t c_t bh^2 \sqrt{1 + \frac{p_{c3}}{f_t}}$

when $T_3 = 0$, $M_3 = -M_{u3} = -\frac{bh^2}{6} f_t \left[1 + \frac{p_{c3}}{f_t}\right]$

and $$\left[\frac{T_3}{T_{u3}}\right]^2 - \frac{M_3}{M_{u3}} = 1 \qquad \ldots (4.23)$$

is the general interaction equation.

4.4.2 Skew Bending Method

It is now assumed that the critical stress is the modulus of rupture and that it occurs at an angle θ_3 to the horizontal on an inclined rectangular plane, fig. 4.7

Taking moments about the neutral axis of the section

$$T_3 \sin\theta_3 - M_3 \cos\theta_3 = \frac{bh^2(f_{r3} + p_{c3}\cos^2\theta_3)}{6\cos\theta_3}$$

The minimum value of T_3 occurs when

$$\tan\theta_3 = \frac{M_3}{T_3} + \sqrt{\left[\frac{M_3}{T_3}\right]^2 + \left[1 + \frac{p_{c3}}{f_{r3}}\right]}$$

and then $$T_3 = \frac{bh^2}{3} f_{r3}\left[\frac{M_3}{T_3} + \sqrt{\left[\frac{M_3}{T_3}\right]^2 + 1 + \frac{p_{c3}}{f_{r3}}}\right]$$

If a distorted, trapezoidal failure plane is assumed, an approximation may be made as previously. The equations are the same as those found by Martin (23), as in Mode 3 shear does not affect the failure.

The general interaction equation becomes

$$\left[\frac{T_3}{T'_{u3}}\right]^2 - \frac{M_3}{M_{u3}} = 1 \qquad \ldots (4.24)$$

where $$T'_{u3} = \frac{f_{r3}bh^2}{3 + \left[\frac{h}{b}\right]^{\frac{1}{2}} + 0.35\left[\frac{h}{b}\right]^{\frac{1}{2}}\left[\frac{p_{c3}}{f_{r3}}\right]^{\frac{1}{2}}} \sqrt{1 + \frac{p_{c3}}{f_{r3}}}$$

for values of $\frac{h}{b}$ between 0.25 and 4 and $\frac{p_{c3}}{f_{r3}}$ between 0 and 10.

For values of $\frac{h}{b}$ between 0.25 and 4 and $\frac{p_{c3}}{f_{r3}}$ between 0 and - 1

$$T'_{u3} = \frac{f_{r3}bh^2}{3 + \left[\frac{h}{b}\right]^{\frac{1}{2}} + \left[\frac{h}{b}\right]^{\frac{1}{2}}\left[\frac{p_{c3}}{f_{r3}}\right]} \sqrt{1 + \frac{p_{c3}}{f_{r3}}}$$

and $$M_{u3} = \frac{bh^2}{6} f_{r3}\left[1 + p_{c3}/f_{r3}\right]$$

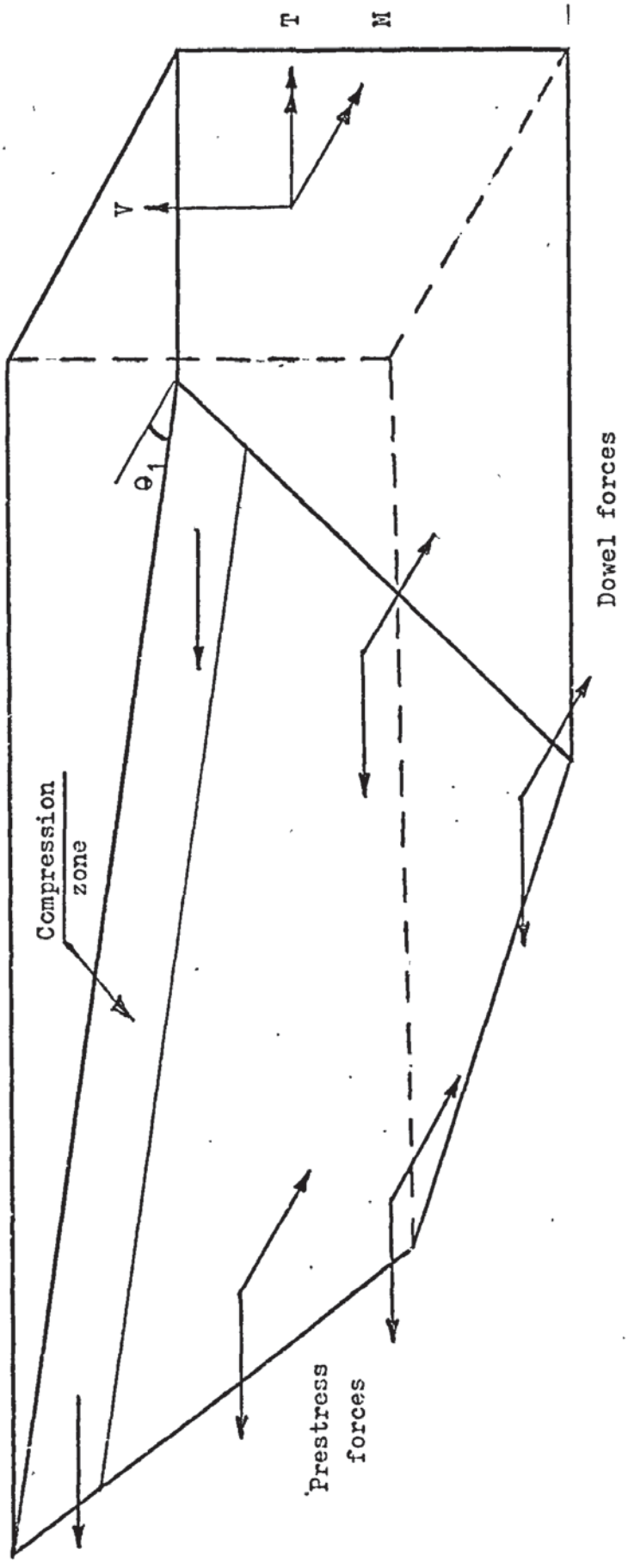

FIGURE 4.1. FAILURE SURFACE - MODE 1

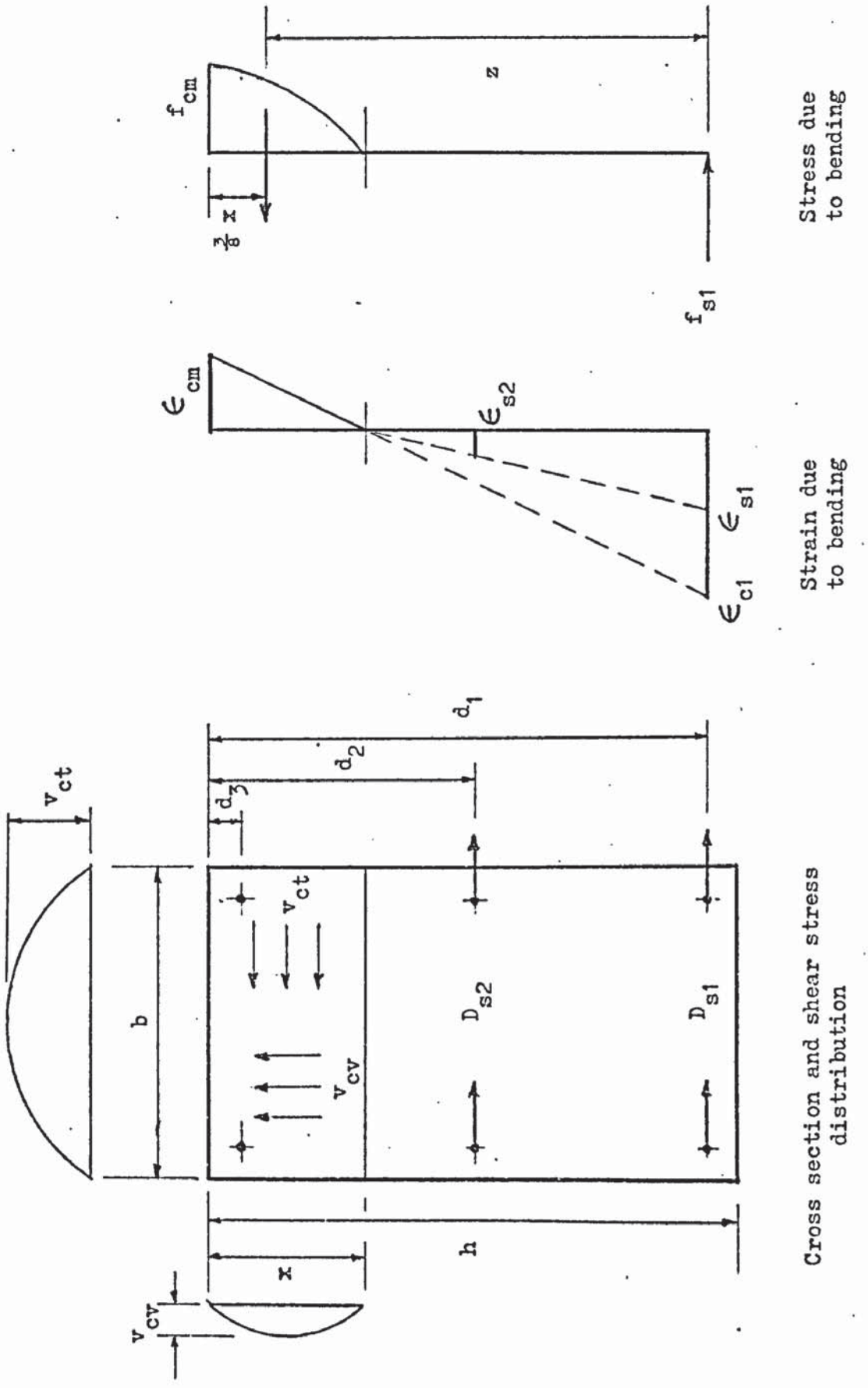

FIGURE 4.2 STRESS AND STRAIN DISTRIBUTION ON PLANE NORMAL TO AXIS - MODE 1

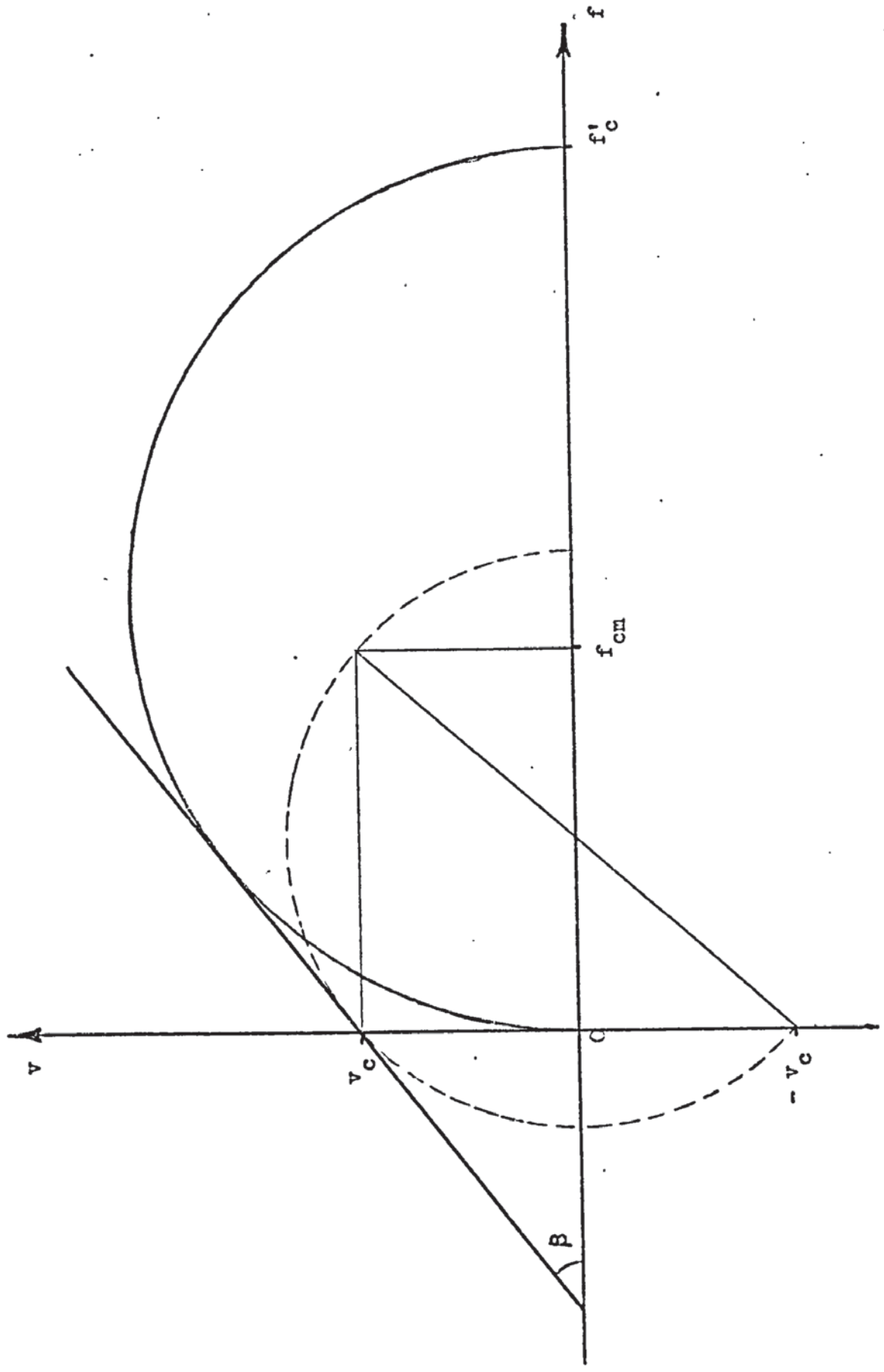

FIGURE 4.3 COWAN FAILURE ENVELOPE

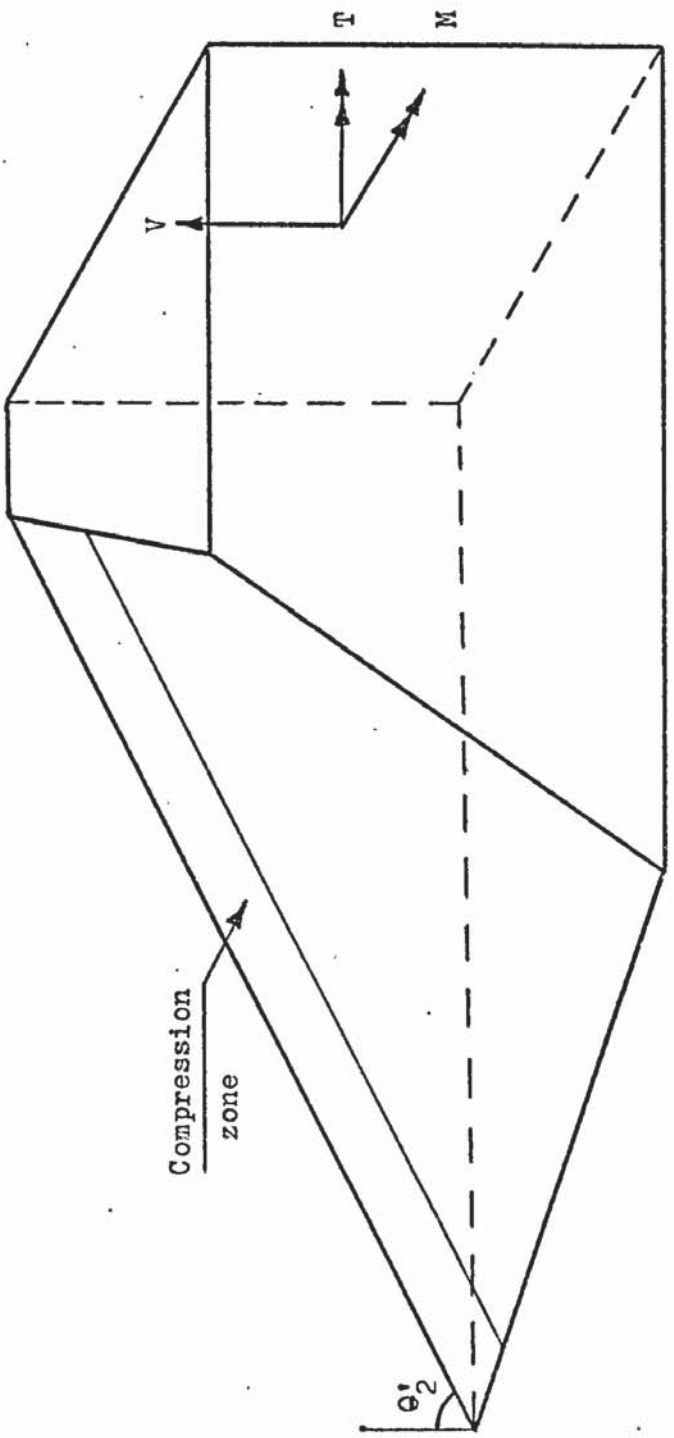

FIGURE 4.4 FAILURE SURFACE - MODE 2

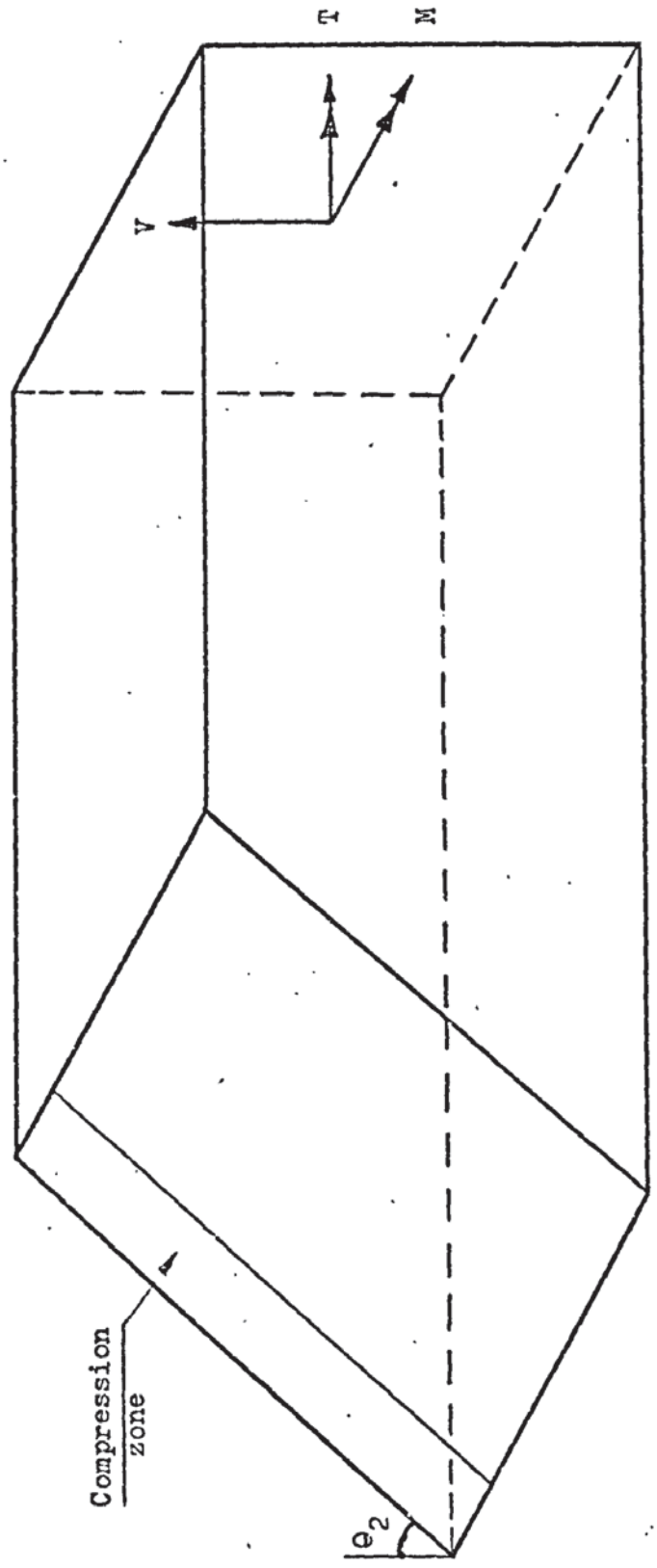

FIGURE 4.5 SIMPLIFIED FAILURE SURFACE - MODE 2

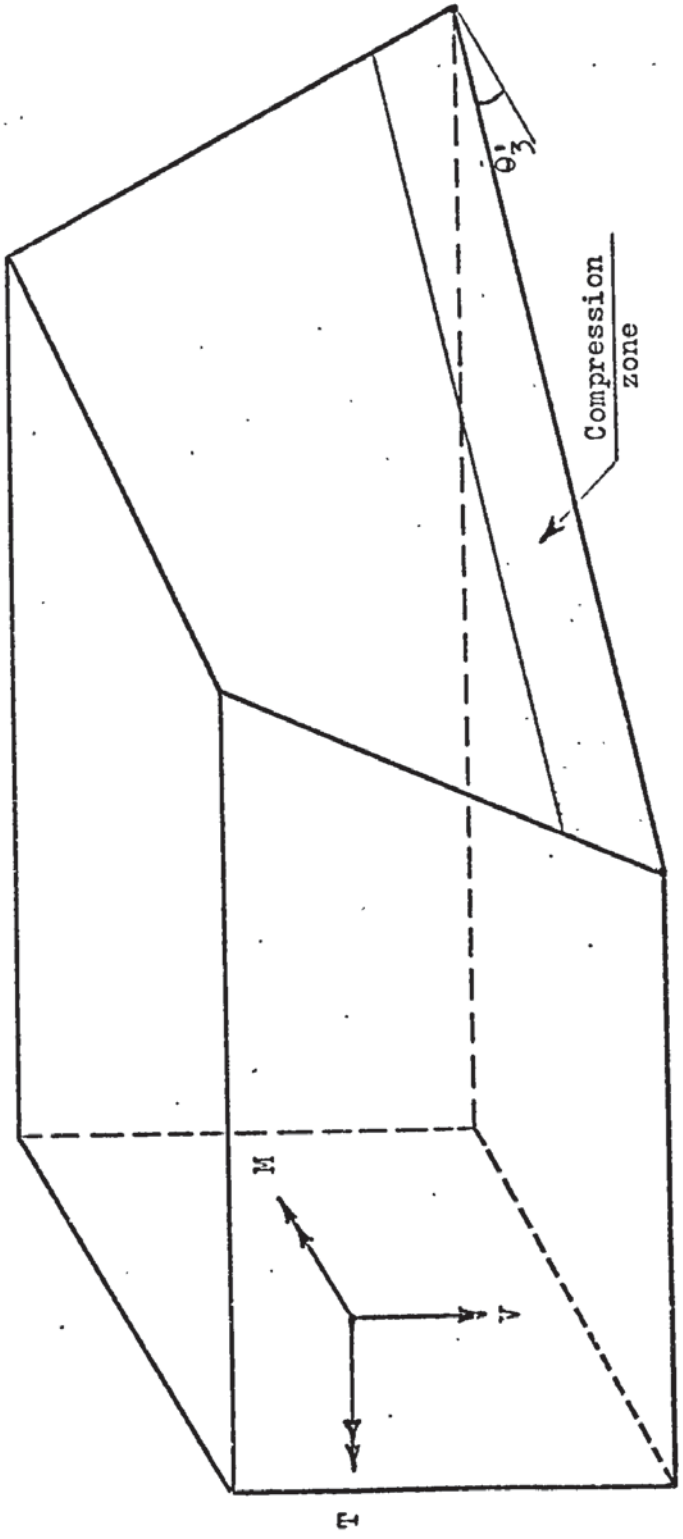

FIGURE 4.6 FAILURE SURFACE - MODE 3

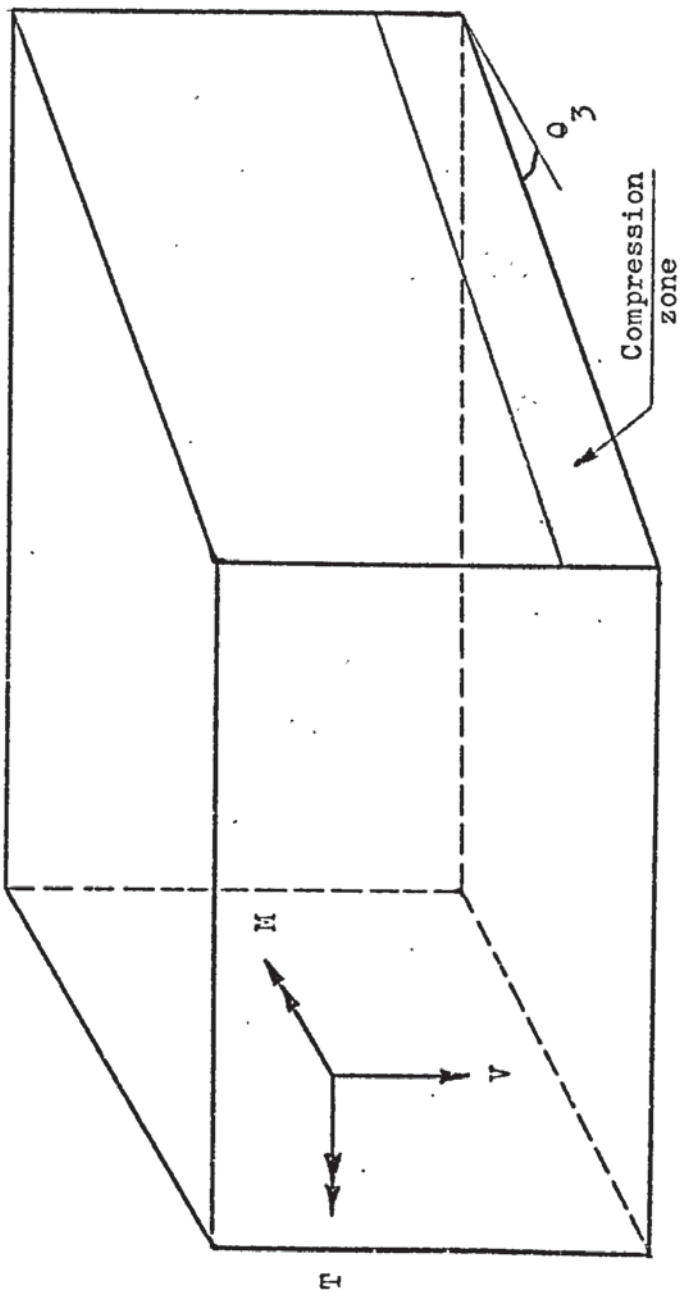

FIGURE 4.7 SIMPLIFIED FAILURE SURFACE - MODE 3

5. TEST RESULTS AND BEHAVIOUR OF BEAMS

The main test results are now presented, and the behaviour of the beams under load discussed. Strain gauge results, deflections, rotations and cracking details are given in Section 8, but discussed here.

5.1 Principal Test Results

These are given in Tables 5.1 and 5.2. The failure moment, torque and shear are given for the critical section, which is assumed to lie on the centre of the compression face, a distance y mm from the left hand support. The values of M_u and T_u are experimental; that for V_u is theoretical, the value of V_{co} from B.S. CP 110 being used, omitting partial safety factors and putting f_t equal to the average experimental value of the modulus of rupture f_r.

5.2 General Behaviour

Four beams were tested under self weight and torsional load only. Due to the position of the torsion arms, the Series 1 beams 20 and 21 were subjected to a small hogging bending moment, whilst the Series 2 beams 23 and 27 were subjected to the sagging self weight moment only. The beams all failed suddenly and it was not possible to see on which face the first crack formed. From an examination of the failure surface it is seen that the compressive hinge is either on the back or on the front face, both indicating a Mode 2 type failure.

Eight further beams were tested with an applied moment such that the M/T ratio was less than or equal to 1.5. In one case, beam 40, slight cracking occurred at the penultimate load. In all other cases

the cracking load and failure load coincided, the resulting failure being of Mode 2 type. Figures 5.7 to 5.10 show the failure cracks of two of these, beams 5 and 6.

For beams with larger applied bending moments, flexural cracks occurred at the bottom of the beam well before failure. As the load increased these widened, spread and branched at approximately 45° towards the right hand support on the front face, in the opposite direction on the back face. The cracks occurred whether the vertical load was applied first, in the first nine beams, or in increments with the torsion, beams 10 to 41.

If the $M/_T$ ratio was between 1.5 and 3.5 the beam again failed in Mode 2, the failure surface not utilising the existing cracks.

Beams 32 and 38 were tested with $M/_T$ ratios of 3.9 and 4.3 respectively. Mode 1 type cracks were formed on loading, but in both cases the final failure mechanism was complex. They have been labelled 1/2, but neither Mode 1 nor Mode 2 cracks were completely formed, whilst some longitudinal and transverse cracks may have been formed subsequently to failure. The failure cracks for beam 38 are shown in figures 5.11 and 5.12.

Beams tested with $M/_T$ ratios greater than 4.5 all failed in Mode 1. Extensive cracking occurred near failure, a compression hinge forming on the top face with, in many cases, local crushing of the concrete. The cracks at failure of beam 16 are shown in figures 5.13 and 5.14.

5.3 Moment/torque Interaction Curves

These are given for each series and each shear span in figures 5.1 to 5.4.

For most specimens, a slight increase in torque occurs for low values of applied moment, as found by other investigators (7, 21, 32). However,

to obtain this rising curve in a beam subjected to varying bending moments implies that failure must be inhibited in regions of low moment. This occurred to a very limited extent in the author's tests due to

(a) the reinforcing cages at the ends of the beams

(b) the length of the failure zone

This could be over 1 m in some Mode 2 type failures.

Apart from this slight rise, the torque remains sensibly constant for all beams failing in Mode 2.

The mode of failure changes to the bending type - Mode 1 - at a moment of approximately 12 kNm for Series 1 and 10 kNm for Series 2. The ultimate torque falls off steeply with increase in moment, although there is some indication that the moment capacity of a section may be slightly enhanced for low torques (beams 16 and 36).

5.4 Shear/torque Interaction Curves

These are shown, for beams failing in Mode 2 only, in figures 5.5 for Series 1 and 5.6 for Series 2 beams.

For all specimens, the torque is sensibly constant over the range of shears considered.

Since the moment has little effect on Mode 2 type failures, the torque/shear curve will have this shape for any value of moment.

For Mode 1 failures, the moment has a very significant effect on torque, and either a three dimensional diagram must be drawn, or a series of torque/shear planes drawn at different points along the moment axis (see section 6).

5.5 Vertical Deflections

Load/deflection curves are shown in figures 8.41 to 8.44, the deflection being that immediately under the loading point.

After some settling down the curves become linear, the slopes being fairly consistent for each set. The average slopes for each set of beams are shown below; the theoretical results are calculated using the second moment of area of the gross concrete area, and a Young's Modulus for concrete of 32.5 kN/mm^2 , the average experimental value.

	Deflections in mm/kN load		
	Theoretical	Experimental	
		Series 1	Series 2
a_v = 600 mm	0.12	0.12	0.15
a_v = 800 mm	0.17	0.19	0.20

The Series 2 beams were less stiff, showing the effect of the prestressing steel.

The first crack was noticed soon after the curves became non-linear. Both the amount of deflection after cracking and the total deflection at failure depended on the $M/_T$ ratio on loading, being low for low $M/_T$ ratios and increasing for higher values. As expected, deflections were also higher for the higher value of a_v .

5.6 Rotations

Overall rotations of the beams were measured as detailed in Section 8.4; torque/rotation curves are shown in figures 8.45 to 8.49.

After some settling down the curves generally become linear, the

slopes being fairly consistent for each series; there appears to be no relationship between the slope and the $^{M}/_{T}$ ratio. The theoretical torsional stiffness K may be calculated for the full concrete section :-

$$K = \frac{0.213\ E_c h b^3}{2(1+\nu)}$$

where the constant 0.213 depends on the ratio $^{h}/_{b}$ and ν is Poisson's ratio for concrete. Putting ν equal to 0.15 and E_c equal to the average experimental value of 32.5 kN/mm^2 , K becomes 524 kNm^2 . This compares with the experimental averages for Series 1 and Series 2 beams, which were 350 and 310 kNm^2 respectively. The calculated torsional stiffness is often reduced to allow for cracking in the section. However, the torsional stiffness of beams 1, 2 and 9 were not affected, even though they were already cracked in bending before any torque was applied. This agrees with Henry (8) , who found the formation of bending cracks hardly changed the torsional stiffness of his beams. Since the value of Young's modulus was that used for deflections, and the value of ν is that usually accepted for concrete, the differences between the values of stiffness cannot be adequately explained.

5.7 Failure Crack Angles

At all stages of loading the positions of cracks were recorded on the beams, see for example, figures 5.13 and 5.14. At failure, some beams disintegrated and part of the information was lost. The crack patterns at failure for each beam have been drawn - see figures 8.1 to 8.40. The loads and torques at which the first crack was observed are generally shown in figures 8.41 to 8.49.

The average crack angles on each of the faces of each beam were measured, where possible, and are given in table 5.3. The experimental angles of the tensile cracks have also been compared with the theoretical, using equations 4.19 and 4.21 for beams failing in Modes 1 and 2 respectively, although these equations were, in fact, derived on the basis of failure on a rectangular plane. The results agree within 15 degrees, in spite of the difficulty found in deciding on an average crack angle on a face on which the crack changes direction.

In figure 5.15 both the experimental and theoretical crack angles have been plotted against the $^{M}/_{T}$ ratio for Mode 1. The scatter of points is large, but the trend is indicated.

In figure 5.16 the crack angles for Mode 2 have been plotted. Using the average values of prestress and modulus of rupture, the theoretical value of θ_2 is constant at about 60 degrees, agreeing reasonably well with the experimental values.

5.8 Increase in Tendon Force

In all beams the tendon force was measured at each increment of load, either indirectly with strain gauges on the tendon (Series 1) or directly with load cells (Series 2).

Table 5.4 compares the actual increase in force at failure for Mode 1 beams with the theoretical value. For Series 2 beams the force is for two wires.

For Series 1 beams, the average increase in force is 16%, the theory predicting 14%. Individual results, however, vary quite widely.

For the top steel in Series 2 beams the results are not so good, the theory predicting larger increases in force than occurred in practice. The experimental values for bottom and top steel are 8% and 0.7%, whilst the theoretical increases are 7% and 1.7%. The theoretical

stress in the top steel is obviously very susceptible to slight errors in the value of x, the depth of the compression zone - see Section 5.9.

The manner in which the longitudinal steel strain increases with applied moment is shown in figure 5.17. For beams tested under moment only the increase in strain in the lower prestressing steel is plotted against M/M_u. The curves are closely spaced and there are no appreciable differences between beams of different series and different shear spans. The near - horizontal portion of the curve for beam 3 is probably missing because of the rather large final increment of load used on this beam.

It should be noted that the strains plotted here are average values over the length of the beam. A similar curve is plotted by Wainwright (7), who has a longer loaded length of beam, and hence slightly higher average strains.

5.9 Longitudinal Concrete Strains

Strain gauges of either 50 or 60 mm gauge length were generally fixed to all faces of the beams in order to measure strains in the longitudinal direction. The positions of the gauges were as shown in figures 8.1 to 8.40, and were placed such that the depths of the compression zone could be determined, either on the front or back faces, or on the top and bottom faces, depending on whether a Mode 1 or a Mode 2 failure was to be expected.

Changes of strain were recorded as each increment of load was applied. Strains due to prestress were calculated from the loads applied and the concrete Young's Modulus, measured on cylinders using identical strain gauges.

Strain gauge plots of beams tested under pure moment were used to determine the bond slip factor 'B' - see Section 8.5.

Strain gauge plots of other beams have been used to determine the depth of the compression zone for beams failing in Mode 1. Normally, readings were taken on both faces of the beam; average values have been used to determine the mean depth of the neutral axis, so that they could be compared with the theoretical values in Table 5.5. The maximum longitudinal concrete compressive strains, either measured directly, or extrapolated from a vertical strain plot, are also compared to the theoretical values of maximum strain in this Table.

All strain gauge results suffer from the same problem; a gauge is never normally placed in quite the right position to record the maximum strain. Thus we should expect higher values of x than the theory predicts, which is usually the case. Theoretical values of x, using both the experimental figures for f'_c and f_{cu} have been included to show that there can be quite large differences due to this. Generally the results for x are quite good.

The experimental values of the maximum longitudinal concrete strains are very variable. Again, this is mainly due to the strain gauges not being affixed exactly at the failure section. In fourteen cases the theoretical strains are higher, as we would expect. Of the eleven values which are lower, all are for beams failing with $M/_T$ ratios greater than 9. At these higher values of M, the theory not only under estimates the ultimate moment, but also the ultimate concrete strain.

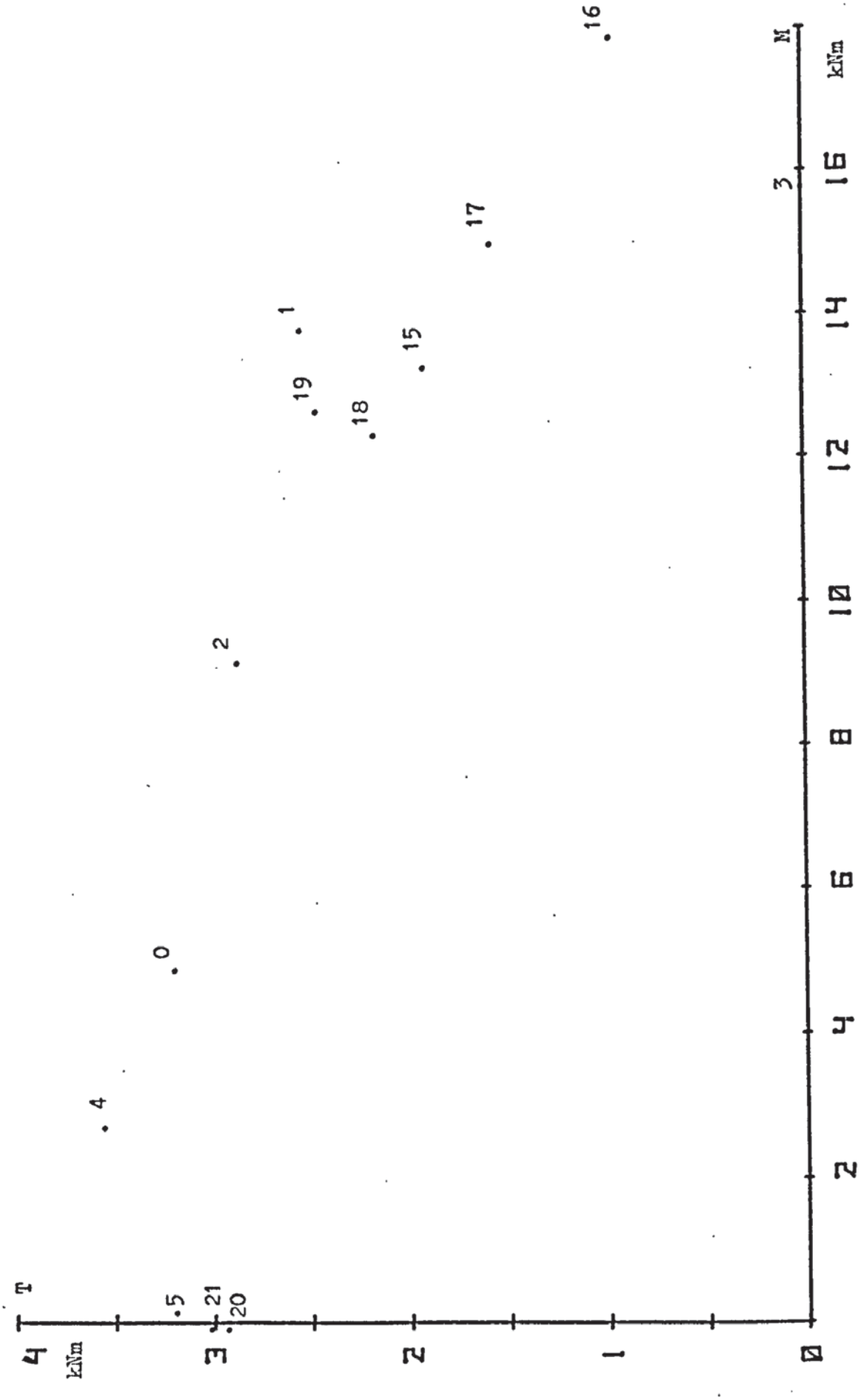

FIGURE 5.1 MOMENT/TORQUE INTERACTION DIAGRAM.

SERIES 1, a_v = 600 mm.

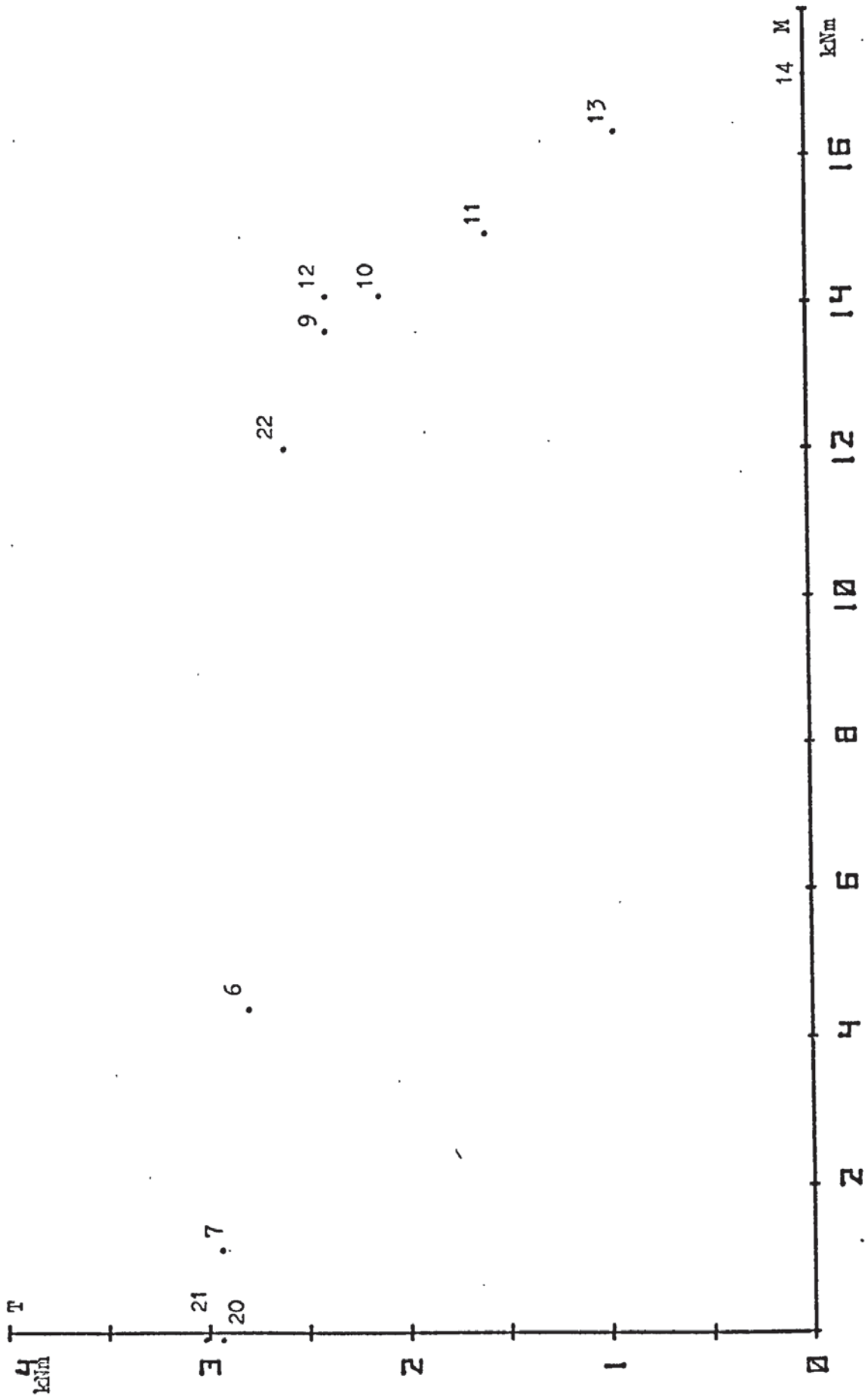

FIGURE 5.2 MOMENT/TORQUE INTERACTION DIAGRAM

SERIES 1, a_v = 800 mm.

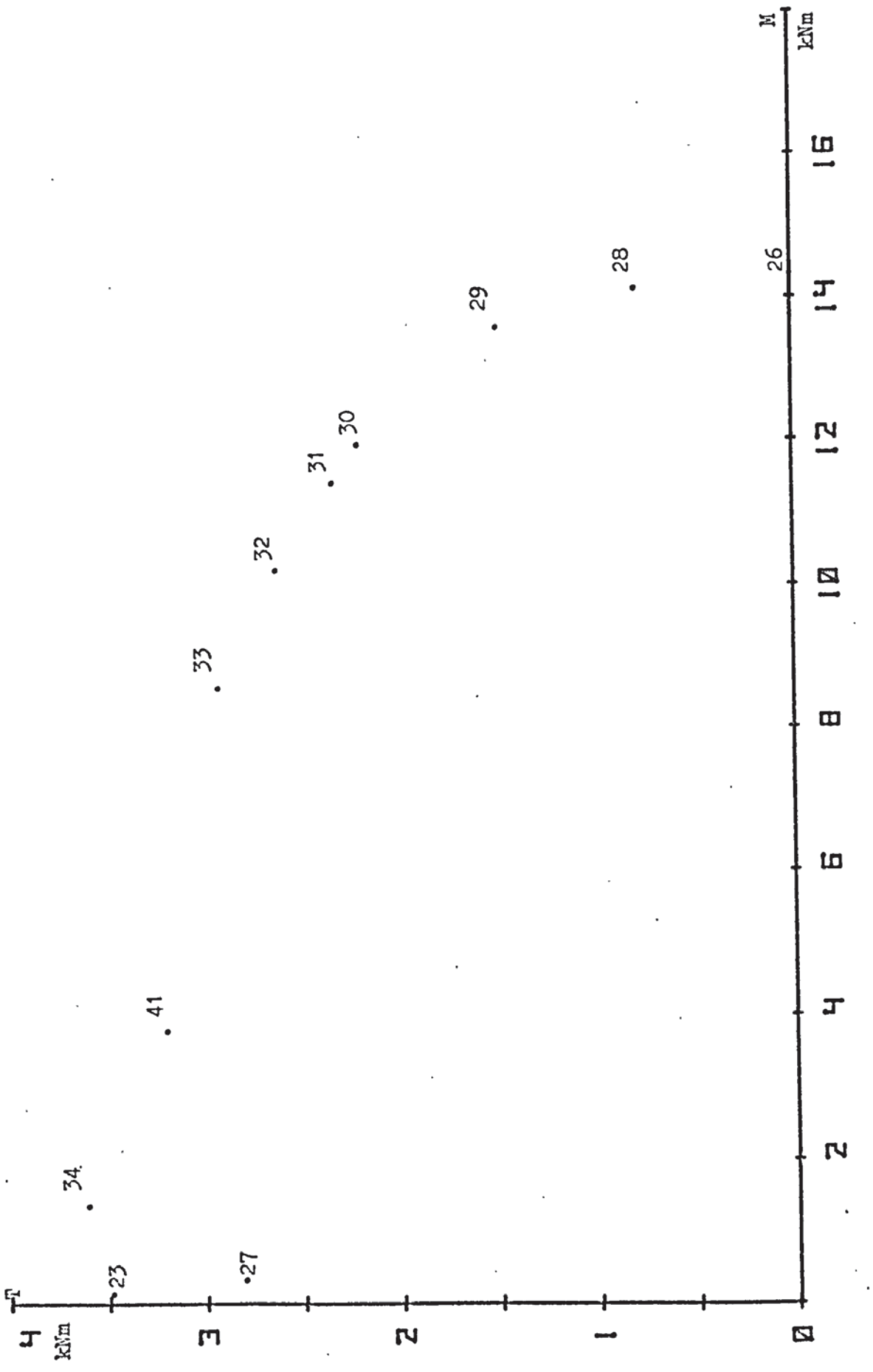

FIGURE 5.3. MOMENT/TORQUE INTERACTION DIAGRAM

SERIES 2, a_v = 600 mm.

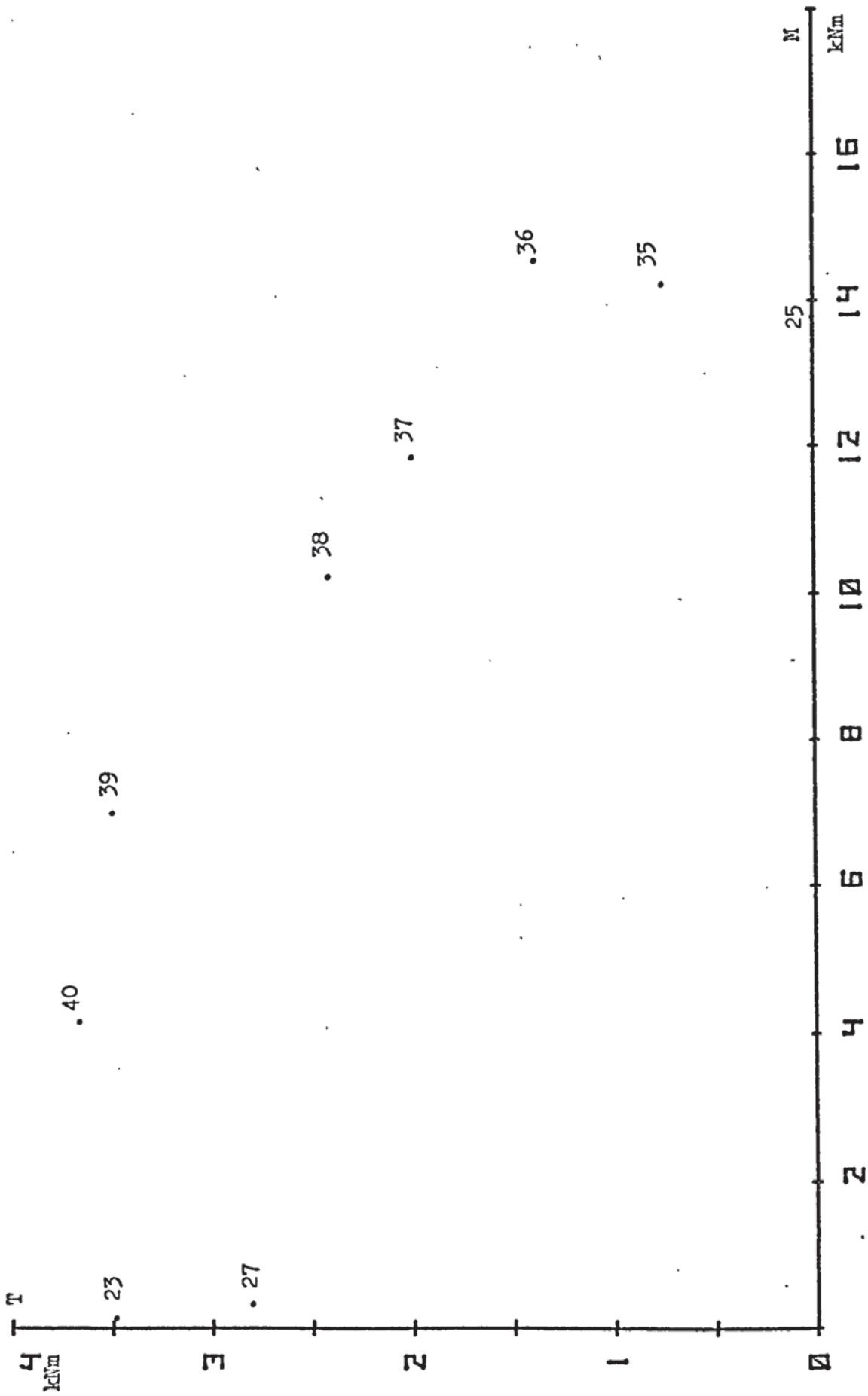

FIGURE 5.4 MOMENT/TORQUE INTERACTION DIAGRAM

SERIES 2, a_v = 800 mm

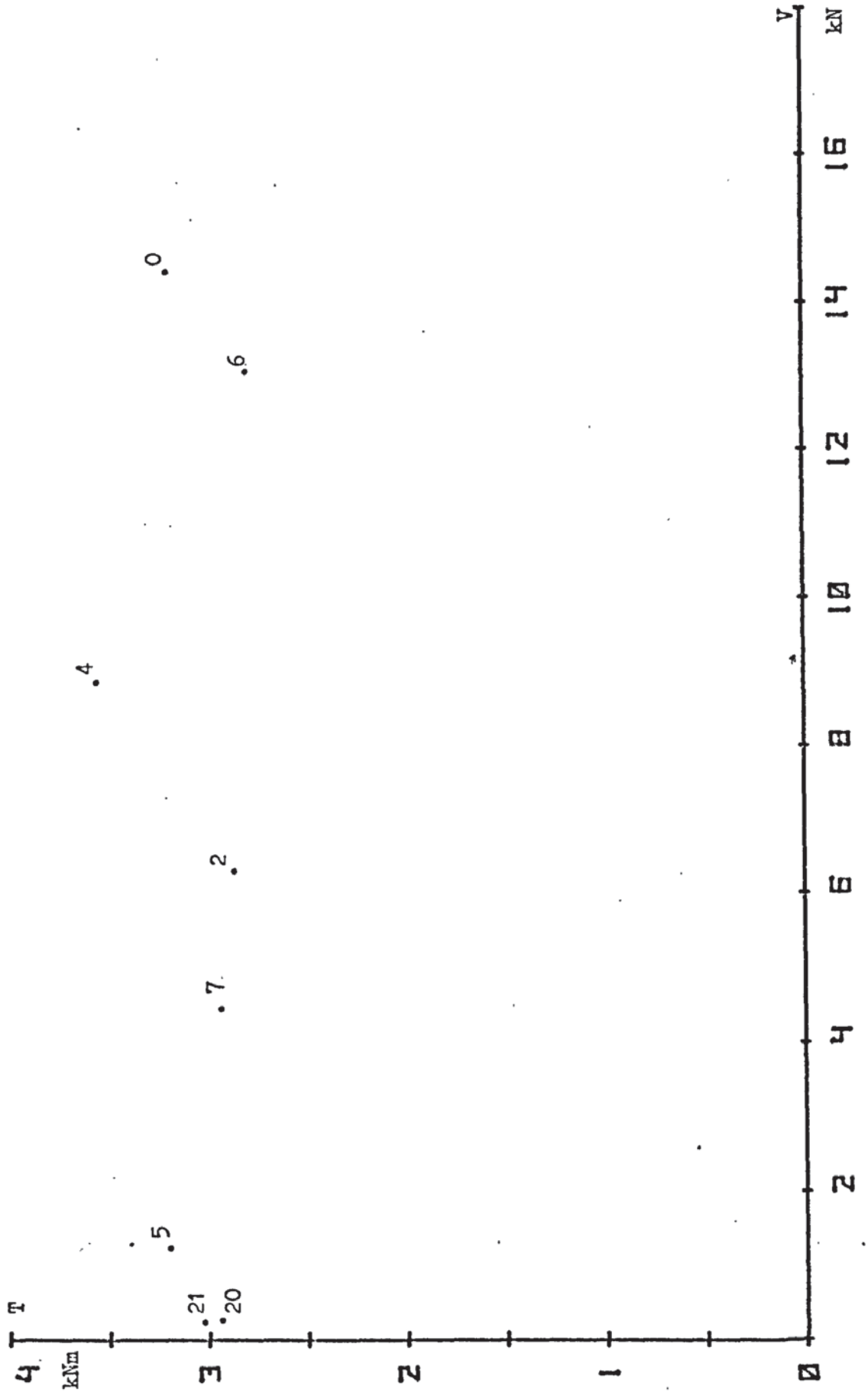

FIGURE 5.5 TORQUE/SHEAR INTERACTION DIAGRAM
MODE 2 - SERIES 1

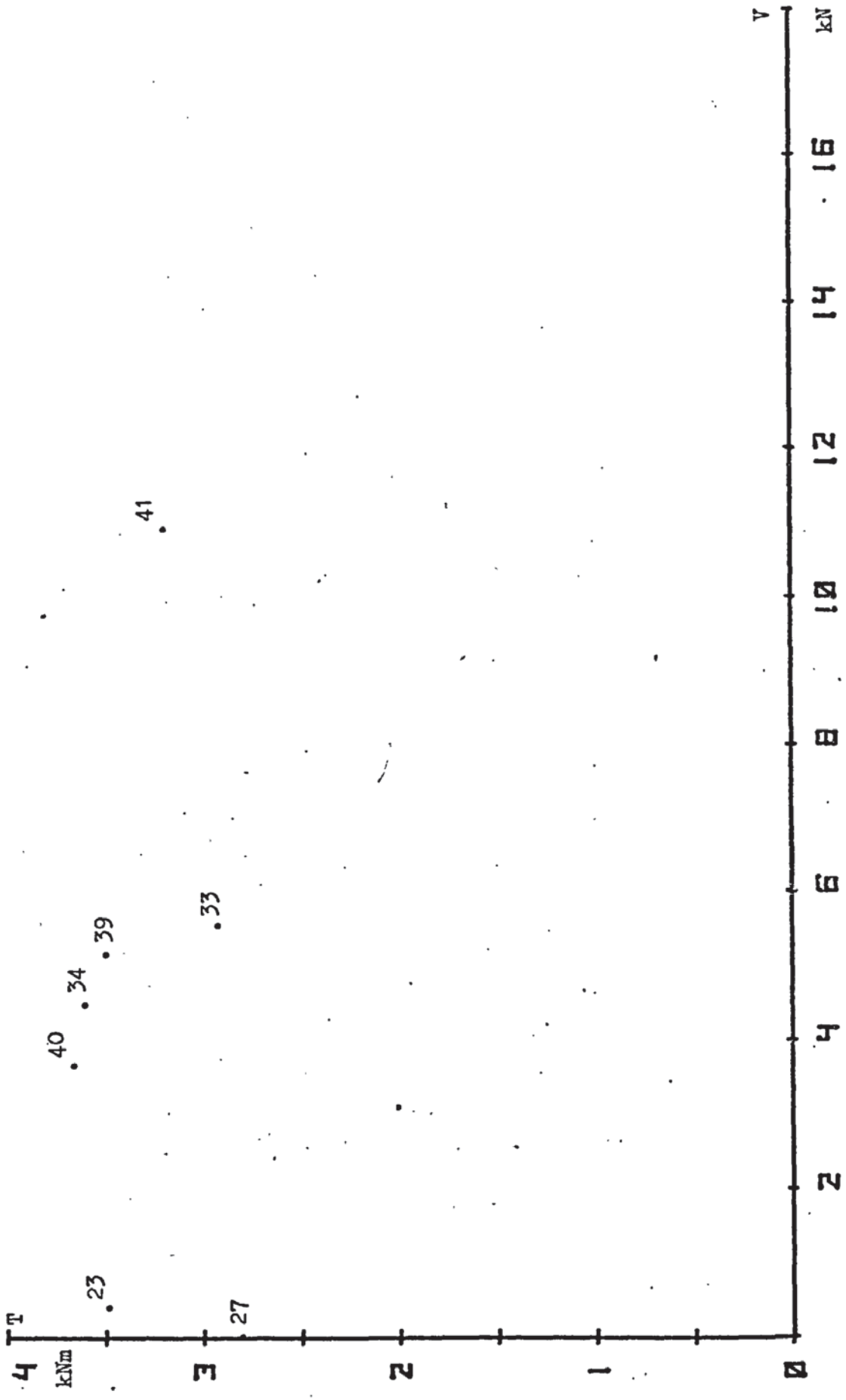

FIGURE 5.6 TORQUE/SHEAR INTERACTION DIAGRAM
MODE 2 - SERIES 2

FIGURE 5.7 MODE 2 FAILURE - BEAM 5
COMPRESSION HINGE ON FRONT FACE

FIGURE 5.8 MODE 2 FAILURE - BEAM 5
TENSILE CRACKS

FIGURE 5.9 MODE 2 FAILURE - BEAM 6
COMPRESSION HINGE ON BACK FACE

FIGURE 5.10 MODE 2 FAILURE - BEAM 6
TENSILE CRACKS

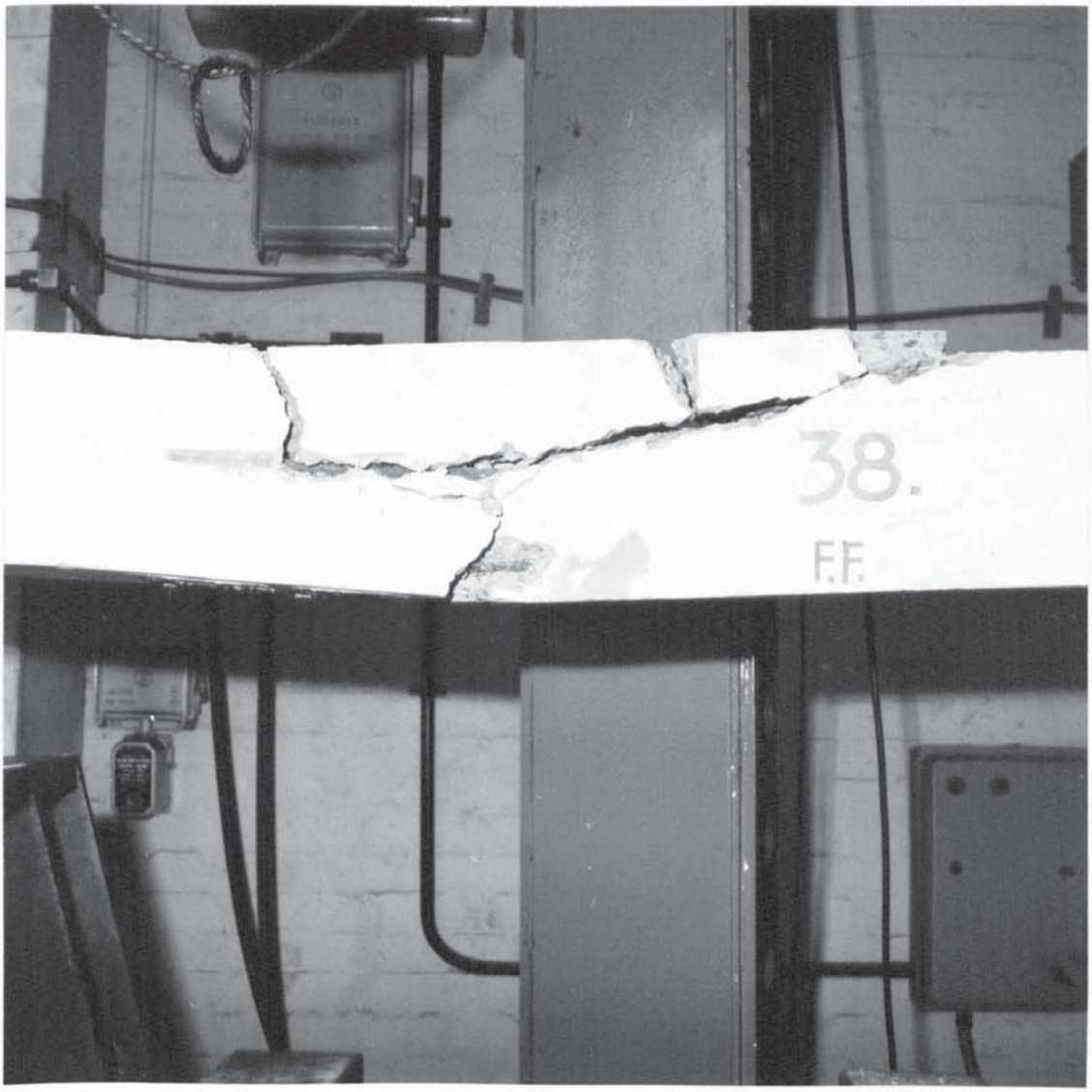

FIGURE 5.11 MODE 1/2 FAILURE - BEAM 38
FRONT FACE

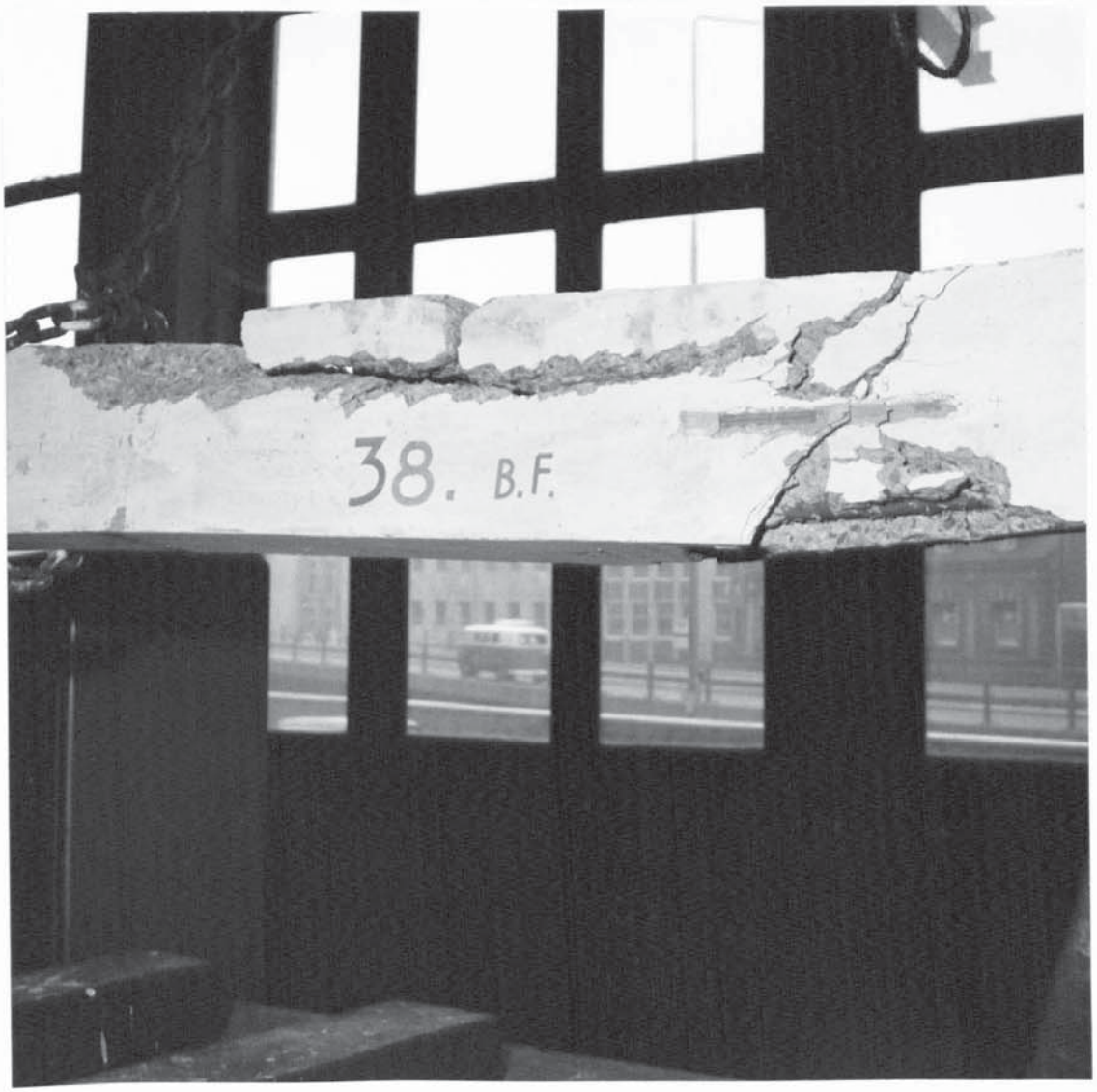

FIGURE 5.12 MODE 1/2 FAILURE - BEAM 38
BACK FACE

FIGURE 5.13 MODE 1 FAILURE - BEAM 16
TENSILE CRACKS AND CRUSHING
OF CONCRETE, FRONT FACE

FIGURE 5.14 MODE 1 FAILURE - BEAM 16
TENSILE CRACKS AND CRUSHING
OF CONCRETE, BACK FACE .

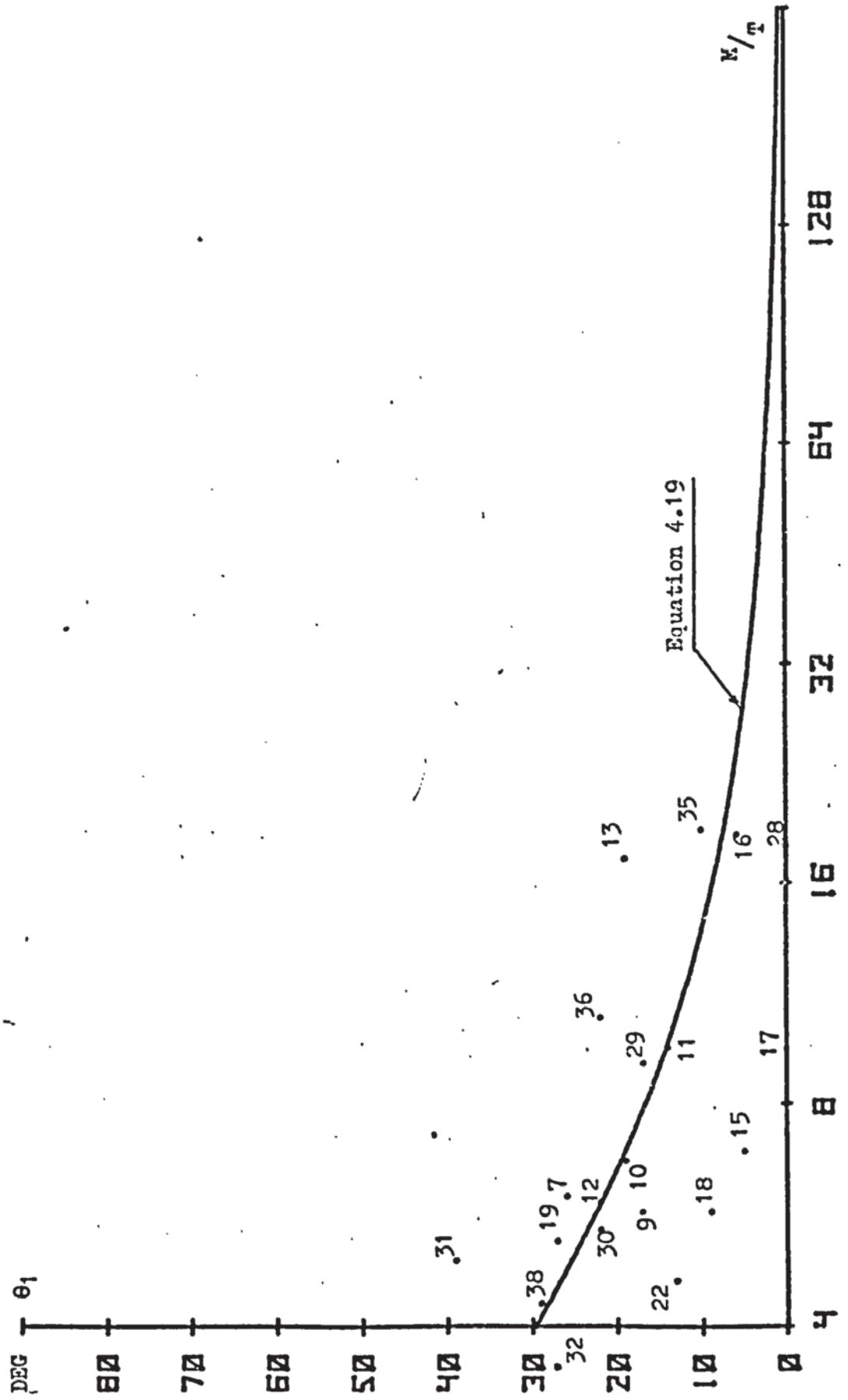

FIGURE 5.15 EFFECT OF $^{M}/_{T}$ RATIO ON CRACK ANGLE θ_1 - MODE 1

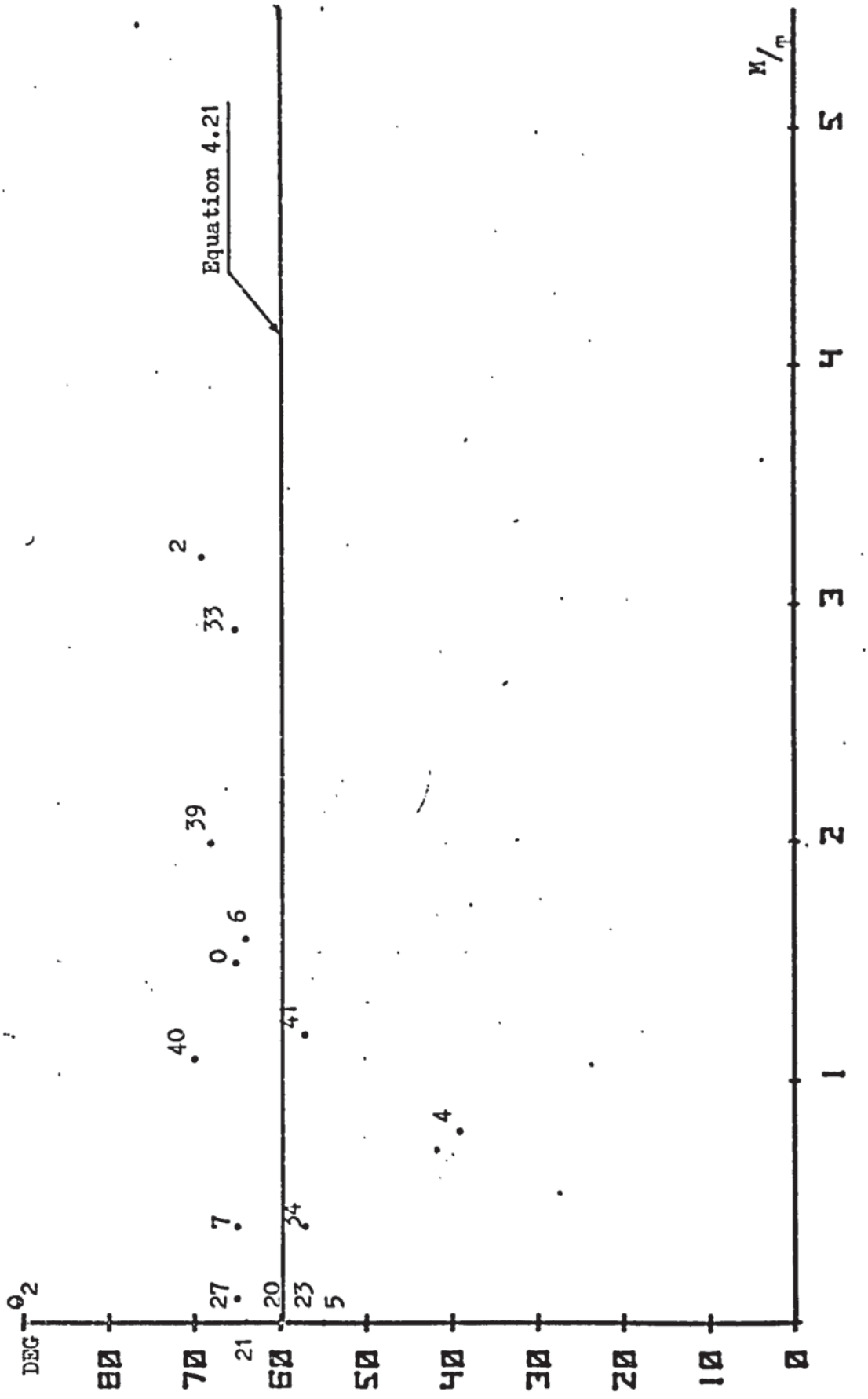

FIGURE 5.16 EFFECT OF $^{M}/_{T}$ RATIO ON CRACK ANGLE θ_2 - MODE 2

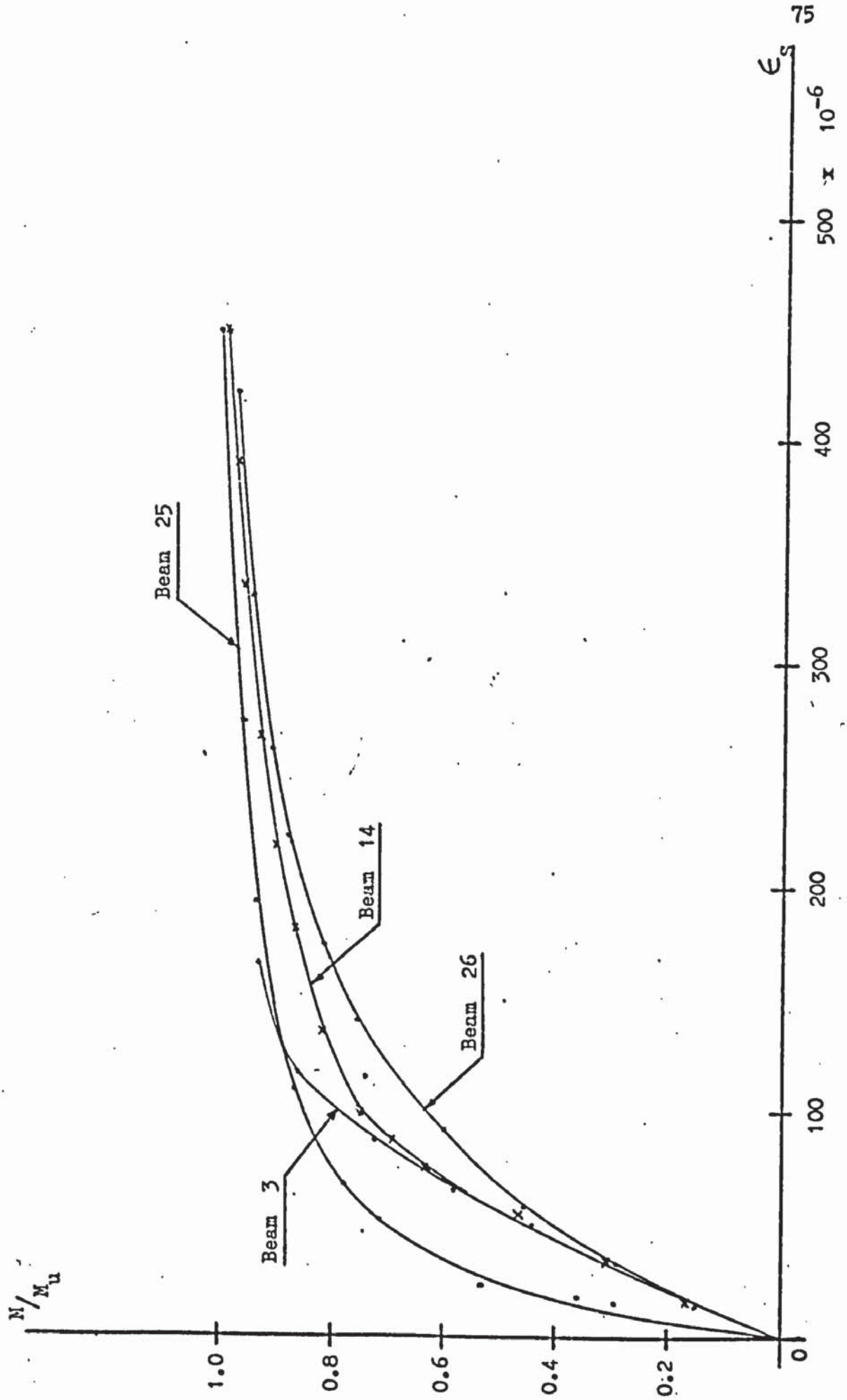

FIGURE 5.17 RELATIONSHIP BETWEEN AVERAGE STEEL STRAIN IN LOWER TENDON AND APPLIED MOMENT

Beam No.	a_v mm	p_{c2} N/mm^2	e mm	M kNm	T kNm	V kN	Series
0	600	7·10	29·0	4·87	3·19	14·43	1
1	600	7·41	29·0	13·77	2·53	8·23	1
2	600	7·75	29·0	9·15	2·86	6·33	1
3	600	7·99	29·0	15·75	0·00	8·63	1
4	600	7·62	29·0	2·71	3·55	8·89	1
5	600	7·70	29·0	0·12	3·19	1·25	1
6	800	7·33	29·0	4·40	2·79	13·09	1
7	800	7·24	29·0	1·12	2·93	4·46	1
9	800	7·64	29·0	13·62	2·38	8·75	1
10	800	8·13	29·0	14·10	2·11	18·98	1
11	800	7·07	29·0	14·94	1·58	9·16	1
12	800	7·15	29·0	14·10	2·38	8·95	1
13	800	7·32	29·0	16·31	0·94	10·08	1
14	800	7·37	29·0	17·10	0·00	10·49	1
15	600	7·17	29·0	13·23	1·91	7·36	1
16	600	8·19	29·0	17·84	0·96	9·94	1
17	600	7·67	29·0	14·96	1·57	8·70	1
18	600	7·07	29·0	12·29	2·16	7·24	1
19	600	7·86	29·0	12·63	2·45	7·26	1
20	–	7·43	29·0	-0·11	2·93	0·26	1
21	–	7·13	29·0	-0·10	3·02	0·24	1
22	800	8·06	29·0	12·00	2·59	7·49	1
23	–	7·70	30·1	0·13	3·48	0·41	2
25	800	7·64	29·8	13·77	0·00	8·44	2
26	600	7·54	29·0	14·31	0·00	7·92	2
27	–	7·24	29·0	0·33	2·80	0·01	2
28	600	7·43	27·9	14·11	0·79	7·74	2
29	600	7·53	27·7	13·57	1·49	7·45	2
30	600	7·69	29·5	11·94	2·20	6·79	2
31	600	7·72	29·1	11·42	2·33	6·65	2
32	600	7·56	29·1	10·23	2·62	5·90	2
33	600	7·38	29·1	8·59	2·92	5·58	2
34	600	7·55	29·2	1·37	3·60	4·50	2
35	800	7·79	29·0	14·21	0·75	8·94	2
36	800	7·74	28·3	14·55	1·38	8·92	2
37	800	7·58	29·1	11·86	1·99	7·41	2
38	800	7·83	29·2	10·25	2·41	6·93	2
39	800	7·64	28·5	7·03	3·49	5·17	2
40	800	7·58	29·5	4·19	3·66	3·69	2
41	600	7·57	27·8	3·80	3·19	10·94	2

TABLE 5.1 AUTHOR'S RESULTS

Beam No.	y * mm	$\frac{M}{M_u}$	$\frac{T}{T_u}$	$\frac{V}{V_u}$	$\frac{M}{T}$	Mode
0	362	0.31	1.07	0.19	1.5	2
1	785	0.87	0.85	0.11	5.4	1
2	1030	0.58	0.96	0.08	3.2	2
3	650	1.00	0.00	0.11	∞	1
4	350	0.17	1.19	0.12	0.8	2
5	2120	0.01	1.07	0.02	0.0	2
6	360	0.26	0.94	0.17	1.6	2
7	325	0.07	0.98	0.06	0.4	2
9	920	0.80	0.80	0.11	5.7	1
10	750	0.82	0.71	0.25	6.7	1
11	850	0.87	0.53	0.12	9.5	1
12	900	0.82	0.80	0.12	5.9	1
13	875	0.95	0.32	0.13	17.3	1
14	875	1.00	0.00	0.14	∞	1
15	640	0.84	0.64	0.10	6.9	1
16	675	1.13	0.32	0.13	18.6	1
17	750	0.95	0.53	0.11	9.5	1
18	755	0.78	0.72	0.09	5.7	1
19	700	0.80	0.82	0.09	5.2	1
20	615	-0.01	0.98	0.00	-0.0	23
21	1825	-0.01	1.01	0.00	-0.0	23
22	860	0.70	0.87	0.10	4.6	1
23	2225	0.01	1.11	0.01	0.0	23
25	875	1.00	0.00	0.11	∞	1
26	670	1.00	0.00	0.10	∞	1
27	1220	0.02	0.89	0.00	0.1	23
28	650	0.99	0.25	0.10	17.9	1
29	650	0.95	0.47	0.09	9.1	1
30	725	0.83	0.70	0.09	5.4	1
31	775	0.80	0.74	0.08	4.9	1
32	750	0.71	0.83	0.08	3.9	12
33	988	0.60	0.93	0.07	2.9	2
34	2200	0.10	1.15	0.06	0.4	2
35	920	1.03	0.24	0.11	18.9	1
36	875	1.06	0.44	0.11	10.5	1
37	910	0.86	0.63	0.09	6.0	1
38	1050	0.74	0.77	0.09	4.3	12
39	1200	0.51	1.11	0.07	2.0	2
40	1430	0.30	1.17	0.05	1.1	2
41	345	0.27	1.02	0.14	1.2	2

* y = distance of Critical Section from left hand support.

TABLE 5.2 AUTHOR'S RESULTS - CONTINUED

Beam No	CRACK ANGLES - DEGREES					
	Front Face	Bottom	Back Face	Top	† Experimental	* Theoretical
0	65	22	63	45	65	60
1	55	0	16	72	0	23
2	69	62	80	75	69	61
3	0	0	0	0	0	0
4	66	64	39	39	39	58
5	68	42	55	42	55	59
6	64	45	73	54	64	60
7	65	0	73	60	65	59
9	48	17	55	-	17	22
10	8	19	45	62	19	22
11	0	14	45	-	14	15
12	7	22	22	-	22	22
13	5	19	0	-	19	8
14	0	0	0	-	0	0
15	5	5	5	-	5	19
16	6	6	6	-	6	8
17	53	0	0	60	0	14
18	63	9	16	76	9	24
19	49	27	5	58	27	24
20	60	72	76	39	60	60
21	75	68	64	44	64	58
22	13	13	13	-	13	26
23	72	48	59	46	59	60
25	0	0	0	-	0	0
26	-	0	-	-	0	0
27	75	61	65	38	65	60
28	0	0	0	-	0	9
29	3	17	10	-	17	15
30	45	22	32	71	22	23
31	13	39	49	-	39	29
32	27	27	10	63	27	30
33	65	52	78	75	65	59
34	74	33	57	65	57	60
35	0	10	37	-	10	7
36	22	22	0	-	22	12
37	14	26	46	66	26	22
38	59	31	76	75	31	29
39	74	43	68	50	68	60
40	77	52	70	50	70	59
41	57	35	65	33	57	60

† Mode 1 - Bottom, Mode 2 - Front Face or Back Face

* Mode 1 - Equation 4.19, Mode 2 - Equation 4.21

TABLE 5.3 CRACK ANGLES OF FAILURE SURFACE

	INCREASE IN TENDON FORCE AT FAILURE kN			
	Bottom Steel		Top Steel	
Beam No.	Experimental	Theoretical	Experimental	Theoretical
1	20.9	15.8		
3	15.1	17.0		
9	19.3	14.6		
10	12.0	11.4		
11	27.3	24.4		
12	18.8	15.1		
13	26.4	19.7		
14	32.0	27.3		
15	16.4	21.7		
16	23.0	19.8		
17	33.1	18.7		
18	21.2	21.6		
19	19.5	18.1		
22	16.5	17.6		
25	3.9	5.4	0.5	1.9
26	6.1	5.3	1.3	1.8
28	6.7	5.1	.7	1.8
29	5.8	4.2	.1	1.3
30	3.8	2.5	.3	.7
31	2.8	2.9	.3	.9
32	2.3	2.2	.3	.6

TABLE 5.4 INCREASE IN TENDON FORCE AT FAILURE, MODE 1
EXPERIMENTAL AND THEORETICAL VALUES

Beam No.	Depth of Compression Zone - mm			Maximum Concrete Strain - με	
	Theoretical		Experimental	Theoretical	Experimental
	Using f'_c	Using f_{cu}			
1	65	68	85	2000	1060
3	61	73	78	2004	940
9	72	70	155	1978	540
10	75	74	95	1927	1320
11	65	63	74	2184	2750
12	75	68	81	1917	1665
13	72	68	74	2023	3000
14	59	64	62	2298	5000
15	60	65	67	2121	1900
16	67	70	63	2173	2500
17	67	69	54	2073	2250
18	60	64	61	2122	1600
19	68	68	69	2148	1350
22	74	68	-	2174	1310
25	51	54	53	2535	2900
26	59	54	52	2494	2800
28	56	54	55	2456	2750
29	60	57	57	2329	2600
30	62	63	66	2098	1500
31	67	60	-	2230	1140
32	65	63	-	2052	1180
35	57	53	87	2580	5500
36	60	57	51	2367	3160
37	59	55	57	2404	1900
38	69	62	98	2183	1060

TABLE 5.5. COMPARISON OF THEORETICAL AND EXPERIMENTAL RESULTS MODE 1

DEPTH OF COMPRESSION ZONE

MAXIMUM CONCRETE STRAIN

6. COMPARISON OF THEORETICAL AND EXPERIMENTAL VALUES FOR THE ULTIMATE STRENGTH

In this section the theoretical failure loads found from the equations determined in section 4 are compared with the experimental values listed in section 5 and with the few comparable results of McMullen (35). Moment, torque and shear interaction curves are presented in each case.

The effect of shear is studied by a comparison of the author's results with those of Wainwright (7), Evans and Khalil (21) and Farley (32).

6.1 Author's Results, Mode 1

The values of M_1 given in tables 6.1 and 6.2 have been calculated from equation 4.5 using either the experimental value of cylinder strength, or the equivalent cylinder strength based on the experimental cube strength.

The values of bond slip factor B were determined from strain gauge readings on the beams tested under moment only - see section 8.5. A variable B based on a_v and the ratio of M/M_u had no significant effect on the pattern of results; the simpler, constant B for each series was thus used. In practice, much of the load is uniformly distributed on a beam, and the value of B will not vary so widely; guidance on its selection is available - in e.g. Rajasekaran (39) and Warwaruk (40). In Series 1 beams, a change in B from 0.1 to 0.3 resulted in an increase in M_1 of less than 11%, whilst in Series 2 beams, a change from .05 to 0.15 increased M_1 by less than 6%. The value of B is thus not critical.

Individual results for M_1 vary quite widely between tables 6.1 and

6.2, but overall the mean of 1.02 and coefficient of variation of 12% are the same. Either cube or cylinder strength tests may thus be used.

Examining table 6.2 the following points are noted :-

(a) taking Series 1 and Series 2 beams separately, the M/M_1 means are slightly greater and slightly less than one respectively.

(b) the beams for which M/M_1 is significantly smaller than one are numbers 22, 32 and 38. These beams have M/T ratios between 3.9 and 4.6, and are thus on the border of both Mode 1 and Mode 2 regions (see section 5.2).

(c) the experimental value of moment varied from 23% above the theoretical to 21% below it.

6.2 Author's Results, Mode 2

The comparisons shown in table 6.3 are based on equation 4.22, and use either the experimental value of modulus of rupture, or a value calculated from the cylinder strength using the equation given by Hsu (13).

Two methods of comparison are used. In the first the torque is predicted for a given value of V; in the second the left hand side of equation 4.22 is compared with the theoretical value of 1. Both lead to similar results. The following points are noted :-

(a) using f_r leads to safe results, only two values of T_2 lying very slightly below the experimental value T.

(b) the Hsu equation gives closer means and lower coefficients of variation, showing that it gives a value of f_t which fits equation 4.22 better than the experimental f_r . It is also useful where only compressive strengths have been measured.

(c) either method may be used to predict the failure torque. In the first method, the experimental value of torque varied from 40% above

to 1% below the theoretical. In the second method the range was + 21% to - 8%.

6.3 Author's Results, Mode 3

None of the author's beams were observed to fail in this mode. Comparisons are made in table 6.4 using equation 4.24 with either experimental values of f_r , or using the equation given by Hsu (13). In this case only values of the mean are given, as the coefficient of variation is not applicable to such a small number of specimens. The first method gives safe results, the experimental value of torque varied from 21% above to 1% below the theoretical.

On comparison of the Mode 3 and Mode 2 results we see that in only one case is a Mode 2 failure predicted - in Beam 27, using method 1.

6.4 Author's Results - Interaction Diagrams

6.4.1 Moment/Torque

The comparison of theory with experiment is shown in Fig. 6.1 for Series 1 beams and in Fig. 6.2 for Series 2 beams. The theoretical curves are based on average f_r and f'_c values, for all beams. The following points are noted :-

(a) the theory is generally conservative, except for the region near the intersection of Modes 1 and 2

(b) in Mode 2 a slight increase in torque appears to occur for moments between 2 and 8 kNm. The theory, in fact, predicts a decrease (due to the increase in shear)

(c) there is some indication that small amounts of torque may increase the ultimate moment of the section

(d) for this size and shape of section, with this level of

prestress, a Mode 3 failure might just occur for small moments.

(e) the $^{M}/_{T}$ curves are also drawn for shears of 10 and 20 kN. The Mode 3 curve is unaltered, whilst both Modes 1 and 2 change as shown.

6.4.2 Shear/Torque

The comparison of theory with experiment is shown in Fig.6.3 for all beams failing in Mode 2. The skew bending method using the experimental value of the modulus of rupture gives a good lower bound to the experimental results. More tests are needed to show, conclusively, that increasing the shear reduces the torque capacity of the section.

6.5 McMullen's Results

The results of McMullen's tests on eight beams with no stirrups are summarised in Table 6.5. The main differences between these tests and those carried out by the author were

(a) the beams were pretensioned with six strands, two of which were near the top of the beam.

(b) the eccentricity of prestress was less than that of the author.

(c) the average value of prestress was 35% lower.

(d) no cube strength or cylinder splitting strength tests were carried out.

(e) the amount of prestress and eccentricity were given, but the distribution between strands was not, except that the 'top strands were stressed to a lower level than the bottom strands'.

(f) the ratio of $^{h}/_{b}$ was greater, at 2.0

(g) the average value of cylinder strength was 17% greater, but the modulus of rupture was 5% less. The latter tests were carried out on 150 mm square prisms.

6.5.1 Mode 1

The values of M_1 given in Table 6.6 have been calculated from equation 4.5 using the experimental value of cylinder strength. The bond slip factor has been taken as 1. A factor of 1.1 gave a mean of 1.08 with the coefficient of variation remaining at 8%. Values between 0.9 and 1.1 are normally suggested. The formula given by Warwaruk (40), using the theoretical value of x, gives B between 0.90 and 0.95 for an ultimate strain in the concrete of .0035 .

The predicted moments are in all cases lower than the actual moments. It should be noted, however, that all four of the beams had high $M/_T$ ratios, the ultimate torque being less than half the Mode 2 type failure torque.

6.5.2 Mode 2

In table 6.7 the beams failing in Mode 2 are examined in a similar manner to the author's beams. Both the experimental value of f_r , and the empirical value based on the cylinder strength have been used. Neither method is very accurate, leading to unsafe results for beam I - 6. On the other hand, beam 5 failed at a much higher torque than expected. The number of tests were, however, very small.

6.5.3 Mode 3

No beams were mentioned as having failed in this manner. Beam I - 5 has been examined in Table 6.6 using experimental and empirical values of f_r , giving very different results. In both cases, however, the theoretical failure torque for Mode 2 is lower and thus limits.

6.5.4 Moment/Torque Interaction Diagram

The theoretical curve is shown in Fig. 6.4, together with the experimental results. The Mode 3 curve is based on the concrete properties of beam I - 5; the other curves are based on averages for beams failing in that mode. For Mode 2, the experimental value of f_r has been used, whilst for Mode 1 that for f'_c .

The following points are noted :-

(a) beams I - 6 and I - 8 lie within their corresponding theoretical curves, i.e., the theory is unsafe (I - 8 very slightly).

(b) beam I - 5 failed at a much higher torque than expected.

(c) all other beams lie quite close to the expected curve.

(d) a Mode 3 failure is most unlikely to occur with this shape of section, and level of compressive prestress on the top face.

6.5.5 Summary

Agreement of the author's theory with the pretensioned beams is disappointing. However, it must be remembered that the number of results is very small and scatter is bound to be a problem, particularly in the modes of failure which depend on the tensile strength of the concrete. It is possible that bonded beams are stronger in torsion, for low moments, than unbonded. One explanation might be that dowel action can take place with well bonded tendons, in this mode.

6.6 The Effect of Shear

This will be studied by comparing the author's results with those of investigators who did not include shear in their tests.

In rectangular beams, the effect of shear is quite small and is often masked by the inevitable scatter of test results. When enough results are available a statistical approach may be used, but this is not the case at the present time.

Shear effects may also be hidden in another manner. The presence of shear implies a changing bending moment, and this in itself may alter the shape of the moment/torque interaction diagram drastically. This will be illustrated in the following paragraph.

6.6.1 Wainwright's Results

These tests were carried out on beams nominally the same as those of the author's Series 1 beams, but the loading arrangement was such as to give a constant bending moment on the test length.

The theoretical moment/torque interaction diagram is shown in Fig. 6.5, together with the experimental results.

For small values of applied moment, the beam fails in Mode 3. If the loading system is such that some section of the beam has zero or small moment whatever the load, the beam will fail at that section, and no Mode 2 failures will be possible. In practice, this will be modified to some extent by the length of the failure zone, and by any reinforcing steel which may be incorporated to prevent failure near the ends of the beams. However, the rising portion of the $M/_T$ curve will not be so pronounced when shear is present.

Comparing Figures 6.1 and 6.5, the following points are noted.

(a) in Mode 3 the shear has theoretically no effect on the

failure torque. The differences apparent are due to the slight differences in level of prestress and in the modulus of rupture. These are such that Mode 3 failures would not really be expected with the author's beams.

(b) in Mode 2, Wainwright's experimental values of torque average 3.96 kNm, much higher than the author's at 3.09 kNm. Theoretically, we should expect the results to be closer; using the Hsu formula for modulus of rupture gives values for T_2 of 3.31 kNm (Wainwright) and 3.03 (author) for no shear. The experimental differences are such that they completely overshadow any effect due to shear, which would be expected to reduce the torque by 0.32 kNm for a 20 kN shear force.

(c) in Mode 1, both theoretical and experimental values of moment are less for the author's beams. This is not wholly due to shear. The moments will be decreased by the bond slip factor being changed from 0.4 to 0.2, and the average prestress being reduced from 8.62 to 7.56 N/mm^2 . The moments will be increased by the cylinder strength being increased from 38.4 to 41.5 N/mm^2 .

6.6.2 Evans' Results

Evans and Khalil tested beams with concentric and eccentric prestress, but only those results from the eccentric case have been used here.

The main differences between their tests and those of the author's Series 2 tests were

(a) the average level of prestress was lower

(b) the ratio of $^h/_b$ was lower, at 1.6

(c) the average cube strength was 14%, and the modulus of rupture 7%, greater

(d) the ducts around the tendons were formed differently.

(e) the loading arrangement gave a constant bending moment on the test length.

The interaction curve is shown in Fig. 6.6, where it is seen that, in a similar manner to the author's results, Modes 2 and 3 nearly coincide at M = 0.

The Mode 2 results are quite close to the theoretical value shown, where the average experimental value of f_r has been used in the equations.

The Mode 1 theoretical curve is much less steep than in previous cases. This is because no dowel force has been assumed to take place at right angles to the tendons.

Since T_{u3} is approximately equal to T_{u2} , the curves have been drawn in a non-dimensional manner in Fig. 6.7, where they can be compared with the author's Series 2 results.

Beams failing in Mode 2 show a similar scatter in both cases, the amount of shear present having no notable effect.

In Mode 1, Evans' results are noticeably to the left of the author's. If shear were the only difference, we should expect them to lie to the right. However, as Wainwright has pointed out, the unbonded tendons had sufficient movement, in Evans' beams, to prevent any dowel action. This has the effect of increasing the shear stresses in the compressive zone, for the same torque, and thus the ultimate moments are reduced. The effect is such as to completely nullify the shear effect, which also reduces the ultimate moment.

6.6.3 Farley's Results

These are the results of tests on micro-concrete models with an external system of prestress. The other major differences between these tests and those carried out by the author were

(a) the average value of prestress was much lower at 3.13 N/mm^2 .

(b) the cube strength of the micro-concrete was much lower at 28.0 N/mm^2 .

(c) the ratio $^h/_b$ was higher at 2.67.

(d) the modulus of rupture, carried out on 100 mm square specimens, was lower at 2.85 N/mm^2 . On 80 mm deep specimens it was 3.08 N/mm^2 .

The interaction curve, shown in Fig. 6.8, is drawn for the experimental value of f_r = 2.86 N/mm^2 and a value of f'_c calculated from 0.8 x f_{cu} .

No Mode 3 failure was observed, and none would be expected from the theoretical curves. Although the prestress at the top of the beam was zero, the beam was of a very deep section, which would inhibit this mode.

The Mode 2 failures are fairly concentrated around the .10 kNm torque value, peaking slightly with moments of about .15 kNm.

As these tests were specifically designed to examine Mode 2, few Mode 1 failures occurred. Since no dowel force can be present, the curve will be less steep than the author's, and, as with Evans' results, the effect of shear will thus be hidden.

Since T_{u3} is greater than T_{u2} , the curves have been drawn in a non-dimensional manner and compared with all the author's results in Fig. 6.9.

The agreement here is close throughout the range, even though there was no shear in Farley's tests.

6.6.4 Summary

The effect of shear has been examined theoretically, but the experimental results are disappointingly inconclusive. In Mode 2, the small shear effects are masked by slight differences in tensile strengths of concrete, and levels of applied prestress. In Mode 1, lack of a dowel force overshadows any effect due to shear. Where dowel forces are present, the effects have again been hidden by changes in bond slip factor and levels of prestress.

6.7 Proposed Interaction Surface

Previous investigators have attempted to define an interaction surface; any point on this surface gives three values of the variables M, T, V which combine to cause failure in the section considered.

The first problem with such a surface is to represent it on a two-dimensional paper. This can be attempted by isometric drawing; the author prefers, however, to use a series of cross sections, parallel to the $^{M}/_{T}$ plane, for different values of V.

The second problem is, generally, the lack of information. Compared with a line, a surface requires much more data to define it, and this is often not available over large regions.

6.7.1 Previous Work

Bishara (33), Warwaruk (28, 29), McMullen (35) and Henry (8, 34) have proposed surfaces, as the result of their tests on prestressed beams incorporating mild steel reinforcement. These surfaces vary widely.

Bishara gives two empirical parabolic equations, one in the $^{M}/_{T}$ plane and the other in the $^{V}/_{T}$ plane.

Warwaruk has an empirical parabolic equation in the $^{M}/_{T}$ plane, but a linear or bi-linear one in the $^{V}/_{T}$ plane.

McMullen has quadrants of a circle in both the $^{M}/_{T}$ and $^{V}/_{T}$ planes, using non-dimensional axes.

Henry has a quadrant of a circle in the $^{M}/_{T}$ plane, and a straight line in the $^{V}/_{T}$ plane, with the axes non-dimensional.

McMullen is the only other investigator to examine the interaction surface for beams with no stirrups or mild steel longitudinal reinforcement. Again, his surface is empirical, the $^{M}/_{T}$ equation being linear, and the $^{V}/_{T}$ parabolic.

6.7.2 Author's Proposals

Using the equations in section 4, interaction surfaces may be deduced. The surfaces are necessarily tentative, as many more tests are needed to prove or disprove the equations in regions remote from the author's results.

Figures 6.10 and 6.11 show the interaction surface for Series 1 and Series 2 beams as a series of $^{M}/_{T}$ curves for constant values of V. The surface is completed by a vertical plane, parallel to the $^{M}/_{T}$ plane, passing through V_u = 76.9 kN or V_u = 78.5 kN respectively for the two series.

The surface so found is not, of course, suitable for design. An approximate load factor for an existing section could, however, be checked by this method. The data required for each Mode is as follows :-

(a) Mode 1. The cylinder strength, prestress forces and positions, areas of tendons, the modulus of rupture across the depth of the beam and the bond slip factor.

(b) Mode 2. The average level of prestress in the concrete and the modulus of rupture across the width of the beam.

(c) Mode 3. The level of prestress in the concrete at the top of the beam and the modulus of rupture across the depth of the beam.

The moduli of rupture may be found from the cylinder strength and the dimensions of the beam by using the Hsu formulae.

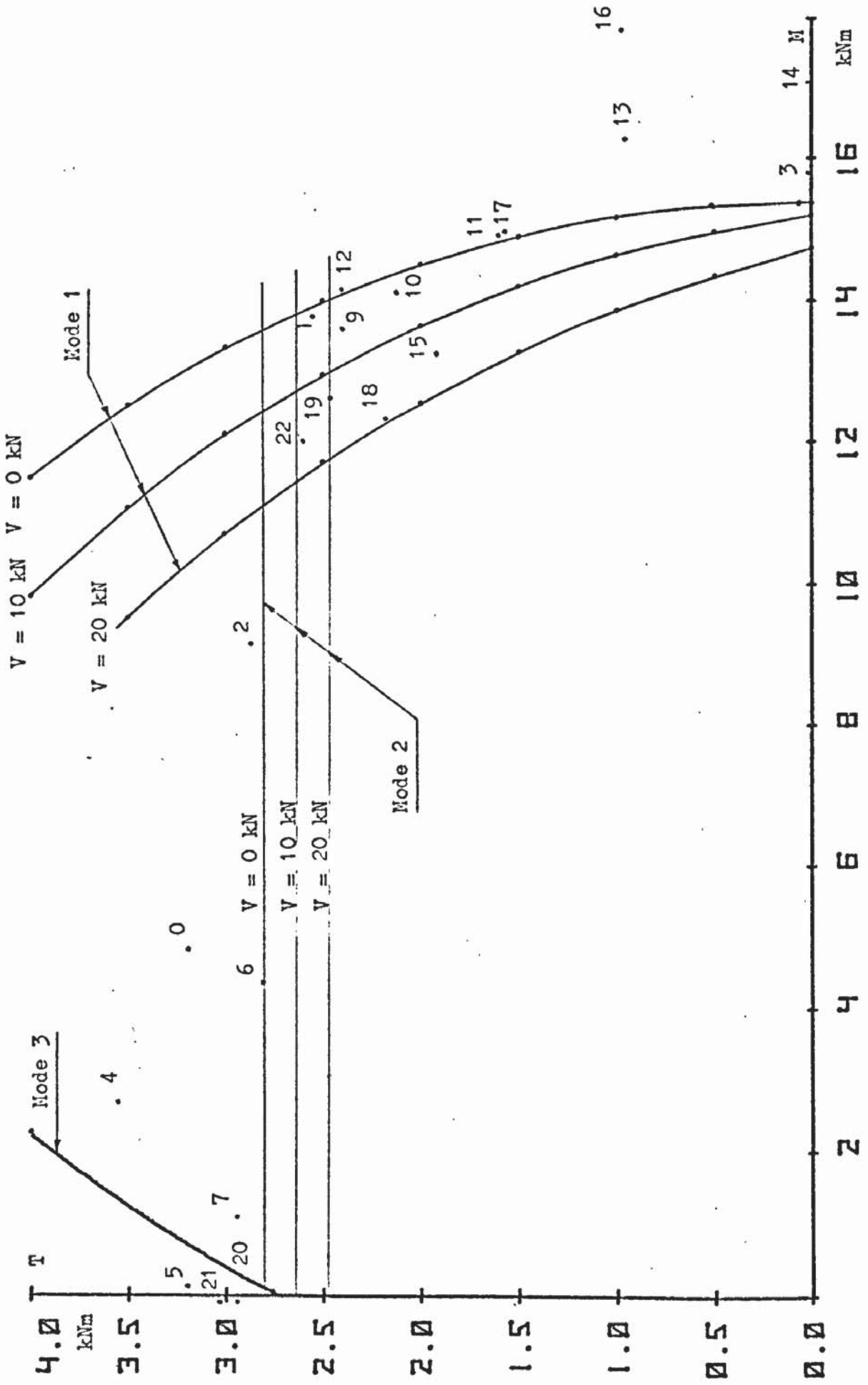

FIGURE 6.1 AUTHOR'S RESULTS MOMENT/TORQUE INTERACTION DIAGRAM

SERIES 1

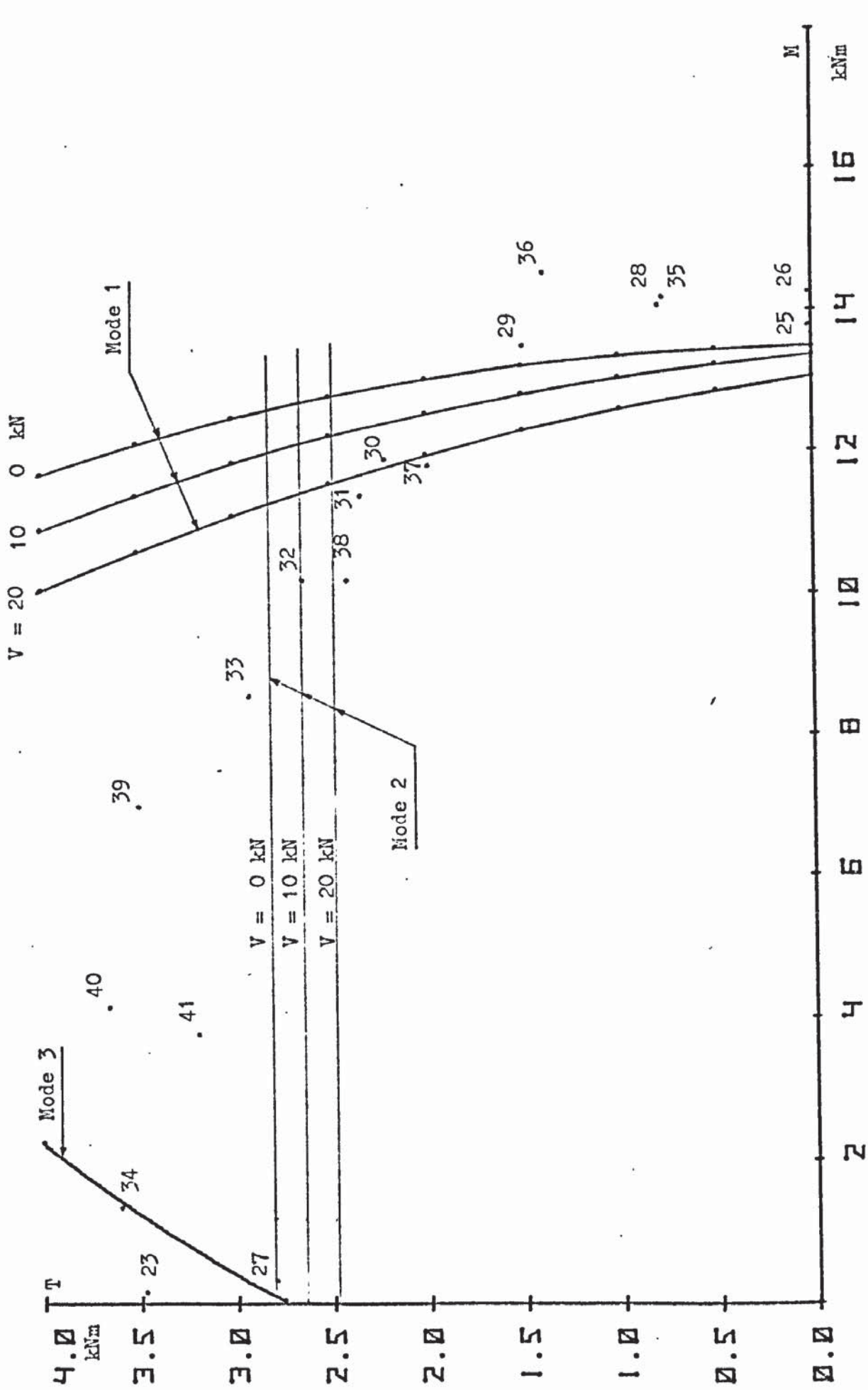

FIGURE 6.2 AUTHOR'S RESULTS MOMENT/TORQUE INTERACTION DIAGRAM

SERIES 2

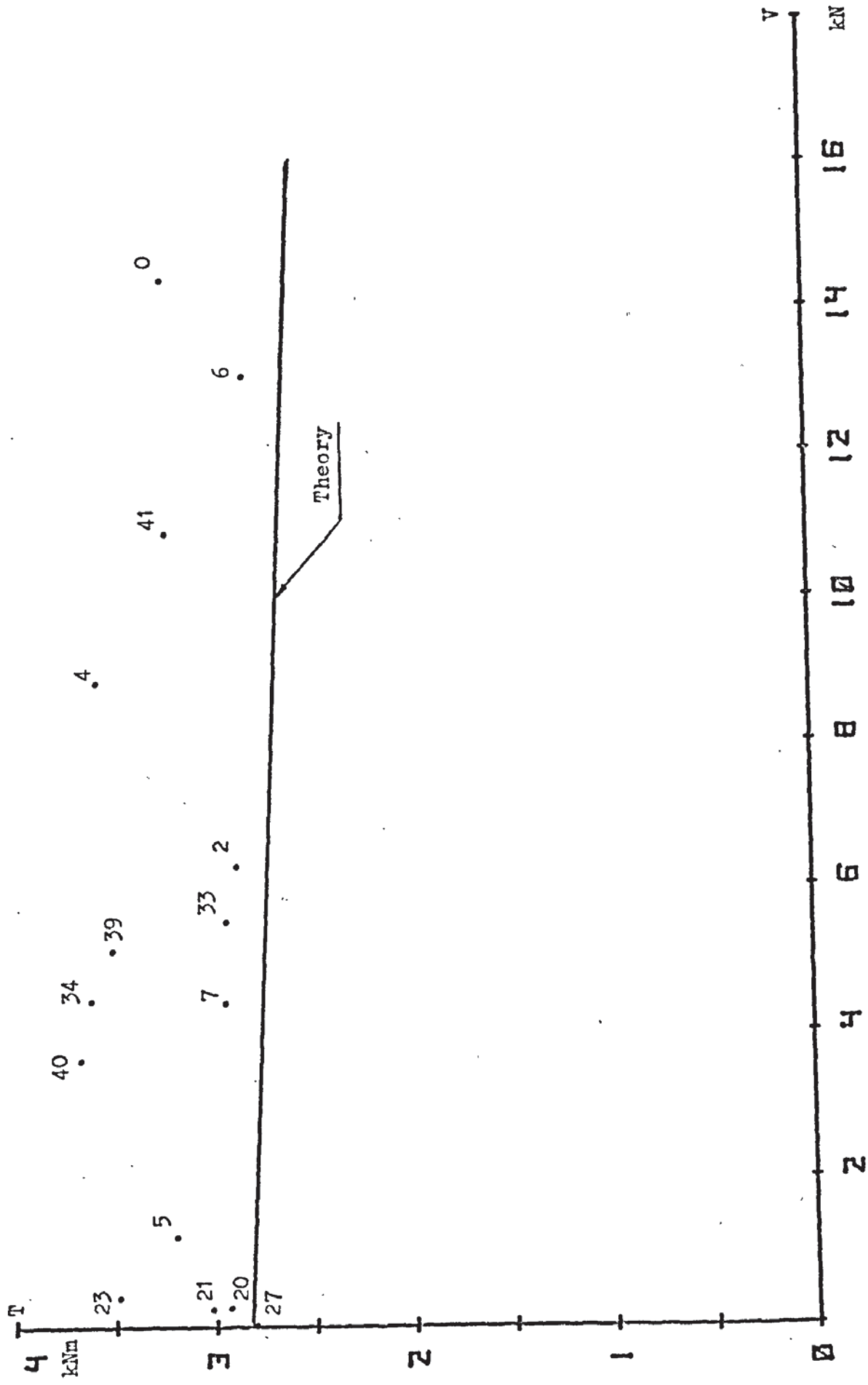

FIGURE 6.3 AUTHOR'S RESULTS SHEAR/TORQUE INTERACTION DIAGRAM MODE 2

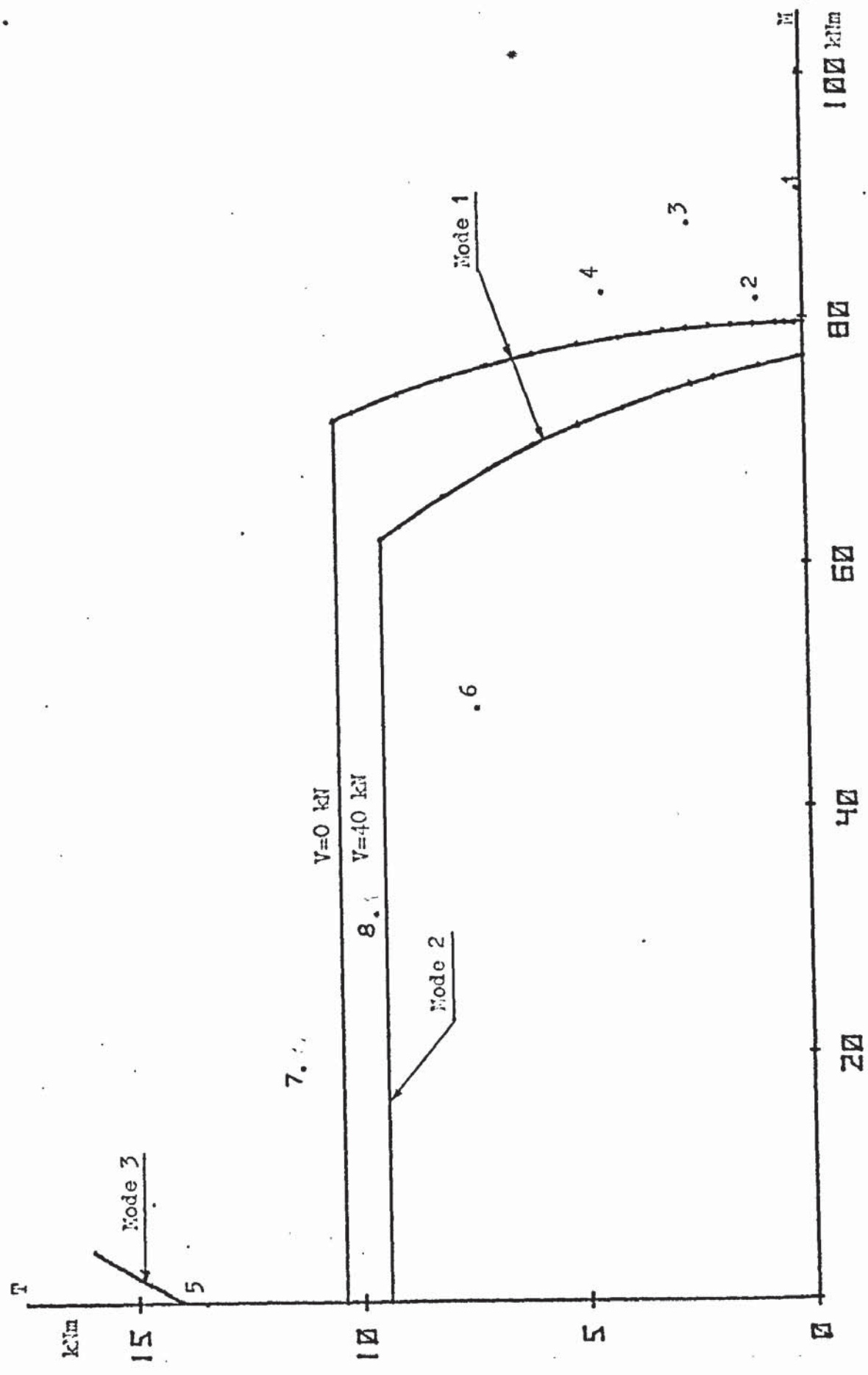

FIGURE 6.4 McMULLEN'S RESULTS MOMENT/TORQUE INTERACTION DIAGRAM

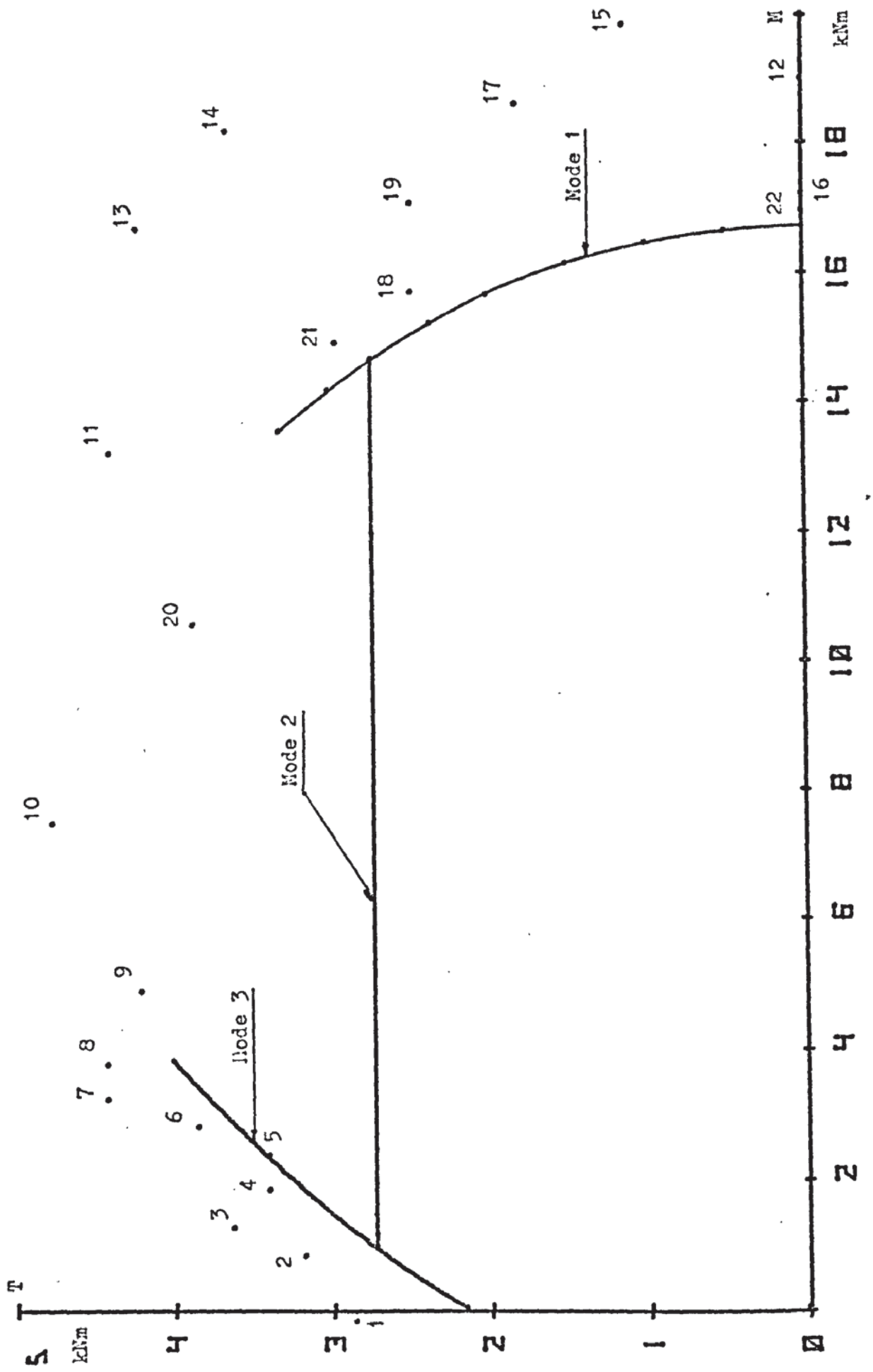

FIGURE 6.5. WAINWRIGHT'S RESULTS MOMENT/TORQUE INTERACTION DIAGRAM

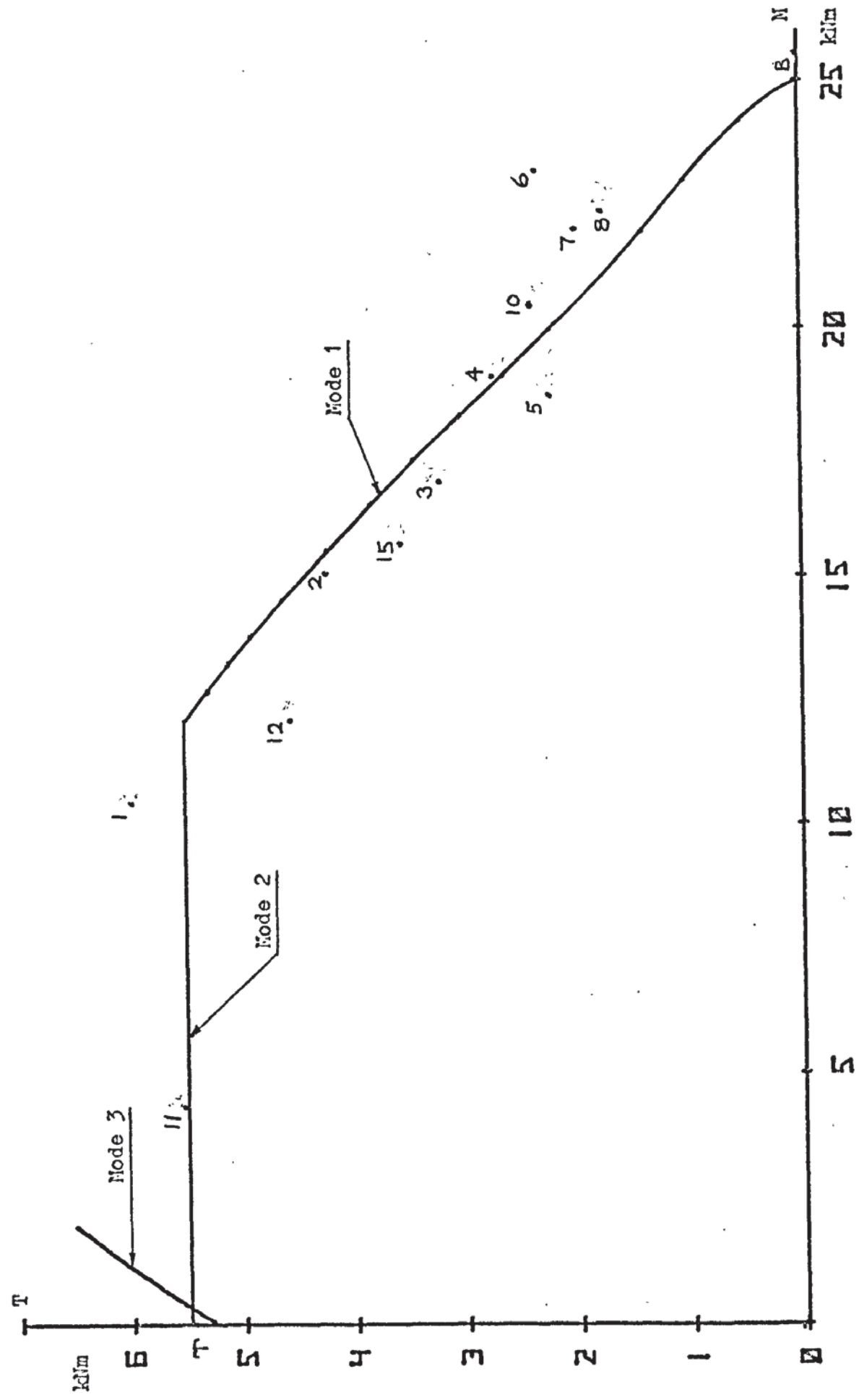

FIGURE 6.6 EVANS' RESULTS MOMENT/TORQUE INTERACTION DIAGRAM

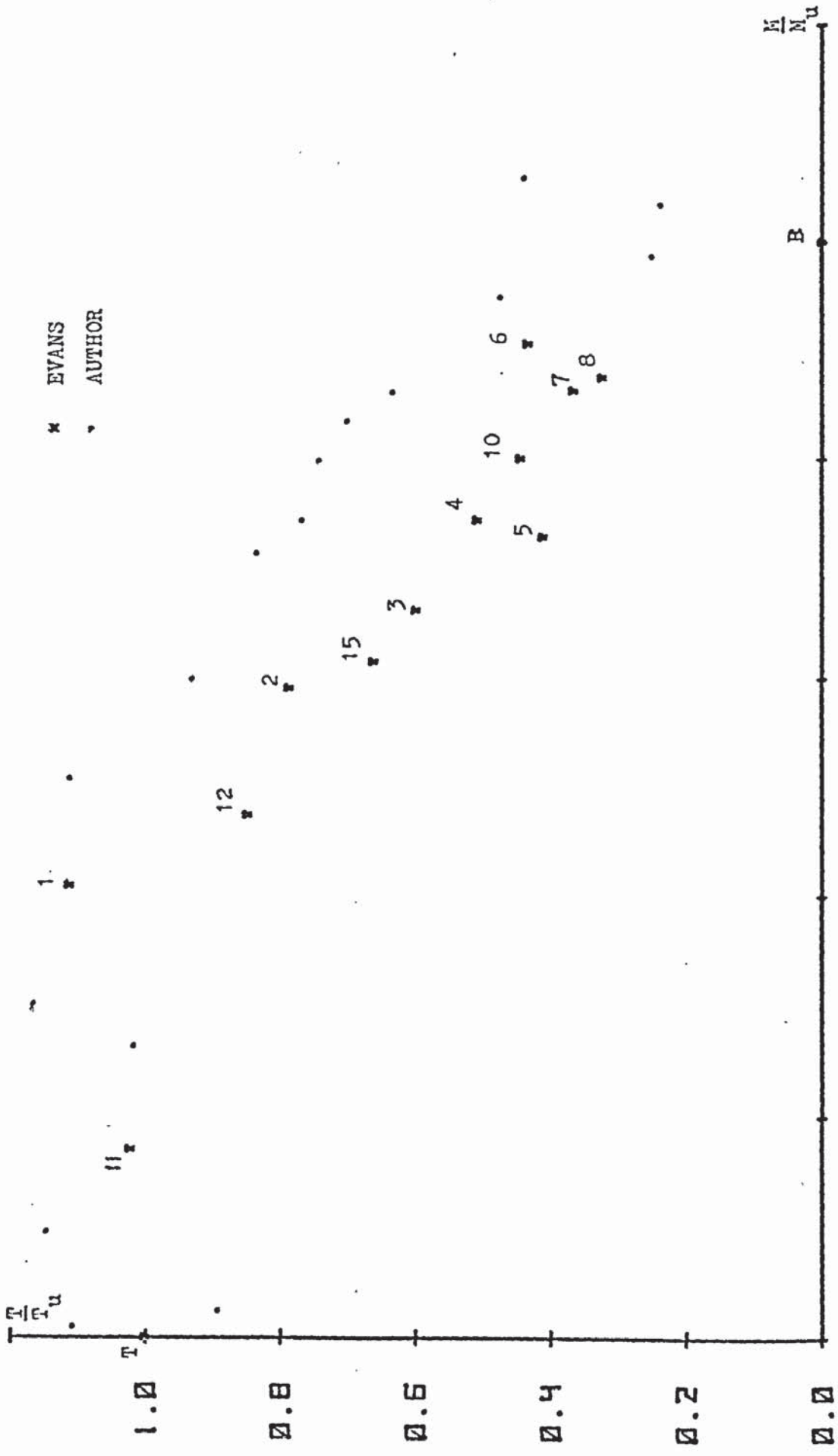

FIGURE 6.7 COMPARISON OF AUTHOR'S SERIES 2 AND EVANS' RESULTS
NON-DIMENSIONAL MOMENT/TORQUE INTERACTION DIAGRAM

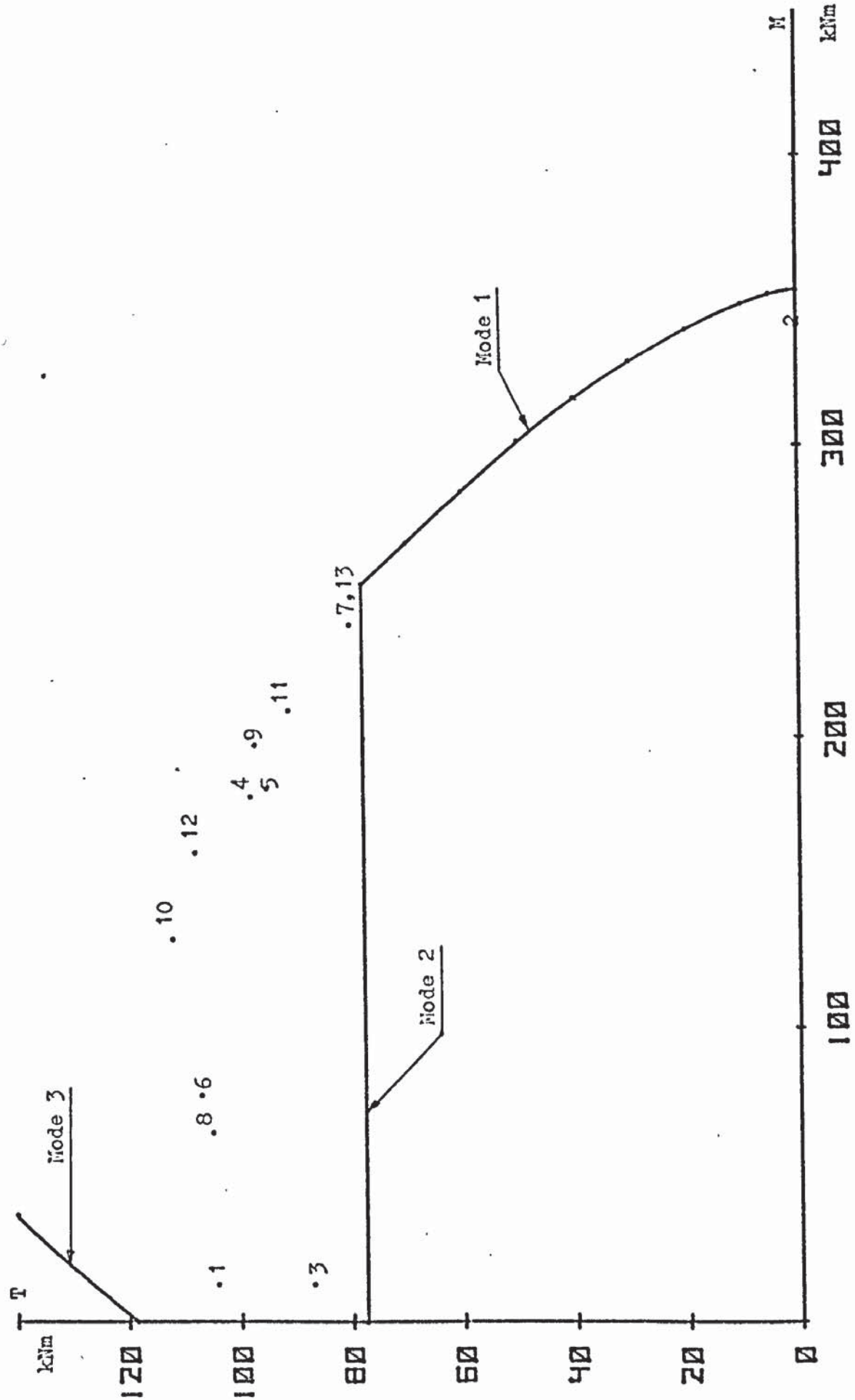

FIGURE 6.8 FARLEY'S RESULTS MOMENT/TORQUE INTERACTION DIAGRAM

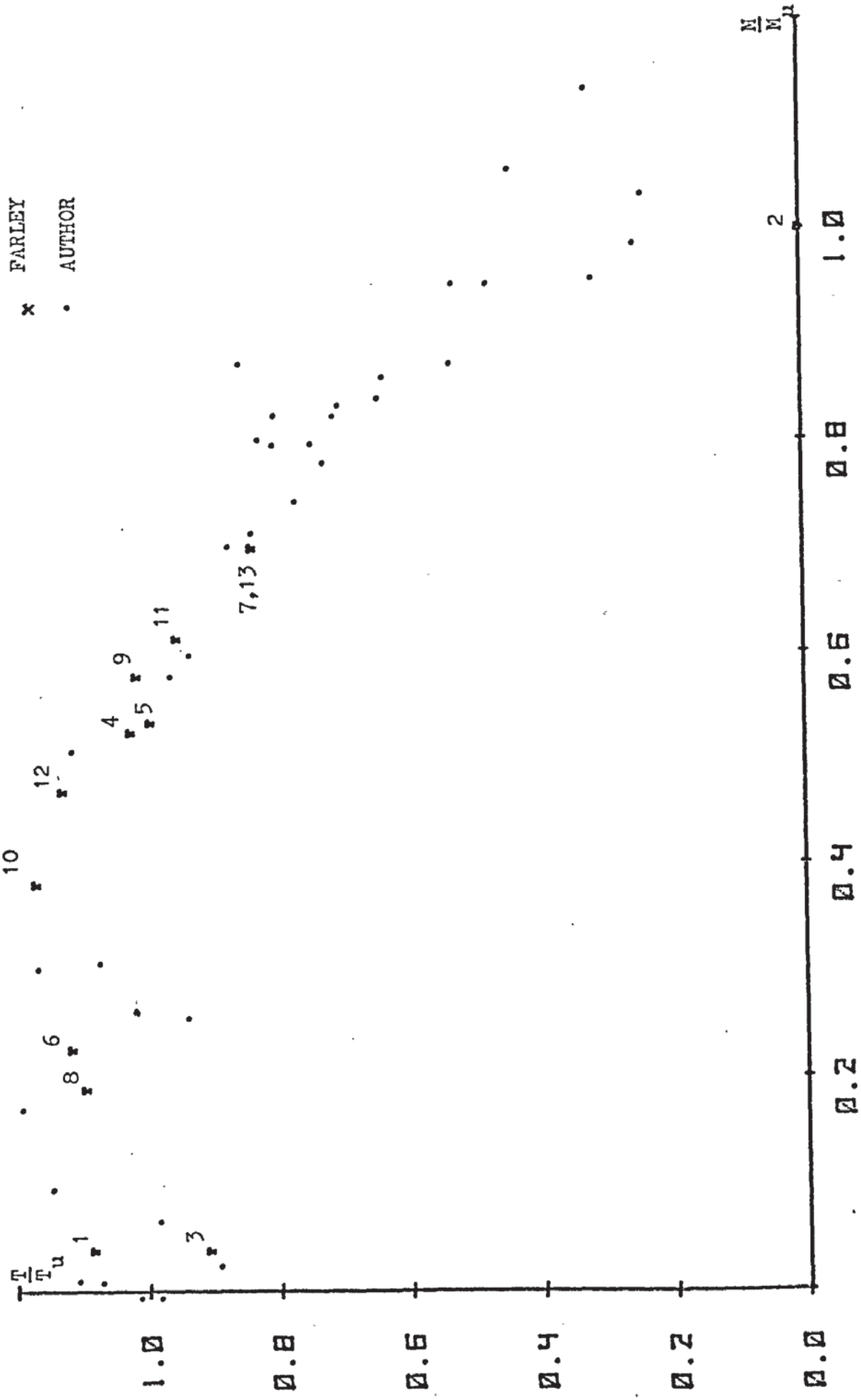

FIGURE 6.9 COMPARISON OF AUTHOR'S AND FARLEY'S RESULTS NON-DIMENSIONAL MOMENT/TORQUE INTERACTION DIAGRAM

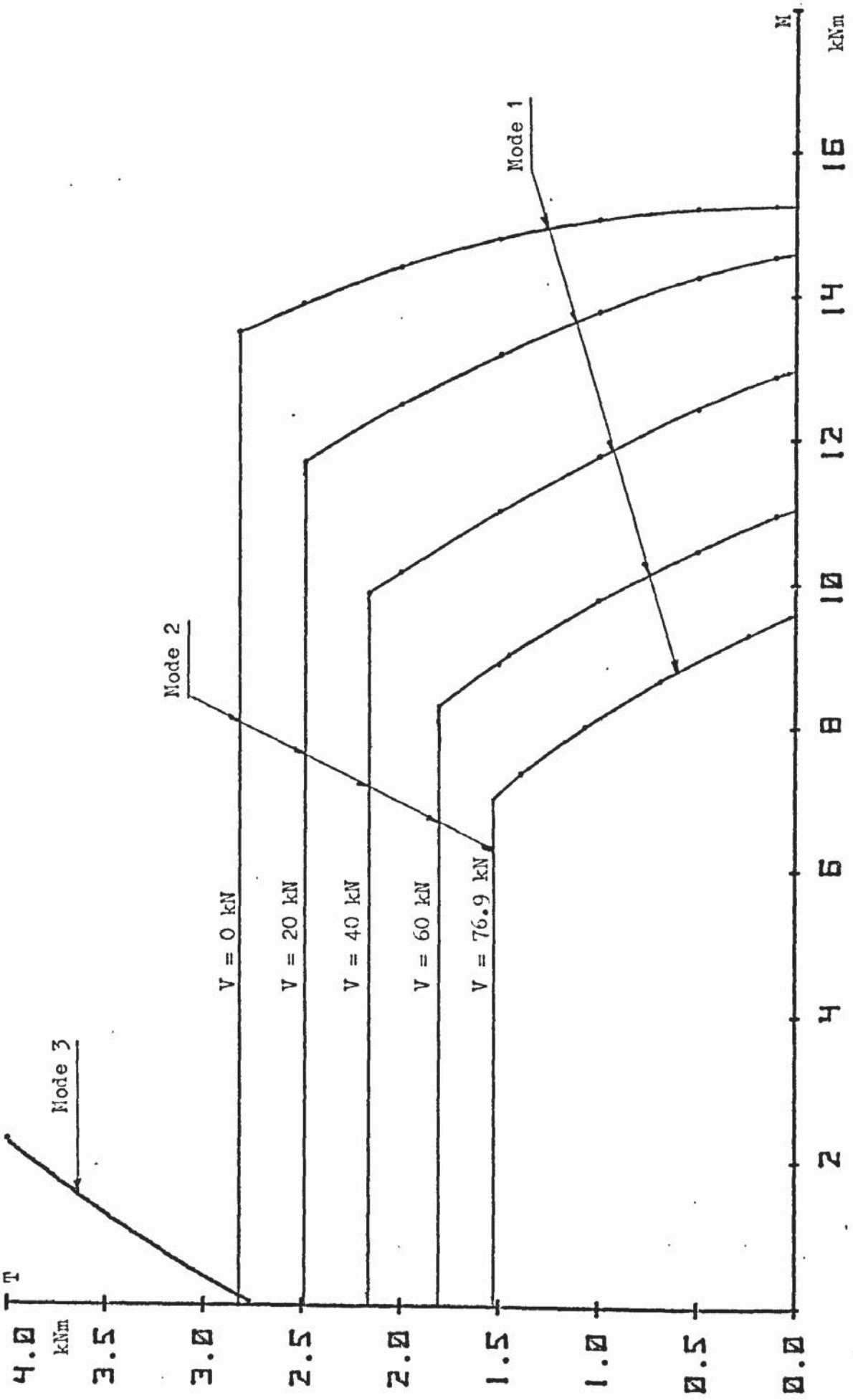

FIGURE 6.10 INTERACTION SURFACE, SERIES 1

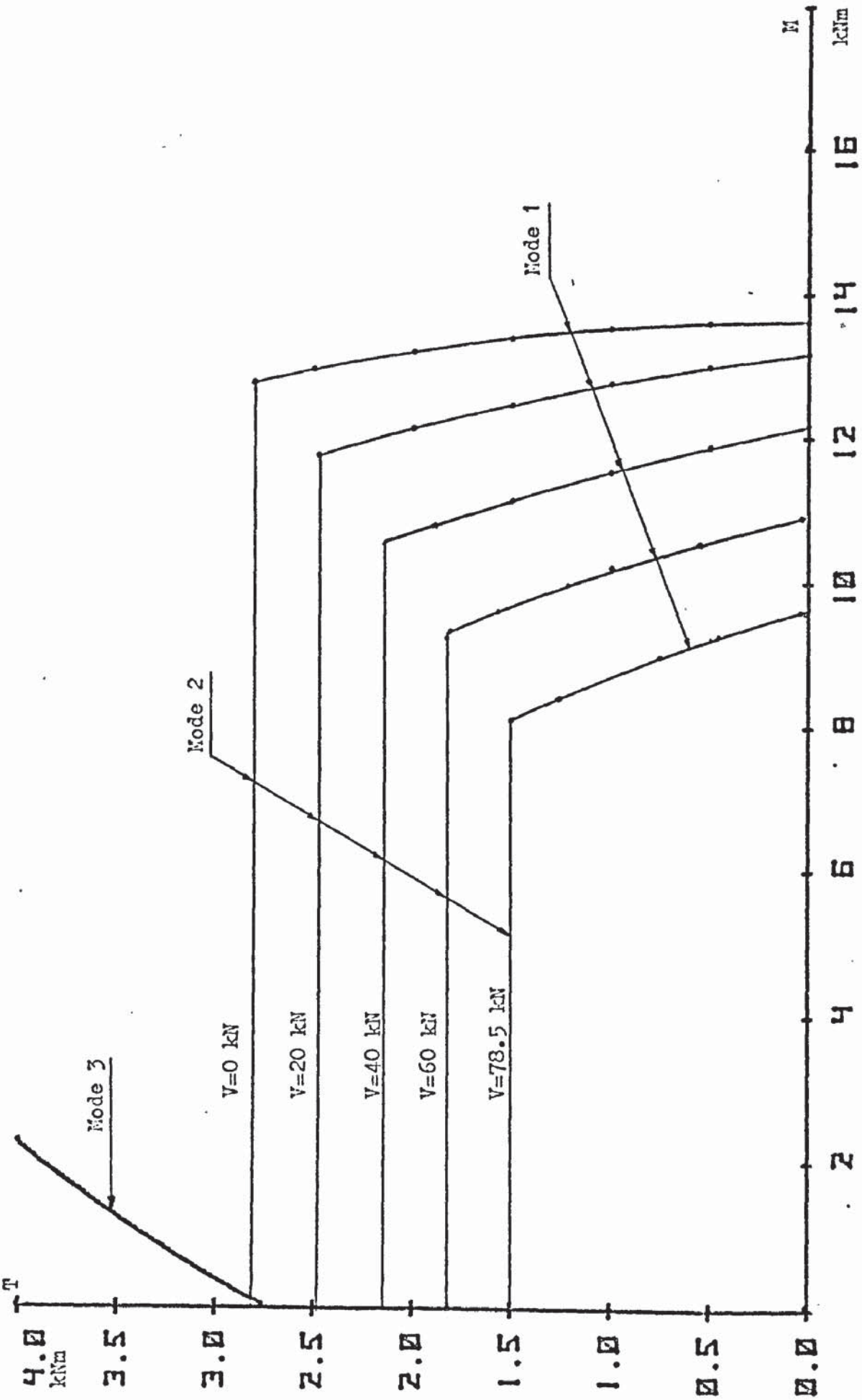

FIGURE 6.11 INTERACTION SURFACE , SERIES 2

Beam No.	B	T kNm	V kN	M kNm	* M_1 kNm	$\frac{M}{M_1}$
1	0.20	2.53	8.23	13.77	13.60	1.01
3	0.20	0.00	8.63	15.75	16.20	0.97
9	0.20	2.38	8.75	13.62	12.96	1.05
10	0.20	2.11	18.98	14.10	13.39	1.05
11	0.20	1.58	9.16	14.94	13.31	1.12
12	0.20	2.38	8.95	14.10	11.57	1.22
13	0.20	0.94	10.08	16.31	12.67	1.29
14	0.20	0.00	10.49	17.10	15.40	1.11
15	0.20	1.91	7.36	13.23	14.60	0.91
16	0.20	0.96	9.94	17.84	15.18	1.18
17	0.20	1.57	8.70	14.96	14.07	1.06
18	0.20	2.16	7.24	12.29	14.27	0.86
19	0.20	2.45	7.26	12.63	14.02	0.90
22	0.20	2.59	7.49	12.00	13.34	0.90
25	0.08	0.00	8.44	13.77	13.93	0.99
26	0.08	0.00	7.92	14.31	12.92	1.11
28	0.08	0.79	7.74	14.11	12.82	1.10
29	0.08	1.49	7.45	13.57	12.62	1.08
30	0.08	2.20	6.79	11.94	12.91	0.93
31	0.08	2.33	6.65	11.42	12.47	0.92
32	0.08	2.62	5.90	10.23	12.35	0.83
35	0.08	0.75	8.94	14.21	13.49	1.05
36	0.08	1.38	8.92	14.55	13.03	1.12
37	0.08	1.99	7.41	11.86	12.93	0.92
38	0.08	2.41	6.93	10.25	12.53	0.82
				MEAN		1.02
				COEFFT. OF VARIATION		12.1%

* Using equation 4.5 with

$V_1 = V$

$T_1 = T$

and experimental values of f'_c

TABLE 6.1 COMPARISON OF EXPERIMENTAL AND THEORETICAL RESULTS - MODE 1

Beam No.	B	T kNm	V kN	M kNm	* M_1 kNm	$\frac{M}{M_1}$
1	0.20	2.53	8.23	13.77	13.10	1.05
3	0.20	0.00	8.63	15.75	13.83	1.14
9	0.20	2.38	8.75	13.62	13.24	1.03
10	0.20	2.11	18.98	14.10	13.47	1.05
11	0.20	1.58	9.16	14.94	13.60	1.10
12	0.20	2.38	8.95	14.10	12.61	1.12
13	0.20	0.94	10.08	16.31	13.30	1.23
14	0.20	0.00	10.49	17.10	14.34	1.19
15	0.20	1.91	7.36	13.23	13.43	0.99
16	0.20	0.96	9.94	17.84	14.56	1.23
17	0.20	1.57	8.70	14.96	13.72	1.09
18	0.20	2.16	7.24	12.29	13.31	0.92
19	0.20	2.45	7.26	12.63	14.04	0.90
22	0.20	2.59	7.49	12.00	14.28	0.84
25	0.08	0.00	8.44	13.77	13.69	1.01
26	0.08	0.00	7.92	14.31	13.40	1.07
28	0.08	0.79	7.74	14.11	13.04	1.08
29	0.08	1.49	7.45	13.57	12.87	1.05
30	0.08	2.20	6.79	11.94	12.78	0.93
31	0.08	2.33	6.65	11.42	13.00	0.88
32	0.08	2.62	5.90	10.23	12.46	0.82
35	0.08	0.75	8.94	14.21	13.84	1.03
36	0.08	1.38	8.92	14.55	13.27	1.10
37	0.08	1.99	7.41	11.86	13.22	0.90
38	0.08	2.41	6.93	10.25	13.05	0.79
				MEAN		1.02
				COEFFT. OF VARIATION		12.0%

* Using equation 4.5 with

$V_1 = V$

$T_1 = T$

$f'_c = 0.8\, f_{cu}$

TABLE 6.2 COMPARISON OF EXPERIMENTAL AND THEORETICAL RESULTS - MODE 1

Beam No.	V kN	T kNm	* T_2 kNm	$\frac{T}{T_2}$	† $\frac{T}{T'_{u2}}$	† $\frac{V}{V'_{u2}}$	$\frac{T}{T'_{u2}} + \frac{V}{V'_{u2}}$
0	14.43	3.19	2.44	1.31	1.19	0.09	1.28
2	6.33	2.86	2.57	1.11	1.07	0.04	1.11
4	8.89	3.55	3.11	1.14	1.09	0.05	1.13
5	1.25	3.19	3.09	1.03	1.03	0.01	1.03
6	13.09	2.79	2.44	1.14	1.05	0.08	1.13
7	4.46	2.93	2.74	1.07	1.04	0.03	1.07
20	0.26	2.93	2.73	1.07	1.07	0.00	1.07
21	0.24	3.02	3.05	0.99	0.99	0.00	0.99
23	0.41	3.48	2.90	1.20	1.20	0.00	1.20
27	0.01	2.80	2.65	1.06	1.06	0.00	1.06
33	5.58	2.92	2.95	0.99	0.96	0.03	0.99
34	4.50	3.60	2.58	1.40	1.36	0.03	1.39
39	5.17	3.49	2.82	1.24	1.20	0.03	1.23
40	3.69	3.66	2.97	1.23	1.21	0.02	1.23
41	10.94	3.19	2.69	1.19	1.11	0.06	1.17
MEAN				1.14			1.14
COEFFT. OF VARIATION				10.2%			9.8%

* Using equation 4.22 with $V_2 = V$

† Using equation 4.22 with $T_2 = T$ and $V_2 = V$

Both using $f_{r2} = f_r$

Beam No.	V kN	T kNm	* T_2 kNm	$\frac{T}{T_2}$	† $\frac{T}{T'_{u2}}$	† $\frac{V}{V'_{u2}}$	$\frac{T}{T'_{u2}} + \frac{V}{V'_{u2}}$
0	14.43	3.19	2.82	1.13	1.04	0.08	1.12
2	6.33	2.86	3.02	0.95	0.91	0.03	0.95
4	8.89	3.55	3.21	1.11	1.06	0.04	1.10
5	1.25	3.19	3.28	0.97	0.97	0.01	0.97
6	13.09	2.79	2.79	1.00	0.93	0.07	1.00
7	4.46	2.93	3.03	0.97	0.94	0.02	0.97
20	0.26	2.93	3.20	0.92	0.92	0.00	0.92
21	0.24	3.02	3.18	0.95	0.95	0.00	0.95
23	0.41	3.48	3.22	1.08	1.08	0.00	1.08
27	0.01	2.80	2.96	0.94	0.94	0.00	0.94
33	5.58	2.92	2.96	0.99	0.96	0.03	0.99
34	4.50	3.60	3.03	1.19	1.16	0.02	1.18
39	5.17	3.49	3.09	1.13	1.10	0.03	1.13
40	3.69	3.66	3.02	1.21	1.19	0.02	1.21
41	10.94	3.19	2.95	1.08	1.02	0.06	1.08
MEAN				1.04			1.04
COEFFT. OF VARIATION				9.3%			9.0%

* Using equation 4.22 with $V_2 = V$

† Using equation 4.22 with $T_2 = T$ and $V_2 = V$

Both using $f_{r2} = 1.32\sqrt[3]{f'_c}$

TABLE 6.3 COMPARISON OF EXPERIMENTAL AND THEORETICAL RESULTS - MODE 2

Beam No.	M kNm	T kNm	* T_3 kNm	$\frac{T}{T_3}$	† $\left[\frac{T}{T'_{u3}}\right]^2$	† $\frac{M}{M_{u3}}$	$\left[\frac{T}{T'_{u3}}\right]^2 - \frac{M}{M_{u3}}$
20	-0.11	2.93	2.57	1.14	1.23	-0.06	1.29
21	-0.10	3.02	3.05	0.99	0.93	-0.05	0.98
23	0.13	3.48	2.88	1.21	1.56	0.07	1.49
27	0.33	2.80	2.77	1.01	1.20	0.18	1.03
MEAN				1.09			1.19

* Using equation 4.24 with $M_3 = M$

† Using equation 4.24 with $T_3 = T$ and $M_3 = M$

Both using $f_{r3} = f_r$

Beam No.	M kNm	T kNm	* T_3 kNm	$\frac{T}{T_3}$	† $\left[\frac{T}{T'_{u3}}\right]^2$	† $\frac{M}{M_{u3}}$	$\left[\frac{T}{T'_{u3}}\right]^2 - \frac{M}{M_{u3}}$
20	-0.11	2.93	2.58	1.14	1.22	-0.06	1.28
21	-0.10	3.02	2.63	1.15	1.25	-0.05	1.30
23	0.13	3.48	2.79	1.25	1.67	0.07	1.60
27	0.33	2.80	2.86	0.98	1.13	0.17	0.95
MEAN				1.13			1.28

* Using equation 4.24 with $M_3 = M$

† Using equation 4.24 with $T_3 = T$ and $M_3 = M$

Both using $f_{r3} = 1.1\sqrt[3]{0.8\, f_{cu}}$

TABLE 6.4 COMPARISON OF EXPERIMENTAL AND THEORETICAL RESULTS - MODE 3

Beam No.	f'_c N/mm^2	f_r N/mm^2	p_{c2} N/mm^2	e mm
I - 1	47.2	3.41	4.55	16.5
I - 2	47.2	3.41	4.55	37.6
I - 3	49.5	3.71	5.51	38.1
I - 4	49.5	3.71	4.83	37.1
I - 5	39.7	3.79	5.35	31.0
I - 6	39.7	3.79	5.17	38.8
I - 7	51.1	3.94	4.69	32.5
I - 8	51.1	3.94	4.69	29.2
Mean	46.9	3.71	4.92	-
Coeff.^{t} of Var.^{n} %	10.0	5.6	7.6	-

Beam No.	M kNm	T kNm	V kN	$\frac{M}{T}$	Mode
I - 1	90.4	0.0	46.3	∞	1
I - 2	81.5	1.0	41.6	81.5	1
I - 3	87.7	2.5	44.8	35.1	1
I - 4	82.1	4.4	41.9	18.7	1
I - 5	0.0	13.5	0.0	0.0	2
I - 6	48.4	7.3	31.7	6.6	2
I - 7	19.2	11.3	12.8	1.7	2
I - 8	31.6	9.6	21.4	3.3	2

TABLE 6.5 McMULLEN'S RESULTS

MODE 1

Beam No.	T kNm	V kN	M kNm	* M_1 kNm	$\frac{M}{M_1}$
I - 1	0.00	46.30	90.40	72.85	1.24
I - 2	1.00	41.60	81.50	77.16	1.06
I - 3	2.50	44.80	87.70	81.25	1.08
I - 4	4.40	41.90	82.10	77.43	1.06
MEAN					1.11
COEFFT. OF VARIATION					8%

* Using equation 4.5 with $V_1 = V$ and $T_1 = T$

with experimental values of f'_c

MODE 3

Beam I - 5 only

	M kNm	T kNm	* T_3 kNm	$\frac{T}{T_3}$	† $\left[\frac{T}{T'_{u3}}\right]^2$	† $\frac{M}{M_{u3}}$	$\left[\frac{T}{T'_{u3}}\right]^2 - \frac{M}{M_{u3}}$
1	0.00	13.50	13.97	0.97	0.93	0.00	0.93
2	0.00	13.50	12.01	1.12	1.26	0.00	1.26

* Using equation 4.24 with $M_3 = M$

† Using equation 4.24 with $T_3 = T$ and $M_3 = M$

Line 1 using $f_{r3} = f_r$

Line 2 using $f_{r3} = 0.93 \sqrt[3]{f'_c}$

TABLE 6.6 COMPARISON OF EXPERIMENTAL AND THEORETICAL RESULTS BY McMULLEN MODES 1 AND 3

Beam No.	V kN	T kNm	* T_2 kNm	$\frac{T}{T_2}$	† $\frac{T}{T'_{u2}}$	† $\frac{V}{V'_{u2}}$	$\frac{T}{T'_{u2}} + \frac{V}{V'_{u2}}$
I - 5	0.00	13.50	10.41	1.30	1.30	0.00	1.30
I - 6	31.70	7.30	9.52	0.77	0.71	0.08	0.79
I - 7	12.80	11.30	10.05	1.12	1.09	0.03	1.12
I - 8	21.40	9.60	9.84	0.98	0.92	0.05	0.98
MEAN				1.04			1.04
COEFFT. OF VARIATION				22%			21%

* Using equation 4.22 with $V_2 = V$

† Using equation 4.22 with $T_2 = T$ and $V_2 = V$

Both using $f_{r2} = f_r$

Beam No.	V kN	T kNm	* T_2 kNm	$\frac{T}{T_2}$	† $\frac{T}{T'_{u2}}$	† $\frac{V}{V'_{u2}}$	$\frac{T}{T'_{u2}} + \frac{V}{V'_{u2}}$
I - 5	0.00	13.50	10.42	1.30	1.30	0.00	1.30
I - 6	31.70	7.30	9.52	0.77	0.71	0.08	0.78
I - 7	12.80	11.30	10.42	1.08	1.05	0.03	1.08
I - 8	21.40	9.60	10.21	0.94	0.89	0.05	0.94
MEAN				1.02			1.03
COEFFT. OF VARIATION				22%			21%

* Using equation 4.22 with $V_2 = V$

† Using equation 4.22 with $T_2 = T$ and $V_2 = V$

Both using $f_{r2} = 1.11 \sqrt[3]{f'_c}$

TABLE 6.7 COMPARISON OF EXPERIMENTAL AND THEORETICAL RESULTS BY McMULLEN - MODE 2

7. CONCLUSIONS AND RECOMMENDATIONS

In this investigation the behaviour of prestressed concrete beams loaded in combined torsion, bending and shear has been examined. Theoretical expressions for the prediction of the ultimate conditions have been derived.

The following conclusions and recommendations are based on tests on forty rectangular post-tensioned, unbonded beams containing no stirrups and are not necessarily applicable to other types of beams.

7.1. Conclusions

1. Under high M/T ratios, failure of the concrete at the top of the beam is considered to be governed by the Cowan failure criteria under a combination of direct and shear stress; the latter is taken as the summation of stress due to torsion and to shear force. This Mode 1 skew bending failure predicted by the analysis occurred in practice in twenty five of the beams tested.

2. The theory for a Mode 1 failure has been presented for use where dowel action is present at right angles to the tension steel, as in the author's beams. It may easily be modified for cases where lateral movement of the steel in the duct is possible.

3. Under lower M/T ratios a Mode 2 type of failure occurs, where a compression hinge forms on a side of the beam. The skew theory developed leads to a linear relationship between torque and shear. Failure is assumed to occur when the maximum tensile stress reaches the modulus of rupture of the concrete. Fifteen of the beams tested failed in this mode.

4. For eccentrically prestressed beams subjected to low moments a Mode 3 type of failure may occur, where the compression hinge is at

the bottom of the beam. This did not take place in the author's test beams. Theory shows the relationship between moment and torque to be parabolic, and independent of shear. Failure is again assumed to occur when the maximum tensile stress reaches the modulus of rupture of the concrete.

5. For the twenty five beams failing in Mode 1, the mean ratio of M_{test} / M_{theory} is 1.02 with a coefficient of variation of 12%.

For the fifteen beams failing in Mode 2, the mean ratio of T_{test} / T_{theory} is 1.04 with a coefficient of variation of 9%.

6. A theoretical moment/torque/shear interaction surface is proposed and has been drawn for the author's beams. It has only been substantiated by test results in regions of low shear force.

7. Flexural stiffnesses of the beams agreed reasonably well with the theoretical values. The Series 2 beams, with four small diameter prestressing wires, were slightly less stiff than the Series 1, with one large diameter alloy bar.

8. Torsional stiffnesses of the beams were less than the theoretical values for both series. The formation of bending cracks hardly affected the torsional stiffness.

9. It is not possible to predict crack angles with any degree of accuracy. The theory proposed is based on a rectangular plane of failure, and takes no account of the changing value of the moment along the length of the beam. This can obviously be very great over a failure length of over 1 m.

10. Longitudinal strain gauge readings were useful on beams tested under moment only, enabling the bond slip factor to be deduced. On other beams the results were not so useful, as only rarely were the gauges placed on the failure section.

7.2 Recommendations

It is not yet possible to formulate good design procedures for prestressed concrete beams under combined loads. The number of test results are so far very few, and do not cover many important aspects. Each investigation requires many tests, in order to reduce the effects of scatter. This might be done by a combination of a small number of full scale tests with a large number of model tests, where appropriate. Investigations into the following are suggested :-

1. The differences between pre- and post-tensioned, with grouted and unbonded tendons.

2. The effect of duct size on the creation of dowel forces.

3. The effect of beam size. This is known to affect the modulus of rupture. If the size effect is not too great, or can be interpreted, then many more model tests may be carried out.

4. The effect of prestress level and eccentricity.

5. The effect of varying the ratio $^{h}/_{b}$ for rectangular beams.

6. The effect of stirrups on the cracking and ultimate conditions.

7. A theoretical analysis into failures near the intersection of Modes 1 and 2.

When these investigations have been completed it should be possible to establish design formulae for rectangular beams.

Finally, the effects of shape of section should be examined, to cover box, tee and I - beams.

8. APPENDIX

8.1 THE DATA LOGGER

The Series 2 test readings were taken using an 'Intercole Systems Compulog'. This data logger incorporated a computer, which processed the readings as required so that the information printed out by the teletype was immediately useful. A programme 'Constrain' was in existence for converting voltages from strain gauges into true strain readings. A new programme 'Constrain 2' was written by the author to enable readings from linear transducers (L T's) and load cells (L C's) to be printed out directly in mm and kN respectively.

The linear transducers (used in place of the dial gauges in Series 1 tests) were Ether PD 20, 10 kΩ potentiometer type with a claimed accuracy of .15% of the maximum voltage. The constant voltage input was somewhat less than 5 volts; an output of this value corresponded to a movement of 50 mm. The actual supply voltage was monitored on one channel of the data logger, but did not vary significantly from the value of 4.86 $\pm$ .01 V originally set up. The constant of 11.25 entered into the computer was an average value obtained from a calibration run on two transducers.

The load cells were used to measure vertical load, torsional load and load in each of the four prestressing wires. They were Mayes Model 403 type compression load cells with capacities of 100, 50, 30 and 10 kN. A constant voltage of 4.90 $\pm$ .01 V was applied, and the constants fed into the computer were obtained from calibration runs of two load cells. The claimed accuracy is 0.25% of applied load.

Notes on the 'Use of Constrain (2)', the programme itself and examples of the data input and output are reproduced overleaf.

USE OF CONSTRAIN (2)

This programme is a development of 'CONSTRAIN' and is contained on a tape in binary form. It is fed into the data logger on the high speed reader.

Entering the Programme

1. Reset
2. Stop
3. P down, enter 2,F,B,B (0010, 1111, 1011, 1011)
4. I, X and A enter 0
5. Run
6. Check A = 0

P = 1, F, E, 0 (0001, 1111, 1110, 0000)

Running the Programme

1. Reset
2. Stop
3. P down, enter 0, 6, 6, A (0000, 0110, 0110, 1010)
4. I, X and A enter 0
5. Run

The teletype now prints - CONSTRAIN (2)

FEED BASIC DATA

PAUSE

and awaits the data tape, which again is fed in via the high speed reader.

Punching the Data Tape

HI	CR	LF	SPACES/TITLE/SPACES (total exactly 50)	HI
	CR	LF	NTYPGA, NTPRO, NTYPLT, NTYPLC	HI
	CR	LF	NOTYGA, NCHANL, NCHANH, GF, GR, E, PR	HI
	CR	LF	(repeat for each type of gauge)	HI
	CR	LF	NOTYGA, NCHANL, NCHANH, NCHANV, CVALUE	HI
	CR	LF	(Repeat for each type of linear transducer and load cell)	HI

CR LF HI

Notes

CR Carriage Return

LF Line Feed

HI Here Is

NTYPGA	Number of types of strain gauge	(0 - 10)
NTYPRO	Zero (at moment)	
NTYPLT	Number of types of linear transducer	(0 - 10)
NTYPLC	Number of types of load cell	(0 - 10)

(BUT total no. of types of GA, LT & LC limited to 10)

NOTYGA	Type number of strain gauge	(1 - 10)
NCHANL	Lowest channel number of GA	(0 - 99)
NCHANH	Highest channel number of GA	(0 - 99)
GF	Gauge factor of strain gauge	e.g. 2.10
GR	Gauge resistance of gauge	e.g. 120.0
E	Young's Modulus	e.g. 12.0E+03
PR	Poisson's Ratio	e.g. 0.15
NOTYGA	Type number of LT or LC	(1 - 10)
NCHANL	Lowest channel number of LT or LC	(0 - 29)
NCHANH	Highest channel limited as above	(0 - 29)
NCHANV	Voltage channel number but maximum no. of 10	(0 - 99)
CVALUE	Conversion factor $\frac{\text{Load}}{\text{Output volts}}$ or $\frac{\text{Deflection}}{\text{Output volts}}$ for LT or LC	e.g. 5.000

Operation of Programme

After PAUSE the computer awaits the data tape.

1. Feed data tape into high speed reader
2. Press Run. The teletype now prints out all the data supplied, and then asks 'LOAD INCREMENT NO. ?'

3. Type 0, CR. The computer zeros all strain gauges, reads LT's and then LC's, storing all the zero readings as VZERO (I,J) and then prints all channels.

4. After the next load has been applied, type 1, CR
   The computer reads and prints all channels.

5. Continue to last reading.

6. To start again type 0, CR and all readings will be re-zeroed.

7. To start a new test, type - 1, CR
   Teletype prints 'FEED BASIC DATA
   PAUSE'
   and return to 1 above

8. If 'SCALE ERROR' is printed, switch to manual, scale 8, and check which reading exceeds 9900. Disconnect that channel, press RUN, then the required load increment no. to restart.

```
          CONSTRAIN   (2)

   DIMENSION NCHANL(10),NCHANH(10),NCHANV(10),DATA(100),
   JBAL(100),KSC
  1ALE(9),CVALUE(10),E(10),PR(10),VZERO(10,30),NOTYGA(10)
   CALL EIN
   KSCALE(1) = 1
   KSCALE(2) = 2
   KSCALE(3) = 5
   KSCALE(4) = 10
   KSCALE(5) = 20
   KSCALE(6) = 50
   KSCALE(7) = 100
   KSCALE(8) = 200
   KSCALE(9) = 500
 1 WRITE(1,2)
 2 FORMAT(/20X,15HCONSTRAIN   (2)//17HFEED BASIC DATA  )
   PAUSE
   WRITE(1,3)
 3 FORMAT(8/)
   READ(3,4)
   WRITE(1,4)
 4 FORMAT(50H                                          )
   READ(3,6)NTYPGA,NTYPRO,NTYPLT,NTYPLC
   WRITE(1,8)NTYPGA,NTYPRO,NTYPLT,NTYPLC
 8 FORMAT(////28H NO OF STRAIN GAUGE TYPES = ,I2/
  1            28H NO OF ROSETTE TYPES      = ,I2/
  2            28H NO OF LINEAR TRANS TYPES = ,I2/
  3            28H NO OF LOAD CELL TYPES    = ,I2/)
 6 FORMAT(4I6)
   WRITE(1,10)
10 FORMAT(68H GAUGE FIRST    LAST  VOLTS  GAUGE
   GGGAUGE  ANGLE    YOUN
  1G'S   POISS /68H TYPE   CHAN    CHAN  CHAN
   FACTOR   RES    DEG
  2  MODULUS   RATIO /)

   IF (NTYPGA) 30,30,31
31 DO 15 I =1,NTYPGA
15 CALL STRGIN(NOTYGA(I),NCHANL(I),NCHANH(I),E(I),CVALUE(I),
   PR(I))
30 NR1=NTYPGA + 1
   NRL= NTYPGA + NTYPRO
   IF (NTYPRO) 32,32,33
33 DO 16  I = NR1,NRL
   CALL STRGIN(NOTYGA(I),NCHANL(I),NCHANH(I),E(I),CVALUE(I),
   PR(I))
   IF (NOTYGA(I) - 100) 16,17,17
   NCHL = NCHANL(I)
   NCHH = NCHANH(I)
17 DO 18 J = NCHL,NCHH
   READ(3,11)ANGLE
18 WRITE(1,12)ANGLE
16 CONTINUE
```

CONSTRAIN (2) - CONTINUED

```
11 FORMAT(F8.2)
12 FORMAT(40X,F7.2)
32  ND1 = NRL + 1
   NDL = NRL + NTYPLT
   NW1 = NDL + 1
   NWL = NDL + NTYPLC
   IF (NTYPLT + NTYPLC) 35,35,34
34 DO 20  I = ND1,NWL
   READ(3,13) NOTYGA(I),NCHANL(I),NCHANH(I),NCHANV(I),
   CVALUE(I)
20 WRITE(1,13)NOTYGA(I),NCHANL(I),NCHANH(I),NCHANV(I),
   CVALUE(I)
13 FORMAT(4I6,F9.4)
35 WRITE(1,14)
14 FORMAT(////22H  LOAD INCREMENT NO?  )
   READ(1,9)  LINC
 9 FORMAT(I10)
   IF (LINC) 1,36,36
36 IF (NTYPGA + NTYPRO) 38,38,37
37 DO 39  I = 1,NRL
   NCHL = NCHANL(I)
   NCHH = NCHANH(I)
   DO 39 J = NCHL,NCHH
   JSCALE = 0
52 CALL CHAN(J,JSCALE,0)
   J1 = J + 1
   IF (LINC) 53,53,54
53 CALL IAUTO(0,IBAL)
   JBAL(J1) = IBAL
54 IBAL =  JBAL(J1)
   CALL COMP(IBAL)
   CALL DVM(JDATA)
   IF (IABS(JDATA) - 9900) 56,56,55
55 JSCALE = JSCALE + 1
   ISCMAX = JSCALE - 9
   IF (ISCMAX) 52,60,60
56 JSCALE = JSCALE + 1
   DATA(J1) = FLOAT(JDATA)*FLOAT(KSCALE(JSCALE))
39 CONTINUE
38 IF (NTYPLT + NTYPLC) 40,40,41
41 DO 42 I = ND1,NWL
   NCHL = NCHANL(I)
   NCHH = NCHANH(I)
   DO 42 J = NCHL,NCHH
   JSCALE = 0
57 CALL CHAN(J,JSCALE,0)
   J1 = J + 1
   CALL DVM(JDATA)
   IF (IABS(JDATA) -9900) 58,58,44
44 JSCALE = JSCALE + 1
   ISCMAX = JSCALE - 9
```

CONSTRAIN (2) - CONTINUED

```
   IF (ISCMAX) 57,60,60
58 JSCALE = JSCALE + 1
42 DATA(J1) = FLOAT(JDATA)*FLOAT(KSCALE(JSCALE))
   DO 62 I = ND1,NWL
   J = NCHANV(I)
   JSCALE = 0
65 CALL CHAN(J,JSCALE,0)
   CALL DVM(JDATA)
   J1 = J + 1
   IF (IABS(JDATA) - 9900)  63,63,64
64 JSCALE = JSCALE + 1
   ISCMAX = JSCALE - 9
   IF (ISCMAX) 65,60,60
63 JSCALE = JSCALE + 1
62 DATA(J1) = FLOAT(JDATA)*FLOAT(KSCALE(JSCALE))
40 WRITE(1,45)
45 FORMAT(/18H CHAN NO    RESULT /)
   IF (NTYPGA + NTYPRO) 68,68,69
69 DO 46  I = 1,NRL
   NCHL = NCHANL(I)
   NCHH = NCHANH(I)
   DO 46  J  = NCHL,NCHH
   J1 = J + 1
   V = (DATA(J1))*CVALUE(I)
46 WRITE(1,47)J,V
47 FORMAT(I6,2X,E12.4)
68 IF (NTYPLT + NTYPLC) 35,35,71
71 DO 48  I = ND1,NWL
   NCHL = NCHANL(I)
   NCHH = NCHANH(I)
   DO 48 J = NCHL,NCHH
   J1 = J + 1
   U = (DATA(J1))*CVALUE(I)
   IF (LINC) 1,49,50
49 VZERO(I,J1) = U
50 V = U - VZERO(I,J1)
48 WRITE(1,47)J,V
   DO 66 I = ND1,NWL
   J = NCHANV(I)
   J1 = J + 1
   V = (DATA(J1))*(1.0E-06)
66 WRITE (1,47) J,V
   GO TO 35
   STOP
60 WRITE (1,61)
61 FORMAT(13H SCALE ERROR )
   PAUSE
   GO TO 35
   STOP
   CALL LPFAIL
   END
```

CONSTRAIN (2) - CONTINUED

SUBROUTINE

```
      SUBROUTINE STRGIN(NOTYGA,NCHANL,NCHANH,E,CVALUE,PR)
      READ(3,10) NOTYGA,NCHANL,NCHANH,GF,GR,E,PR
      WRITE(1,11)NOTYGA,NCHANL,NCHANH,GF,GR,E,PR
      CVALUE   =  (20000.0 + GR)/(GR*GF*8.383333E  7)
   10 FORMAT(3I7,F7.2,F7.2,E10.3,F7.2)
   11 FORMAT(3I6,9X,F6.2,F8.2,8X,E10.3,F7.2)
      RETURN
      END
```

EXAMPLE AND EXPLANATION OF DATA LOGGER INPUT AND OUTPUT

TEST BEAM NO 25

NO OF STRAIN GAUGE TYPES = 1
NO OF ROSETTE TYPES = 0
NO OF LINEAR TRANS TYPES = 1
NO OF LOAD CELL TYPES = 3

GAUGE TYPE	FIRST CHAN	LAST CHAN	VOLTS CHAN	GAUGE FACTOR	GAUGE RES	ANGLE DEG	YOUNG'S MODULUS	POISS RATIO
1	0	14		2.17	100.0		.160E+05	.15
2	15	16	17	11.250				
3	18	18	19	8.299				
4	20	21	19	4.150				
5	22	23	19	2.490				

LOAD INCREMENT NO?
1,

CHAN NO	RESULT		
0	-.1071E-03		
1	-.5745E-04		
2	-.2099E-04		
3	.1270E-03		
4	-.1138E-03		
5	-.5745E-04		
6	-.1767E-04	= 17 $\mu\epsilon$	Values of strain :-
7	-.1347E-03		
8	-.9944E-04		strain gauges 0 - 14
9	-.4972E-04		
10	-.2320E-04		
11	.1403E-03		
12	-.8839E-04		
13	-.6076E-04		
14	-.2430E-04		
15	.8280E+06	= 0.83 mm	Deflection under load
16	.5962E+06	= 0.60 mm	Deflection at y = 1700 mm
18	.4664E+04	= 4.66 kN	Load W
20	.4148E+01	= 0.004kN	Increase in force in P/S wires - top
21	-.4156E+01	= 0.004kN	
22	.0000E+00	= 0.000kN	Increase in force in P/S wires - bottom
23	-.9960E+01	= 0.010kN	
17	.4847E+01	= 4.85 V	Input voltage - L T
19	.4924E+01	= 4.92 V	Input voltage - L C

Ignore signs

8.2 THE HEWLETT-PACKARD 9830 COMPUTER

This desk-top machine, programmed in BASIC was used to calculate the theoretical results. In conjunction with a teletype and an X - Y plotter, comparisons of results were tabulated and graphs plotted.

Examples of the programmes used in the compilation of the tables in Section 6 are given overleaf.

An example of a programme used to compare control tests results graphically, in Section 3, is also printed.

HEWLETT - PACKARD '9830' PROGRAMME - THEORY - MODE 1, SERIES 2

```
10 DIM A$[25]
20 READ D,E,A1,A2,D9,D8,D5,B
30 DATA 70,2.5,77.8,77.8,152,87,0,0.08
40 FOR I=25 TO 41
50 FIXED 2
60 DISP I
70 WAIT 100
80 LOAD  DATA I,A
90 IF A[14]=1 OR A[14]=12 THEN 110
100 NEXT I
110 M=A[11]*1E+06
120 V=A[13]*1E+03
130 T=A[12]*1E+06
132 IF A[6]>0 THEN 140
134 P1=A[8]*(1+6*A[19]/A[21])/A[5]
136 GOTO 150
140 P1=A[8]*(1+6*A[19]/A[21])/A[6]
150 P9=267.7*A[8]*A[19]
160 P8=17400*A[8]-P9
170 P7=0
180 IF T>0 THEN 210
190 T0=0
200 GOTO 220
210 T0=SQR(M↑2/T↑2+1+P1)-M/T
220 Q=ATN(T0)
230 C0=B*12*(D9-D)/D/(COS(Q))↑2
240 L1=D8-0.375*D
250 L2=D9-0.375*D
260 D7=T*L2/(L2↑2+L1↑2)
270 D6=D7*L1/L2
280 C1=B*D7*E*T0/A1
290 C2=(D8-D)/(D9-D)
300 C3=(P7+P8+P9)*COS(Q)+(D6+D7)*SIN(Q)
310 C4=2*A[20]/3*D/COS(Q)
320 C5=A1*COS(Q)
330 C7=A2*COS(Q)
340 F0=(C3-C1*(C5+C7*C2))/(C4-C0*(C5+C7*C2))
350 F2=C2*(C0*F0-C1)
360 C6=((P8+A2*F2)*(D9-D8)+P7*(D9-D5))*COS(Q)
                                        +D6*(D9-D8)*SIN(Q)
370 D1=(D9-(M*COS(Q)+T*SIN(Q)+C6)/(C4*F0))*8/3
380 IF SQR((D-D1)↑2)<1E-02 THEN 420
390 D=(D1+D)/2
400 DISP D
410 GOTO 230
420 A0=(2*A[20]/3)*D*0.8*A[2]*L2
430 M9=0.125*(3*A0+5*SQR(A0↑2-16*(D6+D7+V)↑2*L2↑2))
440 M0=M9-(P8+A2*F2)*(D9-D8) - P7*(D9-D5)
450 DISP M*1E-06,M0*1E-06
460 WAIT 1000
470 IF (M-M0)↑2<1E+06 THEN 500
480 M=M-(M-M0)/4
490 GOTO 180
500 WRITE (15,510)I,B,A[12],A[13],A[11],M*1E-06,A[11]*1E+06/M
510 FORMAT 12X,F3.0,2X,F6.2,2X,F6.2,3X,F6.2,3X,F6.2,3X
                                        F6.2,2X,F6.2
520 NEXT I
530 END
```

HEWLETT - PACKARD '9830' PROGRAMME - THEORY - MODE 2

```
10 DIM A$[25],B$[50],C$[50]
20 S1=Y1=S2=Y2=N=Y3=Y4=M1=M2=S3=S4=V3=V4=0
30 FOR I=0 TO 41
40 LOAD  DATA I,A
50 IF A[14]=2 OR A[14]=2 OR A[14]=2 THEN 70
60 NEXT I
70 F=A[6]
80 GOTO 130
90 F=0.87*(1+6450/A[20]*A[20])*EXP((LOG(A[3]))/3)
95 GOTO 160
100 F=0.87*(1+6450/A[20]*A[20])*EXP((LOG(0.8*A[2]))/3)
105 GOTO 160
110 F=6.13*EXP(LOG(A[3]/A[20])/3)
115 GOTO 160
120 F=6.13*EXP(LOG(0.8*A[2]/A[20])/3)
125 GOTO 160
126 F=1.1*EXP((LOG(0.8*A[2]))/3)
127 GOTO 160
130 IF F<0 THEN 150
140 IF F >= 0 THEN 160
150 F=A[5]
160 P=A[8]
170 V=A[13]
180 T=A[12]
190 B=A[20]
200 H=A[21]
210 K1=SQR(B/H)
220 K2=SQR(1+P/F)
230 T1=B*B*H*F*K2*1E-06/(3+K1+0.35*K1*SQR(P/F))
240 T2=T1-B*V*1E-03/6
250 V2=6000*T1/B
260 S1=T/T2+S1
270 S2=T/T1+V/V2+S2
280 B[N+1]=T/T2
290 C[N+1]=T/T1+V/V2
300 N=N+1
310 FIXED 2
320 WRITE (15,330)A[1],V,T,T2,T/T2,T/T1,V/V2,T/T1+V/V2
330 FORMAT 12X,F3.0,2X,F6.2,2X,F5.2,2X,F5.2,2X,F5.2,2X,
340 NEXT I                                  F5.2,2X,F5.2,2X,F5.2
350 M1=S1/N
360 M2=S2/N
370 FOR J=0 TO (N-1)
380 Y1=B[J+1]-M1
390 Y2=C[J+1]-M2
400 Y3=Y1↑2+Y3
410 Y4=Y2↑2+Y4
420 NEXT J
430 S3=SQR(Y3/(N-1))
440 S4=SQR(Y4/(N-1))
450 V3=S3*100/M1
460 V4=S4*100/M2
470 PRINT
480 PRINT "          ";"NO.OF RESULTS=";N;"MEAN";M1;
490 PRINT                                   "---------  ";M2
500 PRINT "          ";"COEFFICIENT OF VARIATION  ";
510 END                                     "";V3;" --------- ";V4
```

HEWLETT - PACKARD '9830' PROGRAMME - THEORY - MODE 3

```
10 DIM A[25],B[50],C[50]
20 S1=Y1=S2=Y2=N=Y3=Y4=M1=M2=S3=S4=V3=V4=M5=M6=0
30 INPUT I
40 LOAD  DATA I,A
50 GOTO 60
60 F=A[6]
70 GOTO 180
80 F=0.87*(1+6450/A[21]*A[21])*EXP((LOG(A[3]))/3)
90 GOTO 200
100 F=0.87*(1+6450/A[21]*A[21])*EXP((LOG(0.8*A[2]))/3)
110 GOTO 200
120 F=6.13*EXP(LOG(A[3]/A[21])/3)
130 GOTO 200
140 F=6.13*EXP(LOG(0.8*A[2]/A[21])/3)
150 GOTO 200
160 F=1.1*EXP((LOG(0.8*A[2]))/3)
170 GOTO 200
180 IF F >= 0 THEN 200
190 F=A[5]
200 P=A[8]*(1-6*A[19]/A[21])
210 M5=A[11]
220 T=A[12]
230 B=A[20]
240 H=A[21]
250 K1=SQR(H/B)
260 K2=SQR(1+P/F)
270 IF P >= 0 THEN 300
280 T1=B*H*H*F*K2*1E-06/(3+K1+K1*P/F)
290 GOTO 310
300 T1=B*H*H*F*K2*1E-06/(3+K1+0.35*K1*SQR(P/F))
310 M6=B*H*H*F*(1+P/F)*1E-06/6
320 T3=T1*SQR(1+M5/M6)
330 S1=T/T3+S1
340 S2=(T/T1)↑2-M5/M6+S2
350 B[N+1]=T/T3
360 C[N+1]=(T/T1)↑2-M5/M6
370 N=N+1
380 FIXED 2
390 WRITE (15,400)A[1],M5,T,T3,T/T3,(T/T1)↑2,M5/M6,
    (T/T1)↑2-M5/M6
400 FORMAT 8X,F4.0,2X,F6.2,2X,F6.2,2X,F6.2,2X,F5.2,
    2X,F5.2,2X,F5.2,2X,F5.2
410 GOTO 30
420 M1=S1/N
430 M2=S2/N
440 FOR J=0 TO (N-1)
450 Y1=B[J+1]-M1
460 Y2=C[J+1]-M2
470 Y3=Y1↑2+Y3
480 Y4=Y2↑2+Y4
490 NEXT J
500 S3=SQR(Y3/(N-1))
510 S4=SQR(Y4/(N-1))
520 V3=S3*100/M1
530 V4=S4*100/M2
540 PRINT
550 PRINT "          ";"NO.OF RESULTS=";N;"MEAN";M1;
560 PRINT                              "--------- ";M2
570 PRINT "          ";"COEFFICIENT OF VARIATION  ";
580 END                                ""V3;" --------- ";V4
```

HEWLETT - PACKARD '9830' PROGRAMME - TO DRAW FIGURE 3.9

```
10 SCALE 0,75,0,6.5
20 OFFSET 10,1
30 XAXIS 0,5
40 YAXIS 0,1
50 LABEL (*,2,1.7,0,7/10)
60 FOR X=10 TO 60 STEP 10
70 PLOT X,0,1
80 CPLOT -3,-1.5
90 LABEL (320)X
100 NEXT X
110 LABEL (*,2,1.7,0,7/10)
120 FOR Y=1 TO 5 STEP 1
130 PLOT 0,Y,1
140 CPLOT -6,-0.3
150 LABEL (320)Y
160 NEXT Y
170 DIM A[25],B[42,2]
180 INPUT P,Q
190 FOR I=0 TO 41
200 LOAD  DATA I,A
210 B[I+1,1]=A[P]
220 B[I+1,2]=A[Q]
221 IF A[P]<0 OR A[Q]<0 THEN 290
240 PRINT I;A[P];A[Q]
250 X=A[P]
260 Y=A[Q]
270 PLOT X,Y
280 PEN
290 NEXT I
300 STOP
305 LABEL (*,3,1.7,0,7/10)
310 LETTER
320 FORMAT 2F4.0
330 END
340 PLOT X-0.2,Y+0.02
350 PLOT X+0.2,Y-0.02
360 PEN
370 PLOT X+0.2,Y+0.02
380 PLOT X-0.2,Y-0.02
390 PEN
400 NEXT I
410 END
```

8.3 FAILURE CRACK PATTERNS

The cracks at failure of the forty beams tested are shown in Figs. 8.1 to 8.40 which follow.

The legend to each of the figures is as shown below

crack

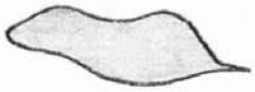

area missing

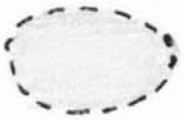

area crushed

strain gauge and no.

'Demec' gauge and no.

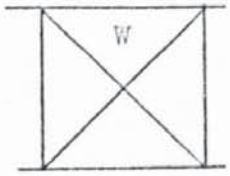

loading plate

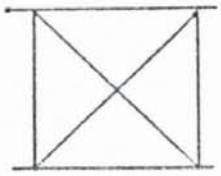

support

distance in mm from left hand support (scale 1/5)

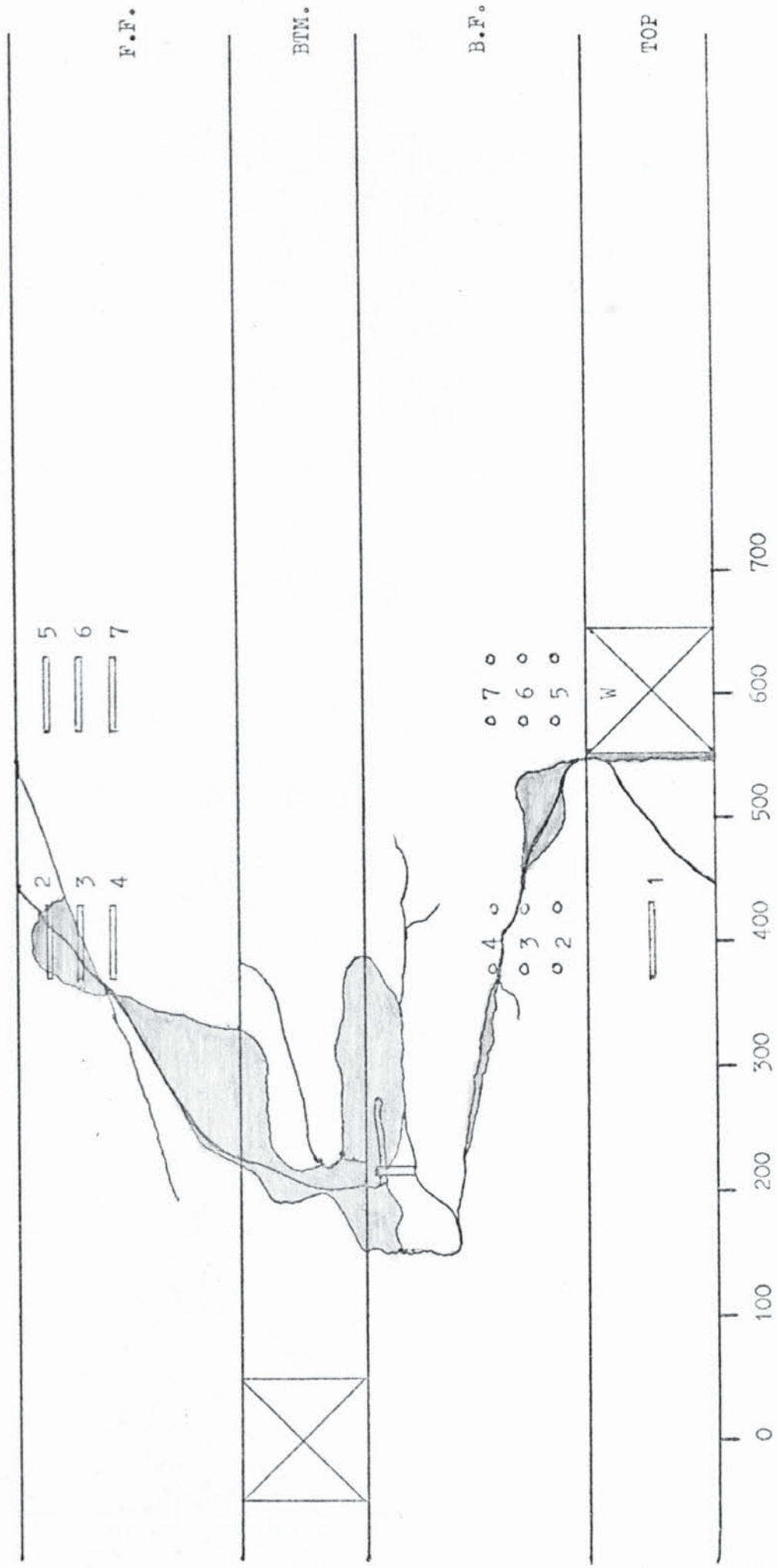

FIGURE 8.1 FAILURE CRACK PATTERNS - BEAM 0 (MODE 2)

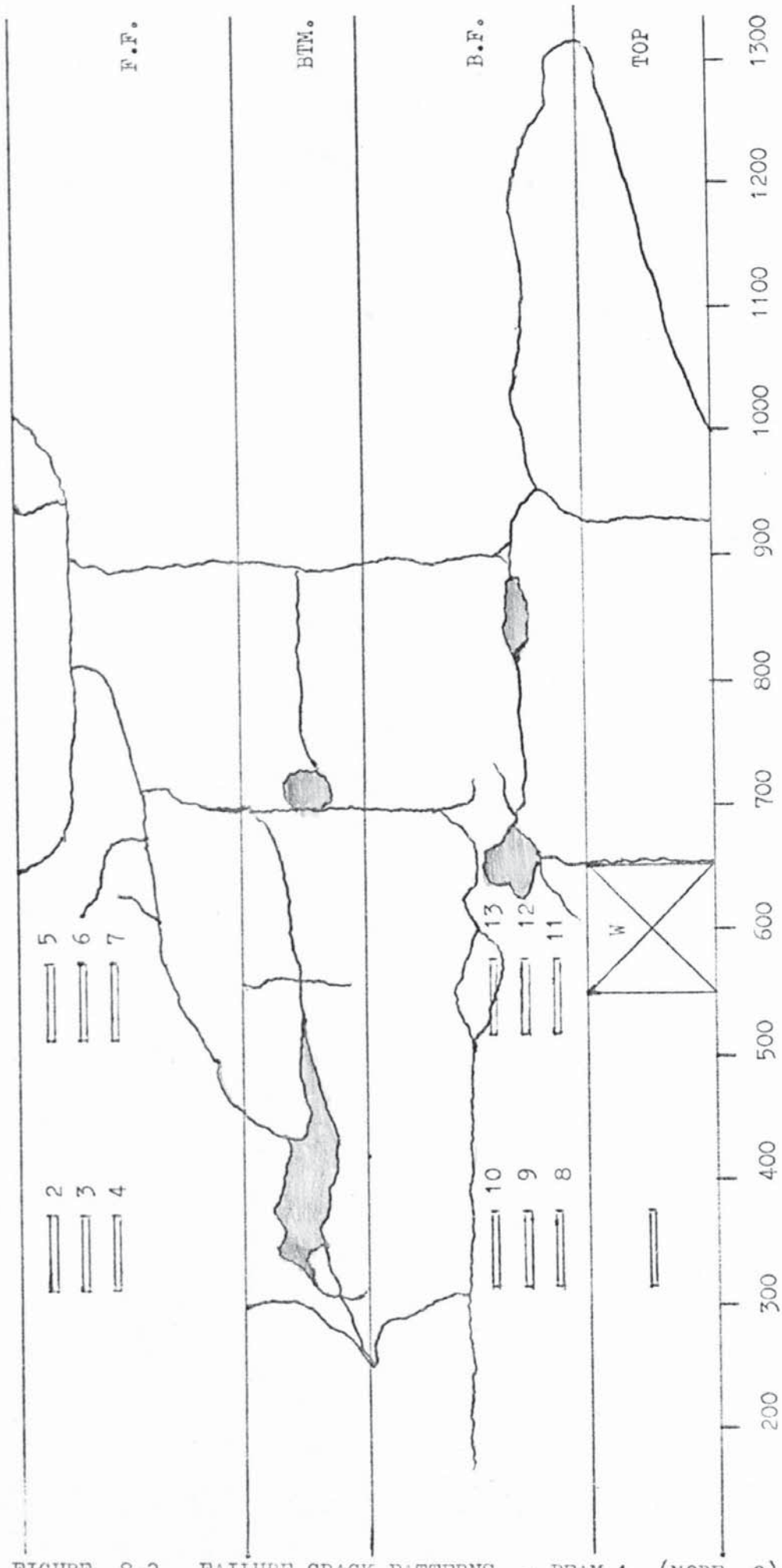

FIGURE 8.2 FAILURE CRACK PATTERNS - BEAM 1 (MODE 2)

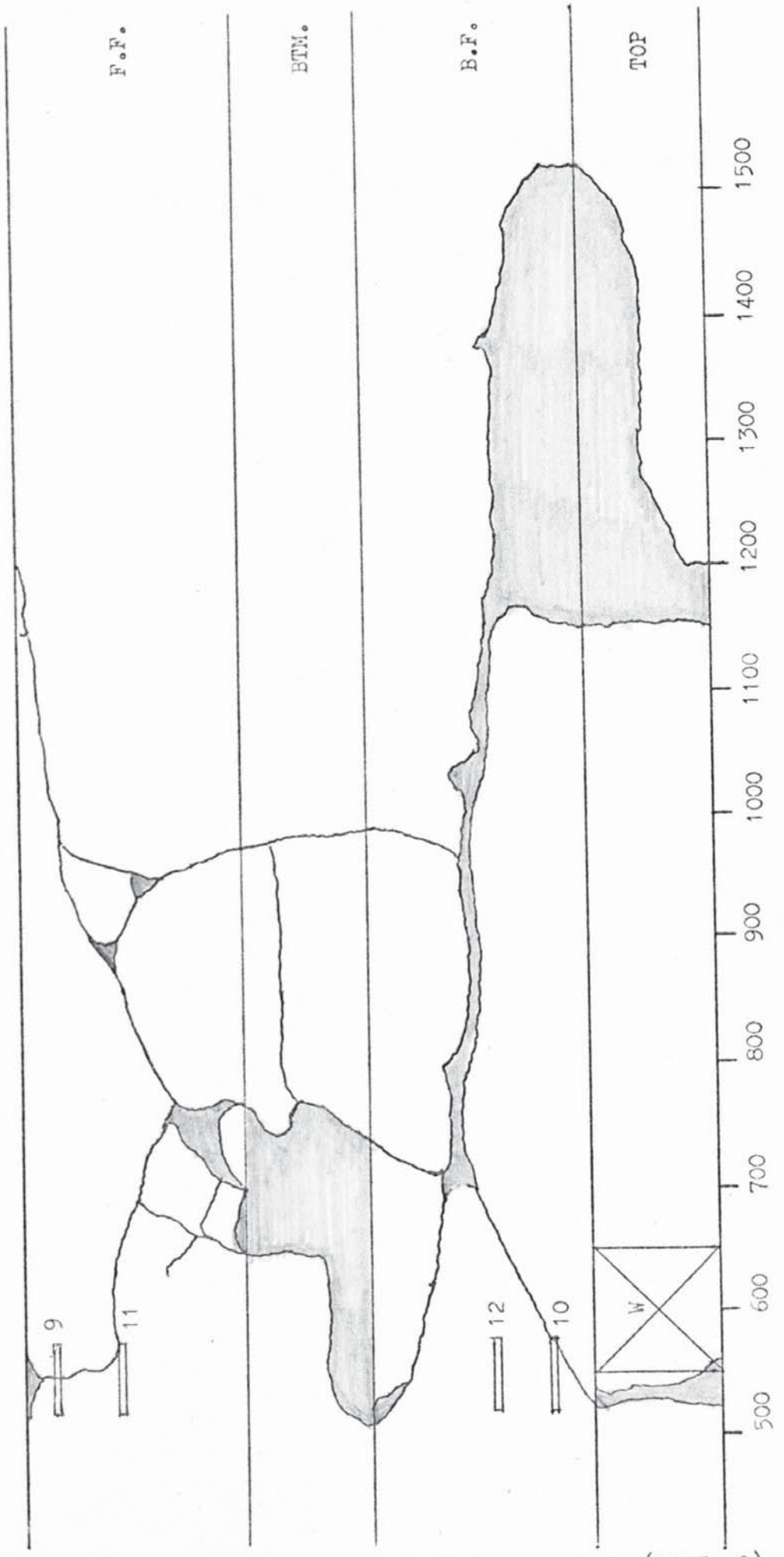

FIGURE 8.3 FAILURE CRACK PATTERNS - BEAM 2 (MODE 2)

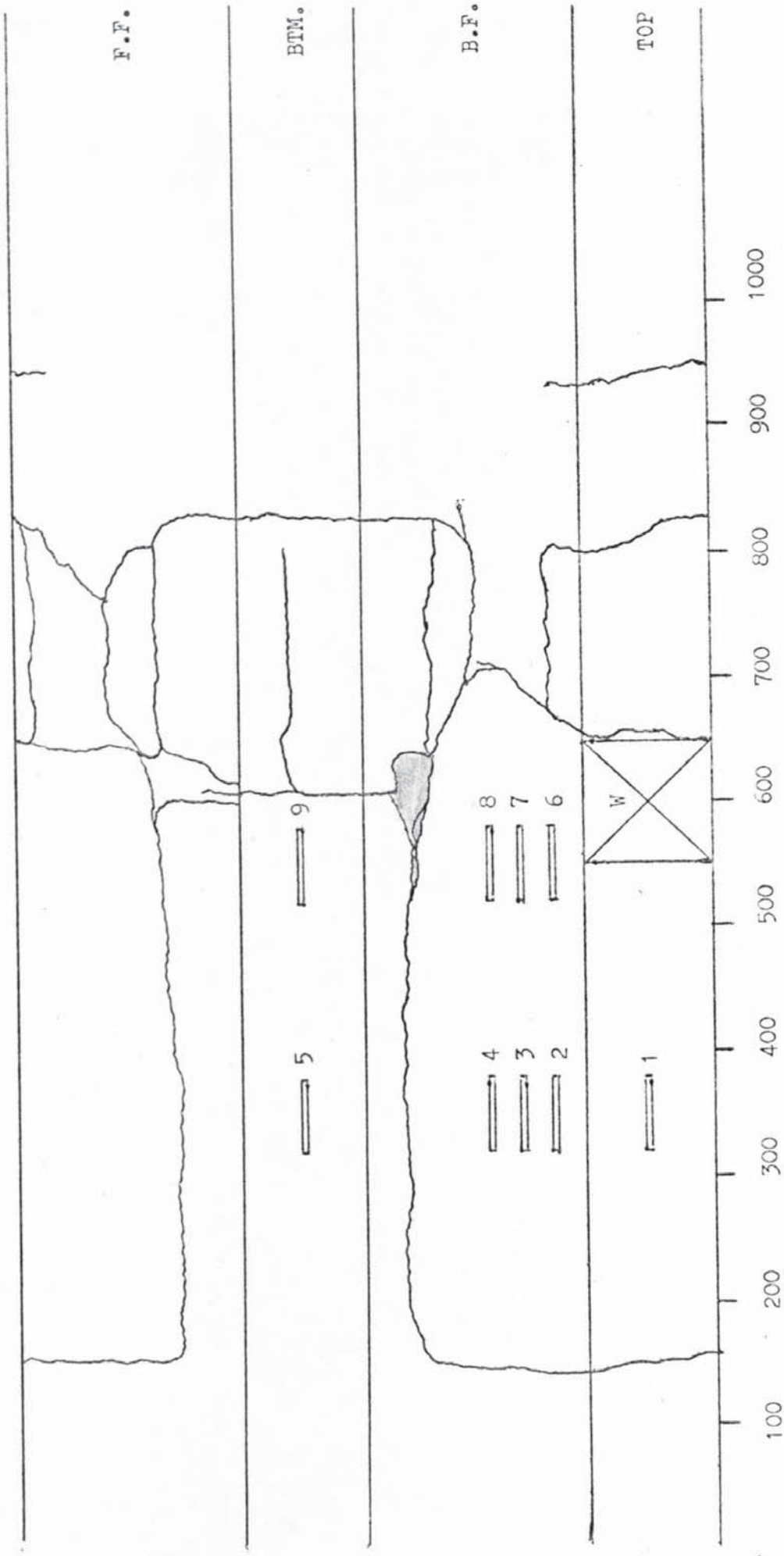

FIGURE 8.4 FAILURE CRACK PATTERNS - BEAM 3 (MODE 1)

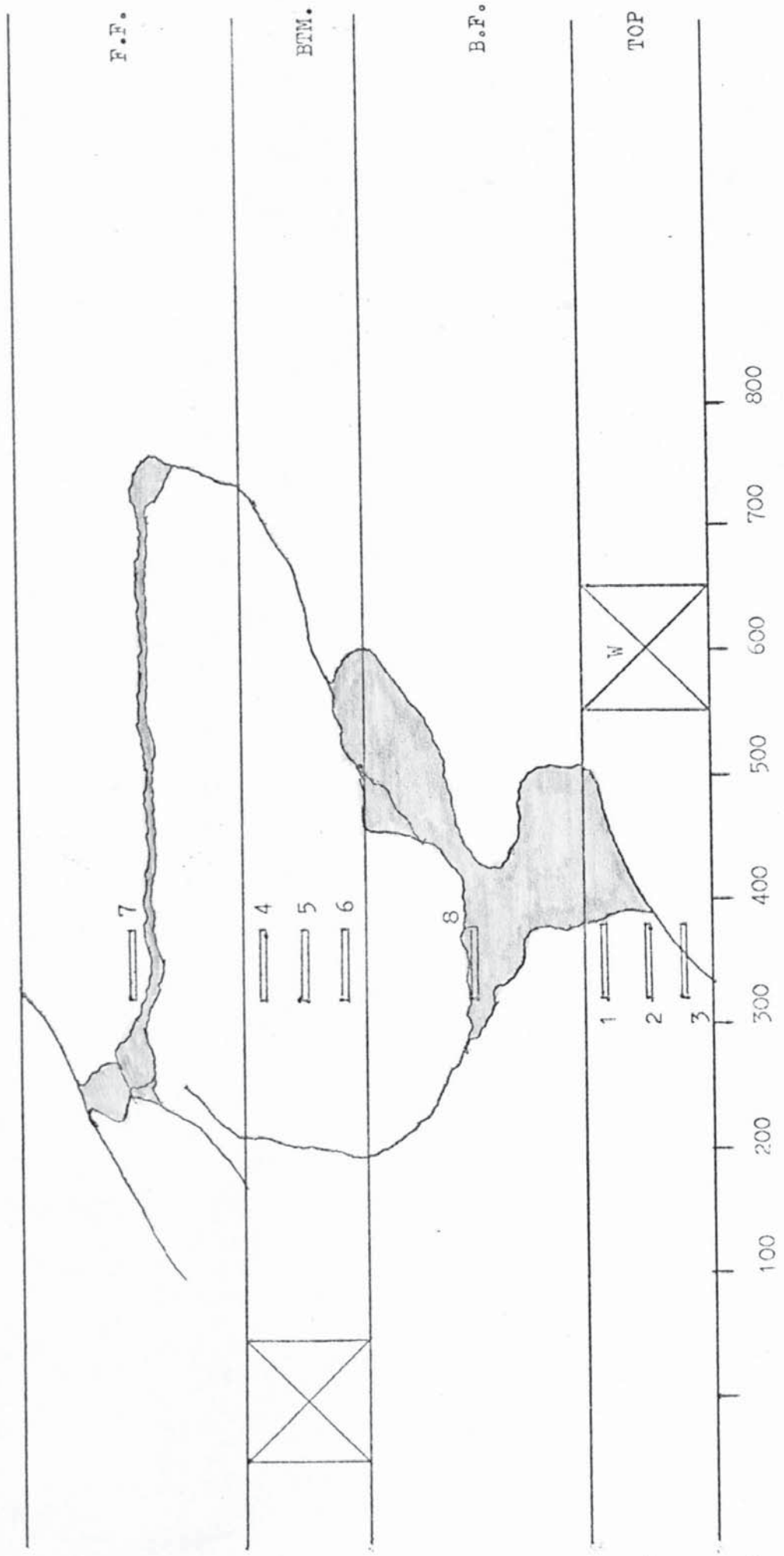

FIGURE 8.5 FAILURE CRACK PATTERNS - BEAM 4 (MODE 2)

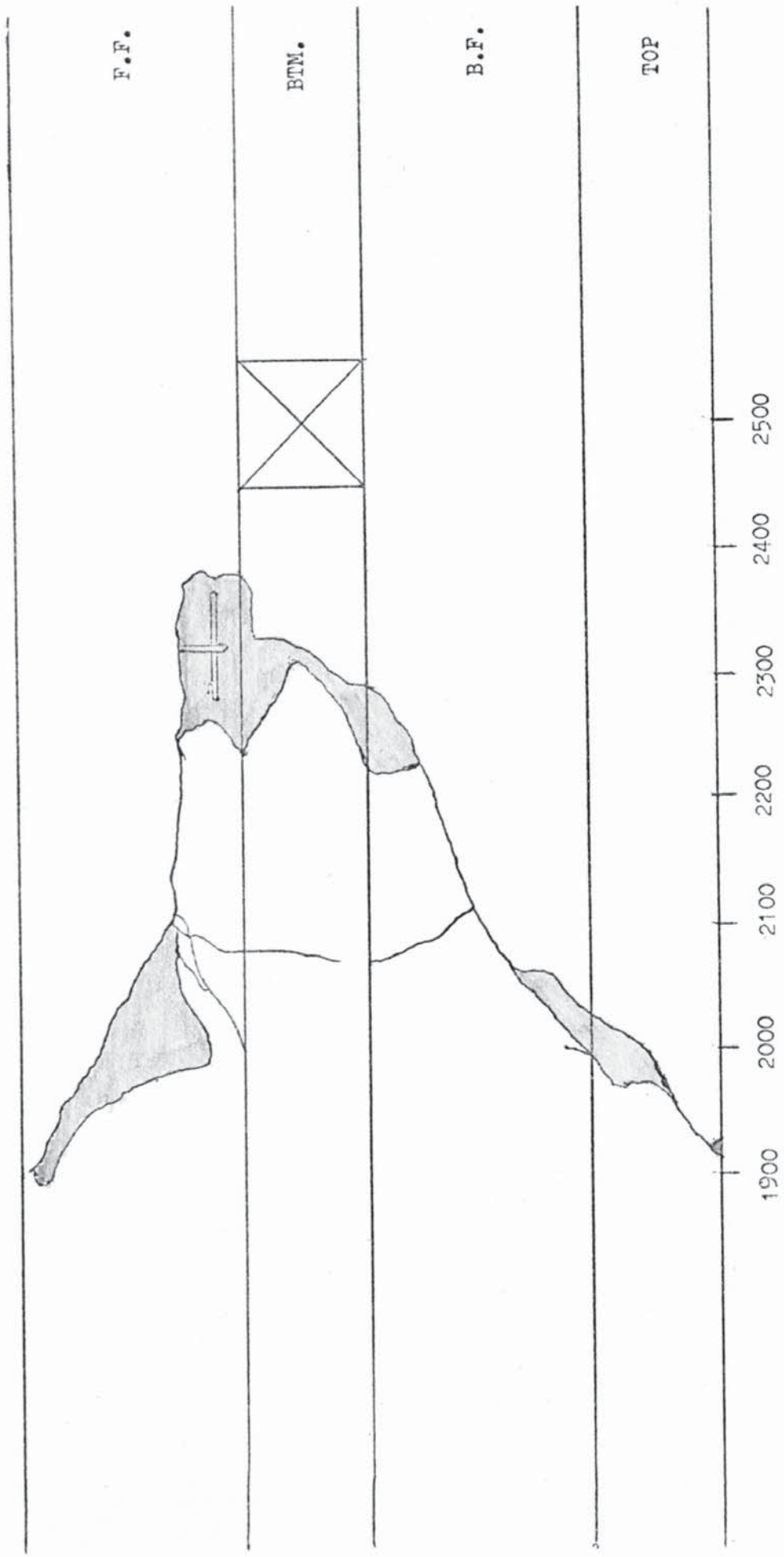

FIGURE 8.6 FAILURE CRACK PATTERNS - BEAM 5 (MODE 2)

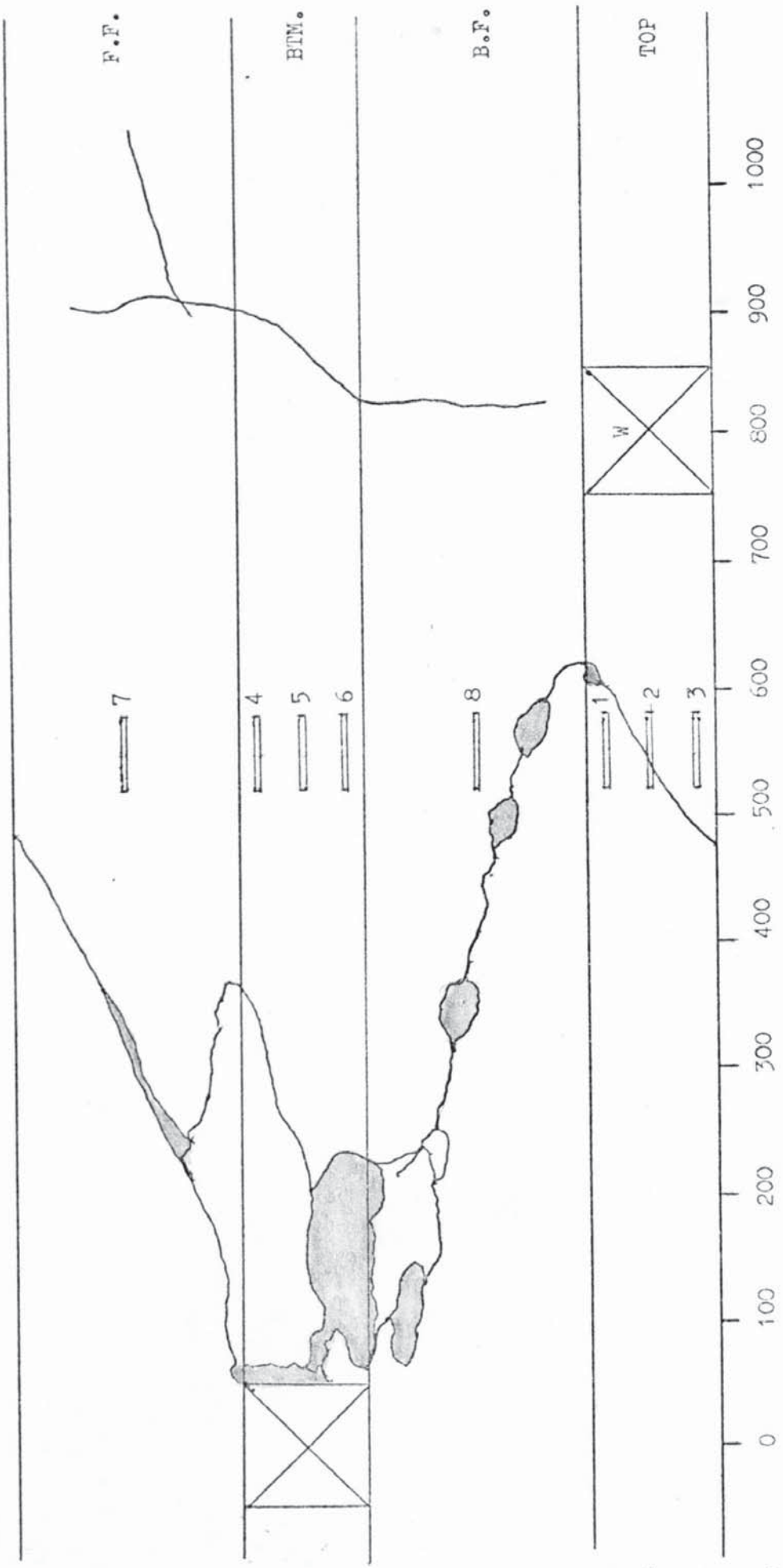

FIGURE 8.7 FAILURE CRACK PATTERNS - BEAM 6 (MODE 2)

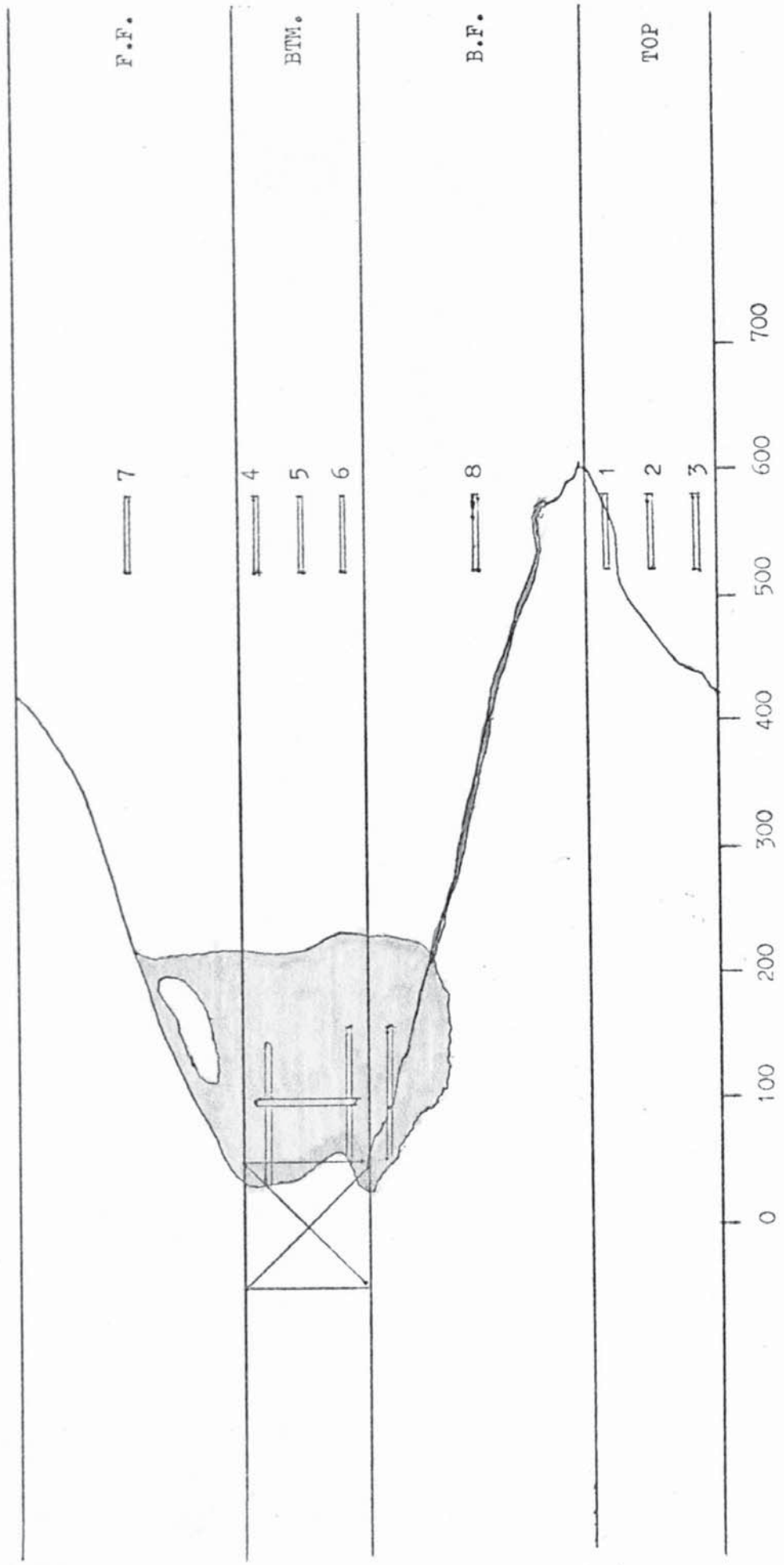

FIGURE 8.8 FAILURE CRACK PATTERNS - BEAM 7 (MODE 2)

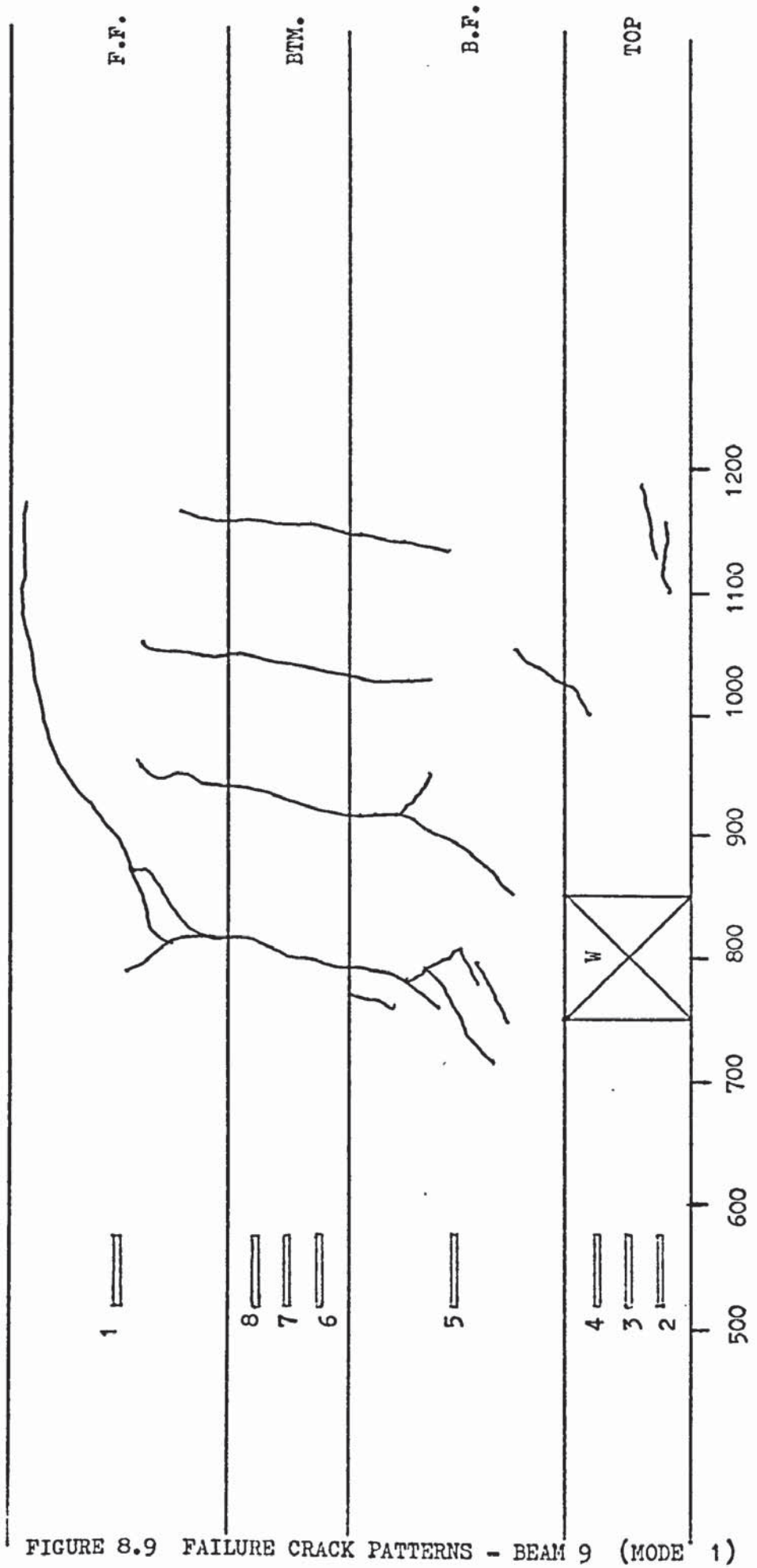

FIGURE 8.9 FAILURE CRACK PATTERNS - BEAM 9 (MODE 1)

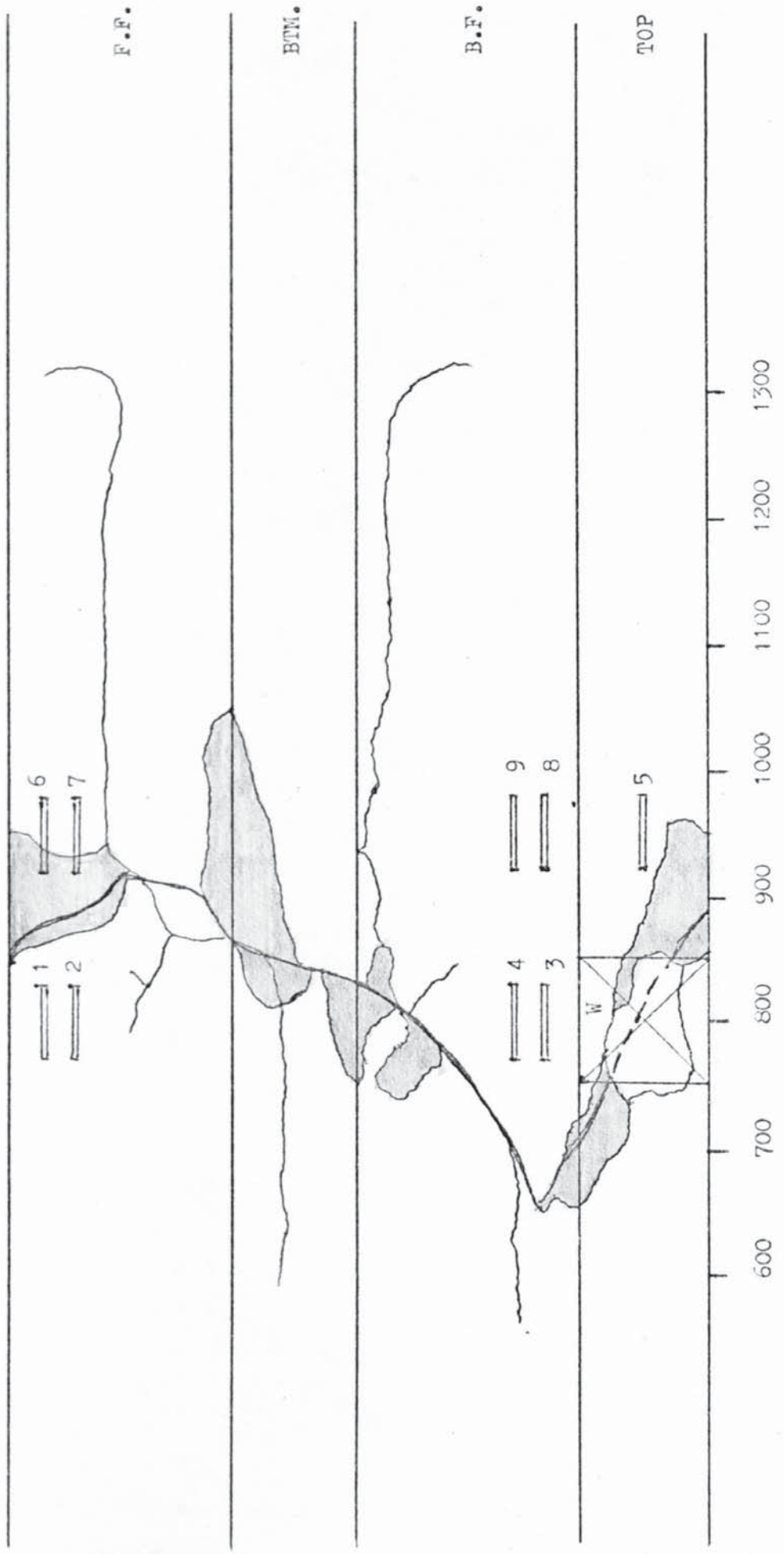

FIGURE 8.10 FAILURE CRACK PATTERNS - BEAM 10 (MODE 1)

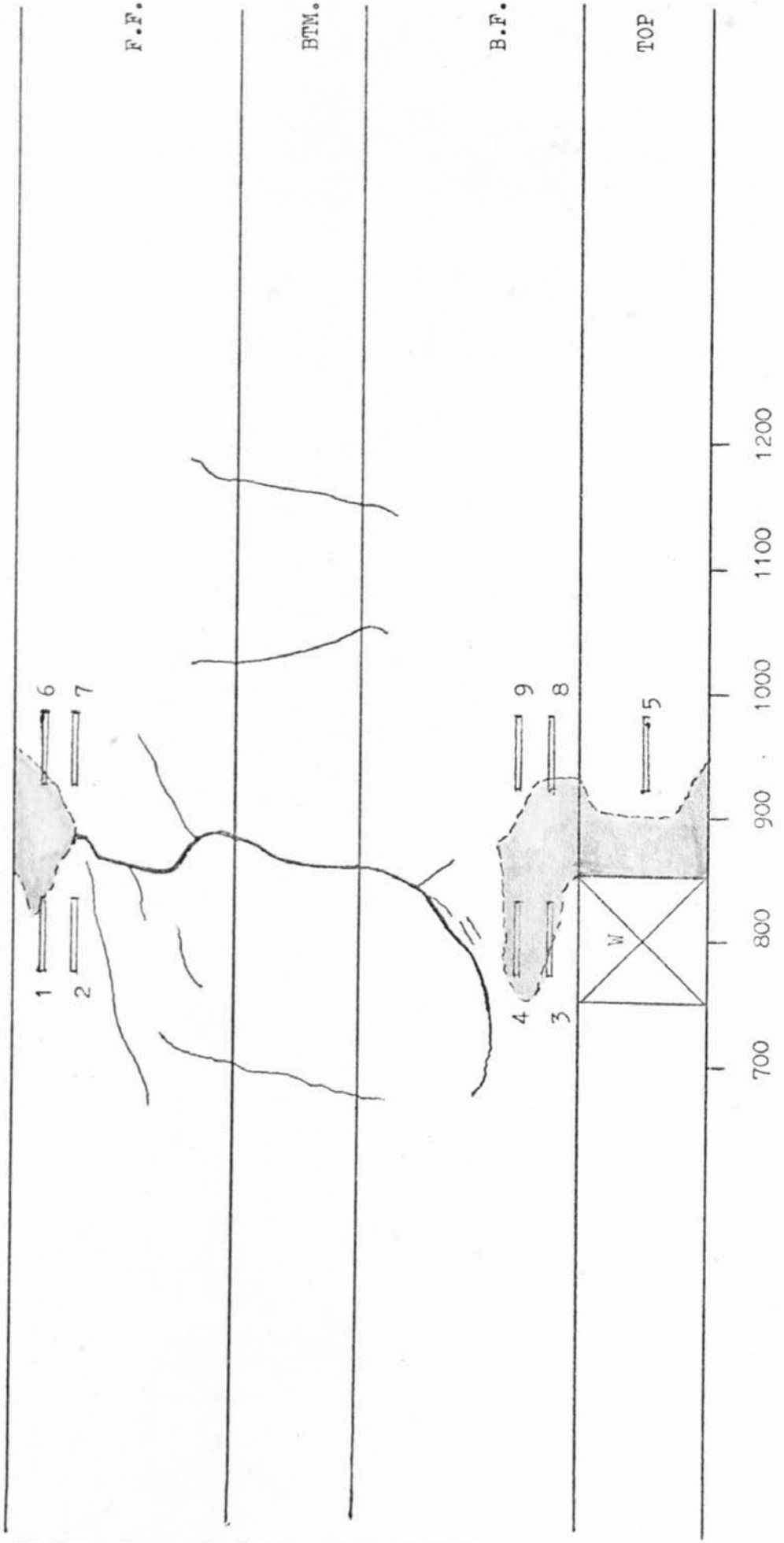

FIGURE 8.11 FAILURE CRACK PATTERNS - BEAM 11 (MODE 1)

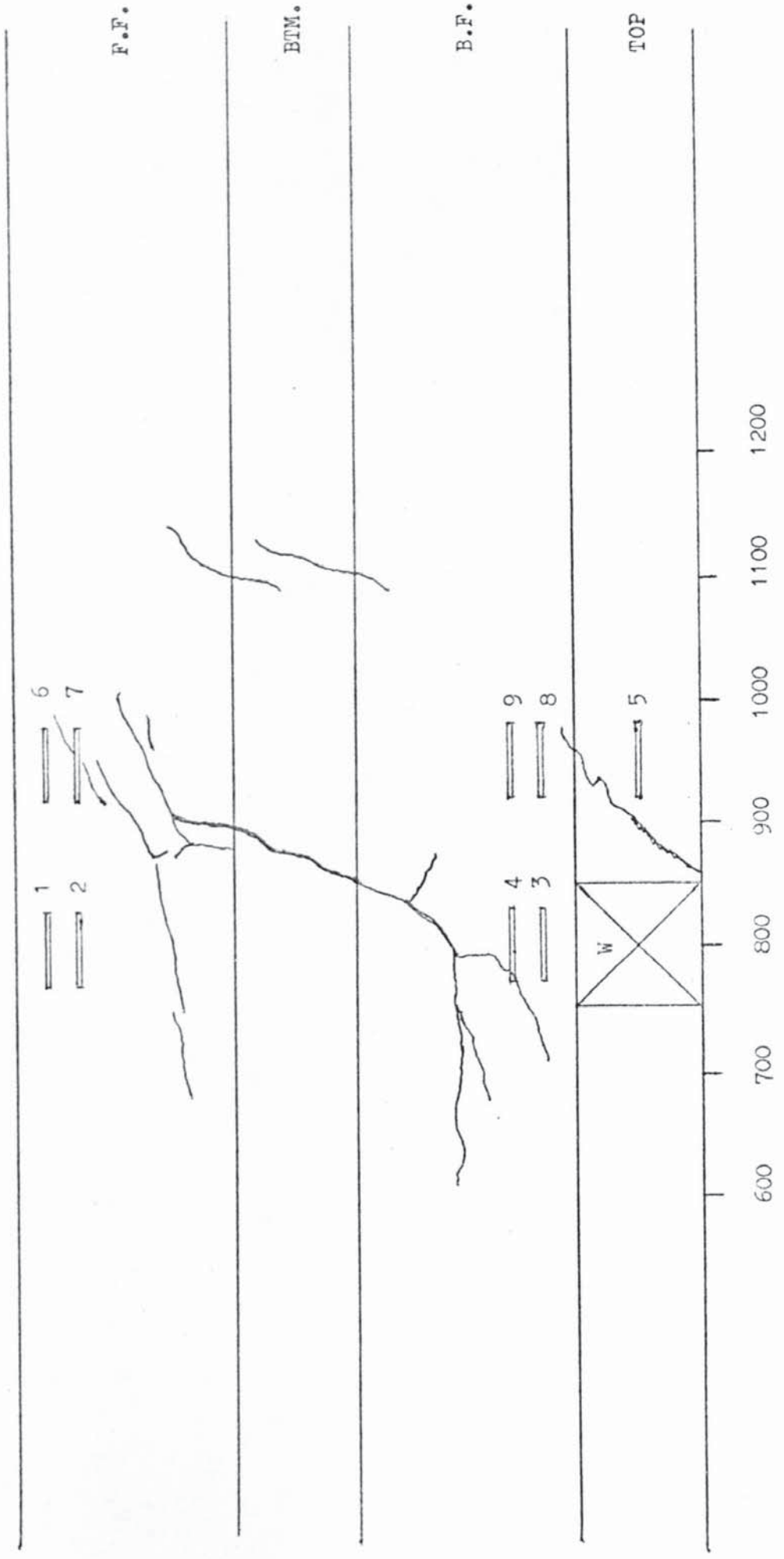

FIGURE 8.12 FAILURE CRACK PATTERNS - BEAM 12 (MODE 1/2)

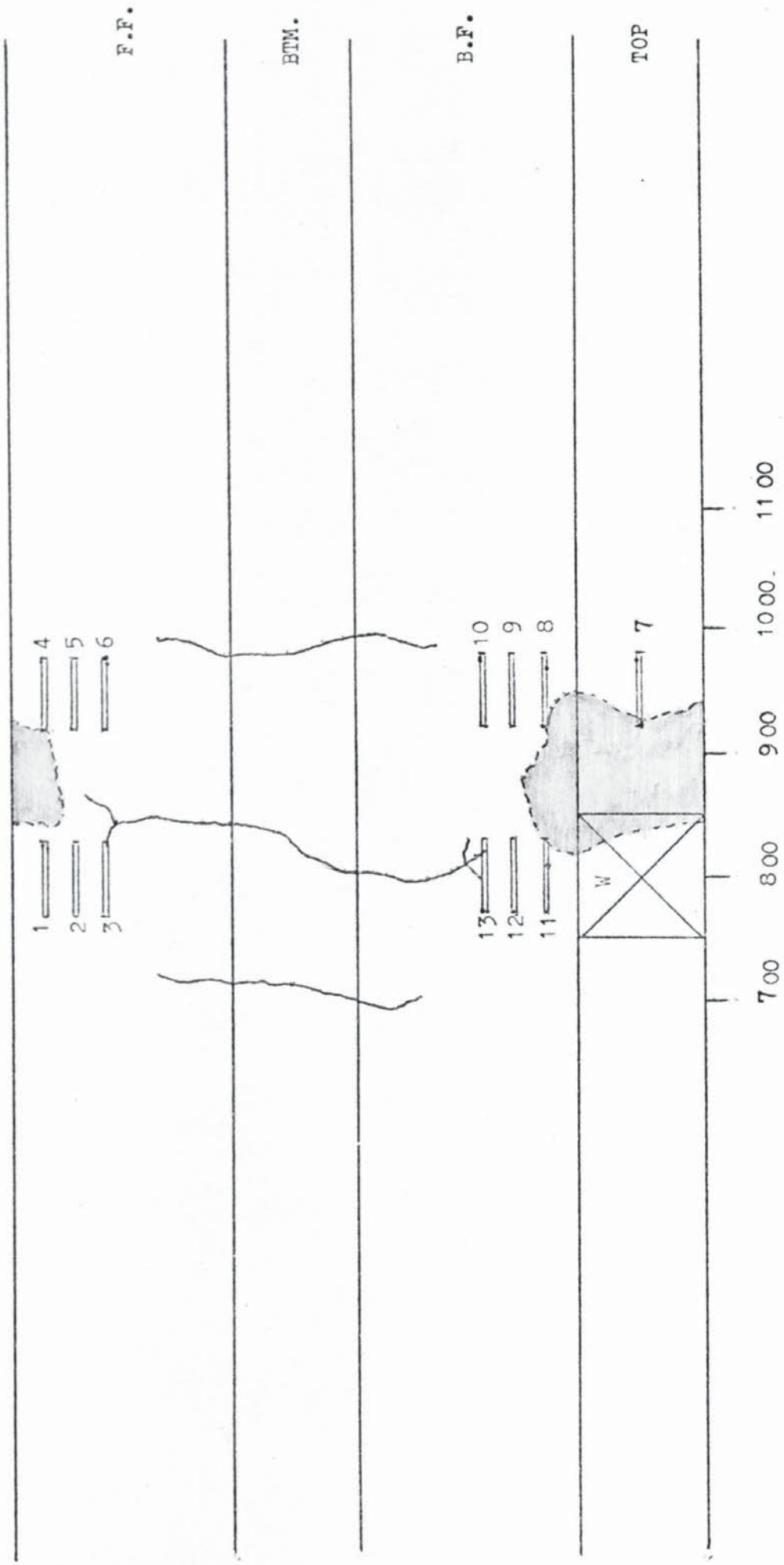

FIGURE 8.13 FAILURE CRACK PATTERNS - BEAM 13 (MODE 1)

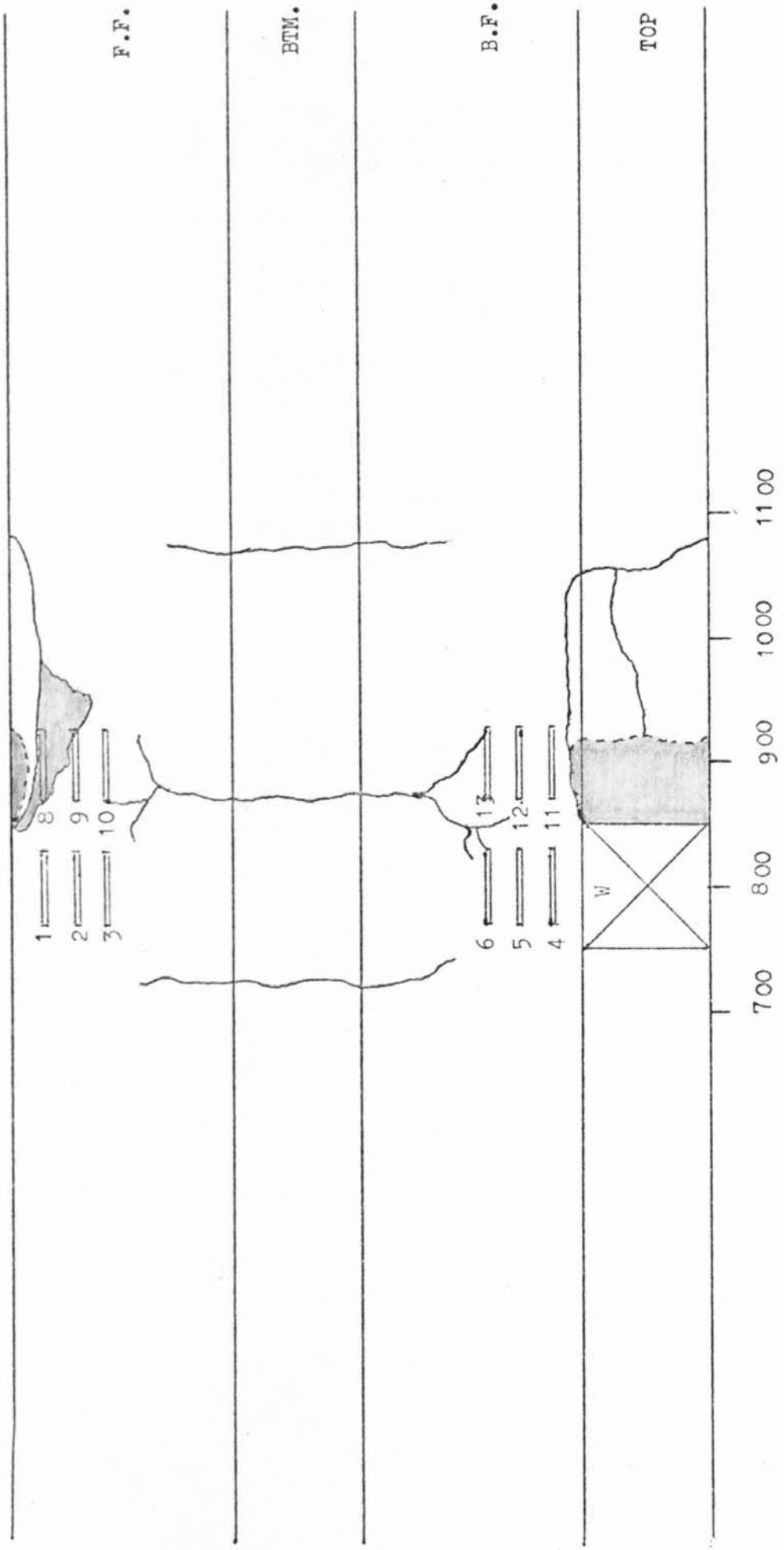

FIGURE 8.14 FAILURE CRACK PATTERNS – BEAM 14 (MODE 1)

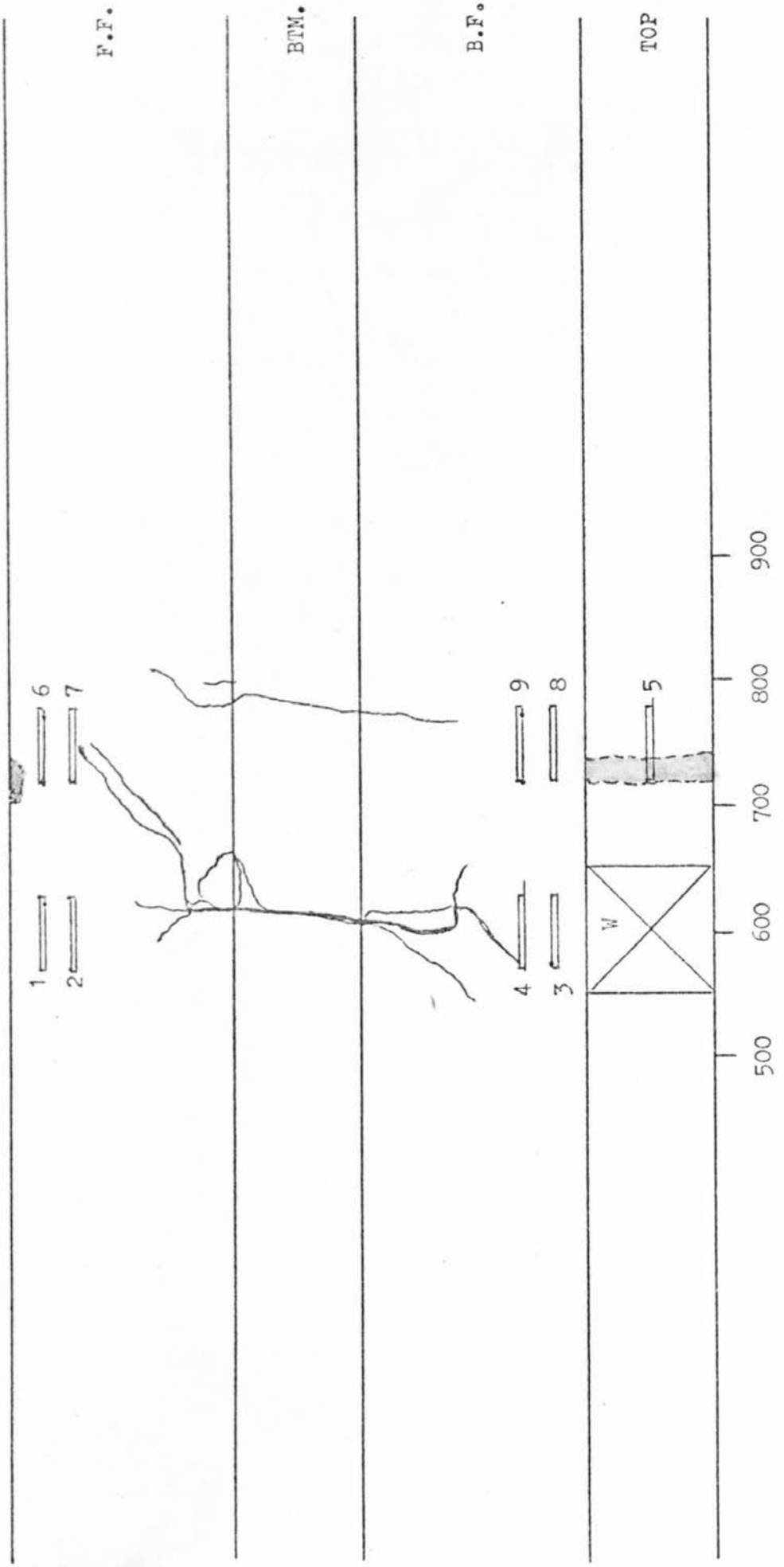

FIGURE 8.15 FAILURE CRACK PATTERNS - BEAM 15 (MODE 1)

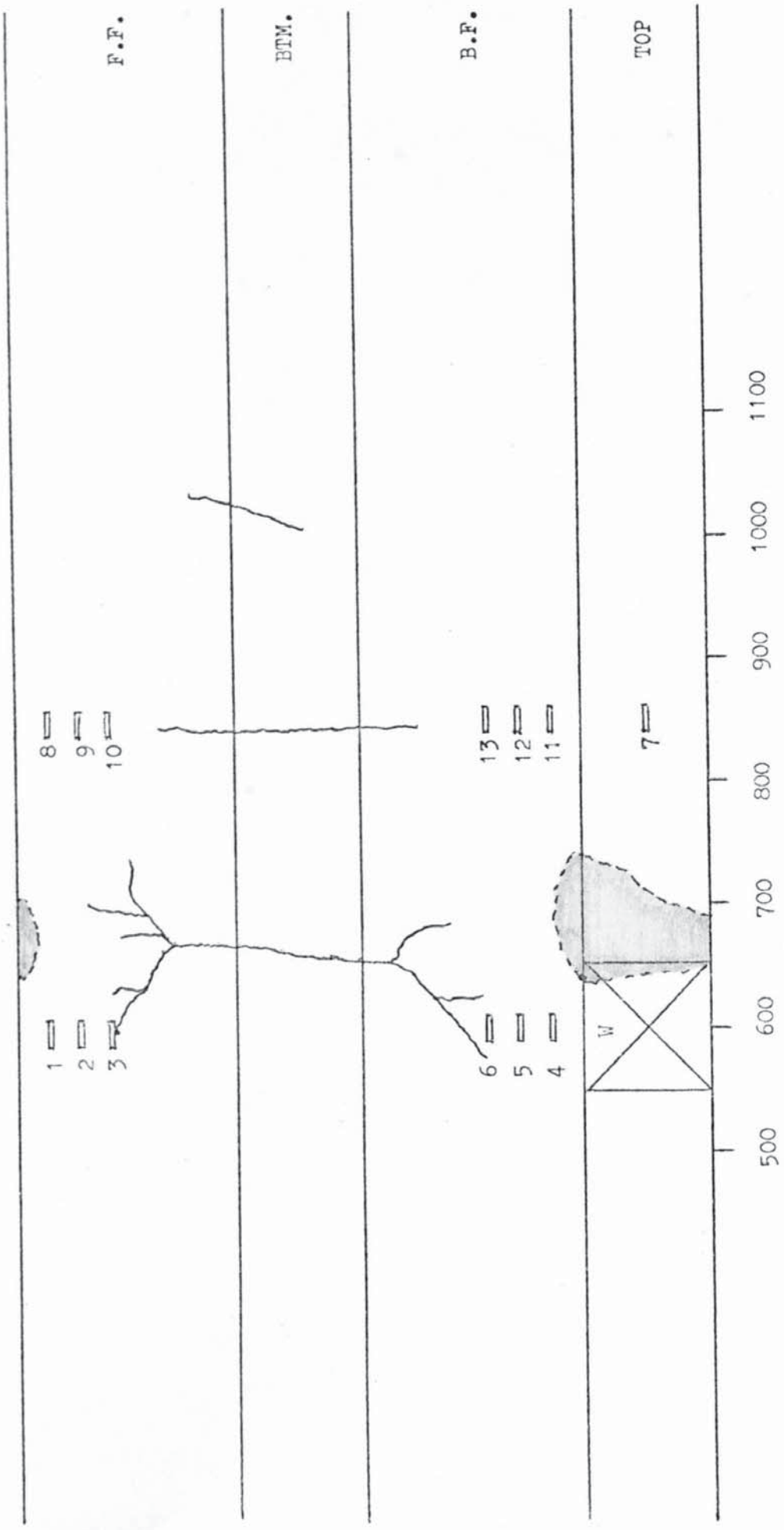

FIGURE 8.16 FAILURE CRACK PATTERNS - BEAM 16 (MODE 1)

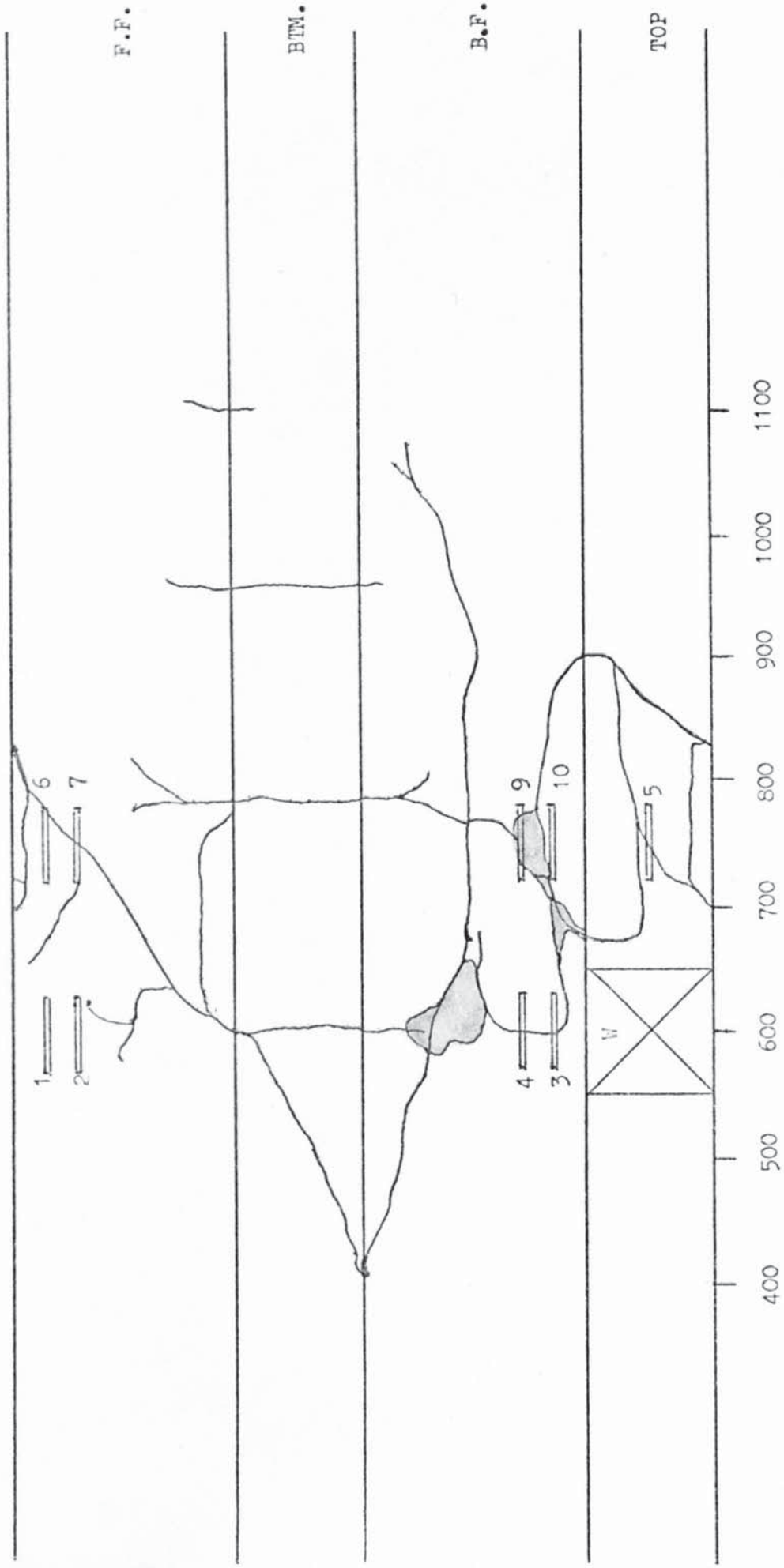

FIGURE 8.17 FAILURE CRACK PATTERNS - BEAM 17 (MODE 1/2)

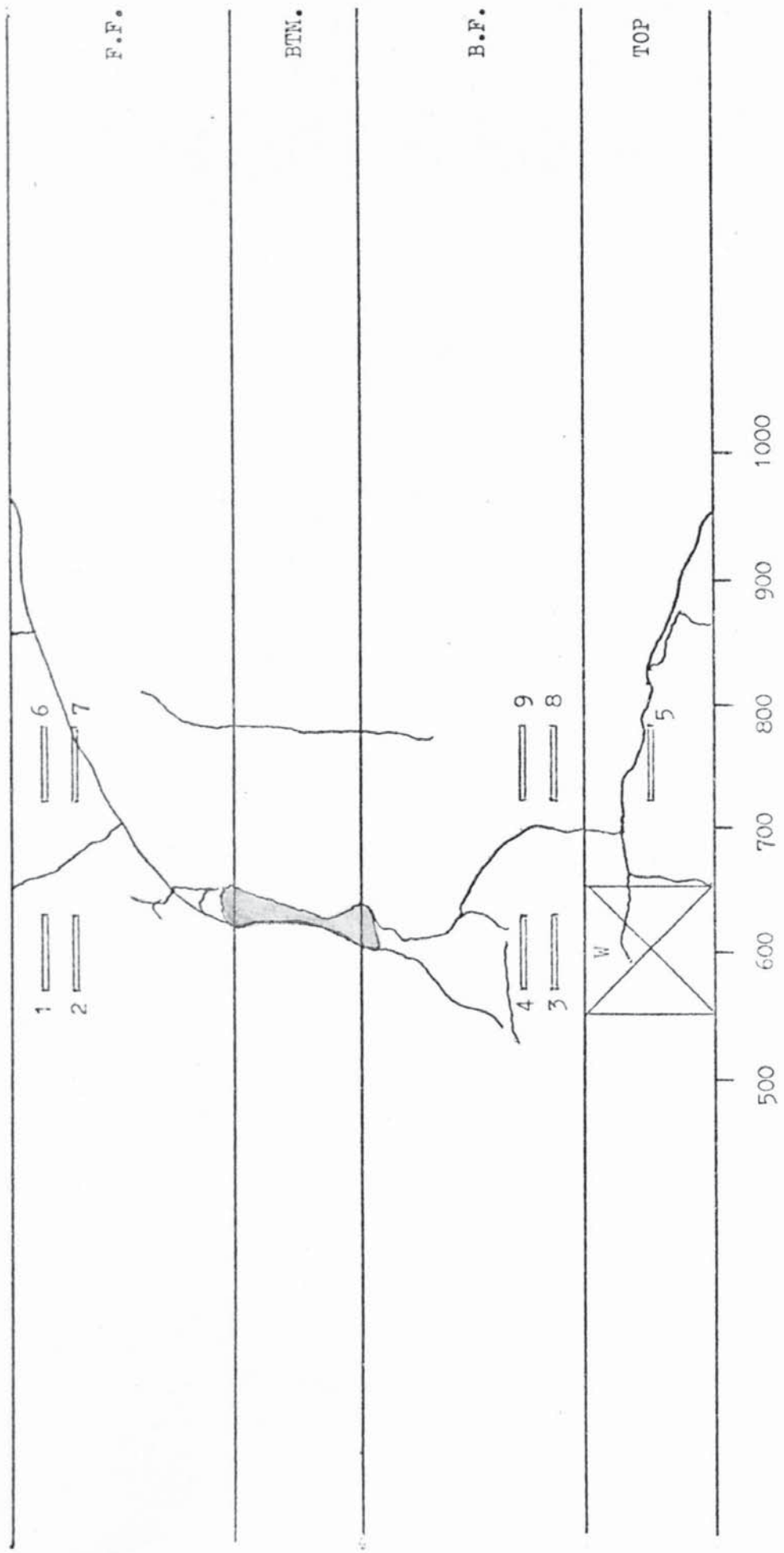

FIGURE 8.18 FAILURE CRACK PATTERNS - BEAM 18 (MODE 1)

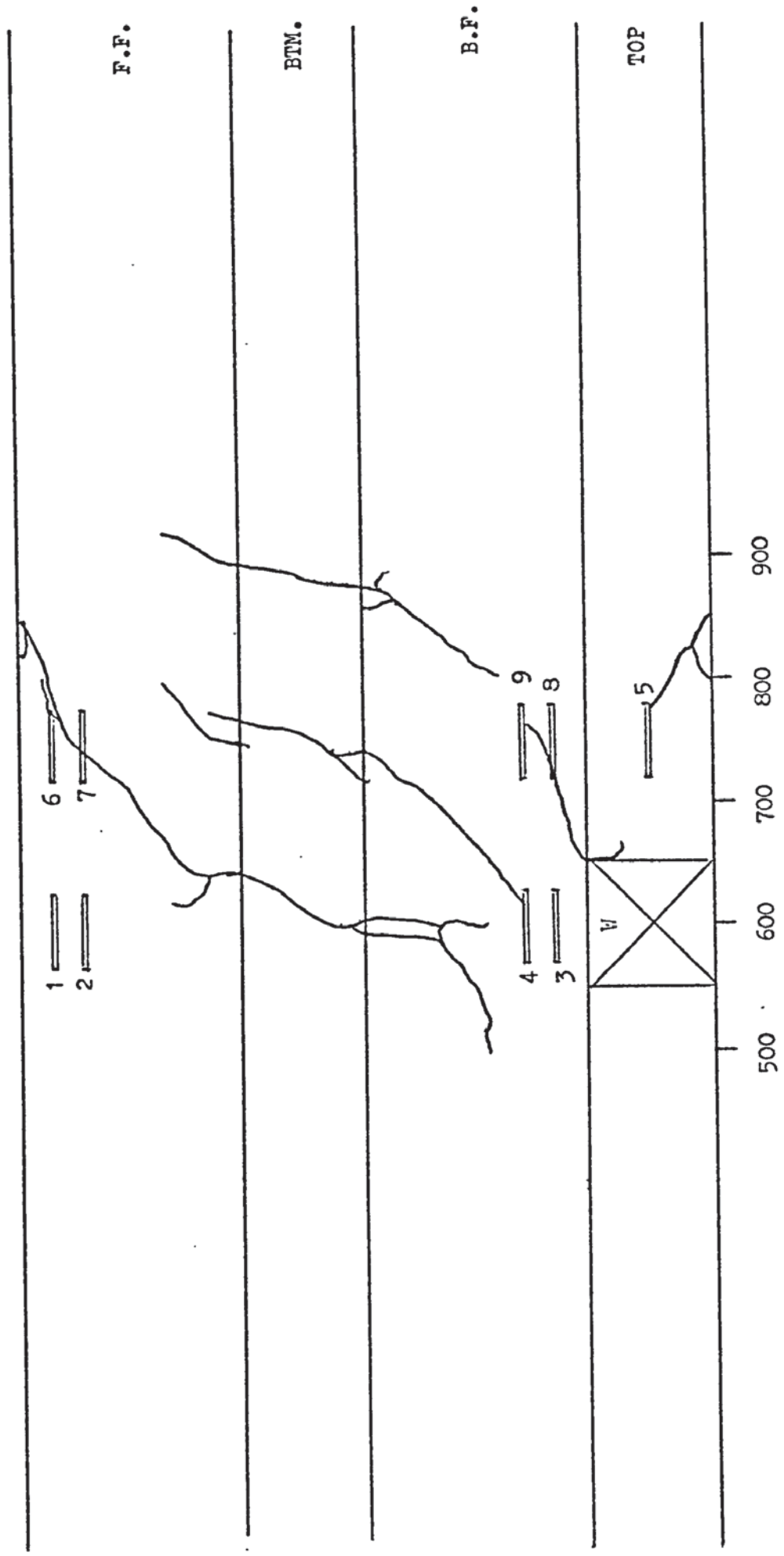

FIGURE 8.19 FAILURE CRACK PATTERNS - BEAM 19 (MODE 1)

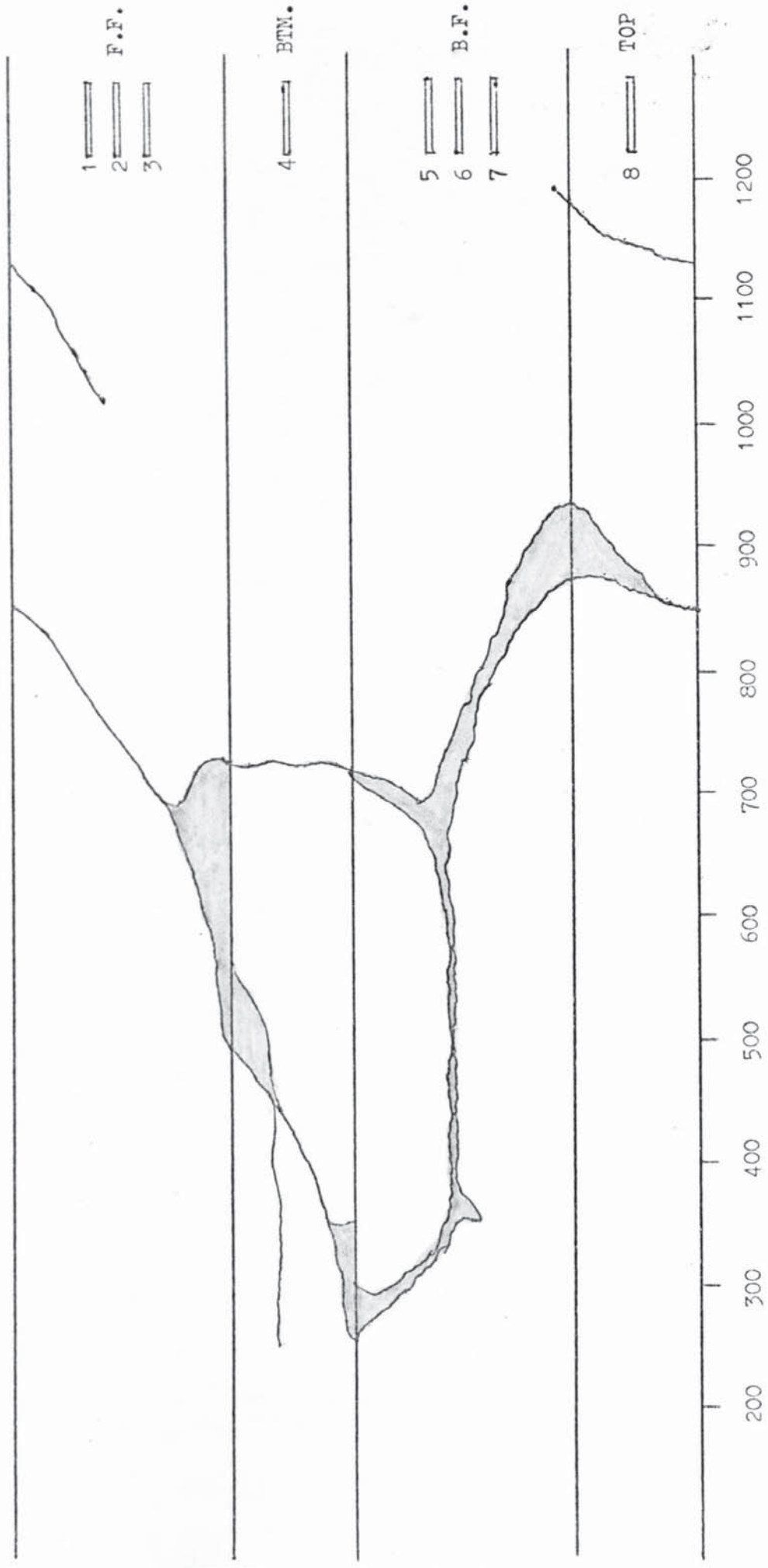

FIGURE 8.20 FAILURE CRACK PATTERNS - BEAM 20 (MODE 2)

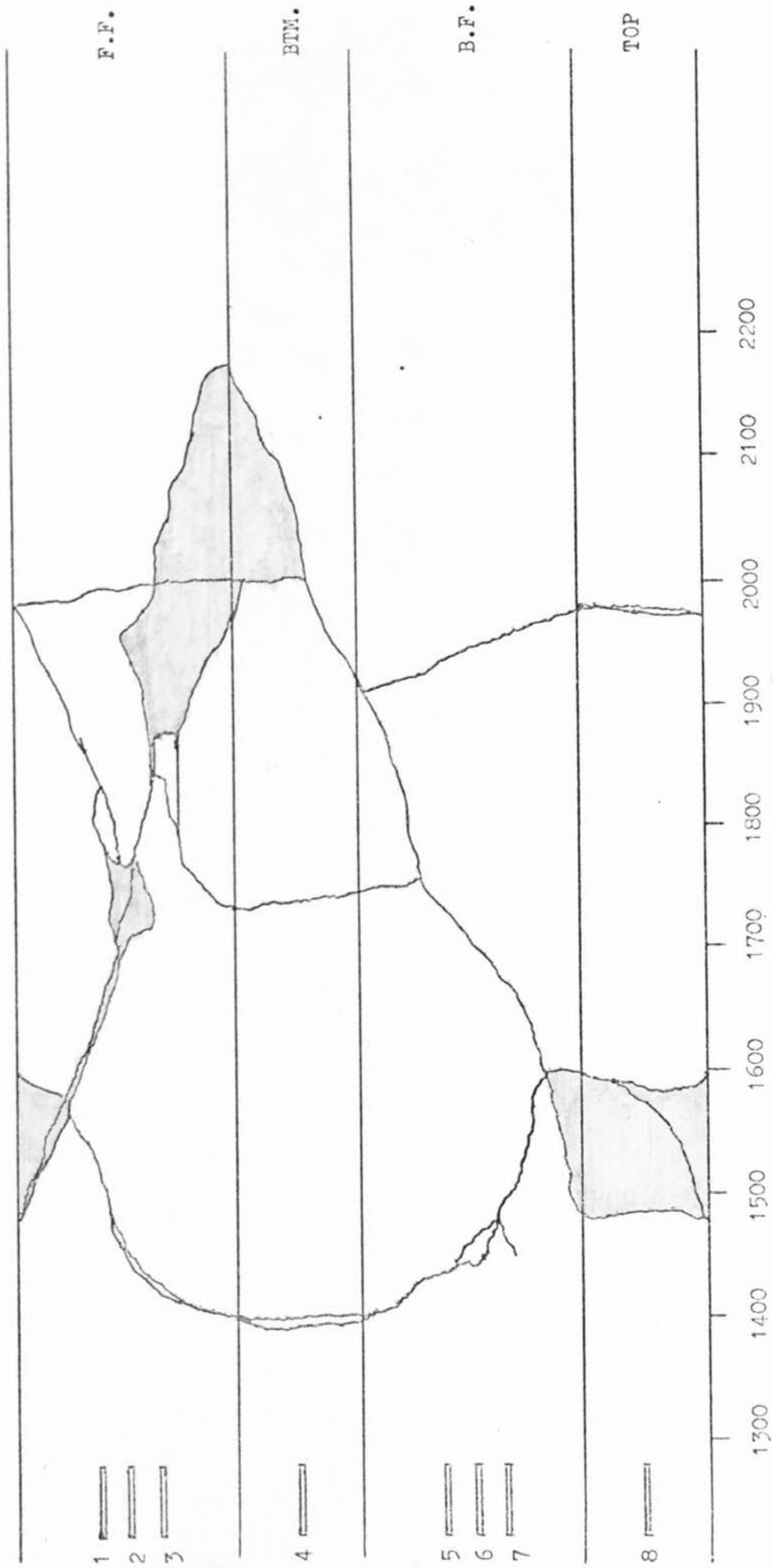

FIGURE 8.21 FAILURE CRACK PATTERNS - BEAM 21 (MODE 2)

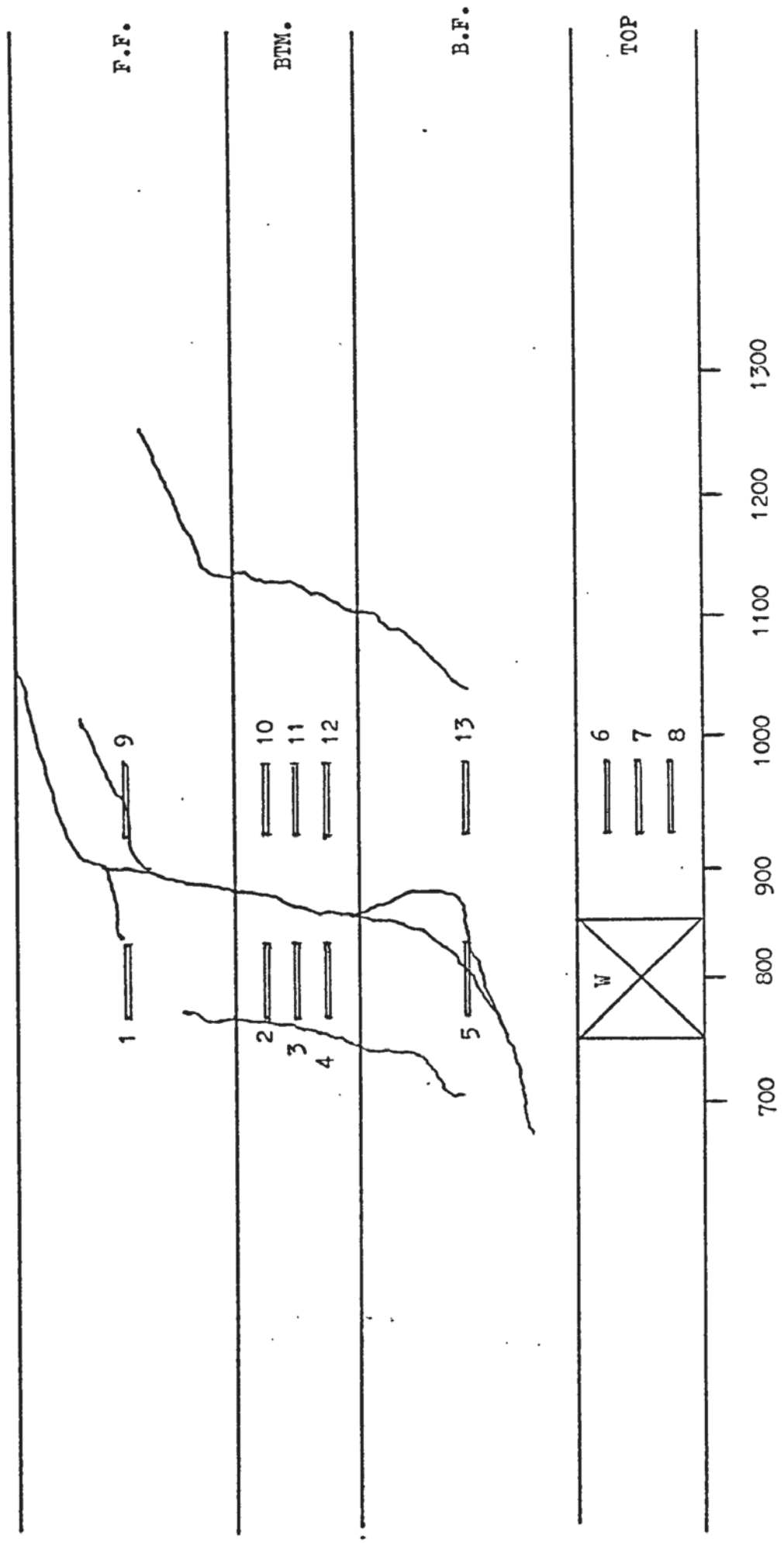

FIGURE 8.22 FAILURE CRACK PATTERNS - BEAM 22 (MODE 1)

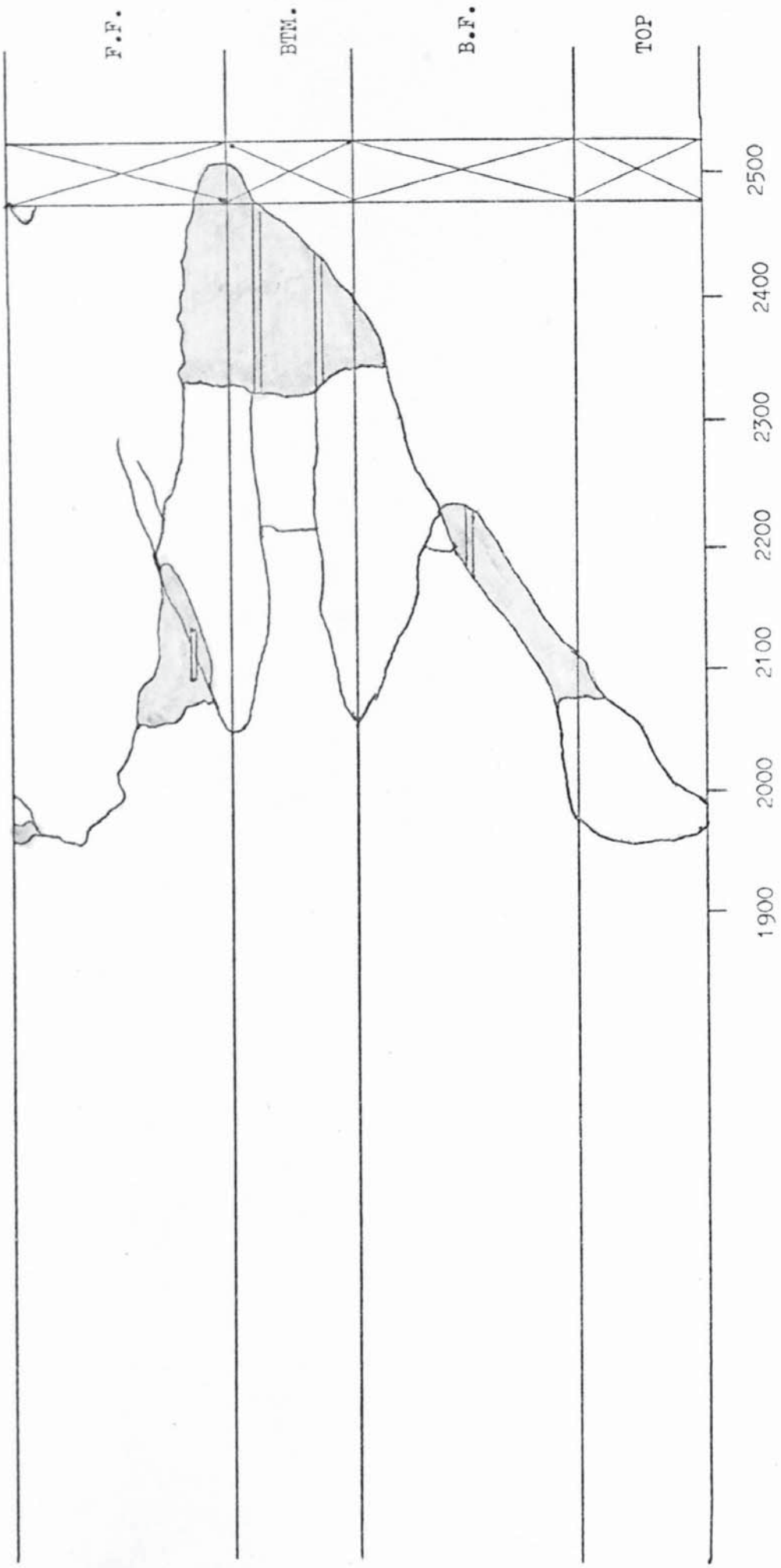

FIGURE 8.23 FAILURE CRACK PATTERNS - BEAM 23 (MODE 2)

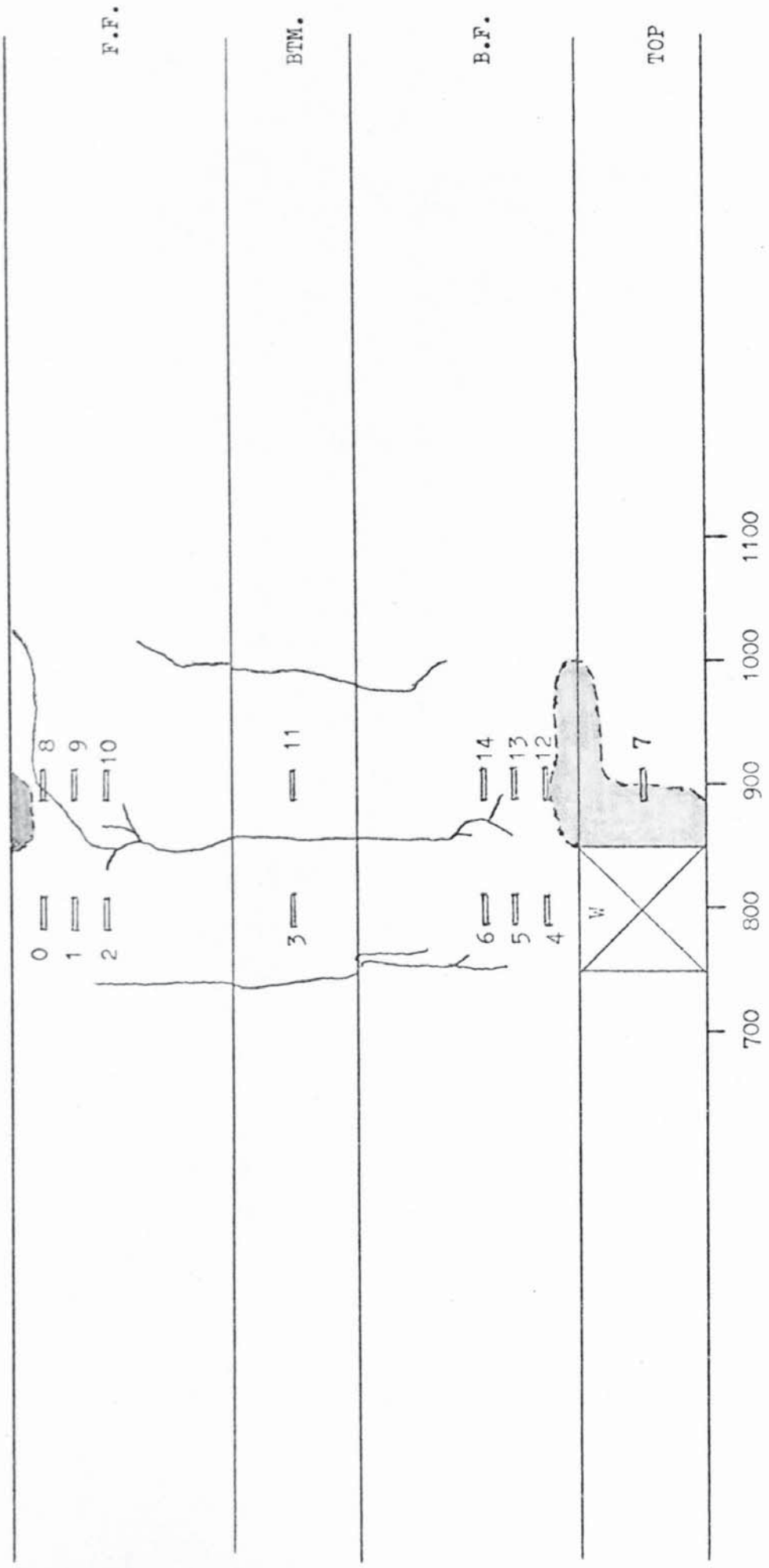

FIGURE 8.2.4 FAILURE CRACK PATTERNS - BEAM 25 (MODE 1)

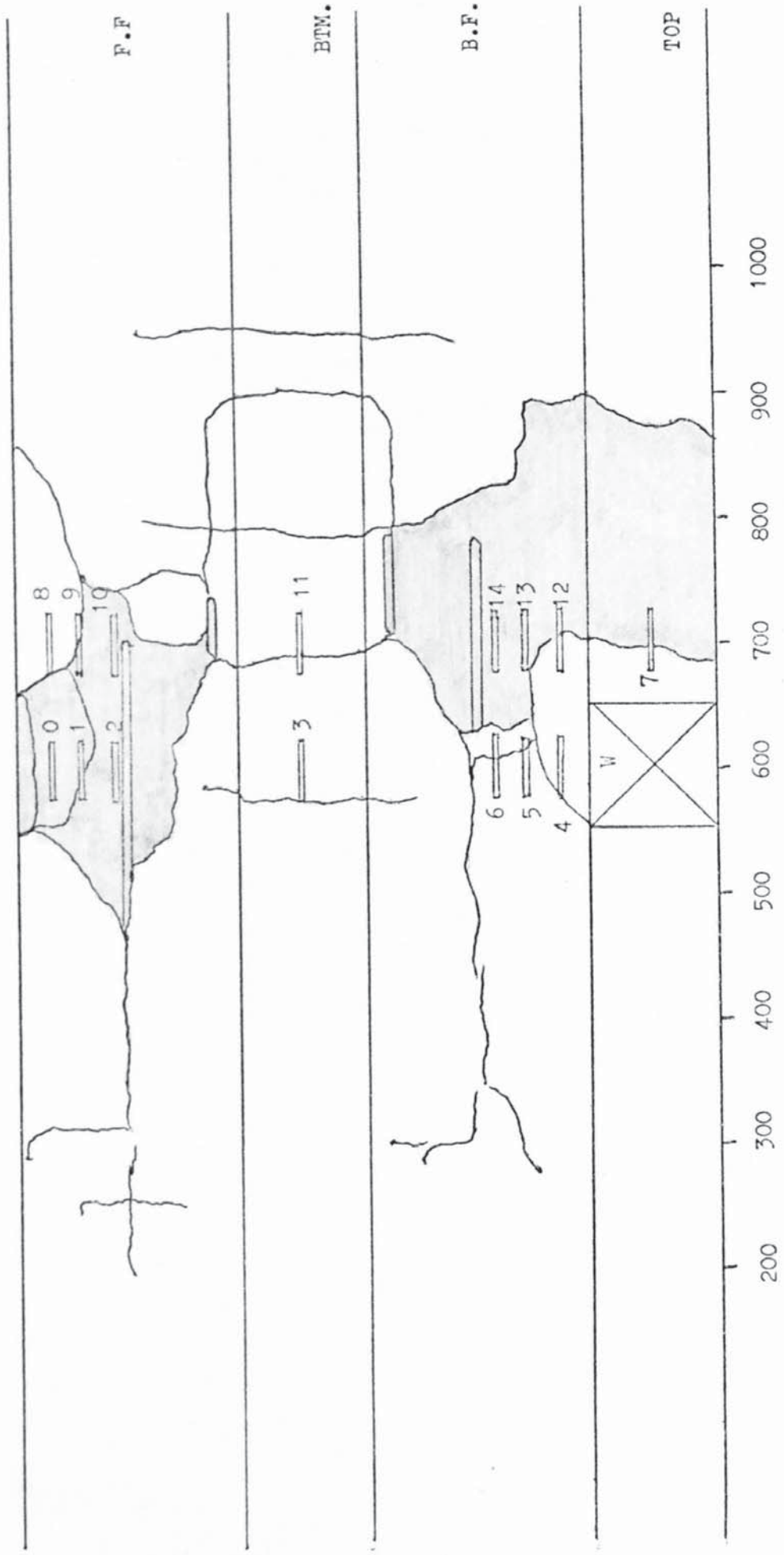

FIGURE 8.25 FAILURE CRACK PATTERNS - BEAM 26 (MODE 1)

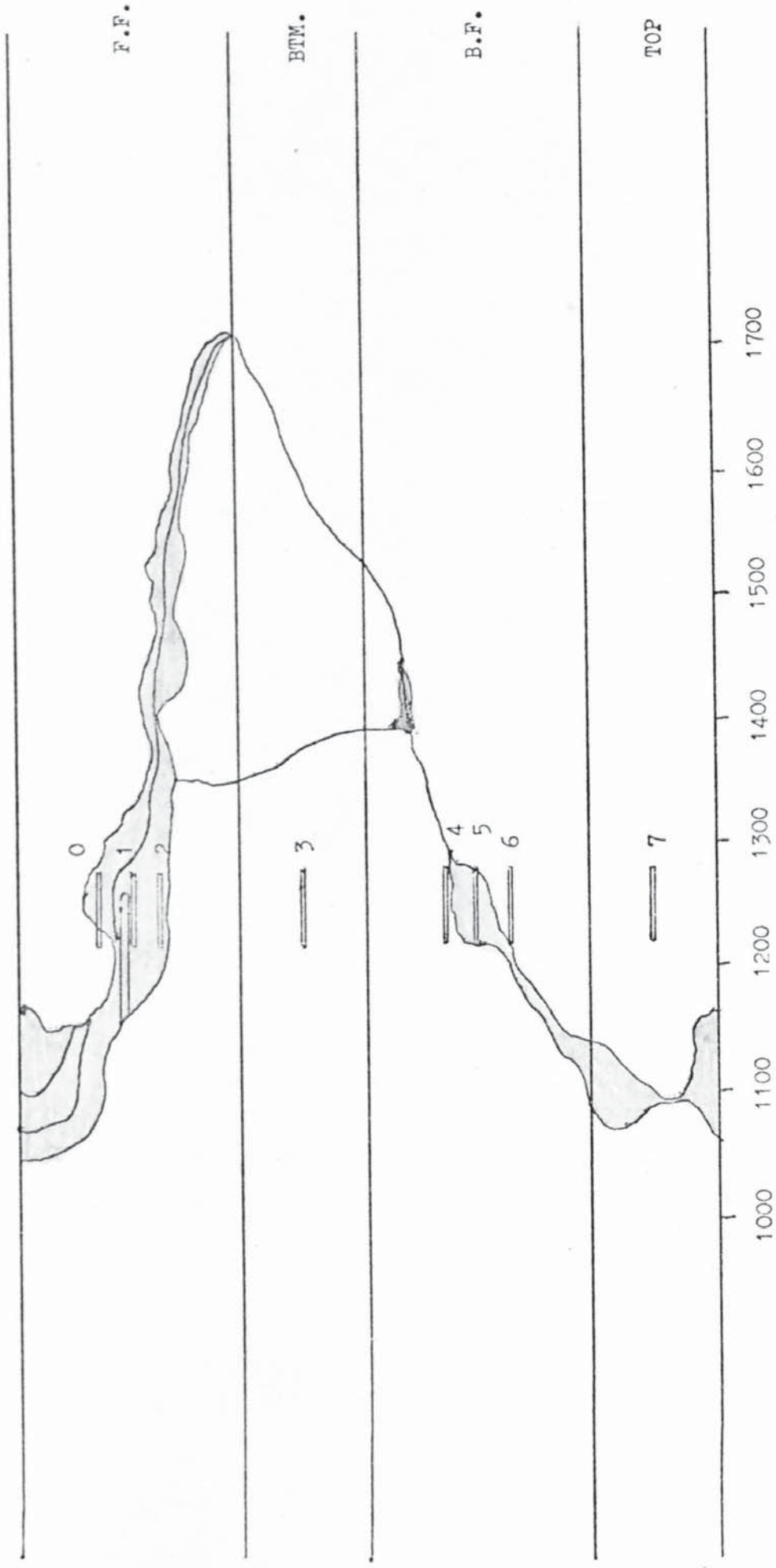

FIGURE 8.26 FAILURE CRACK PATTERNS - BEAM 27 (MODE 2)

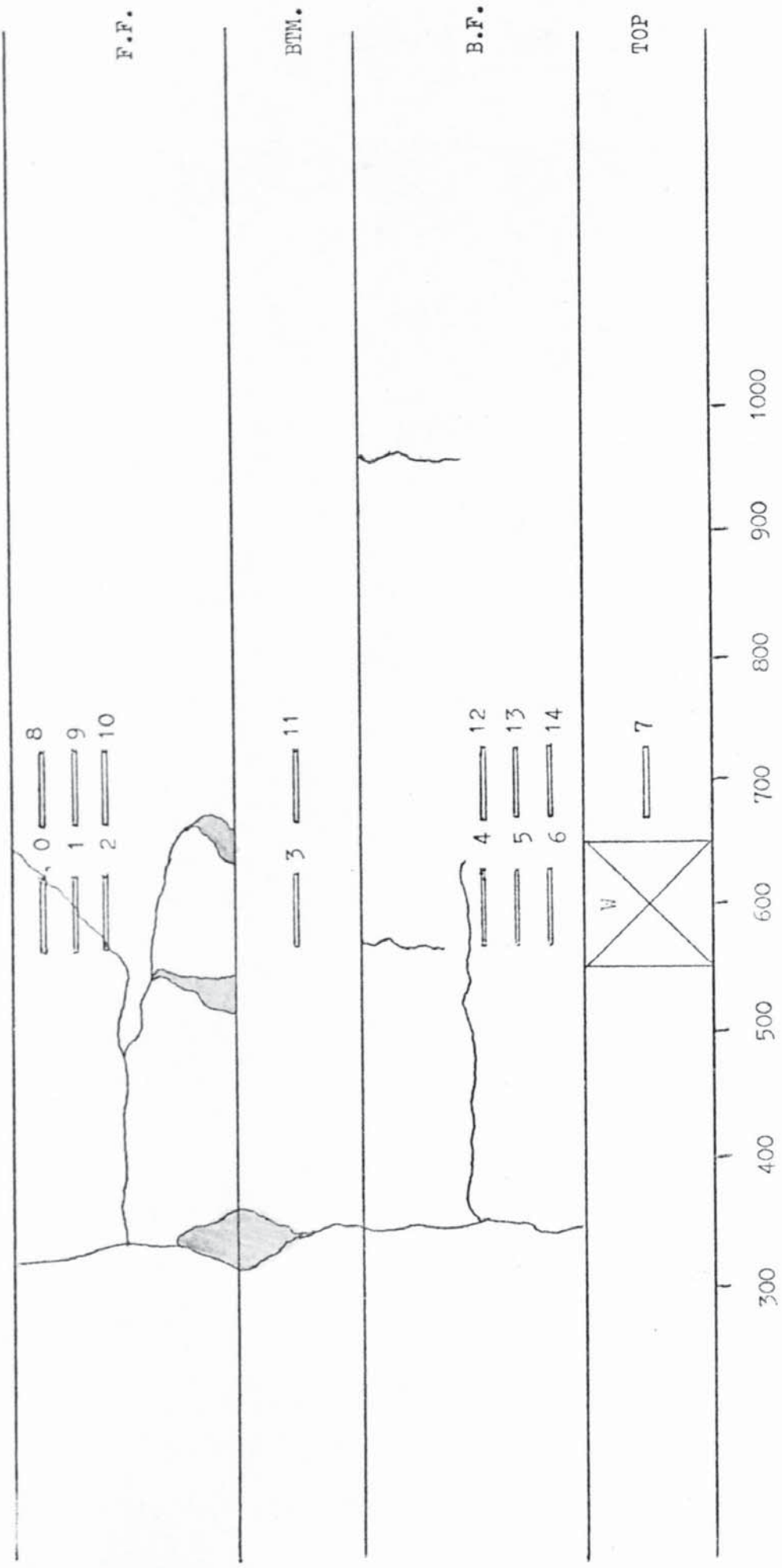

FIGURE 8.27 FAILURE CRACK PATTERNS - BEAM 28 (MODE 1)

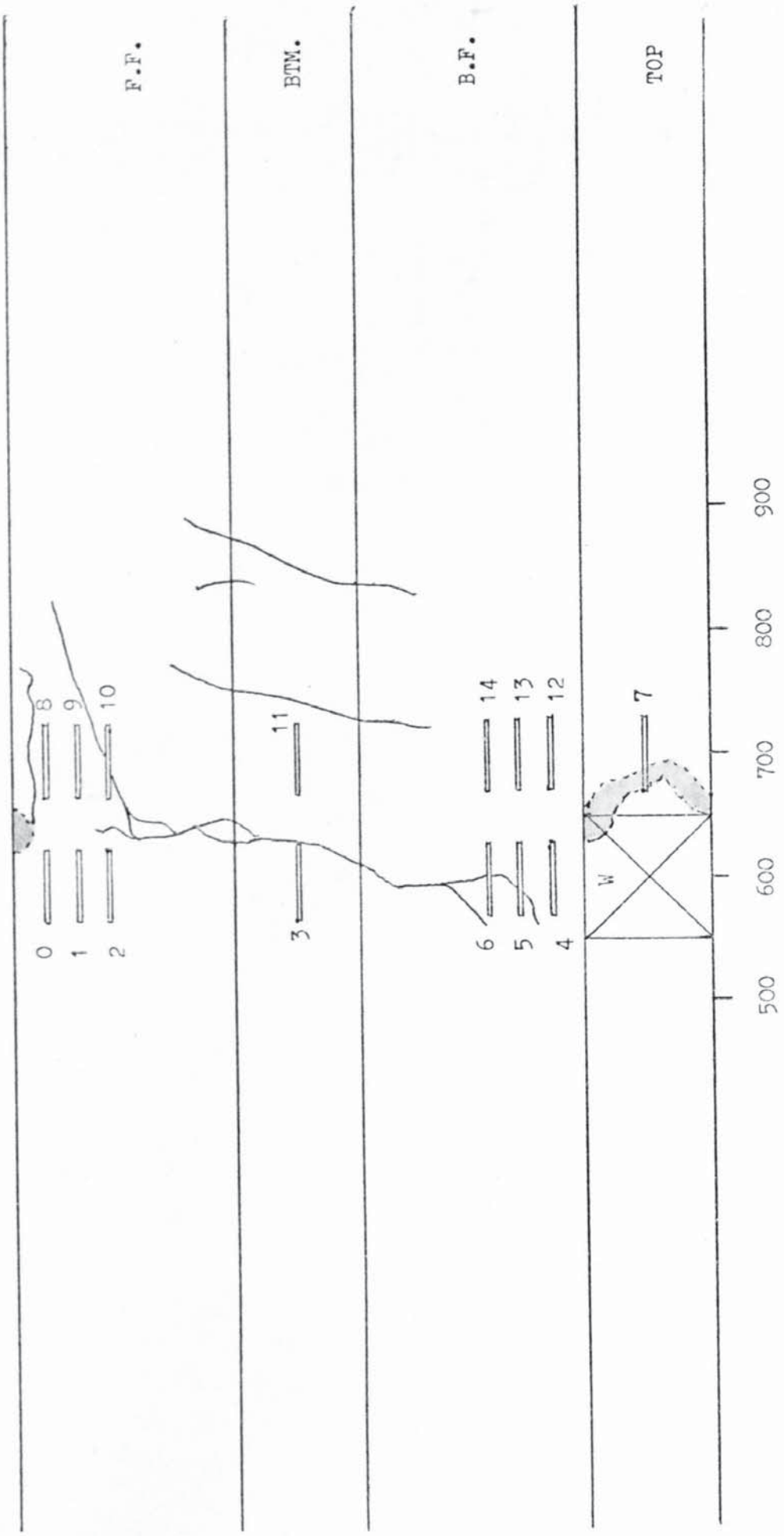

FIGURE 8.28. FAILURE CRACK PATTERNS - BEAM 29 (MODE 1)

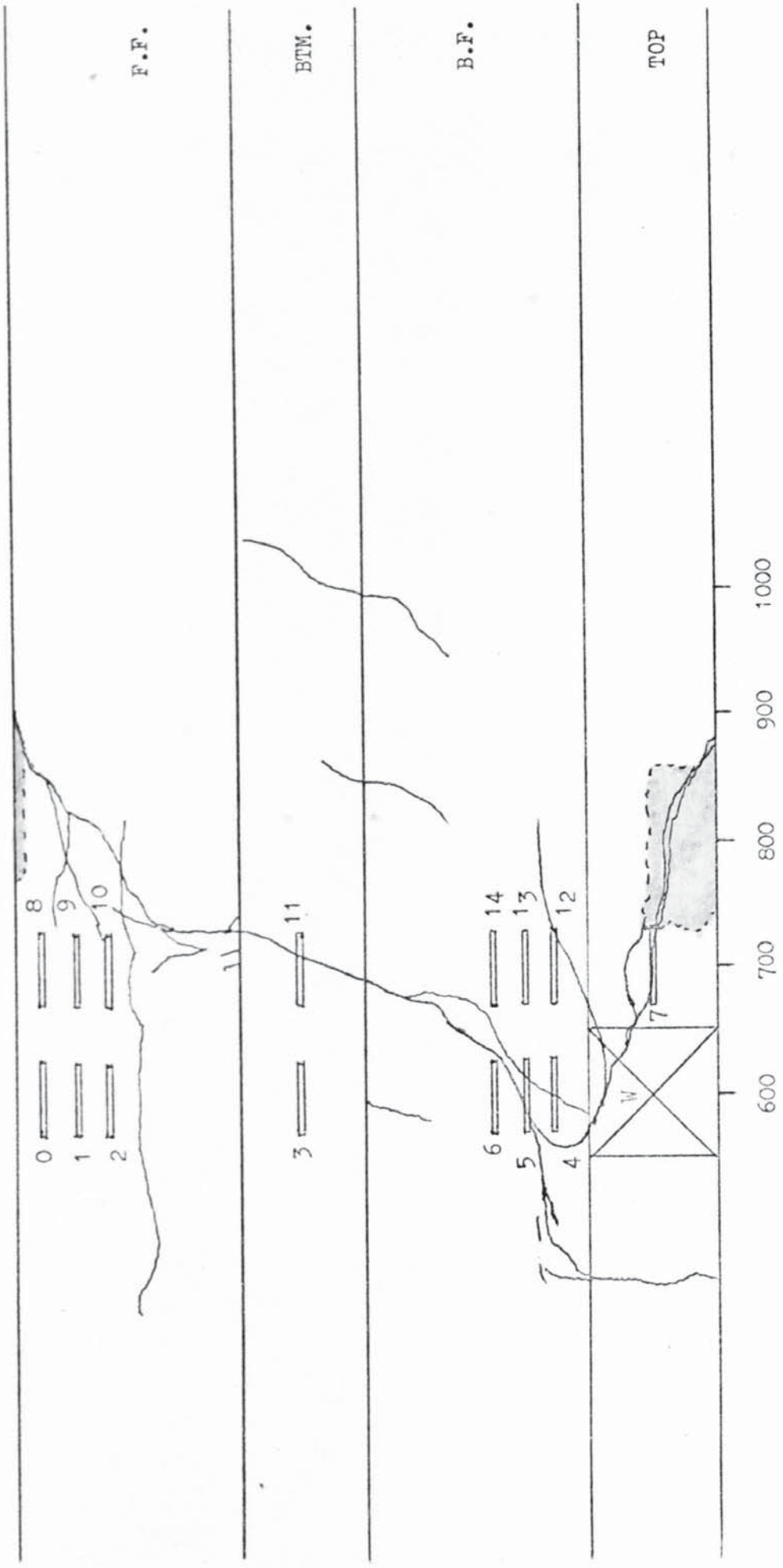

FIGURE 8.29 FAILURE CRACK PATTERNS - BEAM 30 (MODE 1)

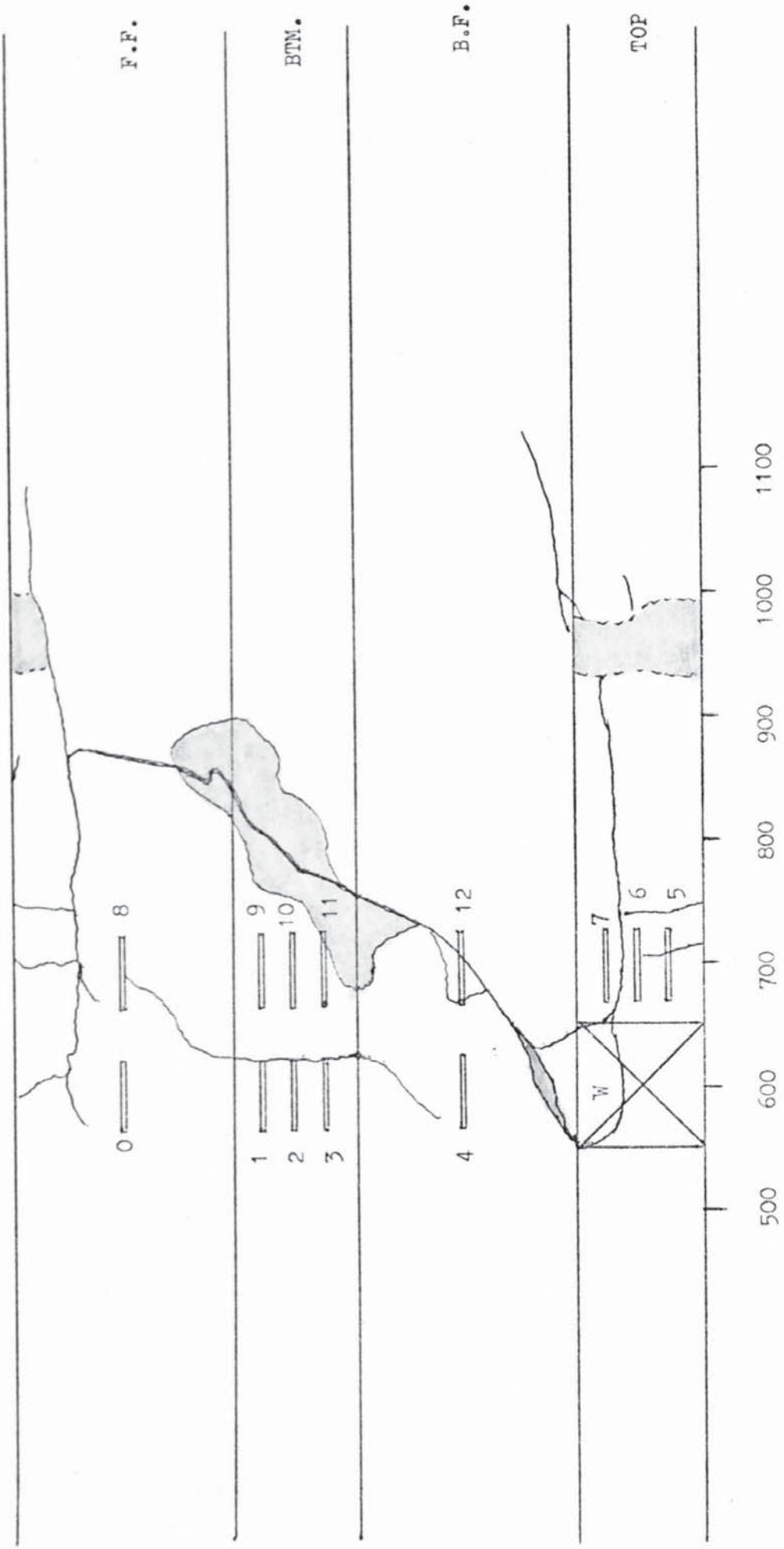

FIGURE 8.30 FAILURE CRACK PATTERNS - BEAM 31 (MODE 1)

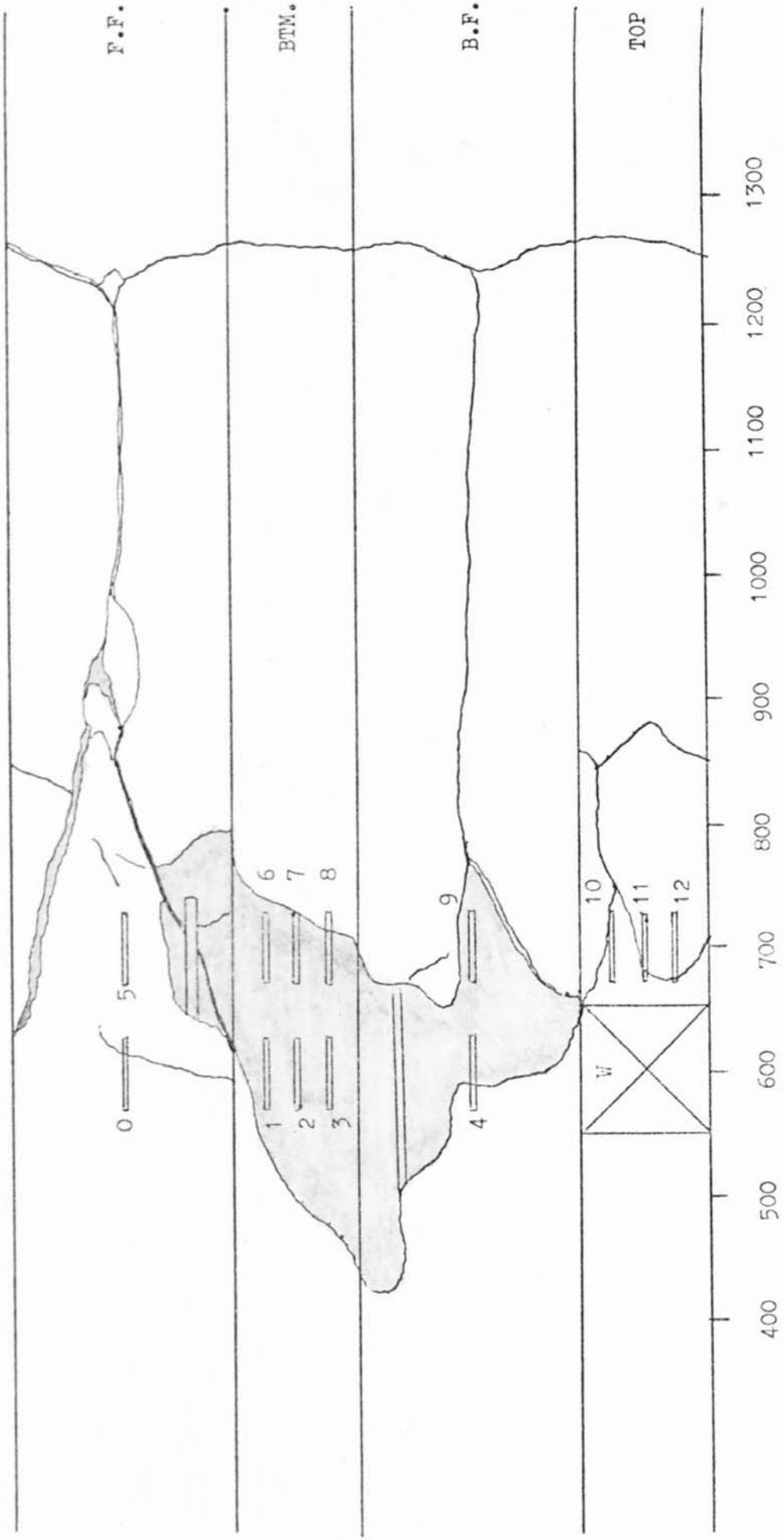

FIGURE 8.31 FAILURE CRACK PATTERNS - BEAM 32 (MODE 1/2)

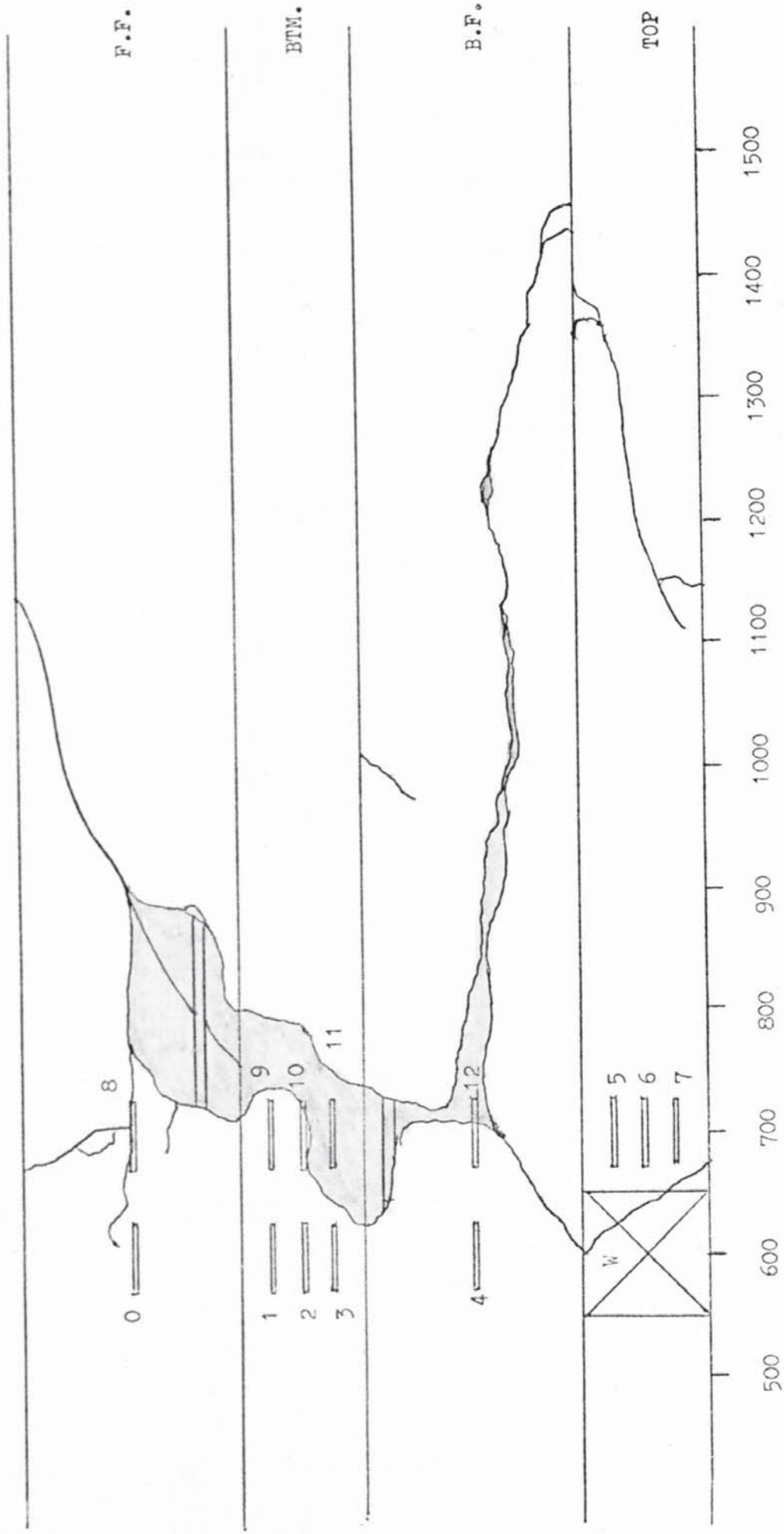

FIGURE 8.32 FAILURE CRACK PATTERNS - BEAM 33 (MODE 2)

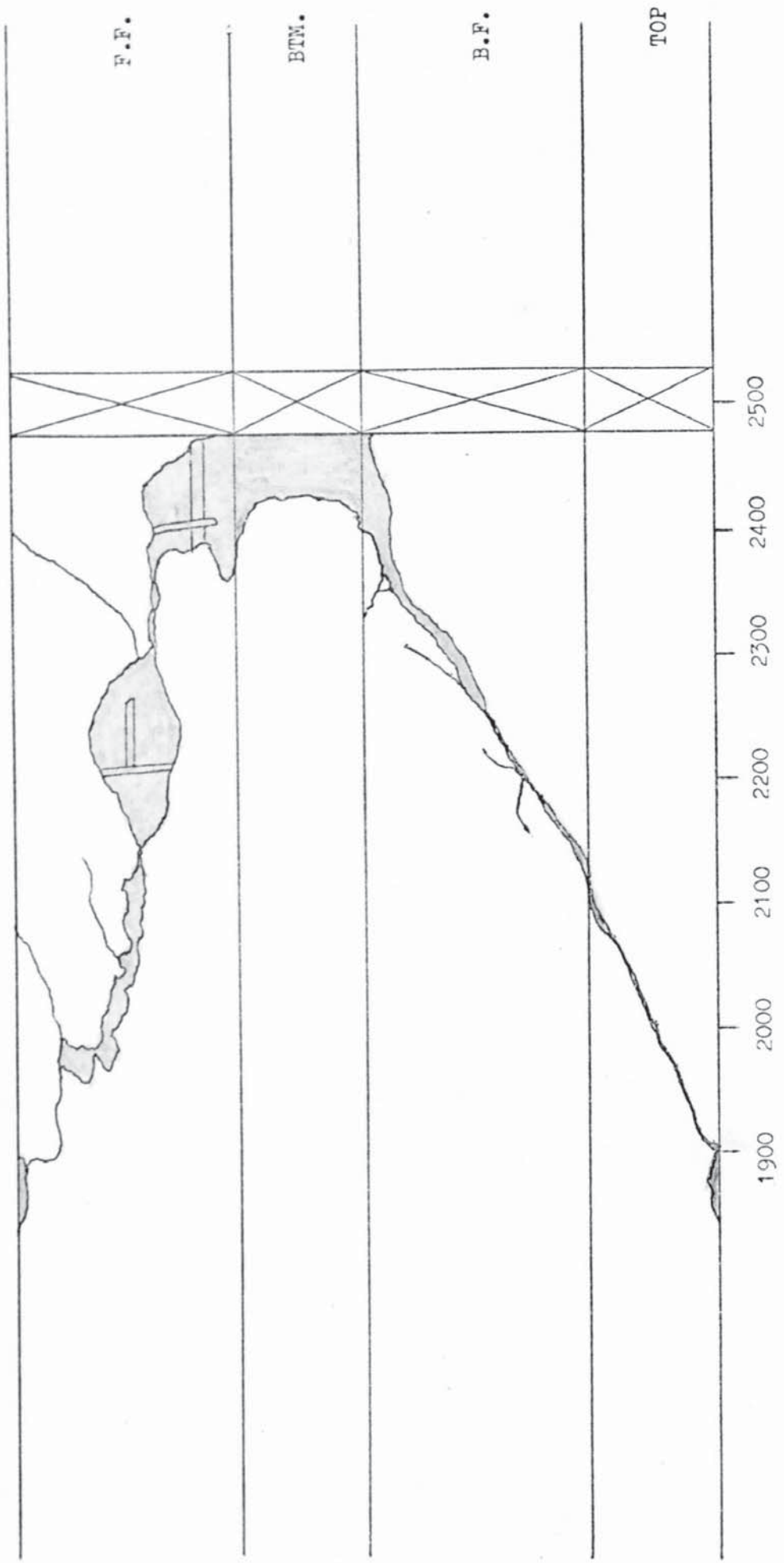

FIGURE 8.33 FAILURE CRACK PATTERNS - BEAM 34 (MODE 2)

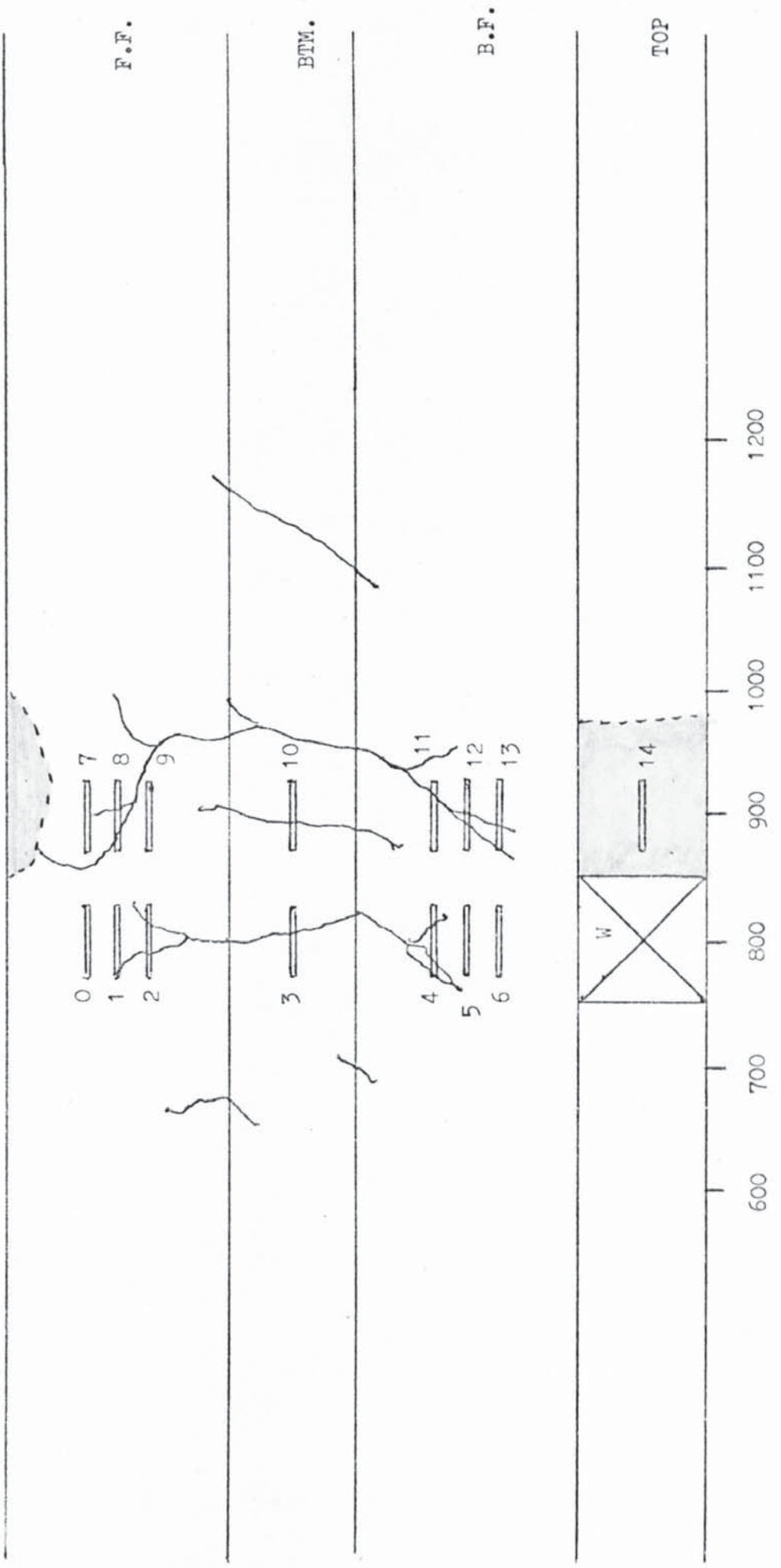

FIGURE 8.34 FAILURE CRACK PATTERNS - BEAM 35 (MODE 1)

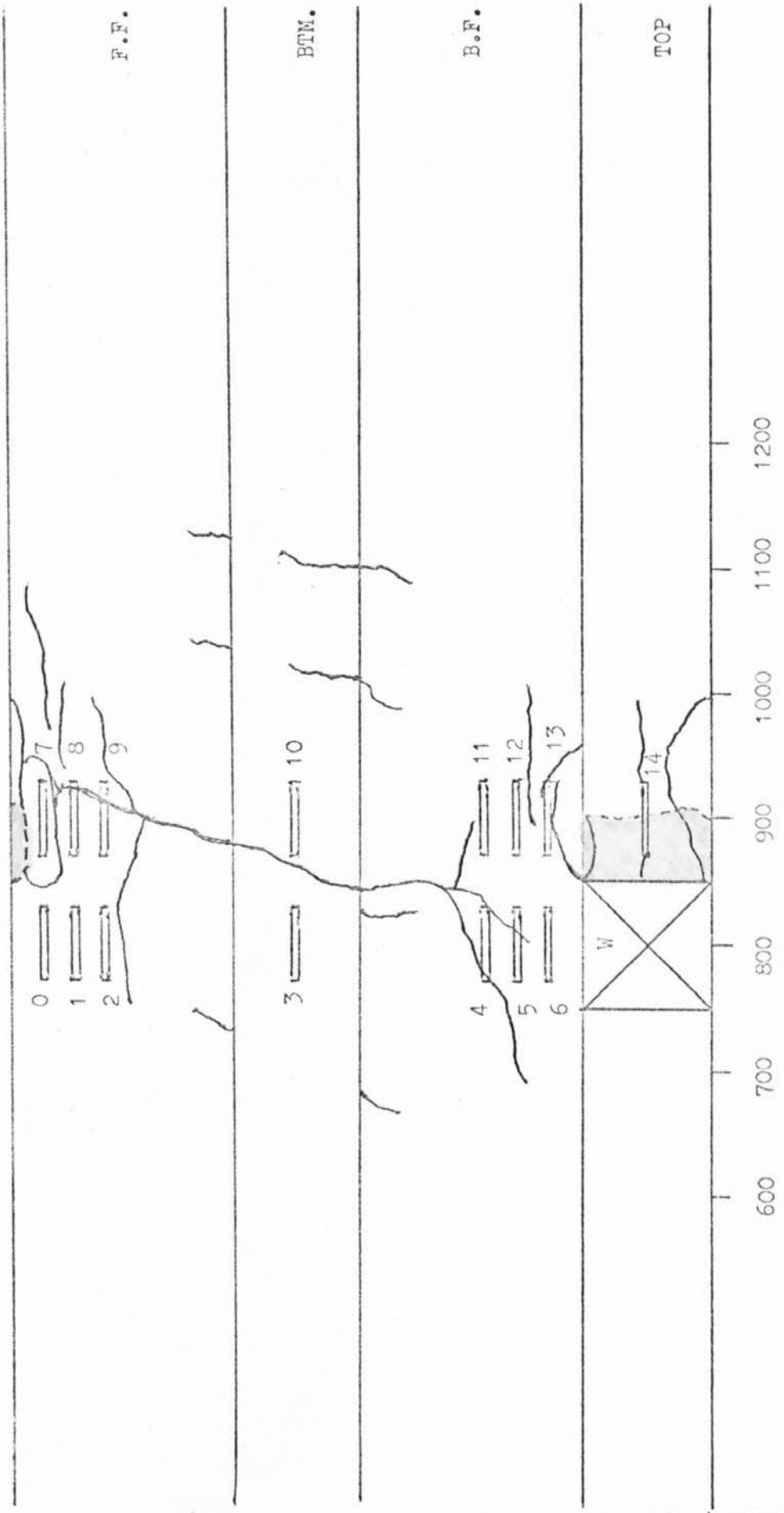

FIGURE 8.35 FAILURE CRACK PATTERNS - BEAM 36 (MODE 1)

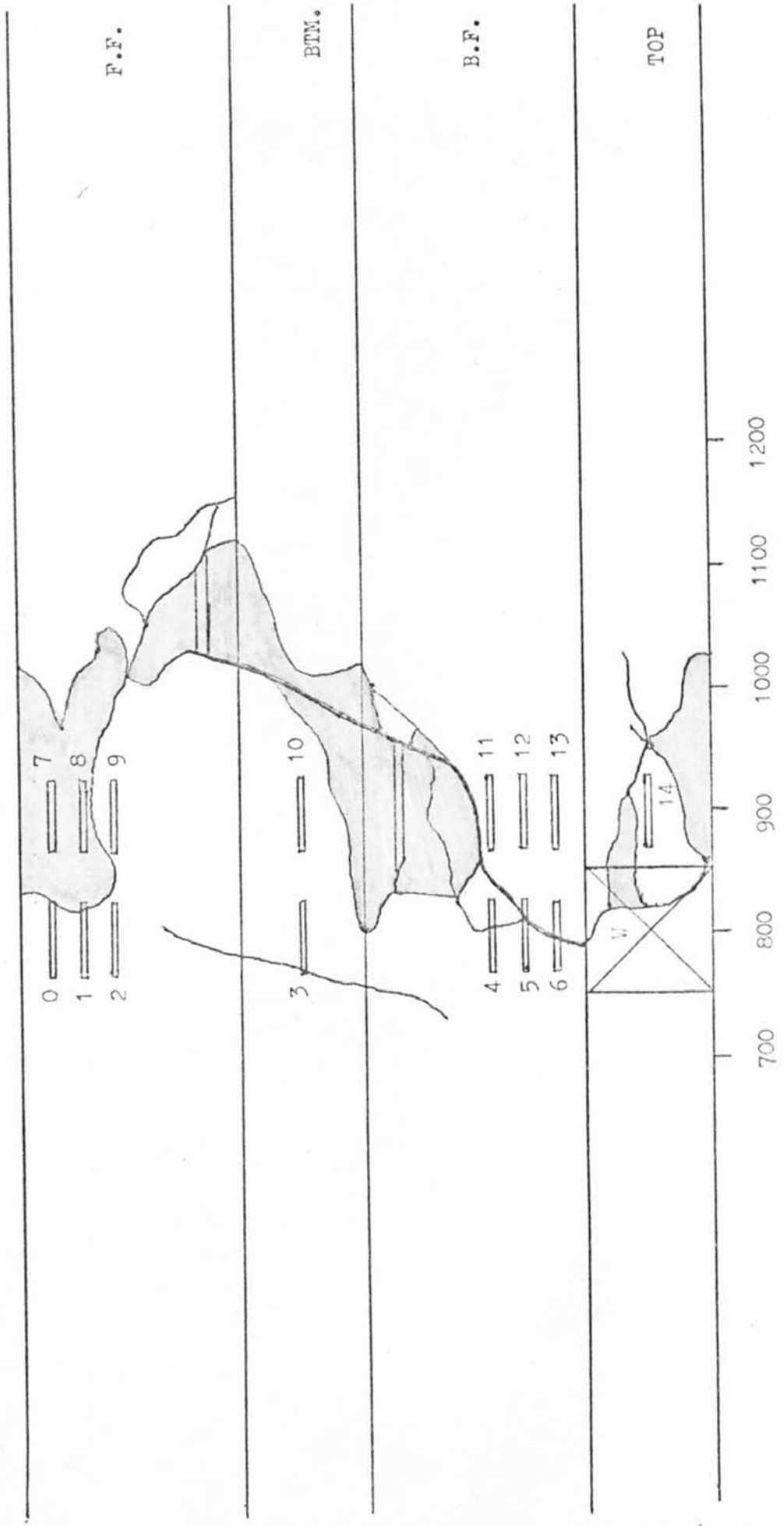

FIGURE 8.36 FAILURE CRACK PATTERNS - BEAM 37 (MODE 1)

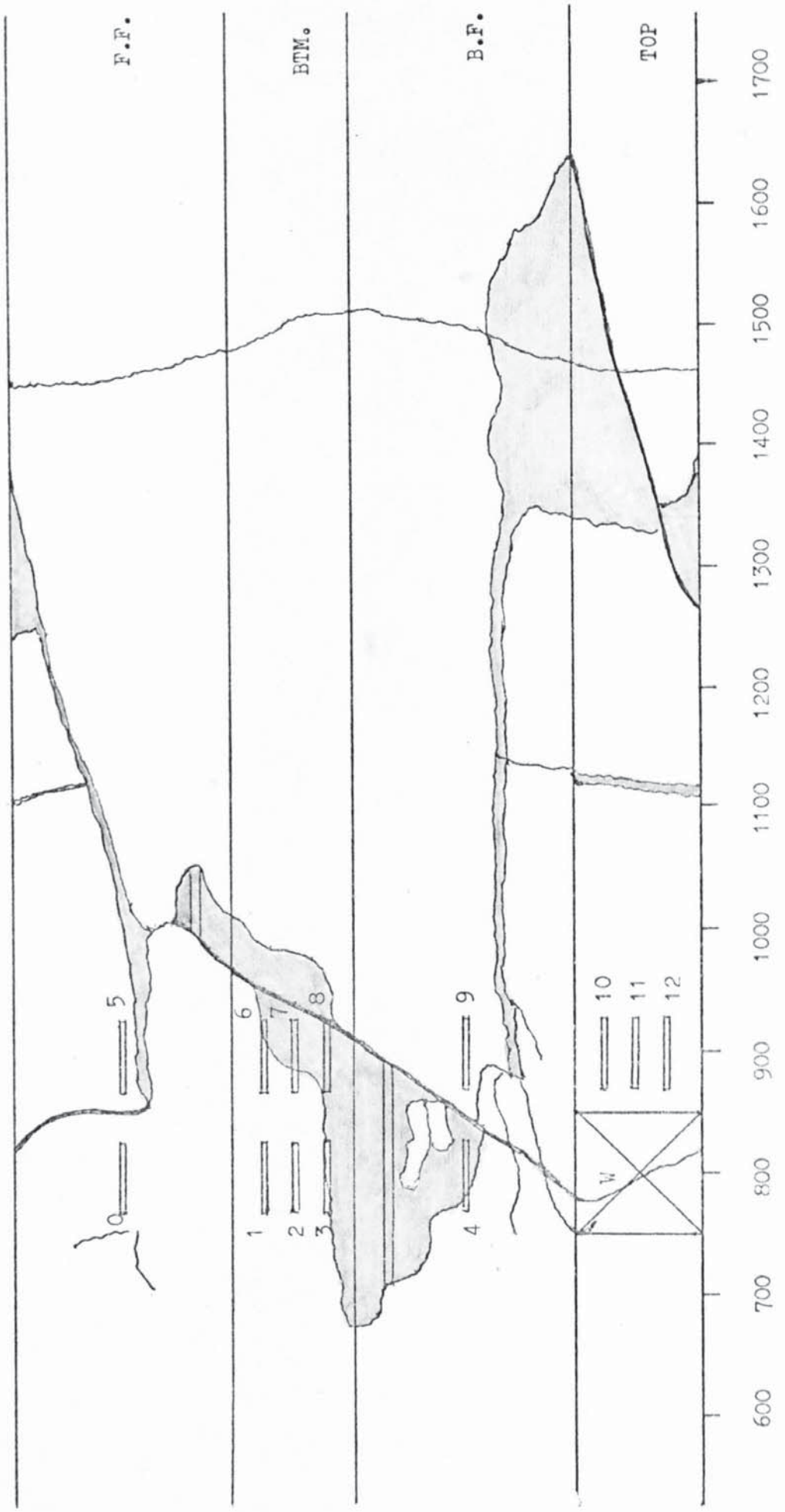

FIGURE 8.37 FAILURE CRACK PATTERNS - BEAM 38 (MODE 1/2)

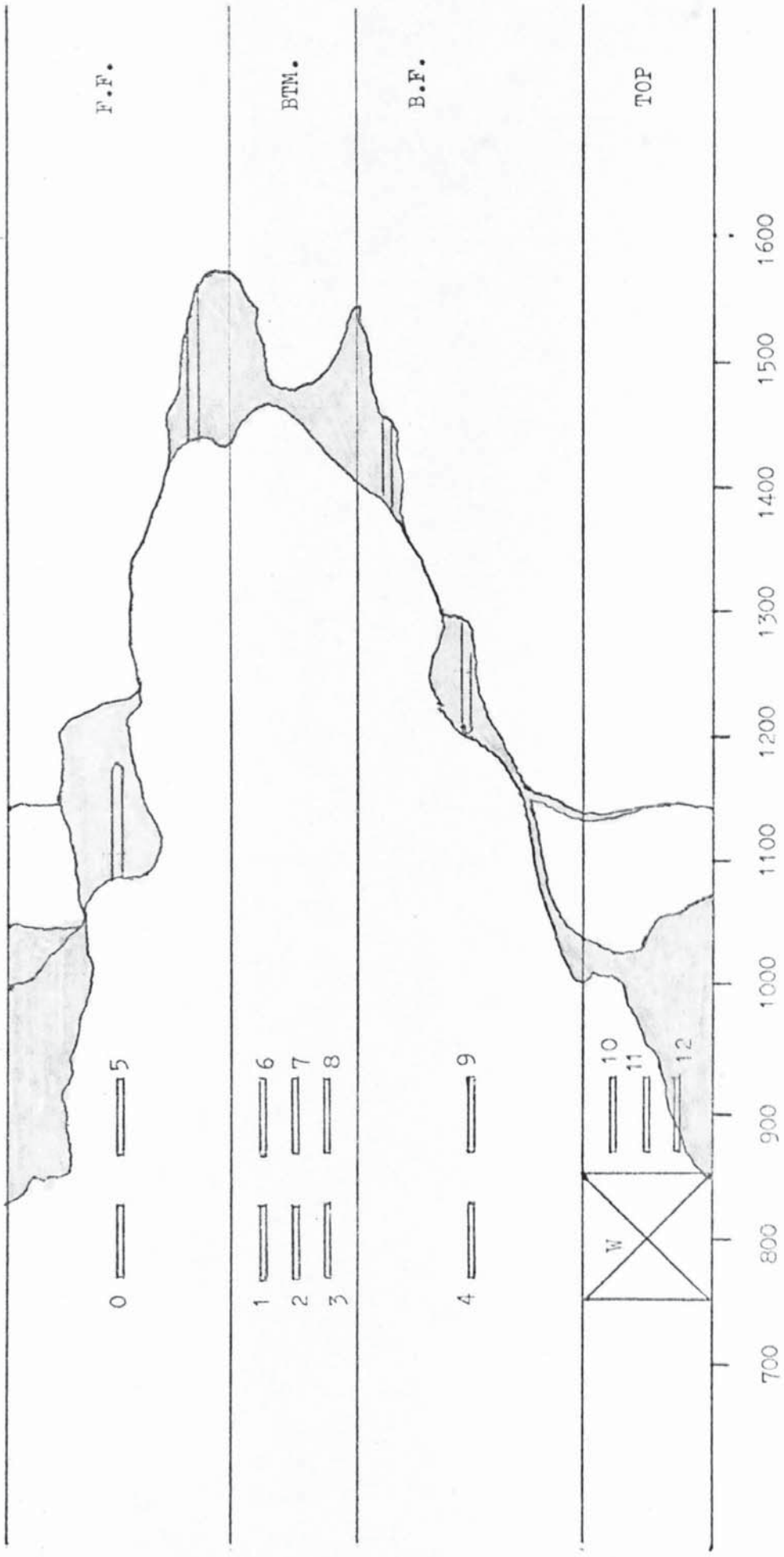

FIGURE 8.38 FAILURE CRACK PATTERNS - BEAM 39 (MODE 2)

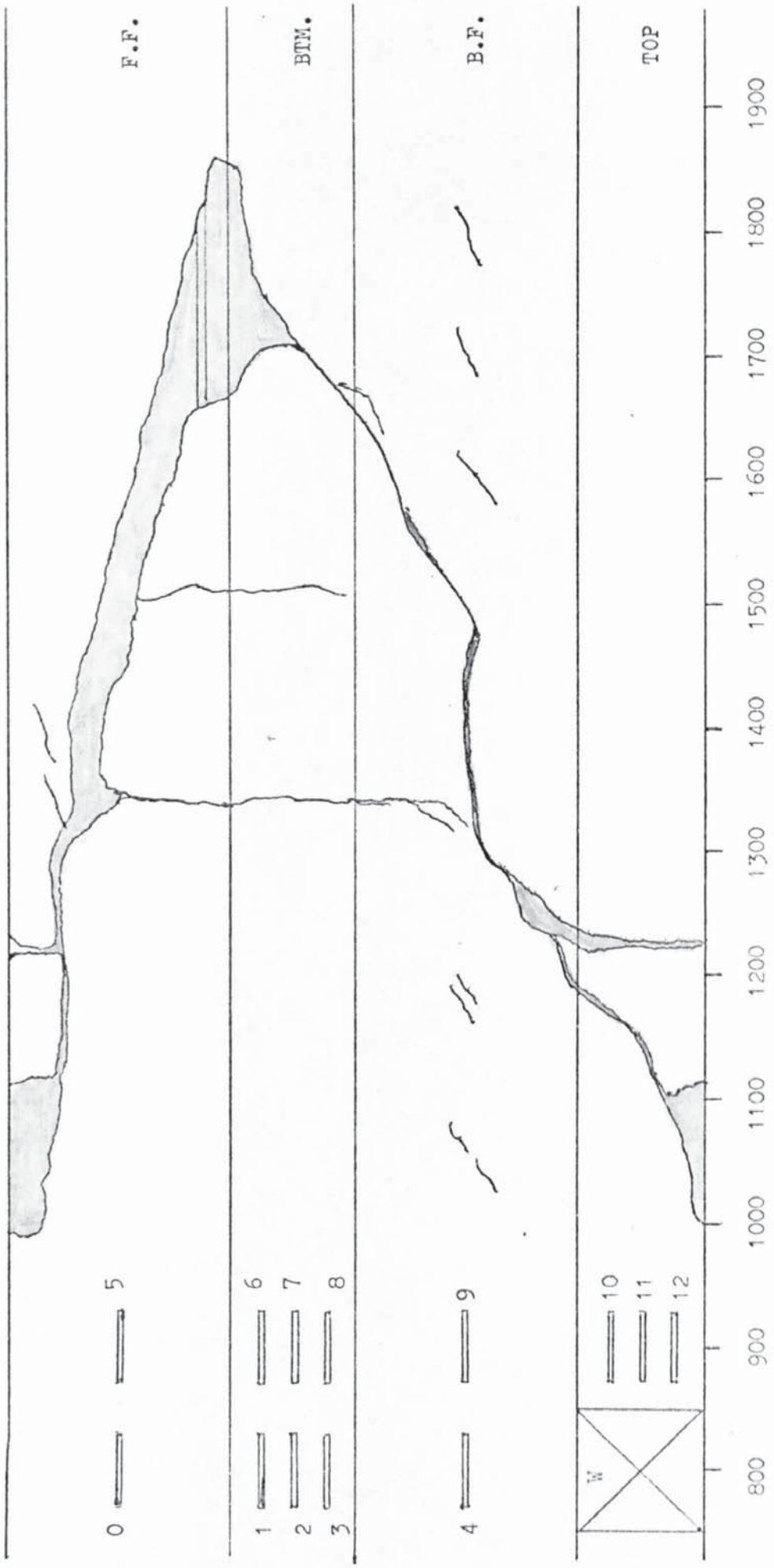

FIGURE 8.39 FAILURE CRACK PATTERNS - BEAM 40 (MODE 2)

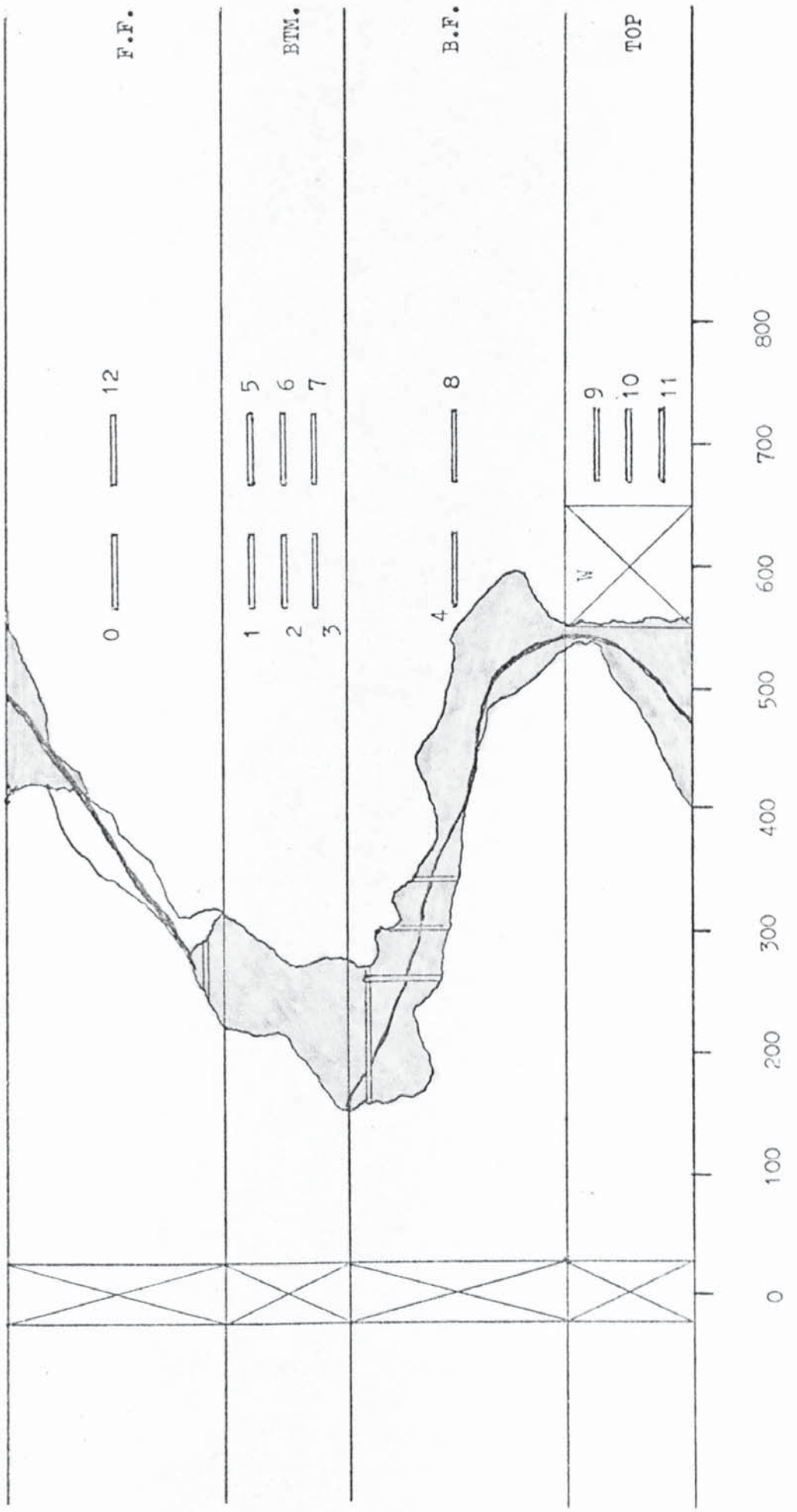

FIGURE 8.40 FAILURE CRACK PATTERNS - BEAM 41 (MODE 2)

8.4 THE MEASUREMENT OF DEFLECTIONS AND ROTATIONS

Deflections

These were measured directly either with dial gauges or with linear transducers at either two or three points along the span. The load/deflection curves have been plotted in Figs. 8.41 to 8.44 for the deflection immediately under the load.

Rotations

The rotations were measured by dial gauges or linear transducers reading to .01 mm on the end of the torsion arms each 457 mm long.

Series 1

In these beams the torsion arms were located 50 mm outside the supports, i.e., at 2600 mm centres. Due to this arrangement, deflections of the beams due to vertical load caused decreased torsion arm readings.

In beams 0 - 9 the vertical load was applied first, and then the torsional load. Change in rotation due to vertical load has in this case been ignored, zero rotation being assumed to be for maximum vertical load and zero torsional load.

For beams 10 - 22 the vertical load and torsional load were increased in the same ratio. The effect of the vertical load has been allowed for by taking a proportion of the readings taken, on the application of the 20 kN settling down load, which was applied at the start of each test.

Series 2

In these beams the torsional arms were modified to be over each support; the measurements thus gave the overall rotation of the beam directly, over a length of 2500 mm.

The torque rotation curves are given in Figs. 8.45 to 8.49.

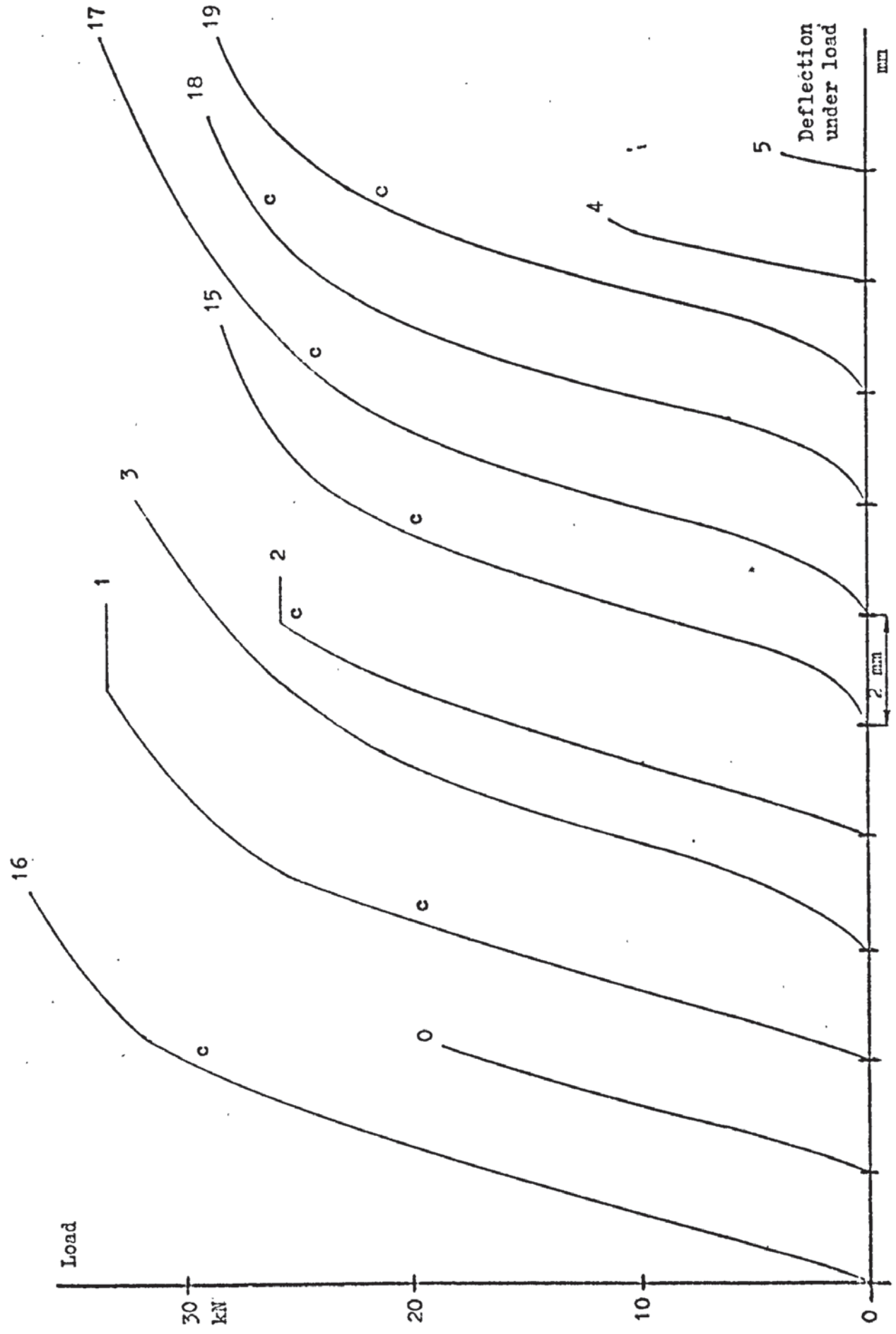

FIGURE 8.41 LOAD/DEFLECTION - SERIES 1, a_v = 600 mm

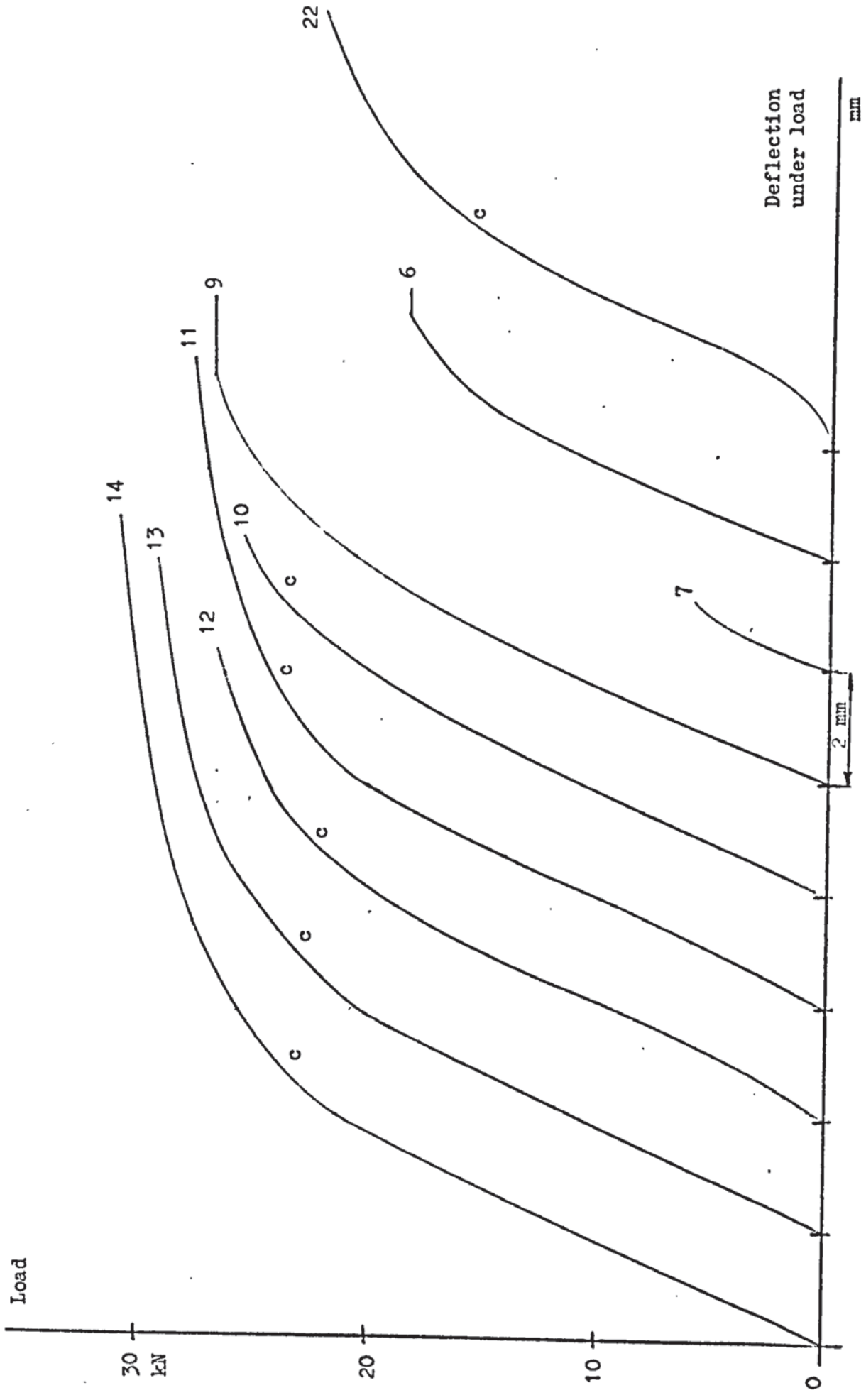

FIGURE 8.42 LOAD/DEFLECTION, SERIES 1, a_v = 800 mm

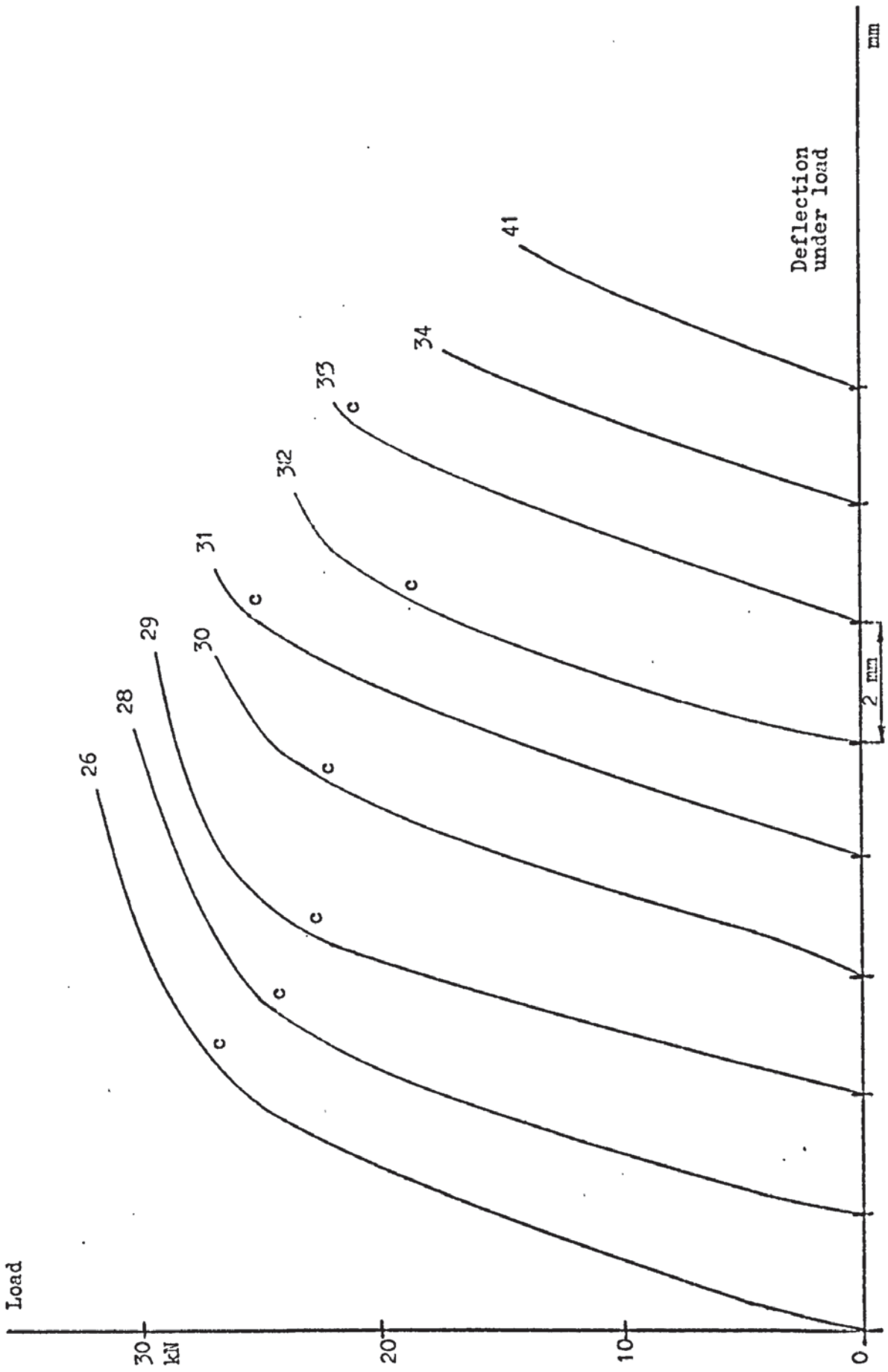

FIGURE 8.43 LOAD/DEFLECTION - SERIES 2, a_v = 600 mm

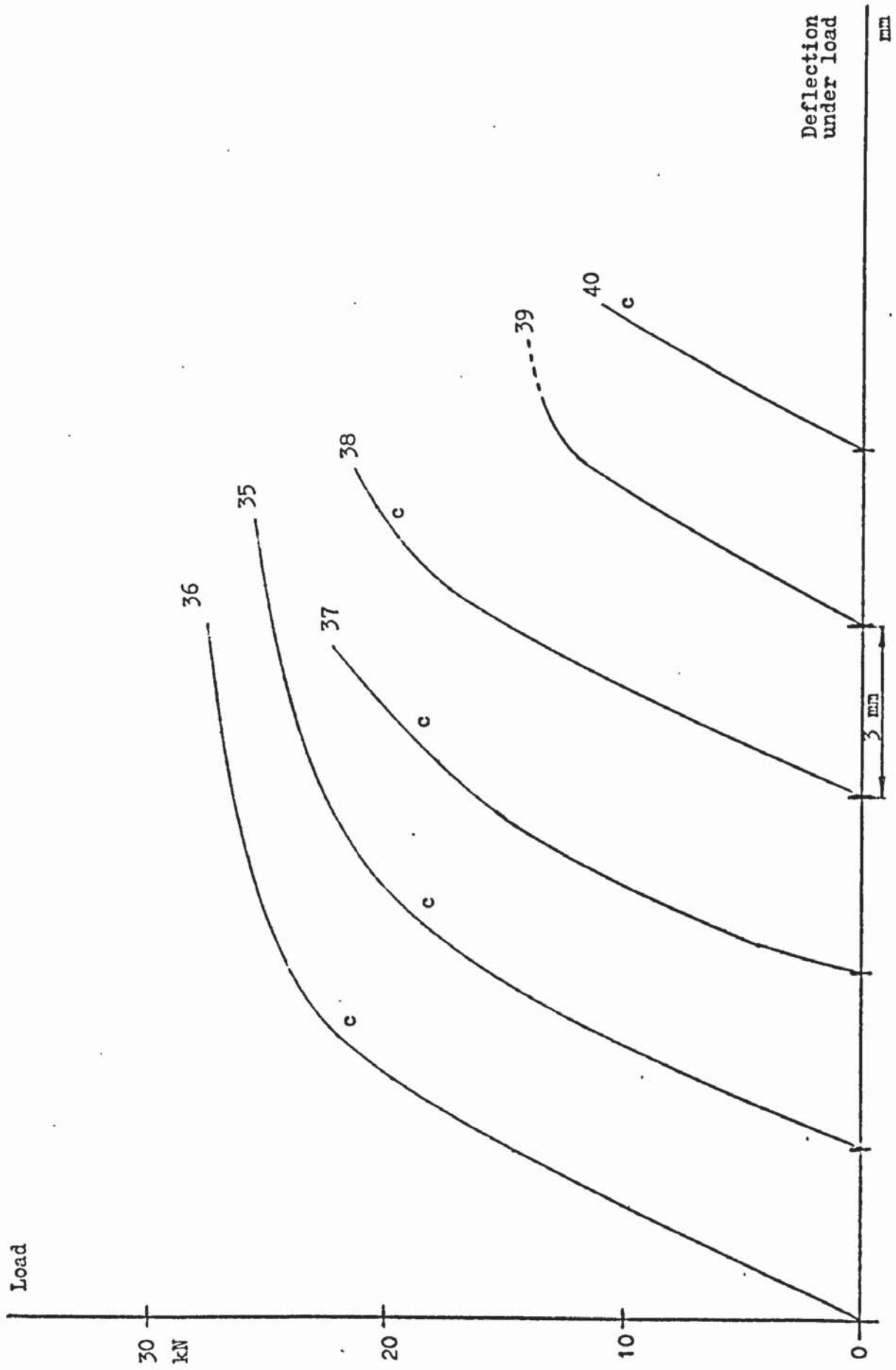

FIGURE 8.44 LOAD/DEFLECTION - SERIES 2, a_v = 800 mm

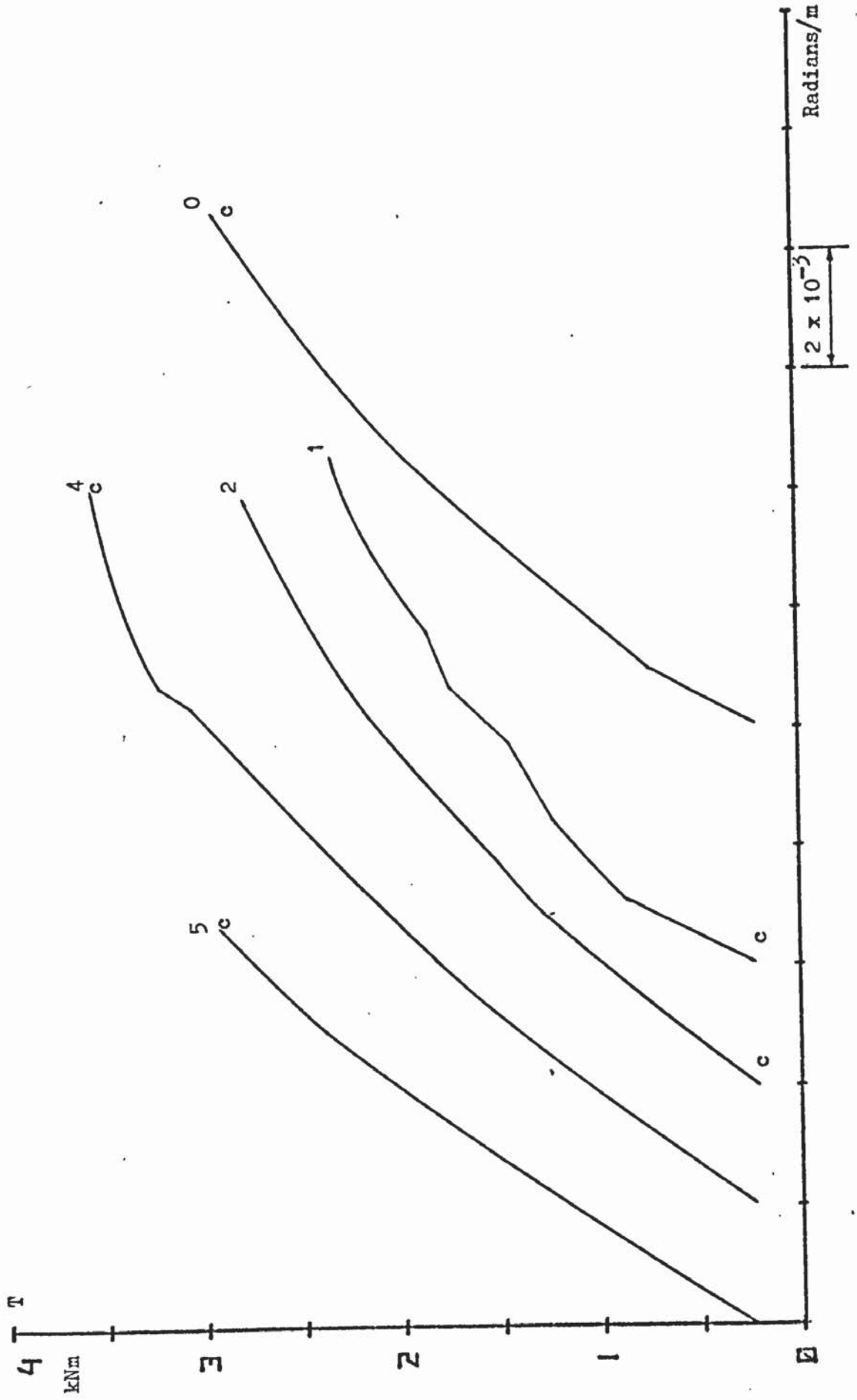

FIGURE 8.45 TORQUE/ROTATION - SERIES 1

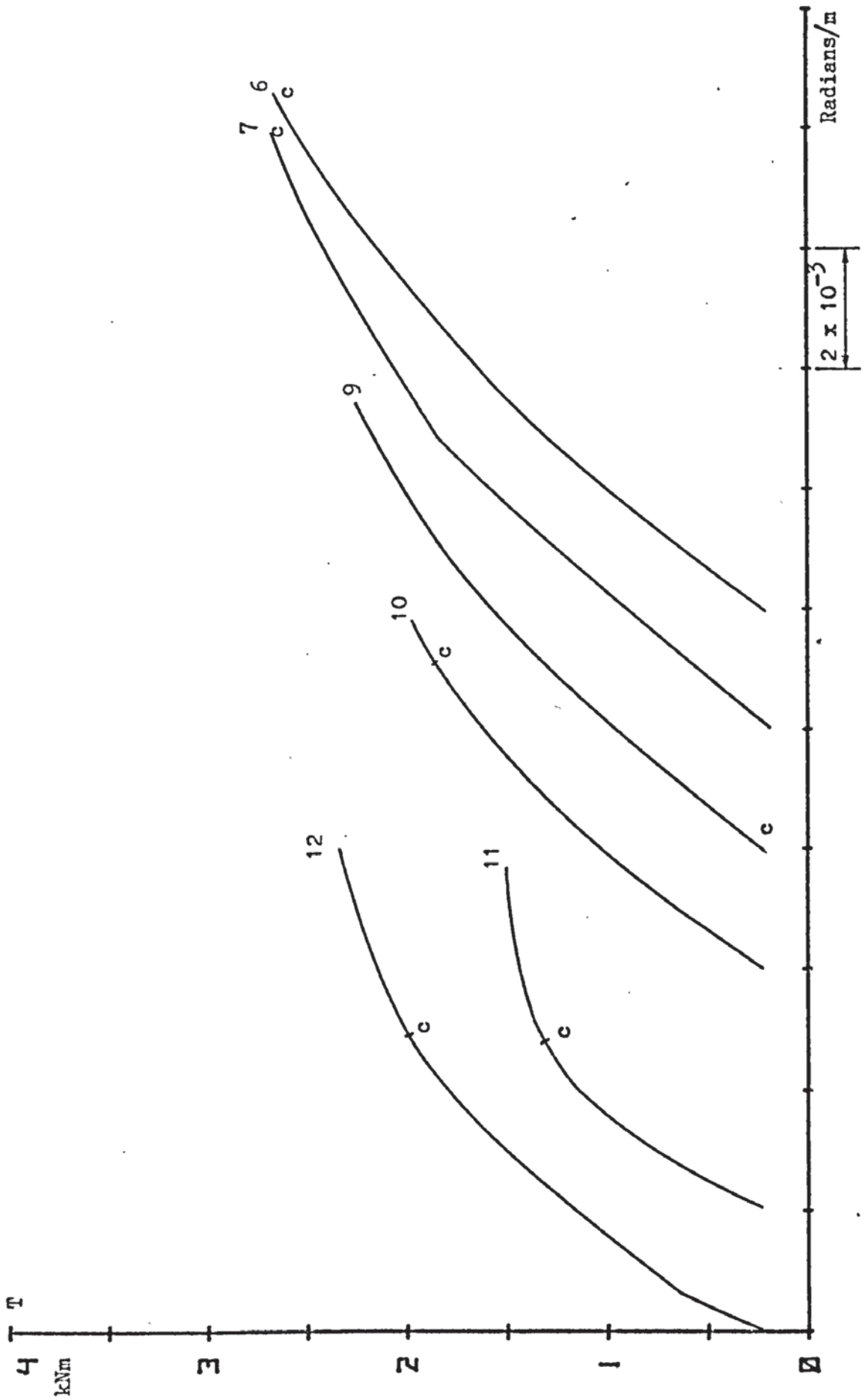

FIGURE 8.46 TORQUE/ROTATION - SERIES 1

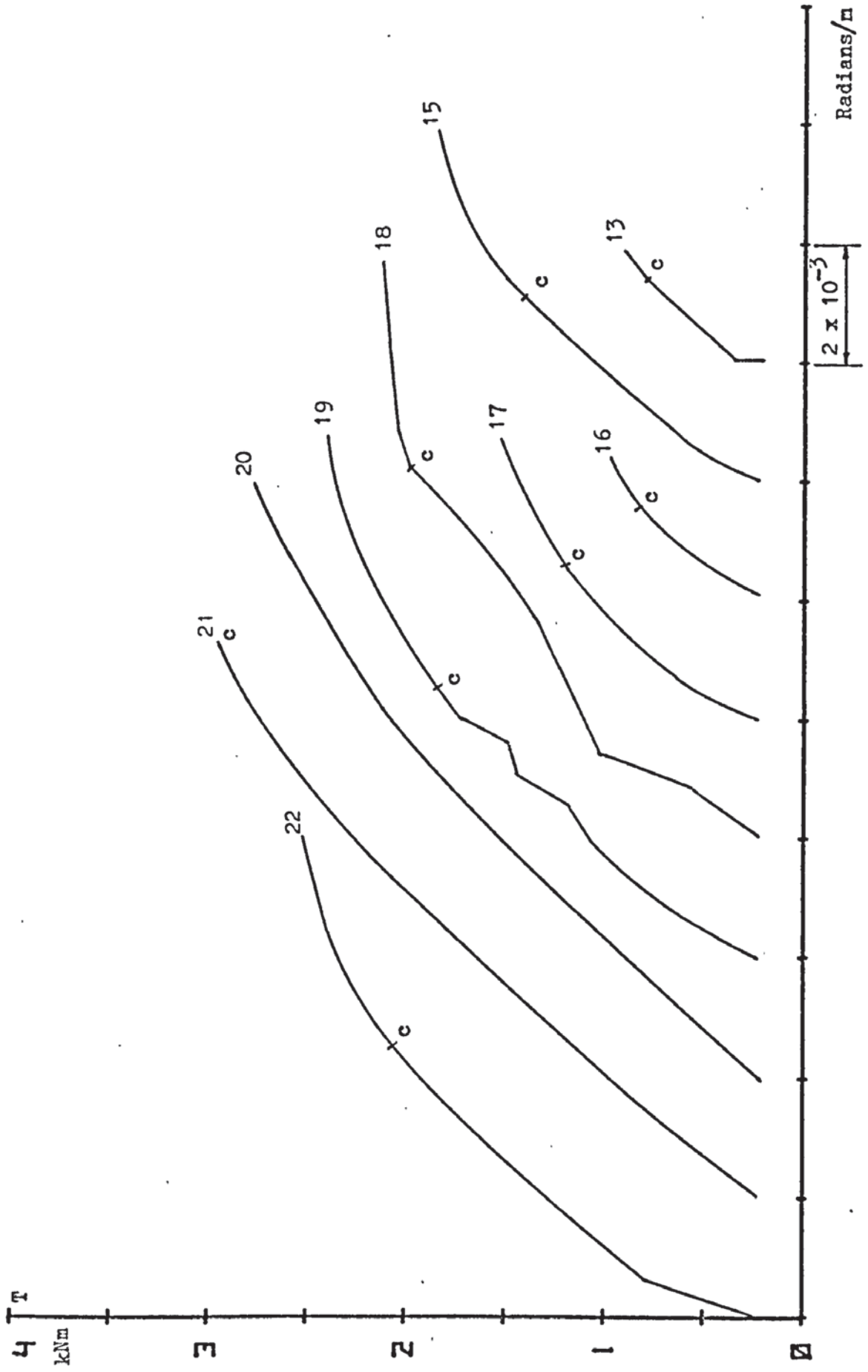

FIGURE 8.47 TORQUE/ROTATION - SERIES 1

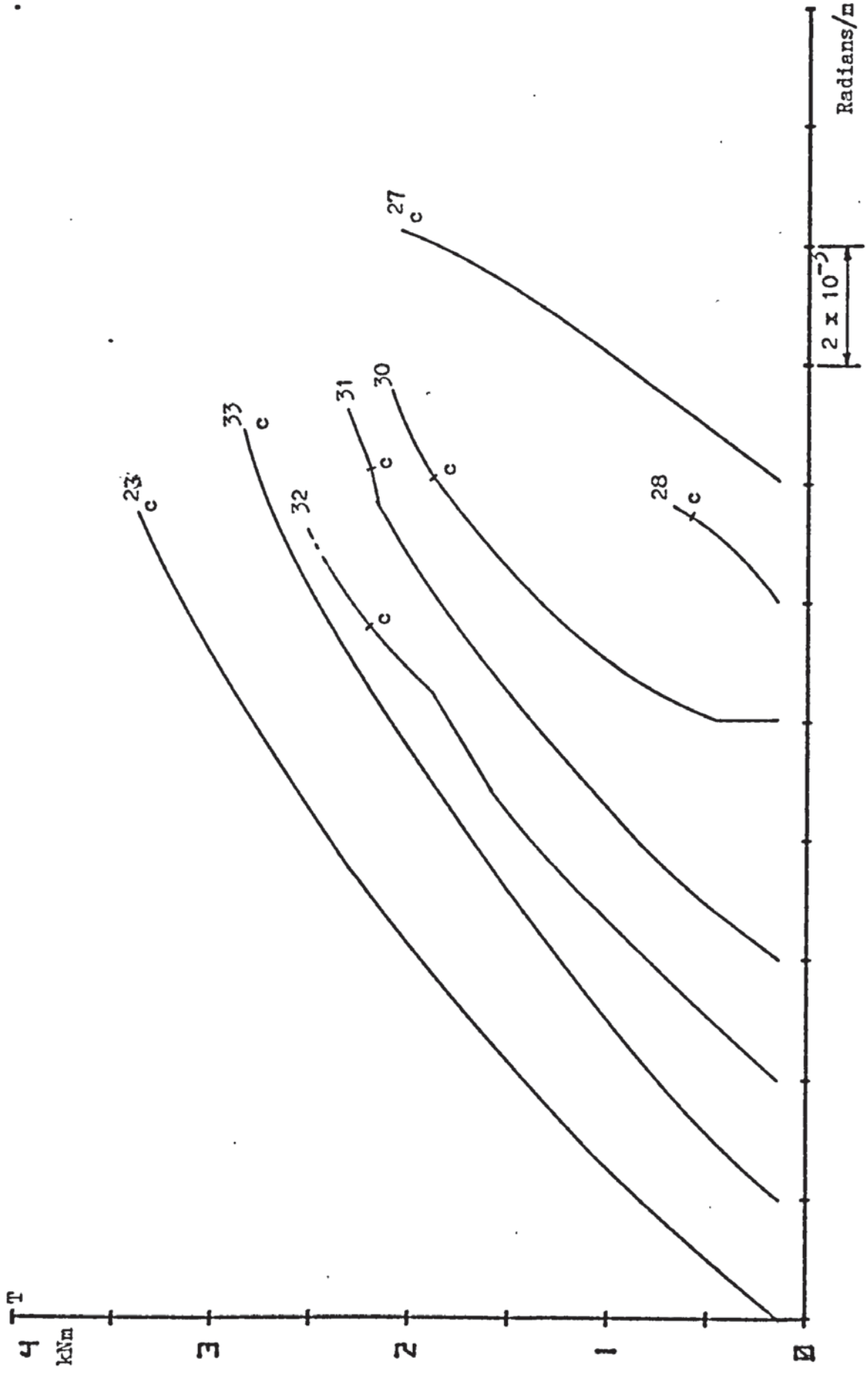

FIGURE 8.48 TORQUE/ROTATION - SERIES 2

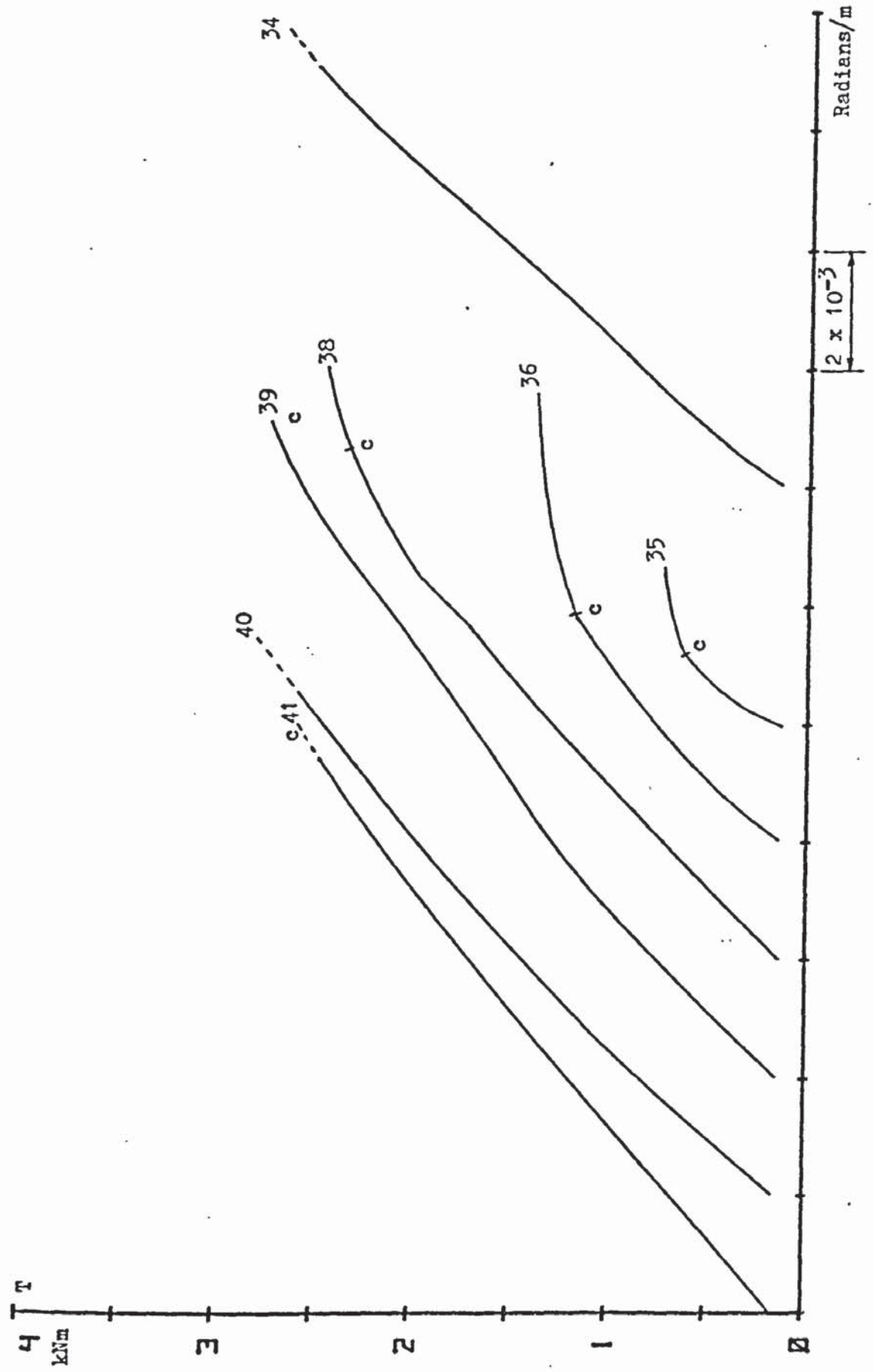

FIGURE 8.49 TORQUE/ROTATION - SERIES 2

8.5 DETERMINATION OF BOND SLIP FACTORS B

The bond slip factors B used in Section 6 have been determined from strain gauge and load cell readings taken during the loading of beams 3 and 14 (Series 1) and 25 and 26 (Series 2).

As strain gauge readings were not taken before prestressing, the initial concrete strains were calculated from the tendon force and position, and the experimental value of Young's Modulus for concrete. Changes of concrete strain on loading were measured directly by gauges. In Series 1 beams, the steel bar was gauged and these readings have been plotted directly. In Series 2 beams the steel strains have been calculated from the load cell readings of force in each wire.

As can be seen from figs. 8.50 to 8.53, the strain distributions were linear, and the ultimate concrete strains at a level with the steel can easily be extrapolated, and hence the value of B determined.

Values of B assumed in the calculations :-

Series 1 beams	0.20
Series 2 beams	0.08

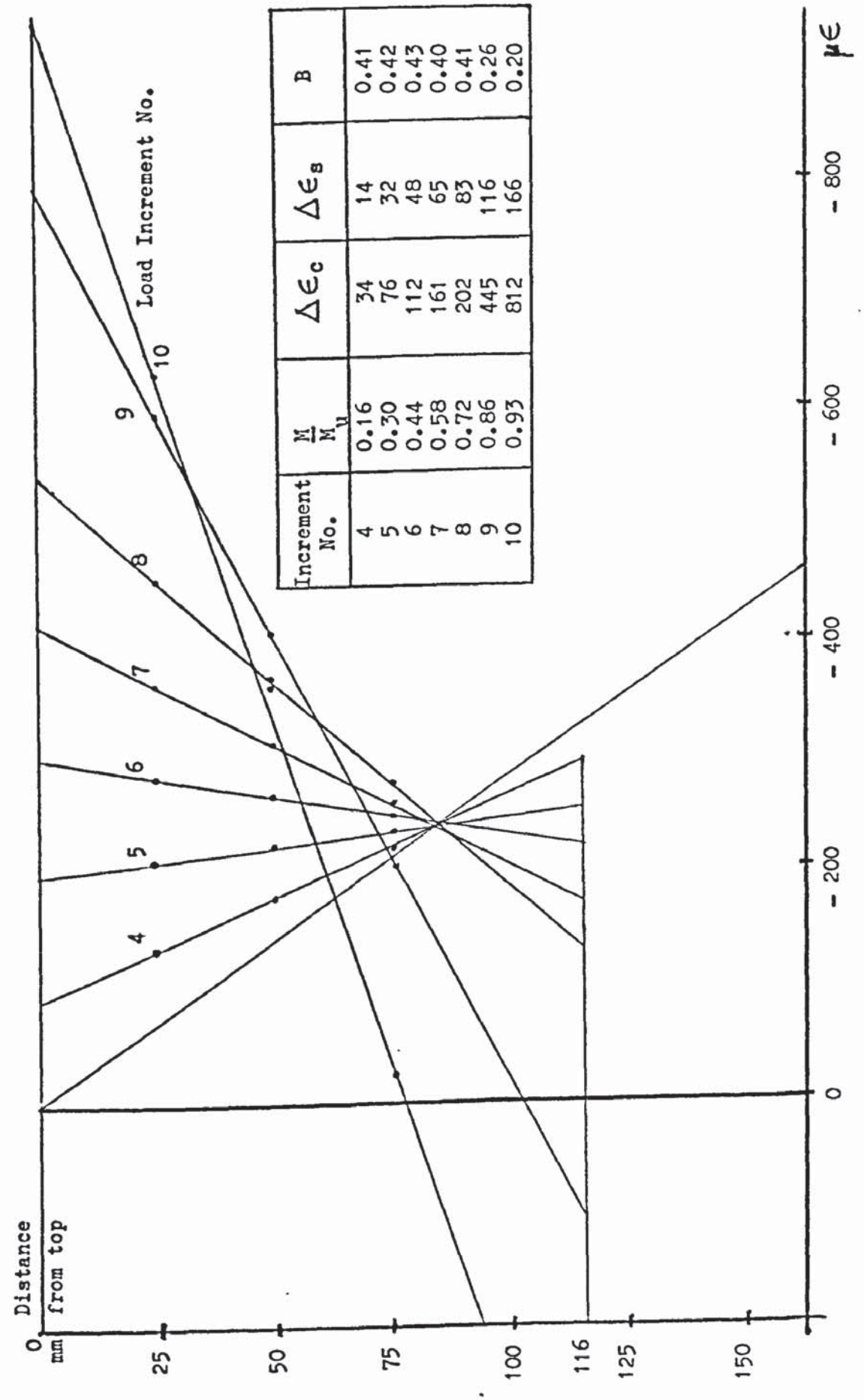

Increment No.	$\frac{M}{M_u}$	$\Delta\epsilon_c$	$\Delta\epsilon_s$	B
4	0.16	34	14	0.41
5	0.30	76	32	0.42
6	0.44	112	48	0.43
7	0.58	161	65	0.40
8	0.72	202	83	0.41
9	0.86	445	116	0.26
10	0.93	812	166	0.20

FIGURE 8.50 DETERMINATION OF BOND SLIP FACTOR, BEAM 3

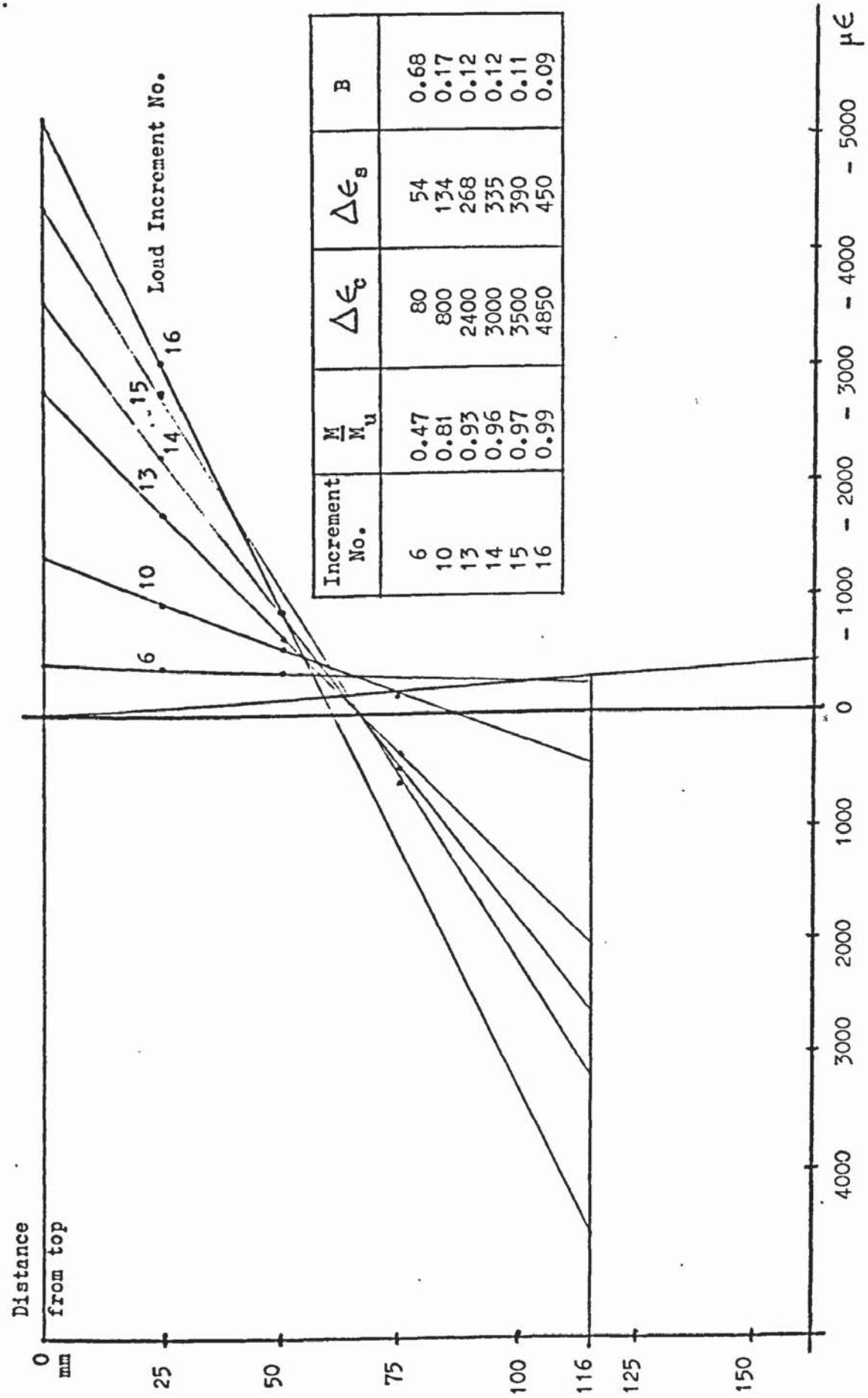

Increment No.	$\frac{M}{M_u}$	$\Delta\epsilon_c$	$\Delta\epsilon_s$	B
6	0.47	80	54	0.68
10	0.81	800	134	0.17
13	0.93	2400	268	0.12
14	0.96	3000	335	0.12
15	0.97	3500	390	0.11
16	0.99	4850	450	0.09

FIGURE 8.51 DETERMINATION OF BOND SLIP FACTOR, BEAM 14

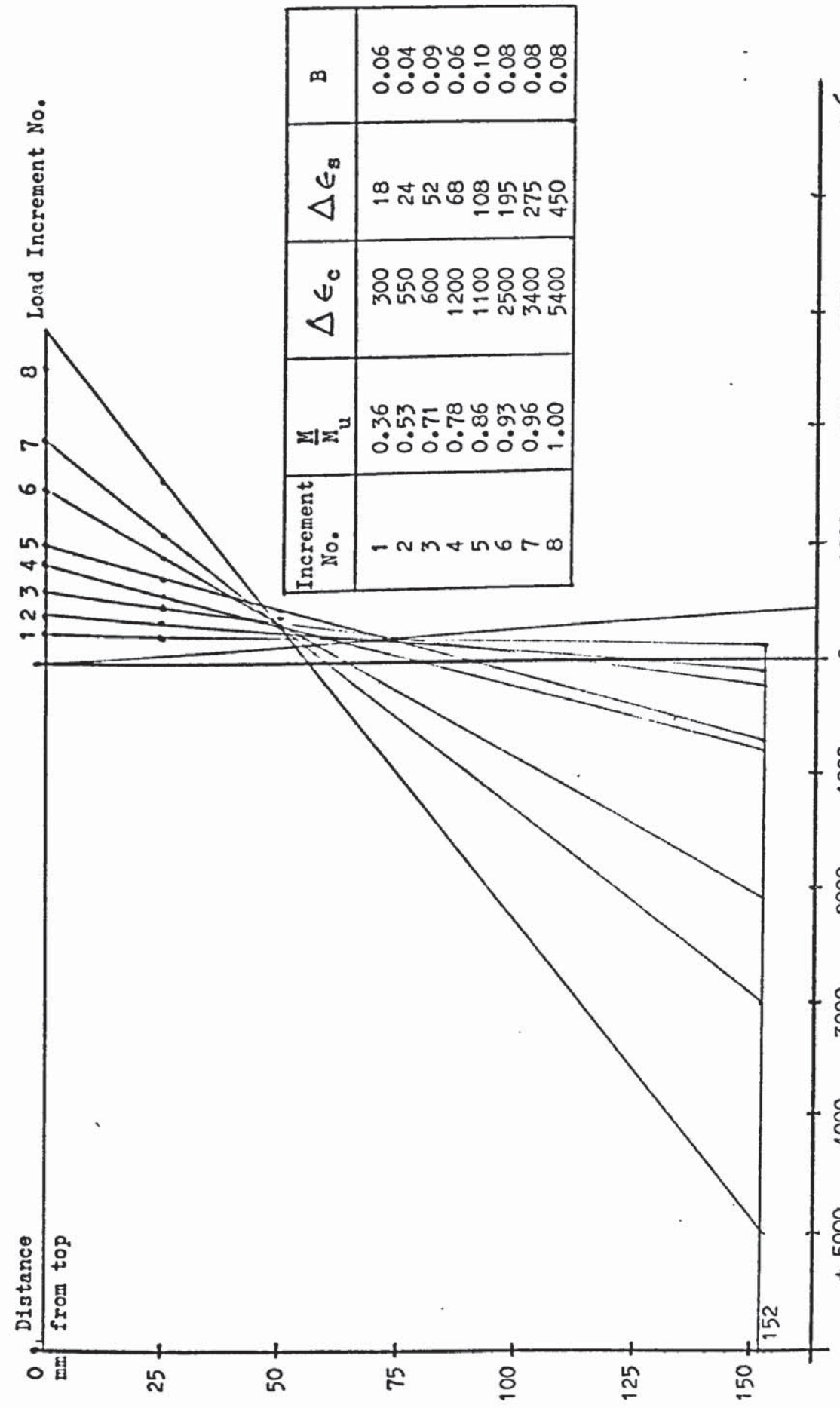

Increment No.	$\frac{M}{M_u}$	$\Delta \epsilon_c$	$\Delta \epsilon_s$	B
1	0.36	300	18	0.06
2	0.53	550	24	0.04
3	0.71	600	52	0.09
4	0.78	1200	68	0.06
5	0.86	1100	108	0.10
6	0.93	2500	195	0.08
7	0.96	3400	275	0.08
8	1.00	5400	450	0.08

FIGURE 8.52 DETERMINATION OF BOND SLIP FACTOR, BEAM 25

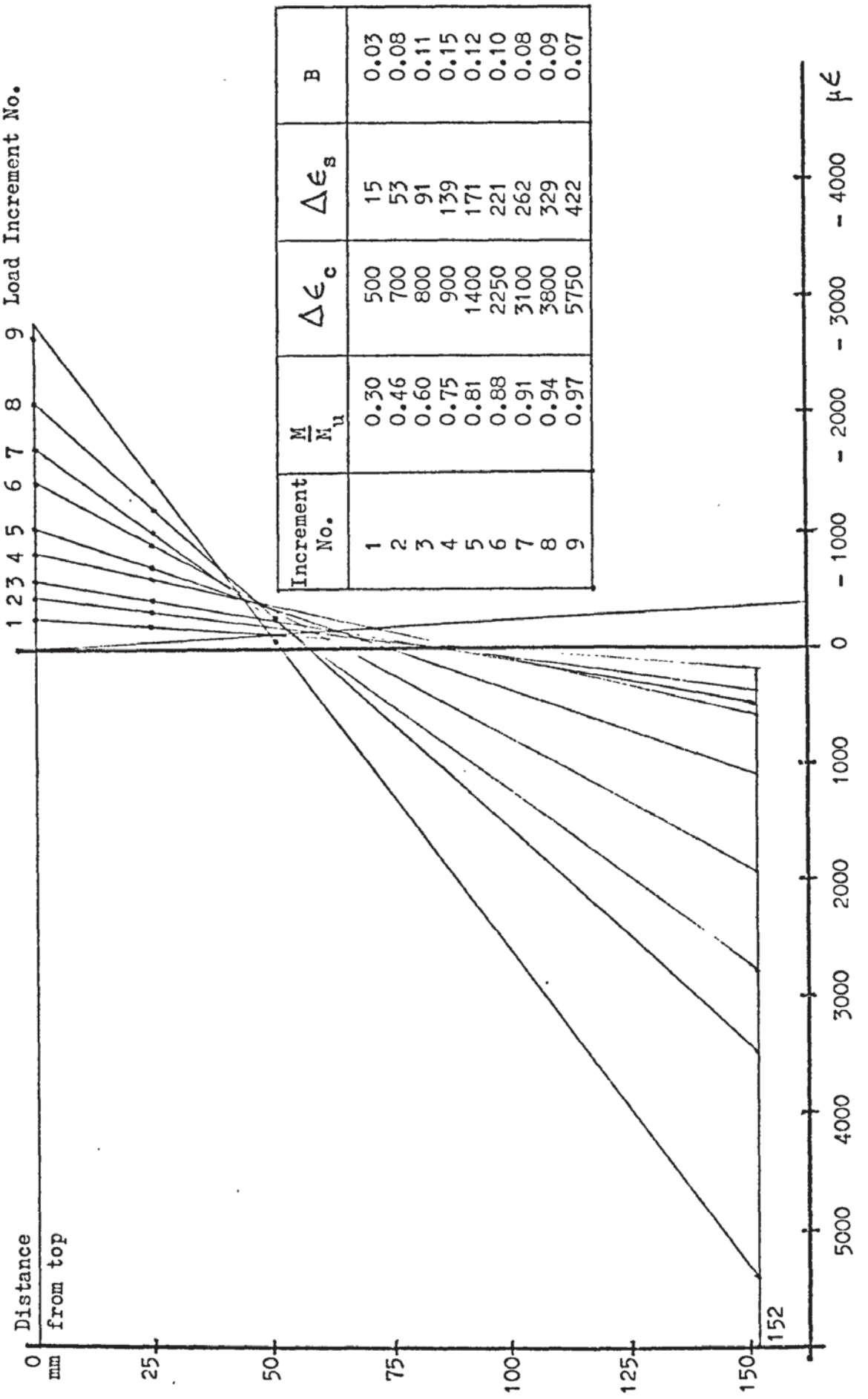

Increment No.	$\frac{M}{M_u}$	$\Delta\epsilon_c$	$\Delta\epsilon_s$	B
1	0.30	500	15	0.03
2	0.46	700	53	0.08
3	0.60	800	91	0.11
4	0.75	900	139	0.15
5	0.81	1400	171	0.12
6	0.88	2250	221	0.10
7	0.91	3100	262	0.08
8	0.94	3800	329	0.09
9	0.97	5750	422	0.07

FIGURE 8.53 DETERMINATION OF BOND SLIP FACTOR, BEAM 26

9. REFERENCES

1. FISHER G.P. and ZIA P.
   Review of Code Requirements for Torsion Design
   Journal of the American Concrete Institute, Vol. 61, Jan. 1964, p 1 - 22

2. British Standard Code of Practice
   CP 110 (1972)

3. S. A. A. Prestressed Concrete Code
   Australian Standard CA 35 - 1973

4. RANGAN B. V. and HALL A.S.
   The Design of Rectangular Prestressed Concrete Beams Subjected to Combined Bending, Shear and Torsion
   UNICIV Report R 93, Aug. 1972, University of New South Wales

5. RANGAN B.V. and HALL A.S.
   Strength of Rectangular Prestressed Concrete Beams in Combined Torsion, Bending and Shear
   Journal of the American Concrete Institute, Vol. 70, April 1973, p 270 - 278

6. RANGAN B.V. and HALL A.S.
   The Design of Rectangular Prestressed Concrete Beams Subjected to Combined Bending, Shear and Torsion
   UNICIV Report R 127, April 1974, University of New South Wales

7. WAINWRIGHT P.J.
   Ultimate Strength in Bending and Torsion of Prestressed Beams Reinforced with Longitudinal Steel Only
   Ph.D. Thesis - 1972, The University of Aston in Birmingham

8. HENRY P.L. and ZIA P.
   Behaviour of Rectangular Prestressed Concrete Beams under Combined Torsion, Bending and Shear

Department of Civil Engineering Report, April 1971, North Carolina State University, Raleigh, N. Carolina

9. ZIA P.

Research on Torsion of Prestressed Members

Journal of the Prestressed Concrete Institute, Vol. 5, Sept. 1960, p 35 - 40

10. ZIA P.

What do we know of Torsion in Concrete Members ?

Journal of the Structural Division, Proceedings of the American Society of Civil Engineers, Vol. 96, No. ST 6, June 1970, p 1185 - 1199

11. MARTIN L.H.

A Theoretical Investigation into the Ultimate Strength in Bending and Torsion of Plain and Reinforced Concrete Members

Ph.D. Thesis, 1973, The University of Aston in Birmingham

12. HSU T.T.C

Torsion of Structural Concrete - Uniformly Prestressed Rectangular Beams Without Web Reinforcement

Journal of the Prestressed Concrete Institute, Vol. 13, April 1968, p 34 - 44

13. A. C. I. COMMITTEE 438

Torsion of Structural Concrete

Publication SP 18, 1968. American Concrete Institute

14. MARTIN L.H.

Bending and Torsion of Plain Concrete Members,

Building Science, Vol. 6, No. 4, Dec. 1971, p 253 - 265

15. GERSH C. and MOORE W.H.

Flexure, Shear and Torsion Tests on Prestressed Concrete I - beam

Highway Research Board Bulletin No. 339, Sept. 1962, p 43- 66

16. ZIA P.

Torsional Strength of Prestressed Concrete Members

Journal of the American Concrete Institute, Vol. 32, 1961,

p 1337 - 1359

17. GARDNER R.P.M.

The Behaviour of Prestressed Concrete I - beams under Combined Bending and Torsion

Technical Report TRA 329, 1960, Cement and Concrete Association

18. GAUSEL E.

Ultimate Strength of Prestressed I - beams under Combined Torsion, Bending and Shear

Journal of the American Concrete Institute, Vol. 67, Sept. 1970,

p 675 - 678

19. REEVES J. S.

Prestressed Concrete Tee - beams under Combined Bending and Torsion

Technical Report TRA 364, 1962

Cement and Concrete Association

20. SWAMY N.

The Behaviour and Ultimate Strength of Prestressed Concrete Hollow Beams under Combined Bending and Torsion

Magazine of Concrete Research, Vol. 14, March 1962, p 13 - 24

21. EVANS R.H. and KHALIL M.G.A.

The Behaviour and Strength of Prestressed Concrete Rectangular Beams Subjected to Combined Bending and Torsion

The Structural Engineer, Vol. 48, No. 2, Feb. 1970, p 59 - 73

22. HUMPHREYS R.

Torsional Properties of Prestressed Concrete

The Structural Engineer Vol. 35, 1957, p 213 - 224

23. MARTIN L.H. and WAINWRIGHT P.J.
Torsion and Bending of Prestressed Concrete Beams
Journal of the Structural Division, Proceedings of the American Society of Civil Engineers, Vol. 99, No. ST 11, Nov. 1973
p 2229 - 2244

24. COWAN H.J. and ARMSTRONG S.
Experiments on the Strength of Reinforced and Prestressed Concrete Beams and of Concrete - encased Steel Joists in Combined Bending and Torsion
Magazine of Concrete Research, Vol. 7, No. 19, March 1955,
p 3 - 20

25. REYNOLDS G.C.
The Strength of Prestressed Concrete Grillage Bridges,
Technical Report TRA 268, 1957
Cement and Concrete Association

26. OKADA K., NISHIBAYASHA S. and ABE T.
Experimental Studies on the Strength of Rectangular Reinforced and Prestressed Concrete Beams under Combined Flexure and Torsion
Transactions of the Japanese Society of Civil Engineers,
No. 131, July 1966, p 39 - 51

27. MURASHKIN G.V.
Influence of Prestressing on the Carrying Capacity and Cracking Loads of Reinforced Concrete Beams under Combined Bending and Torsion
Beton - i - Zhelezabeton (Moscow) No. 10, 1965

28. WARWARUK J. and MUKHERJEE P.R.
Prestressed Concrete Beams with Web Reinforcement under Combined Loading
Structural Engineering Report No. 24, 1970, Department of Civil Engineering, University of Alberta

29. MUKHERJEE P.R. and WARWARUK J.

Torsion, Bending and Shear in Prestressed Concrete Beams

Journal of the Structural Division, Proceedings of the American Society of Civil Engineers, Vol. 97, No. ST 4, April 1971

p 1063 - 1079

30. GANGA RAO H.V.S.

Rectangular Prestressed Concrete Beams under Combined Bending and Torsion

Ph.D. Thesis 1970, Department of Civil Engineering, North Carolina State University, Raleigh, N. Carolina

31. GANGA RAO H.V.S. and ZIA P.

Rectangular Prestressed Beams in Torsion and Bending

Journal of the Structural Division,Proceedings of the American Society of Civil Engineers, Vol. 99, No. ST 1, Jan. 1973,

p 183 - 198

32. FARLEY B.J.

An Investigation into the Combined Effects of Torsion and Bending in Model Prestressed Concrete Beams

Report for B. Sc. - 1972, Department of Civil Engineering and Building, Lanchester Polytechnic, Coventry

33. BISHARA A.

Prestressed Concrete Beams under Combined Torsion, Bending and Shear

Journal of the American Concrete Institute, Vol. 66, No. 7, July 1969, p 525 - 538

34. HENRY R.L. and ZIA P.

Prestressed Beams in Torsion, Bending and Shear

Journal of the Structural Division, Proceedings of the American Society of Civil Engineers, Vol. 100, No. ST 5, May 1974,

p 933 - 952

35. McMULLEN A.E. and WOODHEAD H.R.
Experimental Study of Prestressed Concrete under Combined Torsion, Bending and Shear
Journal of the Prestressed Concrete Institute, Oct. 1973, p 85 - 100

36. LAMPERT P.
Torsion and Bending in Reinforced and Prestressed Concrete Members
Proceedings of the Institution of Civil Engineers, Vol. 50, Dec. 1971, p 487 - 505

37. WOODHEAD H.R. and McMULLEN A.E.
Torsional Strength of Prestressed Concrete Beams
Journal of the Structural Division, Proceedings of the American Society of Civil Engineers, Vol. 100, No. ST 5, May 1974, p 881 - 900

38. COWAN H.J.
The Strength of Plain, Reinforced and Prestressed Concrete under the action of Combined Stresses, with particular reference to the Combined Bending and Torsion of Rectangular Sections
Magazine of Concrete Research, Dec. 1953, p 75 - 86

39. RAJASEKARAN S.
Flexural Strength of Prestressed Concrete Beams - a Graphical Solution
Building Science, Vol. 10, March 1975, p 73 - 78

40. WARWARUK J.
Flexural Strength of Prestressed Concrete Beams using a Graphical Solution for the Reinforcement Stress
Transactions of the Engineering Institution of Canada
Vol. 5, No. 4, 1961, p 213 - 218